Development of Histone Deacetylase (HDAC) Inhibitors with Preferential Isoform Selectivity for HDAC3

THESIS

Submitted in partial fulfillment of

the requirements for the degree of

DOCTOR OF PHILOSOPHY

by

R Ganesh

ID No. 2017PHXF0430H

Under the supervision of

Prof. Balaram Ghosh

BITS Pilani

Pilani | Dubai | Goa | Hyderabad

BIRLA INSTITUTE OF TECHNOLOGY AND SCIENCE, PILANI

2023

BIRLA INSTITUTE OF TECHNOLOGY AND SCIENCE, PILANI

CERTIFICATE

This is to certify that the thesis entitled ***Development of Histone Deacetylase (HDAC) Inhibitors with Preferential Isoform Selectivity for HDAC3*** and submitted by **R Ganesh** ID No.**2017PHXF0430H** for the award of Ph.D. of the Institute embodies original work done by him under my supervision.

Signature of the Supervisor

Name : **Prof. Balaram Ghosh.**

Designation : **Associate Professor.**

Date : 04.05.2023

DECLARATION

I hereby declare that the research work presented in this thesis entitled **Development of Histone Deacetylase (HDAC) Inhibitors with Preferential Isoform Selectivity for HDAC3** is original and has been carried out by myself under the supervision of Prof. Balaram Ghosh, Associate Professor, Department of Pharmacy, BITS-Pilani, Hyderabad Campus, Hyderabad, India. All prior work this thesis is built on is cited at appropriate places. I further declare that this work has not been submitted in part or full for the award of any degree of this or any other university.

R Ganesh

Research Scholar

Department of Pharmacy

BITS-Pilani, Hyderabad Campus

ACKNOWLEDGEMENT

This dissertation would not have been possible without the guidance and help of several individuals who, in one way or another contributed and extended their valuable assistance in the preparation and completion of this study.

First and foremost, my utmost gratitude to my esteemed research guide Prof. Balaram Ghosh, Associate Professor, Department of Pharmacy, BITS-Pilani, Hyderabad Campus, whose sincerity and encouragement I will never forget. His wide knowledge, experience, and logical way of thinking have been of great value to me. His understanding, encouragement, and personal guidance have provided a good basis for the present thesis. His extensive discussions around my work and interesting explorations in operations have been very helpful for this study.

I am heartily grateful to Prof. Swati Biswas, Department of Pharmacy, BITS Pilani- Hyderabad, who acted as a Doctoral Advisory Committee (DAC) member, for her detailed and constructive discussions and suggestions whenever I needed, and for her continuous support throughout this work.

I wish to express my sincere thanks to Prof. Onkar Prakash Kulkarni, Department of Pharmacy, BITS-Pilani, Hyderabad who kindly agreed to serve as a Doctoral Advisory Committee (DAC) member and for his suggestions and valuable time to review my dissertation report.

I would like to thank the Head of the department (HOD), faculty members, and staff of the department of Pharmacy for their kind support and help.

I express my sincere thanks to the Vice Chancellor, BITS-Pilani, Director, Prof. G. Sundar, BITS-Pilani, Hyderabad Campus, Dean, General Administration, Dean and Associate Dean, Academic Research Division (Ph.D. Programme) BITS-Pilani, Hyderabad, for providing excellent working facilities and academic environment.

I gratefully acknowledge the SERB-DST sponsored project for financial assistance in the form of a Project fellow, I acknowledge BITS-Pilani, Hyderabad, for providing an institute fellowship for my research work.

I sincerely admire the contribution of all my lab mates Dr. Prakruti Trivedi, Dr. Yamini, Dr. Soniya, Sravani, Tarun, Himaja, Darakhshan Begum, Sanjay, Asif, Milan, Sri Ganga, and Dr. L. Goverdhan.

I owe my loving thanks to my parents, my family and other family members for their encouragement and understanding.

Last but not least, the omnipresent God, for giving me the strength to undertake this research task and making my destiny to reach this milestone.

Ganesh Routholla

ABSTRACT

First, A series of novel linker-less benzamides with different aryl and hetero aryl cap groups have been designed, synthesized, and screened as potent histone deacetylase (HDAC) inhibitors with promising anti-cancer activity. Two lead compounds amino phenyl quinoline carboxamide **(5e)** and amino phenyl indole carboxamide **(5f)**, were found as potent and highly selective HDAC3 inhibitors over other class-I HDACs and HDAC6. Compound **5e** bearing a 6quinolinyl moiety as the cap group was found to be a highly potent HDAC3 inhibitor (IC_{50} = 560 nM) and displayed 46-fold selectivity for HDAC3 over HDAC2, and 33-fold selectivity for HDAC3 over HDAC1. The synthesized compounds possess antiproliferative activities against different cancer cell lines and are significantly less cytotoxic to normal cells. Molecular Docking studies of compounds amino phenyl quinoline carboxamide **(5e)** and amino phenyl indole carboxamide **(5f)** reveal a similar binding mode of interactions as CI994 at the HDAC3 active site. These observations agreed with the *in vitro* HDAC3 inhibitory activities. Significant enhancement of the endogenous acetylation level on H3K9 and H4K12 was found when B16F10 cells were treated with compounds amino phenyl quinoline carboxamide **(5e)** and amino phenyl indole carboxamide **(5f)** in dose-dependent manner. The compound induced apoptotic cell death in Annexin-V/FITC-PI assay and caused cell cycle arrest at the G2/M phase of the cell cycle in B16F10 cells. These compounds may serve as potential HDAC3 inhibitory anticancer therapeutics.

Second, A series of small molecules having *o*-hydroxy benzamide as the novel zinc binding group (ZBG) has been introduced for the first time that can be able to produce good HDAC3 selectivity over other HDACs. The lead HDAC3 inhibitors, hydroxy phenyl quinoline carboxamide (**11a),** and flouro hydroxy phenyl indole carboxamide (**12b)** displayed promising in vitro anticancer activities with less toxicity to normal kidney cells. These lead compounds significantly upregulate histone acetylation and induce apoptosis with a G2/M phase arrest in B16F10 cells. Compound hydroxy phenyl quinoline carboxamide (**11a)** exhibited potent anti-tumor efficacy in 4T1-Luc breast cancer xenograft mouse model in female balb/c mice. It also showed significant tumor growth suppression with no general toxicity and extended survival rates post tumour resection. It significantly induced highest ROS generation leading to apoptosis. No considerable toxicity was noticed in major organs isolated from the compound hydroxy phenyl quinoline carboxamide (**11a)** treated mice. Compound hydroxy phenyl quinoline carboxamide (**11a)** also induced the upregulation of *ac*-H3K9, *ac*H4K12, caspase-3, and caspase-7 as analyzed by immunoblotting with treated tumor tissue. Overall HDAC3 selective inhibitor hydroxy phenyl quinoline carboxamide (**11a)** might be a potential lead for the clinical translation as an emerging drug candidate.

The main objective behind designing these molecules is to develop novel molecules that exhibit selective HDAC3 inhibitory activity. Further structural optimization of the lead molecules may show better selectivity, potency, stability, and bioavailability. The lead molecules can also be explored further in various other animal models of cancer and can be translated as potential drug candidates for the treatment of cancer.

TABLE OF CONTENTS

List of Tables

List of Figures

LIST OF ABBREVIATIONS

µg	Microgram
µL	Microlitre
µM	Micromolar
1H NMR	Proton Nuclear Magnetic Resonance
A549	Human alveolar adenocarcinoma cell
ADP	Adenine diphosphate
AO	Acridine Orange
B16F10	Murine melanoma cells
CDCl3	Deuterated chloroform
Ch.	Chapter
CTCL	Cutaneous T-cell lymphoma
DAPI	4,6-diamidino-2-phenylindole
DCM	Dichloromethane
DCFH-DA	Dichlorodihydrofluoresein diacetate
DFT	Density functional theory
DMAP	4-Dimethylaminopyridine
DMEM	Dulbecco's modified Eagle's media
DMF	Dimethylformamide
DMSO	Dimethyl sulphoxide
DMSO-d6	Deuterated dimethyl sulphoxide
DNA	Deoxyribonucleic acid
EDC	1-Ethyl-3-(3-dimethylaminopropyl)carbodiimide
ESI	Electron spray ionization
EtOAc	Ethyl acetate

FITC	Fluorescein isothiocyanate
HCl	Hydrochloric acid
HDAC	Histone deacetylase
HDACi	Histone deacetylase inhibitors
HeLa	Human cervical cancer cell line
HPLC	High-performance liquid chromatography
HRMS	High resolution mass spectrometry
HRP	Horseradish peroxidase
IC_{50}	Half maximal inhibitory concentration
LC-MS	Liquid chromatography–mass spectrometry
MCF-7	Human breast cancer cell lineline
mg	Milligram
min	Minute
mL	Millilitre
mm	Millimetre
mmol	Millimole
MS	Mass spectroscopy
MTT	3-(4,5-dimethylthiazol-2-yl)-2,5-diphenyltetrazolium bromide
Na_2SO_4	Sodium sulphate
$NaHCO_3$	Sodium bicarbonate
NCOR1	Nuclear receptor corepressor 1
NMR	Nuclear magnetic resonance
°C	Degree centigrade
PBS	Phosphate buffered saline
PI	Propidium iodide
ppm	Parts per million
PTCL	Peripheral T-cell lymphoma
Py	Pyridine
RIPA	Radio immuno precipitation assay

RNA	Ribonucleic acid
ROS	Reactive Oxygen Species
Rt	Retention time
RT	Room temperature
SAHA	Suberoylanilide hydroxamic acid
SIRT	Sirtuin
t-Boc	tert-Butyloxycarbonyl protecting group
TBST	Tris-buffered serine with 1% tween 20
THF	Tetrahydrofuran
TLC	Thin layer chromatography
TNF-α	Tumor necrosis factor- alpha
TSA	Trichostatin A
TUNEL	Terminal deoxynucleotidyl transferase mediated nickened labelling
USFDA	United states food and drug administrations
ZBG	Zinc binding group

Chapter 1

Introduction

Epigenetic modifications:

Epigenetics had developed into a well-known biological subdiscipline for many decades, and the term had practically come to mean "epigenetic inheritance." For instance, epigenetics was defined as “the study of changes in gene function that are mitotically and meiotically inheritable and that do not necessitate a change in the DNA sequence” in a 2001 issue of science that focused on the subject (Wu & Morris, 2001). Epigenetic alterations frequently take place over the course of an organism's existence, but if they happen in germ cells, they can be passed on to the following generation (Chandler, 2007). Paramutation, bookmarking, imprinting, gene silencing, X chromosome inactivation, position effect, changeable disorder, reprogramming, maternal attributes, carcinogenic process, teratogenic effects, regulation of histone modification, hetero chromatin states, and cloning are epigenetic processes known to be involved. The epigenetic machinery consists basically of three interconnected components: DNA methylation, histone posttranslational modification, and non-coding RNAs.

DNA methylation, which is greatly studied, is a commonly repressive epigenetic signal while placed at promoters, happens predominantly at the carbon five positions of symmetrical CpG (cytosine and guanine separated with the aid of phosphate) dinucleotides (Li & Zhang, 2014). The state of DNA methylation is maintained after the cellular division via the reaction of DNA methyltransferase 1 (DNMT 1), which methylates hemi methylated CpG dinucleotides in the daughter cell. DNA methylation has a complex relationship; it can be quite helpful in regulating the (Wu & Morris, 2001), epigenetic alterations frequently take place over the course of an organism's existence, but if they happen in germ cells, they can be passed on to the following generation (Chandler, 2007). Epigenetic processes involve Gene silencing, bookmarking, position expression of genes, X chromosome inactivation, imprinting, Paramutation, changeable disorder or phenotypic severity, material attributes, teratogenic effects, reprogramming, carcinogenic processes, regulation

histone modification, heterochromatin states, and cloning, but its effect can be disease-causing such regions. The previous study discovered 5-hydroxy methyl cytosines (5hmc) were oxidised to 5-methyl cytosines by using a family of catalysing enzymes, has added a new dimension to the study of DNA methylation (Kriaucionis & Tahiliani, 2014).

1.2 Chromatin structure and modifications:

Chromatin is the state in which DNA is packaged in the cell. The nucleosome is the basic unit of chromatin and consists of an octamer of the four nuclear histones (H_3, H_4, H_2A, H_2B) around which 147 base pairs of DNA are wrapped. The core histone is spherical, except for its *N*- terminal tails, which are unstructured. Chromatin modifications include covalent modification (PTM) of protruding amino-terminal histone tails with acetyl, methyl, phosphate, ubiquitin, or other groups (H. Huang *et al*., 2014).

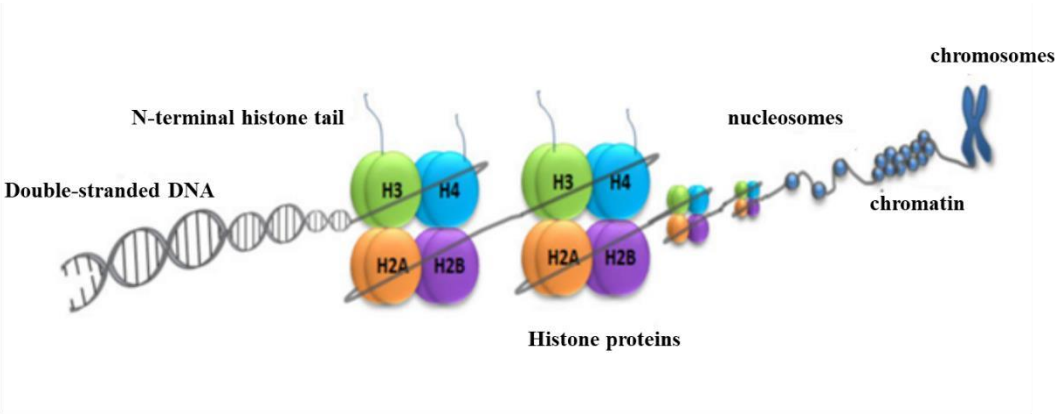

Figure 1.1. Structure of histone octamer coiled with DNA double helix

In the case of lysine, methyl modification can be mono, di, or trimethylation. These modifications contribute to the regulation of gene expression by directly affecting or attracting or repelling effector-binding proteins, referred to in this collection as PTM writers, readers, and erasers. Sin chromatin consists of tightly packed DNA stand wrapped around histone octamers, the folding pattern of DNA in chromatin is clearly the cause of changes in gene activity. Although chromatin

structures and histone PTMs can be stably transferred from a mother cell to a daughter cell, the mechanism underlying the replication of such structures is not fully understood (Almouzni & Cedar, 2016)

1.3. Histone deacetylases (HDACs):

Histone deacetylases are expressed through diverse tumors and are involved in critical chromosomal translocation-mediated oncogene protein fusion and carcinogenic activities (Falkenberg & Johnstone, 2014a). These enzymes removes acetyl groups from the amino acid of lysine on a histone(Inoue & Fujimoto, 1969).

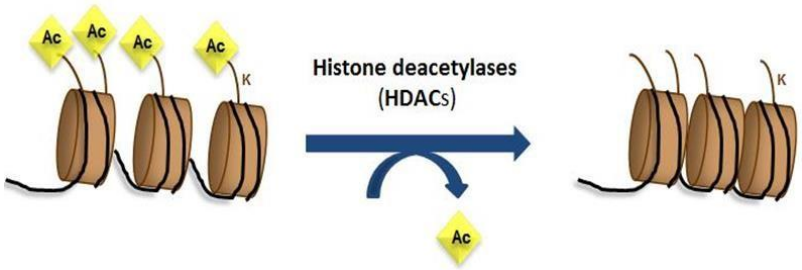

Figure 1.2. The role of histone deacetylases (HDACs) in epigenetic regulation.

In humans, so far 18 HDACs have been identified, and those are grouped into four classes (Seto & Yoshida, n.d.). Class I, Class II, Class III and Class IV. Class I contains HDAC 1, HDAC 2, HDAC 3, and HDAC 8; Class II HDACs are subdivided into two groups: Class IIa and Class IIb. HDACs 4,5,7 and 9 are included in class IIa, and HDACs 6 and 10 are included in Class IIb. Class IV contains only one HDAC, "i.e., HDAC 11. These three classes HDACs (11 HDACs) are Zndependent HDACs. Class III was known as the sirtuins. SIRTs are nicotinamide adenine dinucleotide-dependent enzymes (Imai *et al*., 2000).

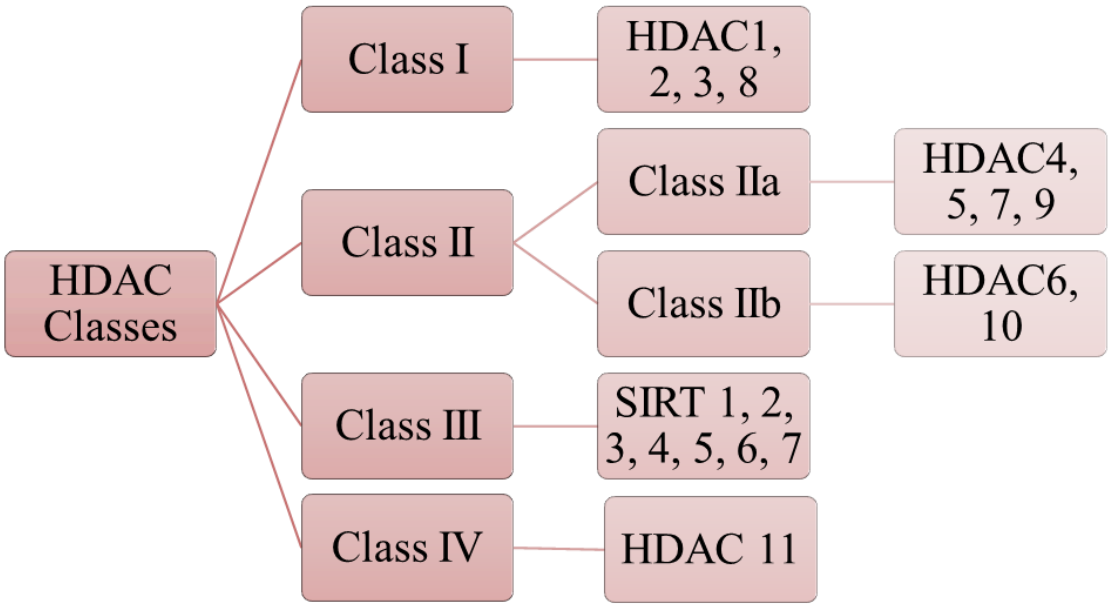

Figure. 1.3. Classification of the histone deacetylases (HDACs) family enzymes

1.4. Histone deacetylases in cancer:

Despite the widespread use of HDAC inhibitors in cell cultures, animal models, and early clinical trials, surprisingly, little is known about the expression of their targets in cancer tissues. As a result, there are a few systematic studies examining the function of all family members in the context of tumors. According to a recent study, cells lacking HDAC2 expression are resistant to HDAC inhibitors of clinical significance (Ropero *et al*., 2006). The genetics, expression, and function of the classical HDAC family members 1-11 in cancer are depicted in **Figure 1.4.**

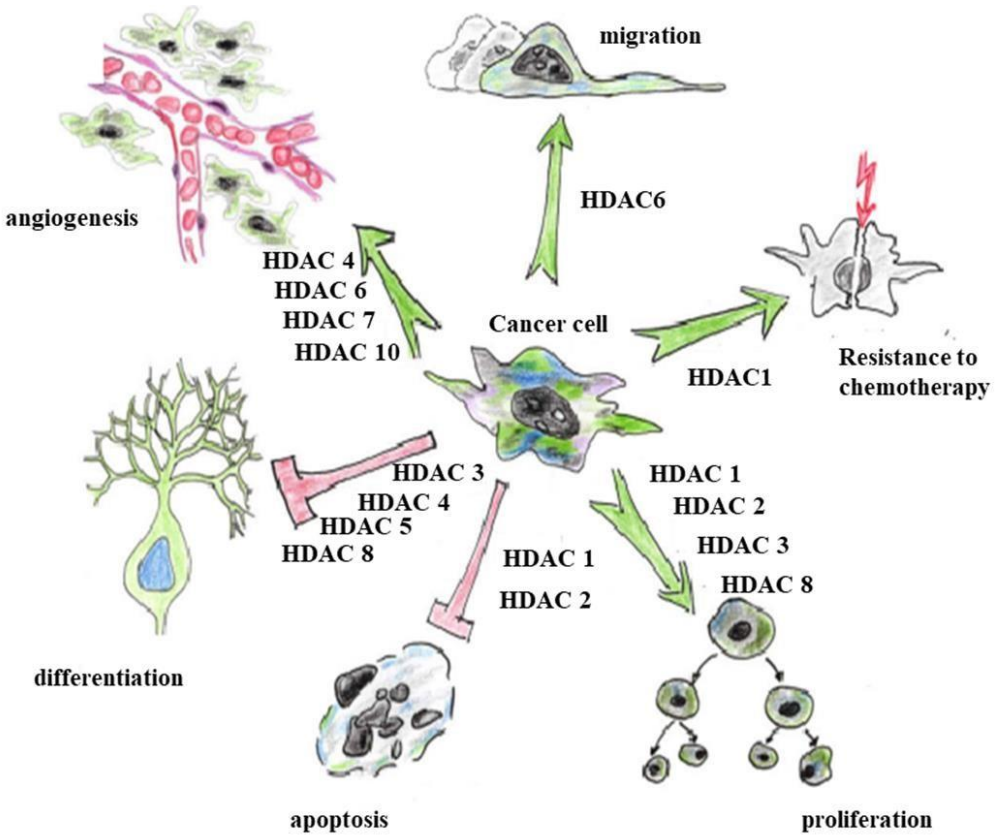

Figure. 1.4. HDAC family members control hallmarks of cancer cell biology. Selective targeting of individual HDACs causes differentiation, apoptosis, cell cycle inhibition, inhibition of migration, susceptibility to chemotherapy, and anti-angiogenesis. See the text for further information and references (Witt *et al*., 2009a).

1.4.1. Class I HDACs:

Class I HDAC participants are deregulated in many cancers. HDAC 1 expression was elevated in 17/25 instances (60%) of gastric cancer in the first research compared to normal tissue. The prognostic value of HDAC 1, 2, and 3 expressions are investigated by 293 gastric cancer samples; this observation was confirmed by a recent study, and also elevated class I HDAC expression was found to be an independent predictor of survival in that study, gastric cancer patients. (Weichert, Röske, Gekeler, Beckers, Ebert, *et al.,* 2008a). In a group of 39 pancreatic carcinomas, increased HDAC1 expression in conjunction with HIF1a used to be a poor prognosis (Miyake *et al.,* 2008). High HDAC 1, 2, and 3 expressions have been additionally linked to differentiation and increased

pancreatic cancer cell proliferation in large investigations comprising 192 pancreatic carcinoma samples (Weichert, Röske, Gekeler, Beckers, Stephan, *et al*., 2008). Compared to HDAC1, upregulation of HDAC2 in colorectal cancer is more frequent and stronger, starting at the polyp stage. Similarly, HDAC 2 expression confirmed a distinct demarcation of high-intensity in cervical dysplasia and aggressive cancer compared to HDAC 1 (B. H. Huang *et al.*, 2005). In gastric, colorectal, and prostate cancer, HDAC 2 expression together with HDAC 1 and 3 was correlated with advance stage disease and a poor prognosis (Weichert, Röske, Gekeler, Beckers, Ebert, *et al*., 2008b) . A high level of HDAC8 expression in childhood neuroblastoma is significantly associated with advanced-stage disease, poor prognostic markers, and poor survival in children. However, none of the other 10 HDAC family members investigated the correlation with the disease stage (Oehme *et al*., 2009).

1.4.2. Class II HDACs:

Class II HDACs are further subdivided into two types. 1. Class IIa

2. Class IIb

1.4.2.1. Class IIa HDACs:

During the past few years, Class II HDACs have also been associated with cancer. The expression of HDAC4 was higher in breast cancer samples than in renal, bladder, and colorectal cancer samples. In the observation, HDAC5 and HDAC7 expression is increased in colorectal cancer, whereas it is downregulated in renal, bladder, and breast cancer (H. Ozdag *et al.*, 2006). The overexpression of HDAC9 was reported in cervical cancer (Y. W. CHOI *et al*. 2007), and elevated HDAC9 levels are also correlated with decreased survival induction of medulloblastoma patients (Milde *et al*. 2010), and in childhood, acute lymphoblastic leukemia patients (Moreno *et al*. 2010).

1.4.2.2. Class IIb HDACs:

In oral squamous cell carcinoma, extensively higher HDAC 6 expression was observed in carcinomas versus normal oral squamous tissue, and HDAC6 expression upregulated in advancedstage cancers comparison with early stage in 90 samples (T. Sakuma *et al*. 2006). HDAC 6 expression was correlated with better survival, and it was a higher expression in breast cancers of low histological grade, estrogen and progesterone receptor, and small tumors. The higher level of HDAC6 mRNA was correlated with a good response to endocrine treatment. Therefore, HDAC6 can be used as a prognostic indicator of breast cancer progression and response to endocrine treatment (Zhang *et al.*, 2004).

1.4.3. Class III HDACs:

Cancer is also being linked to sirtuins in recent years. Sirtuins appear like other HDACs, and function as both pro-oncogenic and tumor suppressors. In a similar manner to classical HDACs, several sirtuins have abnormal expressions. Acute myeloid leukemia, prostate cancer, and nonmelanoma skin cancer these three have increased levels of SIRT1(Bradbury *et al.* 2005; Hida *et al*. 2007; Huffman *et al.* 2007). There are SIRT3 and SIRT7 increased expressions in breast cancer (Ashraf *et al*. 2006). In gastric cancer and gliomas, downregulation of SIRT2 is observed (Hiratsuka *et al*. 2003).

1.4.4. Class IV HDACs:

HDAC 11 is the lone class of IV HDAC and is crucial for the growth and survival of oncogenic jak2-driven MPN cells (Yue *et al.*, 2020).

1.5. Histone deacetylase inhibitors (HDACi) as anticancer agents:

Cancer cells induce cell cycle arrest, cell differentiation, and cell death and reduce angiogenesis as well as modulate immune response when exposed to HDAC inhibitors. It has been suggested by Dawson and kouzarides, that the epigenetic vulnerability of cancer cells causes the relative specificity of HDAC inhibitors. Epigenetic regulatory mechanisms are multiplied in normal cells in contrast to those in some cancer cells. As a result, HDAC may maintain a set of key genes required for the survival and growth of cancer cells, not those required for normal cells (Dawson & Kouzarides, 2012). HDAC inhibitors work differently and may have different mechanisms of anticancer action based on cancer type, individual HDAC inhibitor dose, and other factors (Kretsovali *et al.,* 2012). As an example, valproic acid inhibited bladder cancer invasiveness but not prostate cancer (Chen *et al.,* 2006), did not inhibit the cell cycle in some neuroblastoma cell lines such as SH-SY-5Y and SK-N-BE (Stockhausen *et al.,* 2005).

1.5.1. FDA-approved HDAC inhibitors:

To date, there are five HDAC inhibitors have been approved for cancer treatment by the US Food and Drug Administration (FDA). The first commercial non-selective HDAC inhibitor was vorinostat (SAHA), developed by Merck. It was approved in October 2006 for the treatment of cutaneous T-cell lymphoma (CTCL). The second marketed drug is naturally occurring Romidepsin (FK228). It was isolated from the cultures of chromo bacterium violaceum, a gram-negative bacterium isolated from a japanese soil sample. In June 2011, it was approved for the treatment of both cutaneous T-cell lymphoma and peripheral T-cell lymphoma (CTCL & PTCL) (Mann et al., 2007, Vandermolen *et al.,* 2011). The drugs panobinostat (LBH589) and belinostat (PXD101), both pan HDAC inhibitors, were made available to patients with multiple myeloma (MM), cutaneous T-cell lymphoma (CTCL), and peripheral T-cell lymphoma (PTCL)(Laubach *et al.,* 2015, Poole,

2014). Panobinostat was approved in 2015 by Novartis pharmaceutical company. Belinostat was approved on July 3, 2014, and developed by Spectrum Pharmaceuticals. The Chinese FDA (CFDA) has approved tucidinostat (Chidamide), a 2-aminoanilide, is used to treat resistant peripheral T-cell lymphoma (PTCL) by inhibiting the activity of HDAC 1, 2, 3, and 10 (Lu *et al.,* 2016a).

1.5.2. Classes of HDAC inhibitors:

According to the chemical structure, the five main kinds of HDAC inhibitors include short-chain fatty acids, benzamides, hydroxamic acids, cyclic peptides (Falkenberg & Johnstone, 2014b), and recently hydrazide-based HDAC inhibitors also described (McClure *et al*., 2016).

1. Hydroxamates **:** Vorinostat (SAHA), Belinostat, Panobinostat.
2. Cyclic peptides **:** Romidepsin.
3. Benzamides **:** Tacedinaline (CI-994), Entinostat, Mocetinostat, Chidamide.
4. Short-chain fatty acids **:** Valproic acid, Phenylbutyrate.
5. **5.** Hydrazides **:** UF010

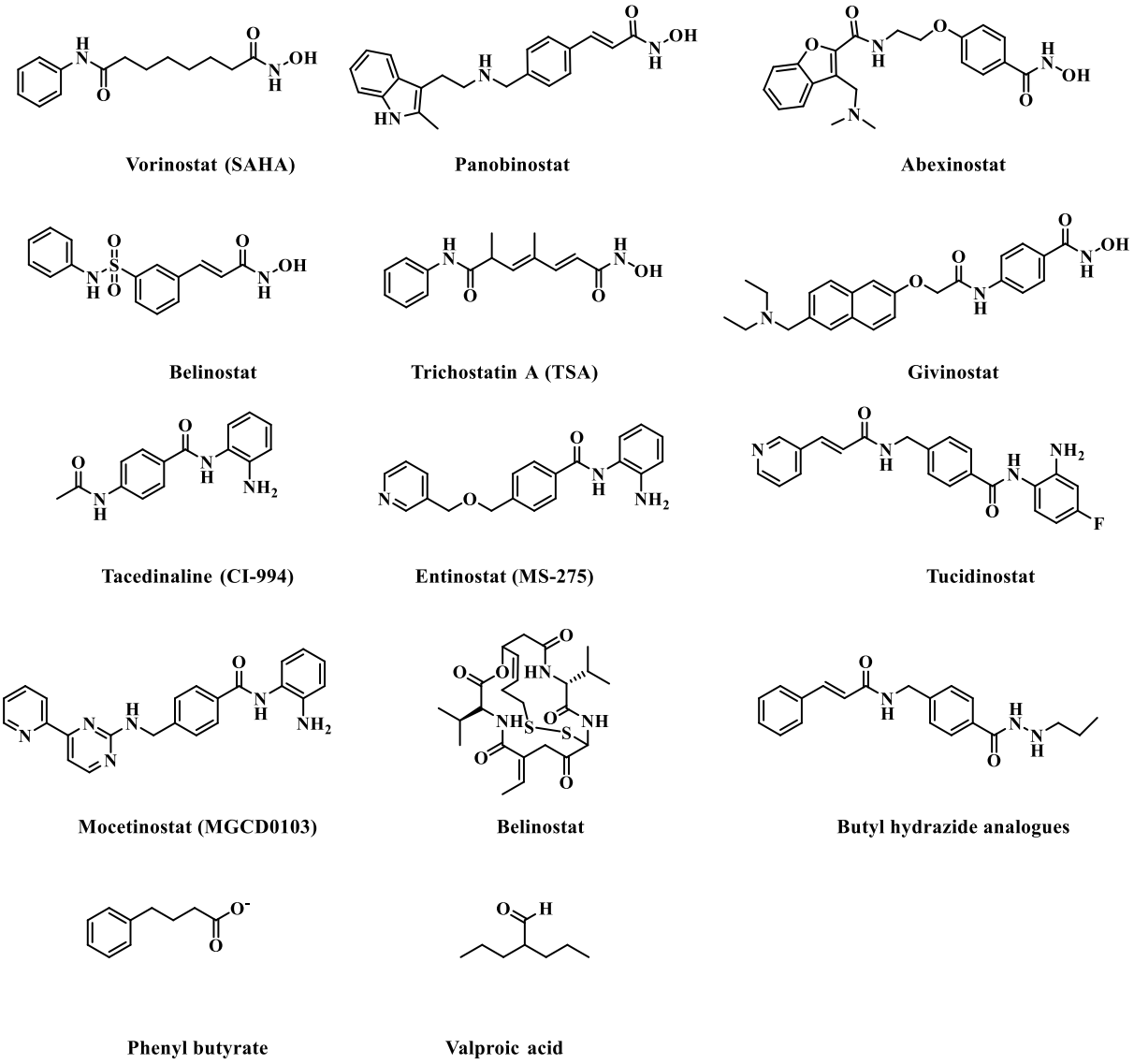

Figure 1.5. HDAC inhibitors contain Hydroxamates, Benzamides, cyclic peptides, carboxylic acids, and hydrazides.

1.5.3. Basic Structure of Zinc Binding HDAC Inhibitors:

HDAC inhibitors (hydroximic acid, benzamide, cyclic peptide, short-chain fatty acid) have been tested in clinical trials in a variety of structurally different classes, as we discussed here. Generally, the majority of zinc-dependent HDAC inhibitors consist of three different pharmacophores. (1) Cap group or a surface recognition unit, usually a hydrophobic and aromatic group, which interacts with the rim of the binding pocket; (2) Zinc binding domain (ZBD), such as the hydroximic acid,

carboxylic acid or benzamide groups, which coordinates to the Zn^{2+} ion in the enzyme active site, and (3) a saturated or unsaturated linker domain with linear or cyclic structure, that connect the cap group to the ZBG (Miller *et al.*, 2003a).

(**CAP**: Surface cap group; **Linker:** hydrophobic linker region**; ZBG**: Zinc Binding Group)

Figure 1.6. General pharmacophore model of HDAC inhibitors

The capping group interacts with the amino acids close to the active site's entrance and is located inside the protein, and become the part of the complex formed by ZBG and Zn-metal which is reported in crystallographic analyses of HDAC in complex with hydroxamate compound (Finnin *et al*., 1999; Somoza *et al*., 2004; Vannini *et al*., 2004; Lauffer *et al*., 2013). Using the linker, the capping group and the high-affinity interaction with proteins are appropriately provided by the metal binding domain. **Figure 1.7**. shows the structures of a few selected HDAC inhibitors.

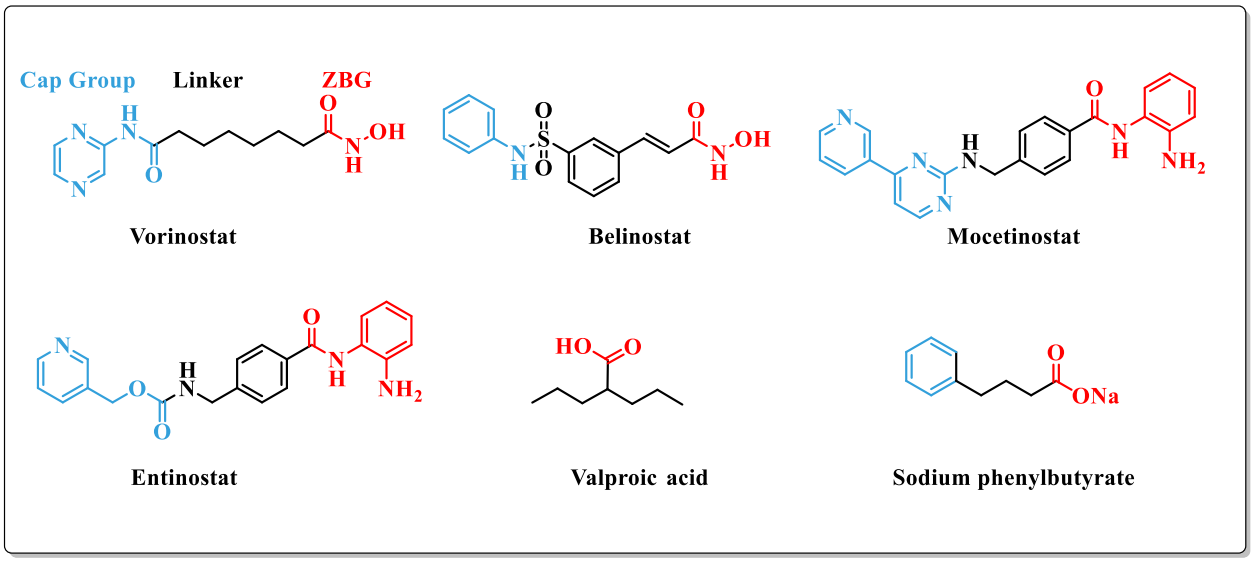

Figure 1.7: Representative HDAC inhibitors and their pharmacophores. Cap, linker, and zinc binding domain (ZBD) are coloured indigo, black and red respectively.

The potency and selectivity of many HDAC inhibitors have been affected by variations in any or all three if these domain (Saito *et al.*, 1999a) or a carboxylate (50M) (Phiel *et al.*, 2001) in the clinically significant three drugs vorinostat, entinostat, and valproic acid, which contain a hydroxamate, benzamide, and carboxylate metal binding moiety, respectively. As a result, the presence of a carboxylate acid or a benzamide led to decreased inhibitory efficacy, possibly as a result of their poorer ability to bind metals compared to a hydroxamate group. According to several investigations, hydroxamic acid is a more potent HDAC inhibitory than carboxylic acid (Luo *et al*., 2011). Variations in the inhibitory activity have been replaced by a modification to the linker group, with various chain lengths, hydrocarbons (saturated or unsaturated), and cyclic hydrocarbons. Therefore, these three modifications have been involved in the design of HDAC inhibitors, as shown by numerous articles and reviews (Rajak *et al.*, 2014; Taddei *et al*., 2014; Tashima *et al.*, 2014).

1.5.4. Mechanism of action of HDAC inhibitors:

Histone acetylation is increased by HDAC inhibitors, and HDAC activity inhibition is the mechanism for these drugs' antiproliferative effects. However, despite having little clinical effect, multiple trials have shown increased histone acetylation in tumor samples, indicating that this effect is insufficient to induce efficacy (Siu *et al*., 2008; Schrump *et al.*, 2008). HDACs have a wide range of biological substrates and targets, including proteins that are involved in tumor development, cell cycle regulation, apoptosis, angiogenesis, and cell invasion. HDACs can also act on other different cellular proteins. As a result, HDAC inhibitors have a variety of cellular effects, and the mechanism of action involves cell cycle arrest, activation of the apoptotic pathway, induction of autophagy, production of reactive oxygen species, and angiogenesis. The primary cause of HDACi-mediated

tumor cell death is the induction of apoptosis, which can be isolated by intrinsic (mitochondrial) or extrinsic (death receptor) pathways and result in caspase activation and cell death. The activation of the extrinsic pathway occurs when ligands (Such as Fas ligand (FasL), tumor necrosis factor, (TNF)-related apoptosis-inducing ligand) bind to their respective cell surface death receptor and the activation of the intrinsic pathway occurs when cellular stresses like chemotherapy, ionizing radiation, and the removal of growth factor and disruption of growth factors (Johnstone *et al.*, 2002). Suberic bishydroxamate down-regulates the expression of antiapoptotic X-linked inhibitor of apoptosis, B-cell lymphoma-extra-large (Bcl-XL), and myeloid cell leukaemia while upregulating BIM, BAX, and BAK in melanoma cells to cause apoptosis (Mcl1) (X. D. Zhang *et al.*, 2003). In transformed fibroblast, vorinostat treatment resulted in the widespread transcriptional induction of gene encoding BH3-only pro-apoptotic proteins (BAD, BIM, BIX, Noxa), the multi-domain pro apoptotic gene BAK1, and genes encoding death effector components downstream of mitochondrial damage (Diablo, Apaf1, Casp9, HtrA2, and CytC) (Bolden *et al.*, 2013). Additionally, these cells simultaneously suppressed the pro-survival genes Bcl2A1, Bcl2L1, and Bcl2L2. HDAC inhibitors increased the expression of the Bcl2 family's antiapoptotic proteins, such as Bcl2 and Bcl-x, and decreased the expression of the pro-apoptotic proteins Bmf, Bid, and Bim (Bolden *et al*., 2006). HDACi can additionally induce cell cycle arrest at G1/S or G2/M transition, leading to differentiation and apoptosis. HDACi- mediated increase in expression of the CDK inhibitor p21wAF1/CIP1 leads to cell cycle arrest in G1/S (Z. Zhang *et al.*, 2013). Silencing of HDAC3 was found to induce p21WAF/CIP1 and cellular expression cell cycle arrest in the G2/M phase of colon cancer cells (Wilson *et al.*, 2006). Vorinostat has been found to promote cell cycle arrest at G1/S and G2/M subsequent apoptosis in leukemia K562, HL60, and THP1 cells (Silva *et al.*, 2013). Another mechanism action of HDACi, can involve inhibiting molecules that cause hypoxia-inducible factor (HIF), which can stop tumor angiogenesis. The transcription factor HIF

1α is stabilised during hypoxia and is degraded by the tumour suppressor gene Von Hippel Lindau (VHL), which increases the production of the VEGF gene. When a downregulating of VEGF and HIF 1α to block angiogenesis, Trichostatin A (TSA) was shown to upregulate VHL and p53 under hypoxic conditions (M. S. Kim *et al.*, 2001). HDACi interferes with the function of Hsp90-mediated chaperone and exposes HIF 1α to proteasomal degradation, which also contributes to the anti-angiogenic pathway (Qian *et al.*, 2006). HDAC inhibitors cause chromatin conformational changes upon histone acetylation, which may expose the DNA to UV radiation, ionising radiation, ROS, and chemotherapeutic genotoxic chemicals. The complex biochemical reaction can eventually lead to double-strand breaks (DSBs) in DNA. Vorinostat, a pan HDAC inhibitor, has been shown to cause DSBs in both cancers (LNCaP, A549) and normal (HFS) cells (Lee *et al.*, 2010a). While transformed cells increased the level of the phosphorylated histone variant γH2AX, a biomarker of DNA damage, with continued culture with vorinostat, normal cells, unlike cancer cells, repair the DSBs despite continued culture with vorinostat. Two distinct pathways, homologous recombination, and non-homologous end joining, are used to repair DNA double-strand breaks (Munshi *et al.*, 2005; C. S. Chen *et al*., 2007). The gene expression of DNA repair proteins such as RAD51, BRCA1, and BRCA2 was also decreased by HDACi (Adimoolam *et al*., 2007). Another crucial process in HDACi-induced cell death that results in DNA damage is the generation of reactive oxygen species (ROS). ROS generation is decreased by free radical scavengers like N-acetylcysteine, which prevents HDACi-mediated cell death (Lee *et al*., 2010b, Rosato *et al*., 2003). Thioredoxin, a thiol reductase that scavenges ROS, and thioredoxin binding protein-2 (TBP-2), a protein that binds to Thioredoxin and inhibits its reducing activity, are both downregulated by HDACi, which results in an increase in ROS generation (Marks, 2006). TBP-2 expression was induced by vorinostat treatment, and afterward, Thioredoxin expression was

suppressed (Butler *et al*., 2002). Together, these varied methods by which HDACi effect cancer cell survival and death are depicted in **Figure 1.8.**

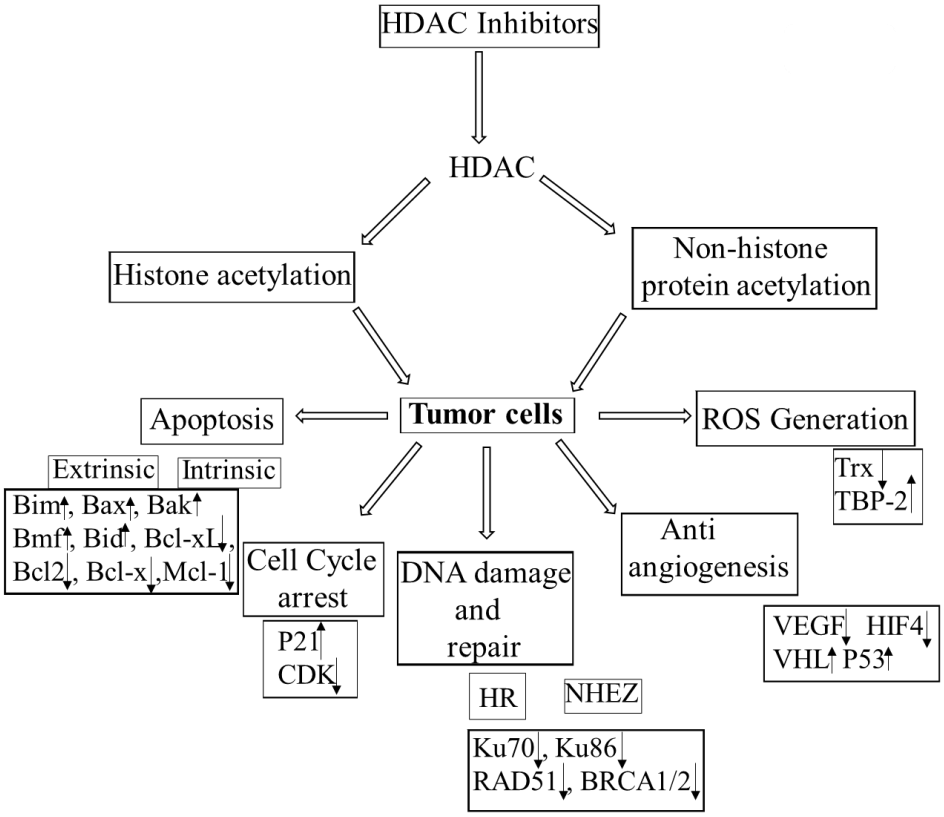

Figure. 1.8. Multiple anti-tumor pathways activated by HDACi. Extrinsic and intrinsic refer to two apoptosis pathways, and HR and NHEJ refer to two DBS repair pathways (Mottamal *et al*., 2015).

1.5.5. Toxicity in Clinical Trials of HDAC inhibitors:

Like any class of anticancer drugs, HDAC inhibitors have some side effects. The Side effects of the inhibitors (grades III and IV) include thrombocytopenia, neutropenia, anemia, fatigue, and diarrhea (Madsen *et al*., 2014; Younes *et al*., 2011). HDAC can sometimes result in thrombocytopenia, but it can be quickly treated by stopping the medication (Pili *et al*., 2012). Nausea, vomiting, anorexia, constipation, and dehydration were some of the side effects that were observed. Clinical trials using HDAC inhibitors have recorded the deaths of study participants. Four people died during a mocetinostat study among those with serious Hodgkin's lymphoma, and

two of those deaths were treatment-related (Bishton *et al.,* 2011). The clinical studies for vorinostat and givinostat also included several other deaths (Younes *et al.,* 2011; Galli *et al*., 2010). Therefore, to reduce the toxicity of HDACi and decrease the cytotoxicity effect in patients, some modifications are necessary before starting clinical trials.

1.5.6. Isoform selective HDAC inhibitors:

Most of the HDACi drugs in and out of clinical trials non-specifically inhibit all HDAC isoforms (so-called pan-inhibitors). SAHA and TSA are canonical pan-inhibitors, which had roughly equivalent potency in influencing HDAC1- 9 (Khan *et al*., 2008). The best pharmacological tools to understand the unique roles of each HDAC isoform would be selective HDAC inhibitors, which can either target a single HDAC isoform (isoform-selective HDACi) or a number of isoforms within a single class (class-selective HDACi). The molecular mechanism linking HDAC activity to the development of cancer will be better understood with the use of specific HDAC inhibitors. Furthermore, compared to *pan*-inhibitors, a class- or isoform-selective HDAC inhibitor might provide more potent chemotherapy. The design of selective HDAC inhibitors has been difficult despite their usefulness and potential therapeutic advantage. Designing effective inhibitors is challenging because of the isoforms' active sites' considerable sequence similarity. The minor variation between the active sites of each human isoform is not well described, due to the restricted crystallographic analysis; the only available crystal structures are of HDAC7 and HDAC8 (Somoza *et al.,* 2004;Vannini *et al*., 2004), although the structures of bacterial homologues related to class I and class II HDAC proteins have been useful (Finnin *et al.,* 1999; Nielsen *et al.,* 2005). Despite these challenges, various class and isoform selective HDAC inhibitors have been identified in the past decade.

Inhibitors	HDAC isoform selectivity	HDAC isoforms
Trapoxin A and derivatives	HDAC 1	640 – 570000-fold vs. HDAC6
Apicidin	HDAC 2,3	5 –83-fold vs. HDAC1, 4-9
Romidepsin	HDAC1,2	10-fold vs. HDAC4
Azumamide E	HDAC1-3	37-500-fold vs. HDAC4-9
MS-275	HDAC1,3	135fold vs. HDAC 6,8
CI-994	HDAC 1,3	133fold vs. HDAC 6,8
MGCD0103	HDAC 1,3	40fold vs. HDAC 6,8
SK-7041	HDAC 1,2	HDAC 3-6
SK-7068	HDAC 1,2	HDAC 3-6
VPA	HDAC1-5,7	>20-fold vs. HDAC 6,10
SB429201	HDAC1	20-fold vs. HDAC 3,8
PCI-34051	HDAC8	>290-fold vs. HDAC 1-3,6,10
SB-379278A	HDAC8	60-fold vs. HDAC1,3
Tubacin	HDAC6	4-fold vs. HDAC1

Table 1.1: Isoform selective HDAC inhibitors.

In the following two chapters, novel linker-less benzamide-based potent and selective HDAC3 inhibitors and novel linker-less o-hydroxy benzamides were designed and characterized. Determination of potency and selectivity of the synthesized molecules against different isoforms of HDACs by biochemical assay and the anti-proliferative effect of the compounds was assessed in various cancer cell lines. One of the lead molecules was taken further for the assessment of in vivo therapeutic efficacy of the compound against breast cancer animal models, showing significant

tumor growth rate inhibition at 25mg/kg with the least toxicity, which can be explored further as an effective treatment strategy for cancer treatment.

Chapter 2

Synthesis, biological evaluation, and molecular docking analysis of novel linker-less benzamide-based potent and selective HDAC3 inhibitors

ABSTRACT

A series of novel linker-less benzamides with different aryl and heteroaryl cap groups have been designed, synthesized, and screened as potent histone deacetylase (HDAC) inhibitors with promising anticancer activity. Two lead compounds 5e and 5f were found as potent and highly selective HDAC3 inhibitors over other Class-I HDACs and HDAC6. Compound 5e bearing a 6-quinolinyl moiety as the cap group was found to be a highly potent HDAC3 inhibitor (IC_{50} = 560 nM) and displayed 46-fold selectivity for HDAC3 over HDAC2, and 33-fold selectivity for HDAC3 over HDAC1. The synthesized compounds possess antiproliferative activities against different cancer cell lines and significantly less cytotoxic to normal cells. Molecular Docking studies of compounds 5e and 5f reveal a similar binding mode of interactions as CI994 at the HDAC3 active site. These observations agreed with the in vitro HDAC3 inhibitory activities. Significant enhancement of the endogenous acetylation level on H3K9 and H4K12 was found when B16F10 cells were treated with compounds 5e and 5f in a dose-dependent manner. The compounds induced apoptotic cell death in Annexin-V/FITC-PI assay and caused cell cycle arrest at G2/M phase of cell cycle in B16F10 cells. These compounds may serve as potential HDAC3 inhibitory anticancer therapeutics.

2.1. Introduction:

According to WHO, cancer is the second leading cause of death worldwide, claiming about 9.6 million deaths (approximately 1 in 6) in 2018 (World Health Organization (WHO)). “Cancer is caused by the mutations in tumour suppressor genes and oncogenes due to epigenetic manipulations that lead to cell proliferation and differentiation” and this is considered the most acceptable hypothesis in cancer pathogenesis (Biswas & Rao, 2017). It is also well-established that genetic and epigenetic modifications contribute to the development of cancer (Sadikovic *et al*.,

2008a). Epigenetic modifications leading to structural changes in chromatin include DNA methylation, and post-translational modifications of histone proteins. Among the post-translational modifications, histone acetylation and deacetylation have been found to play a pivotal role in the regulation of expression of genes involved in cancer pathogenesis (Sharma *et al*., 2010). Histone acetyl transferases (HATs) and histone deacetylases (HDACs) are the two key enzymes involved in the regulation of gene expression through acetylation and deacetylation of histone proteins at ϵamino group of lysine residues present in the *N*-terminal end of histone proteins. The imbalance between the activities of HATs and HDACs often results in aberrant gene expression leading to several epigenetic disorders (Yang & Seto, 2007). Moreover, HDACs play a prominent role also in cancer cell proliferation, invasion, and metastasis (Pulya, Amin, *et al*., 2021a). It has also been reported that HDAC inhibitors are well-implicated in apoptosis or programmed cell death as well as cell cycle arrest (Singh *et al*., 2005; Frew *et al*., 2009; Sarkar *et al*., 2020). whereas abnormal HDAC expression lead to various cancers such as cancers of the colon, breast, liver, lung, pancreas, prostate, along with melanoma, lymphoma, multiple-myeloma and leukaemia (Y. Li & Seto, 2016a). There are 18 different HDACs categorized into four classes according to their homology with yeast proteins, subcellular localization, and mechanism of action. Basically, Class I (HDAC1, 2, 3 and 8), Class II (IIa: HDAC4, 5, 7 and 9; IIb: HDAC6 and 10) and Class IV (HDAC 11) HDACs are Zn^{+2}-dependent whereas Class III HDACs are NAD^{+}-dependent also known as Sirtuins (SIRT 1-7) (Pulya *et al.*, 2021; Witt *et al*., 2009b). HDAC3 has garnered lot of attention due to its implication in various life-threatening disease conditions namely cancers (Sarkar *et al*., 2020a), cardiovascular diseases (Xu *et al*., 2017), memory and learning disorders (Amin *et al*., 2019; McQuown *et al*., 2011), neurodegenerative diseases (Bardai & D'Mello, 2011), diabetes (Sathishkumar *et al*., 2016) and rheumatoid arthritis (Angiolilli *et al*., 2017). Most importantly,

HDAC3 has been validated and well-studied as a potential target for cancer therapy, due to its crucial role in transcriptional repression through hypoacetylation of histones in different cancers (Adhikari *et al.,* 2018a). HDAC3 has been found to modulate various cancers such as colon cancer (Spurling *et al*., 2008a), breast cancer (H. C. Kim *et al*., 2010), multiple myeloma (Minami *et al.,* 2014a), melanoma (Shan *et al*., 2014), prostate cancer (Jeong *et al.,* 2016), gastric cancer (Ma *et al*., 2015a) and leukemia (Mehdipour *et al*., 2017), and selective HDAC3 inhibitors have been extensively studied in recent years for various applications (Sarkar *et al.,* 2020; Johnstone, 2002). However, still lot of work needs to be carried out to identify highly potent and selective HDAC3 inhibitors to combat such disease states with minimum off target side effects. HDAC3, a wellexplored Class I HDAC, is structurally characterized by a unique C-terminal domain and it forms a stable complex with NCoR and SMRT for carrying out the deacetylase activity (Guenther *et al*., 2001). Several amino acid residues (such as Tyr198, Asp92, Phe199, Tyr107) at the active site of HDAC3 contribute to the substrate specificity over other Class I HDAC isoforms. Nevertheless, the interactions of Ins(1,4,5,6)P_4 and DAD with HDAC3 contribute to the activation of the enzyme(Watson *et al*., 2012; Karagianni & Wong, 2007) The general pharmacophore model of HDAC active site includes a surface binding domain that interacts with the cap group, the hydrophobic channel that recruits the linker region, and the catalytic zinc binding domain where the Zn^{+2} ion interacts with the zinc binding group (ZBG) of the HDAC inhibitors (**Figure 2.1**). There is also an internal cavity adjacent to the zinc binding domain in case of HDAC3 isoform that might contribute its substrate specificity (Lombardi *et al.*, 2011).

(**CAP**: Surface cap group; **Linker:** hydrophobic linker region**; ZBG**: Zinc Binding Group)

Figure 2.1. General pharmacophoric structure of HDAC inhibitors.

Quite a few numbers of HDAC*i*s have been reported so far and they are widely studied in preclinical and clinical phases as anticancer agents (Sarkar *et al.*, 2020a). Based on various ZBGs, different classes of HDAC*i*s have been reported such as hydroxamates, benzamides, short chain fatty acids, cyclic tetrapeptides, hydrazides and thiols (Sarkar *et al*., 2020a). Six HDAC*i*s have been clinically approved so far namely vorinostat, belinostat, panobinostat, romidepsin, Chidamide and pracinostat for the treatment of different cancers such as cutaneous T-cell lymphoma, peripheral T-cell lymphoma, multiple myeloma and acute myeloid leukemia (Dokmanovic *et al.*, 2007a). With the multiple side-effects and dose-limiting toxicities associated with this pan HDAC is, the need for developing novel isoform-specific inhibitors has been realised urgently to overcome these limitations and to improve the potency and specificity towards individual HDAC isoforms.

The above mentioned clinically approved HDAC inhibitors belong to the hydroxamate class except Chidamide which is the only benzamide compound approved by Chinese FDA for the treatment of relapsed peripheral T-cell lymphoma (Lu *et al*., 2016b). Interestingly, several studies have been carried out and are still continuing on benzamide class of compounds to come up with selective HDAC inhibitors with minimum or no off target side effects (Sarkar *et al*., 2020a).

Notably, the benzamide based class-I HDAC selective inhibitors such as entinostat (MS-275, **1**) (Knipstein & Gore, 2011a) and tacedinaline (CI994, **4**) (Loprevite *et al.*, 2005; Prakash *et al.*, 2001) and HDAC3 selective inhibitors, RGFP109 (**2**) (Z. yang Li *et al.*, 2016), and BG45 (**3**) (Minami et al., 2014a) have been studied extensively as promising anticancer agents (**Figure 2.2**). Recently, several other benzamides designed with varying cap groups have been reported with enhanced HDAC3 selectivity and inhibition potential (Sarkar *et al.*, 2020a).

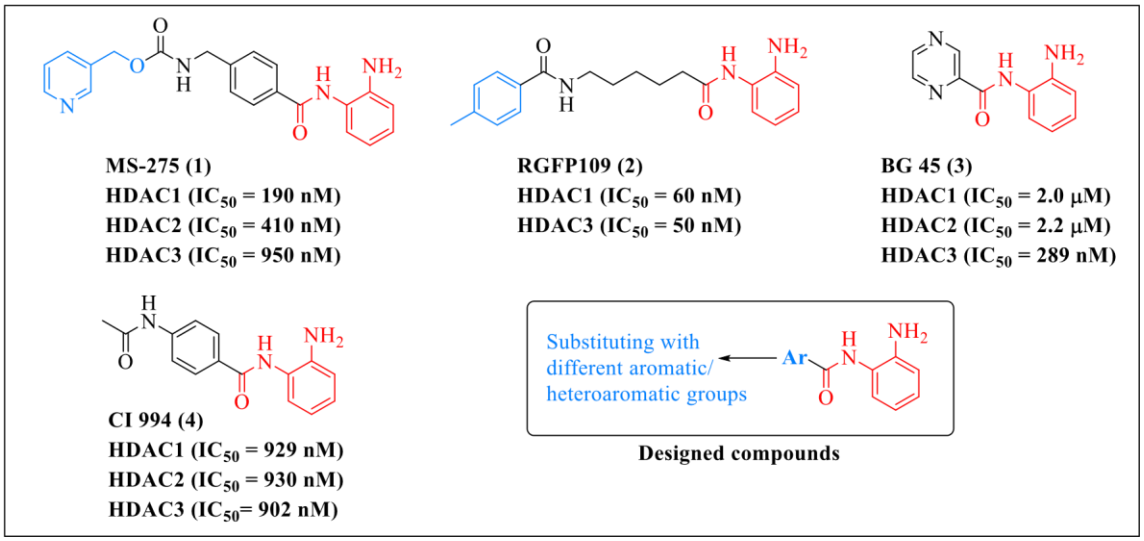

Figure 2.2. Structures of benzamide derivatives and design of our new benzamides derivative.

Benzamide has been established as a promising moiety responsible for chelating the Zn^{2+} ion for various HDACs and thereby responsible for potent inhibition along with selectivity towards specific HDACs (Amin *et al.*, 2019; Adhikari *et al.*, 2018; Beckers *et al.*, 2007) (Wagner *et al.*, 2016). Since last 10 years, a number of research works have been carried out on this scaffold to design compounds reflecting potent HDAC3 inhibition along with selectivity over other HDACs [(Y. Chen *et al.*, 2009; He *et al.*, 2010; Boissinot *et al.*, 2012; Suzuki *et al.*, 2013; Marson *et al.*, 2013; Marson *et al.*, 2015; X. Li *et al.*, 2017) Hsieh *et al.*, 2017; Zang *et al.*, 2018). Interestingly, these compounds also comprise the typical features as HDAC inhibitors, i.e., the cap group, the

linker moiety and the ZBG. However, only a few group of researchers tried to design linker-less atypical selective HDAC3 inhibitors (H. C. Kim *et al*., 2010; Zang *et al.*, 2018., Minami *et al*., 2014a) first reported BG45, which is a linker-less benzamide based HDAC3 selective inhibitor, showed promising efficacy against multiple myeloma. Another series of linker-less HDAC3 selective compounds have been reported by McClure et al. (McClure *et al*., 2017). They used benzofuran scaffold instead of pyrazine scaffold of BG45 to obtain potent and selective HDAC3 inhibitors. Our group has been actively working on the development of HDAC3 selective inhibitors with an emphasis on benzamides involving the structural modifications of the cap and linker region (Adhikari *et al.*, 2018; Trivedi *et al*., 2018; Trivedi *et al.*, 2019; Aminetal.,2018; Hamoud *et al.*, 2020; Pulya, Mahale, *et al.*, 2021). We, here by, report a series of linker-less benzamide compounds with different cap groups derived from the basic pharmacophore scaffold of **CI994** which has been studied most extensively in preclinical and clinical applications (Loprevite *et al.*, 2005; (**Figure 2.2)**. In-order to enhance the HDAC3 selectivity, modification of the cap region with different aromatic or heteroaromatic functions of the linker-less benzamides have been reported. Herein, we report the synthesis schemes, HDAC3 isoform selectivity study and detailed biological characterization of the synthesized small molecule HDAC3 inhibitors.

2.2. Results

2.2.1. Chemistry

2.2.1.1. Design and synthesis of novel benzamides

Keeping the benzamide scaffold intact as the ZBG, several aryl (such as phenyl, naphthyl) and heteroaryl (such as quinolinyl, indolyl, thienyl and pyrazinyl-aminophenyl) cap groups have been incorporated. Most of these benzamides (**5a**–**5h**) were synthesized as per **Scheme 1** whereas compound **5i** was synthesized following the **Scheme 2**.

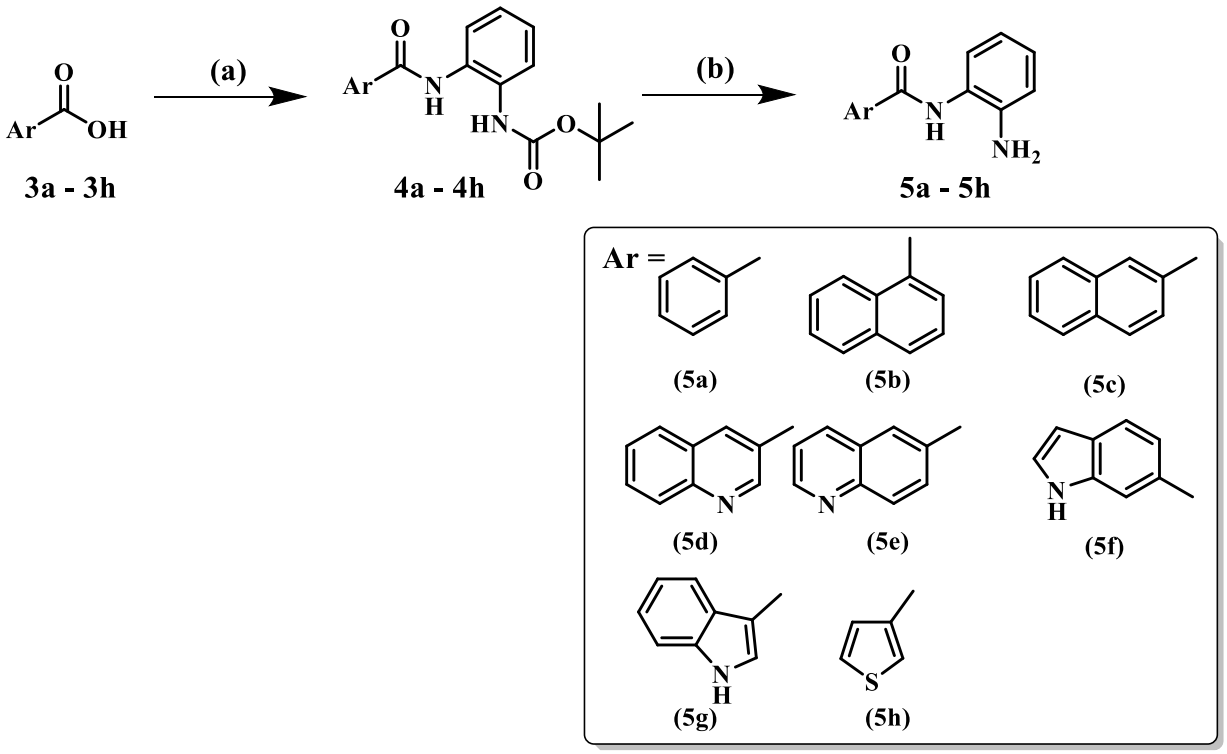

Scheme 1. Reagents and conditions: (a) *tert*-butyl 2-amino phenyl carbamate, EDC, DMAP, DCM: pyridine (1:1), RT (b) 4M HCl in dioxane, 0°C, 2h.

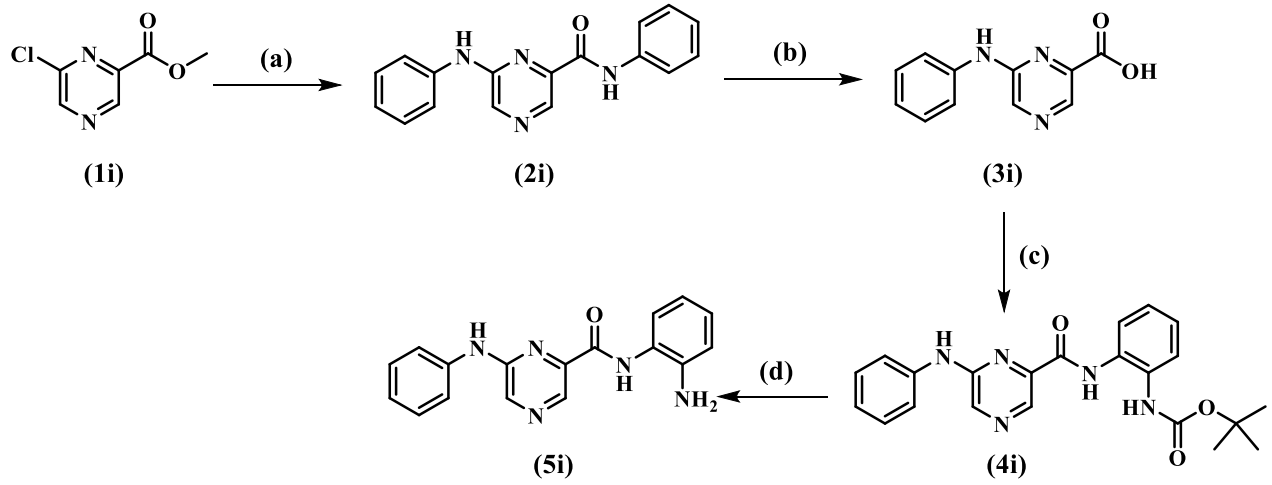

Scheme 2. Reagents and conditions: (a) Aniline, *N*-methyl 2-pyrrolidone (NMP), DIPEA, 160°C, 20h, reflux (b) NaOH, MeOH, H_2O, 1h (c) *tert*-butyl 2-amino phenyl carbamate, EDCI, DMAP, DCM: pyridine (1:1), RT (d) 4M HCl in dioxane, 0°C, 2h.

As per **Scheme 1**, the aromatic or heteroaromatic carboxylic acids (**3a–3h**) were purchased commercially and were coupled with *tert*-butyl (2-aminophenyl) carbamate synthesized as per protocol reported previously (Trivedi *et al*., 2018) Under the conditions, the acid-amine coupling reactions were done using EDCI as coupling agent to obtain (**4a-4h**) as the intermediates, which upon deprotection of carbamate group in acidic medium afforded the final compounds (**5a5h**). Considering the contribution of pyrazine scaffold to the enhanced HDAC3 selectivity as in the case of BG45, another molecule with amino phenyl as the cap group attached to the pyrazine scaffold at its 2nd position with the benzamide has been designed and synthesized. **Scheme 2** describes the synthesis of compound **5i**. There 6-chloro pyrazine 2-carboxylate (**1i**) was converted to methyl 6-(phenylamino) pyrazine-2-carboxylate (**2i**) using aniline in the presence of NMP as a solvent and DIPEA as a base. The 6-(phenylamino) pyrazine-2-carboxylic acid (**3i**) was obtained through alkaline hydrolysis of the carboxylate (**2i**). The acid **3i** was coupled with *tert*-butyl (2aminophenyl) carbamate synthesized as per our previous report (Trivedi *et al.*, 2018) Under the conditions, acid – amine coupling was conducted using EDCI as coupling agent to obtain (**4i**) as the intermediate, which upon deprotection of carbamate group in acidic medium resulted in the final compound **5i**. **Table 2.1**. Structures of the designed compounds along with their % yield and physicochemical properties.

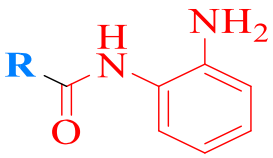

Compound	R	% yield	HBD	HBA	Log P
5a	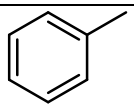	87.00	2	2	2.04

5b	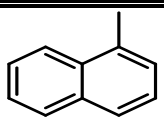	70.00	2	2	3.03
5c	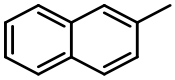	71.85	2	2	3.03
5d	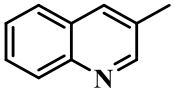	55.00	2	3	1.87
5e	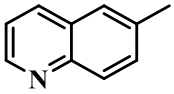	80.00	2	3	1.87
5f	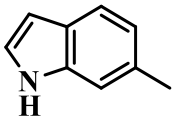	70.00	3	3	1.58
5g	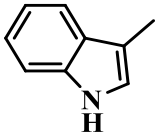	57.30	3	3	1.58
5h	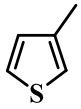	86.00	2	2	1.96
5i	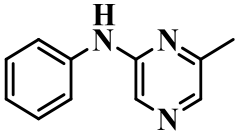	88.80	3	5	1.97

The structures of the designed and synthesized compounds along with their % yield and physicochemical properties are listed in **Table 2.1**. Physicochemical characterisations of the synthesized molecules were done using ^{1}H NMR, ^{13}C NMR, HRMS analysis and the spectral data is given in the supporting information section (**Spectra S1 – S36**).

2.2.2. Biological evaluation

2.2.2.1. Pan-HDAC and HDAC3 inhibition

All the synthesized compounds (**5a-5i**) were screened for enzyme inhibitory activity towards *pan* HDAC (HeLa Nuclear extract) and recombinant human HDAC3 enzymes initially (supporting **Figure S1 and S2**). All the compounds exhibited effective % inhibition of pan HDAC activity at 10 µM compound concentration and effective % inhibition HDAC3 activity at 1 µM compound concentration are depicted in **Table 2.2**.

Table 2.2. The % inhibition values of enzymatic activity by the synthesized compounds as well as the reference molecule **CI994** against Hela nuclear extract (*Pan*-HDAC activity) and recombinant HDAC3 enzymes. Data represents mean ± SD (n = 2).

Compound	***Pan*-HDAC % Inhibition (**at 10 µM**)**	**HDAC3 % Inhibition (**at 1 µM**)**
5a	38.46±1.68	19.35±1.17
5b	15.11±2.27	22.74±0.24
5c	32.88±0.95	33.06±1.88
5d	22.40±3.12	21.83±0.83
5e	12.9±0.85	59±0.46
5f	31.67±1.07	21.13±2.67
5g	22.42±4.15	21.38±2.75
5h	27.86±0.56	34.45±2.81
5i	17.78±0.61	7.93±1.25
CI994	53.8±0.91	53.65±1.21

It was interesting to note that all these compounds (**5a-5i**) exhibited comparatively less *pan*-HDAC inhibitory activity compared to the reference molecule **CI994** and compound **5e** showed least pan HDAC inhibition in the series. However, in case of HDAC3 inhibition, compound **5e** (59%) was found be most active and even better inhibitor than **CI994** (53.65%). Further, it can be inferred from the % inhibition values, that though **5a** exhibited considerable HDAC inhibitory activity but the selectivity factor towards HDAC3 is less when compared to that of compound **5e** which is

highly potent with 59% inhibition at 1 µM. It was noteworthy that the pyrazine scaffold containing benzamide compound, **5i** neither exhibited any significant *pan*-HDAC or HDAC3 inhibition when compared to other compounds in the series.

2.2.2.2. HDAC isoform inhibition

From the result of initial screening based on their inhibition potency, we have further selected compounds **5e and 5f** for the determination of IC_{50} values which will give more précised potency and selectivity towards HDAC3. The selected compounds **5e** and **5f** along with the standard reference **CI994** were subjected to their IC_{50} determination towards HDAC1, HDAC2, HDAC3, HDAC6 and HDAC8 isoforms (**Figure 2.3**, **Table 2.3**).

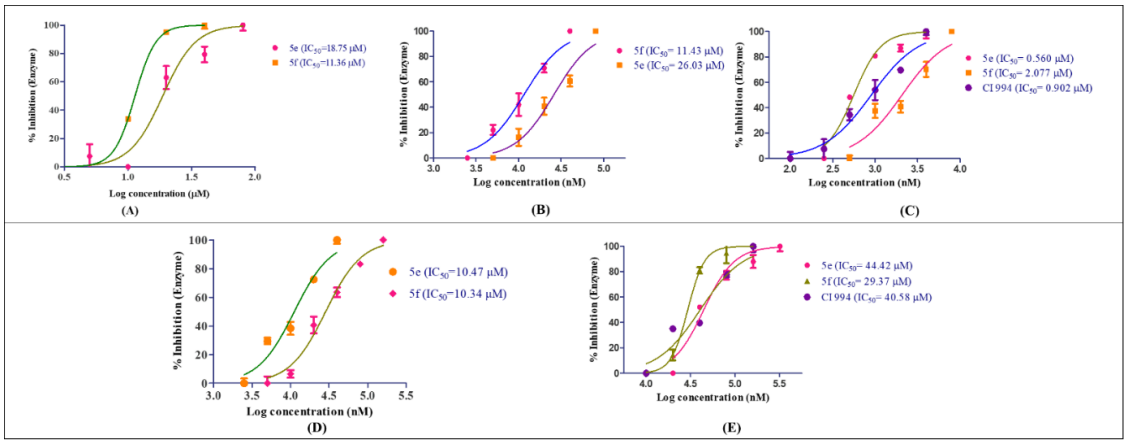

Figure 2.3. The dose response curve for IC_{50} determination of compounds **5e** and **5f** using **CI994** as positive control. **(A)** Using kit based human recombinant HDAC1 enzyme assay. **(B)** Using kit based human recombinant HDAC2 enzyme assay. **(C)** Using kit based human recombinant HDAC3/NCOR1 enzyme assay. **(D)** Using kit based human recombinant HDAC8 enzyme assay. **(E)** Using kit based human recombinant HDAC6 enzyme assay [IC_{50} determinations were carried out in the concentration range of 0.061 – 80 µM of the compounds in duplicate as per the protocol given in the HDAC enzyme assay kits purchased from bio nova. The IC_{50} values of these compounds were determined using nonlinear regression analysis method using Graph Pad Prism

5. Data represent mean ± SD (n = 2)].

Cpd	IC_{50} (μM)					Selectivity for HDAC3 over other HDACs			
	HDAC 1	HDAC 2	HDAC 3	HDAC 8	HDAC 6	HDAC 1/3	HDAC 2/3	HDAC 8/3	HDAC 6/3
CI 994	0.929± 0.06	0.93± 0.09	0.902± 0.14	19.57± 2.1	40.58± 3.2	1.03	1.03	21.7	44.99
5e	18.75± 1.98	26.03± 1.2	0.560± 0.11	10.47± 0.71	44.42± 2.31	33.48	46.48	18.7	79.32
5f	11.36± 0.87	11.43± 0.89	2.077± 0.69	10.34± 1.01	29.37± 1.32	5.47	5.5	4.98	14.14

Table 2.3. The IC_{50} values of compounds **5e** and **5f** using **CI994** as positive control on human recombinant HDAC1, 2, 3, 8 and 6 isoforms and their HDAC3 selectivity profile. Data represent mean ± SD (n = 2).

Compounds **5e** and **5f** displayed IC_{50} values of 0.560 μM and 2.077 μM against HDAC3 respectively and that are the highest potency towards HDAC3 compare to that of other HDAC isoforms (**Table 3)**. Interestingly, compound **5e** was found be more effective towards HDAC3 than even the reference molecule **CI994** (IC_{50} = 0.902 μM). The IC_{50} determining dose response curves of the selected compounds **5e** and **5f** against different HDAC isoforms are shown in the **Figure 3**. It was interesting to observe that the reference molecule **CI994** was nonselective towards HDAC3 over HDAC1 and HDAC2 (**Table 3**). However, Compound **5e** bearing a 6-quinolinyl moiety as the cap group was found to be highly potent HDAC3 inhibitor (IC_{50} = 560 nM) and displayed 46-fold selectivity for HDAC3 over HDAC2 and 33-fold selectivity for HDAC3 over HDAC1. Interestingly, there was about 4-fold reduction of HDAC3 inhibition (IC_{50} = 2.077 μM) compared to the former one when the quinolone cap group of **5e** was replaced by 6-indolyl cap in compound **5f** but still retained a minimum of 5-fold HDAC3 selectivity over other HDAC isoforms tested. Conclusively, compound **5e** is the most potent HDAC3 inhibitor and has been considered to be a

lead molecule from this series with excellent selectivity towards HDAC3 while compared to other compounds including reference compound **CI994**.

2.2.2.3. Anti-proliferative assay against cancer cell lines

All these final compounds (**5a-5i**), along with the reference molecule **CI994** were evaluated for their antiproliferative activity against human triple-negative breast cancer cell line (MDA-MB231), mouse breast cancer cell line (4T1) and murine melanoma cancer cell line (B16F10) by MTT assay (**Figure 2.4A-2.4C**).

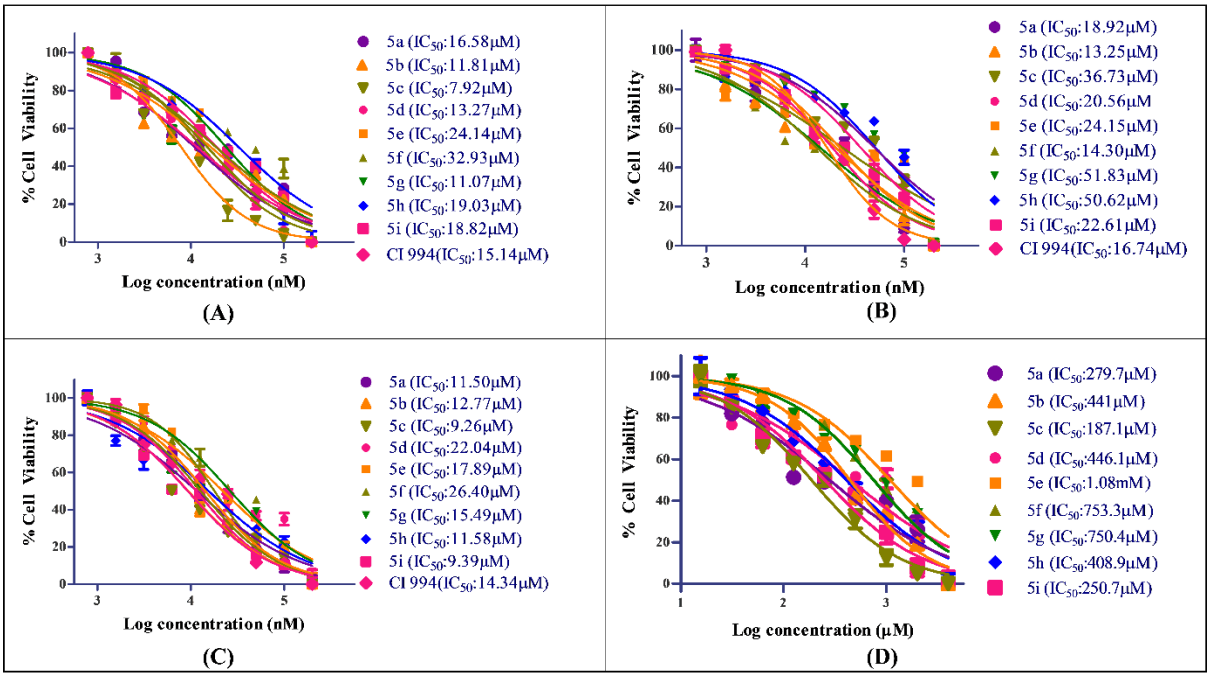

Figure 2.4. Dose response curve and IC_{50} values of all novel compounds (**5a-5i**) along with reference molecule **CI994** as positive control on (**A**) MDA-MB-231, (**B**) 4T1, (**C**) B16F10 cells when treated with the compounds at concentration range of 0.7-200 μM (n=2) for 72h. Figure **D** represents *in vitro* cytotoxicity data on HEK293 cells when treated with the compounds at concentration range of 7-2000 μM (n=2) for 72h. Data represent mean ±SD. IC_{50} values were calculated using nonlinear regression analysis method using Graph Pad Prism 5.

Initially, all the synthesized compounds were tested at two different concentrations (100 μM and 10 μM) in duplicate taking **CI994** as reference molecule (**supporting Figure S3 – S6**) to have an idea about the cell growth inhibition potential of the compounds. Based on the results from initial two dose screen the IC_{50} values of all the compounds were determined with a wider range of compound concentrations. The compounds displayed effective anticancer efficacies against the tested cancer cell lines with good selectivity for cancer cell lines over normal cell lines (**Table 2.4.)**.

Table 2.4. The tabular presentation of IC_{50} (μM) values of these novel benzamides against cancer cell lines 4T1, B16F10 and MDA-MB-231 and normal cell line HEK293 and their selectivity profile for cancer cell lines over normal cell line. Data represent mean ± SD (n = 2).

Compound	IC_{50} (μM)				Selectivity for cancer cells over normal cell line		
	4T1	B16F10	MDA-MB-231	HEK293	HEK293 / 4T1	HEK293 / B16F10	HEK293 / MDAMB-231
5a	18.92±1.2	11.5±0.98	16.58±1.54	279.7±8.76	14.78	24.32	16.87
5b	13.25±0.87	12.77±1.23	11.81±0.87	441±7.69	33.28	34.53	37.34
5c	36.73±1.54	9.26±0.69	7.92±0.89	187.1±4.54	5.09	20.20	23.62
5d	20.56±1.35	22.04±0.86	13.27±1.68	446.1±8.65	21.69	20.24	33.61
5e	24.15±0.89	17.89±1.31	24.14±3.54	1084±10.6	44.88	60.59	44.90
5f	14.30±0.65	26.40±2.14	32.93±3.68	753.3±6.8	52.67	28.53	22.87
5g	51.83±2.35	15.49±1.03	11.07±1.56	750.4±10.8	14.47	48.44	67.78
5h	50.62±3.45	11.58±0.78	19.03±2.34	408.9±2.4	8.07	35.31	21.48
5i	22.61±1.65	9.39±0.68	18.82±1.98	250.7±6.9	11.08	26.69	13.32
CI994	16.74±1.65	14.34±0.99	15.14±1.41	216.2±8.9	12.92	15.07	14.28

The data signifies that the antiproliferative activity of all the compounds was comparable to the reference **CI994** in all the cancer cell lines tested. In fact, some of these compounds (Compounds **5a**, **5b**, **5d** and **5i**) resulted in more or less similar anticancer efficacy to **CI994** (**Table 4**). Regarding the cytotoxicity against mouse breast cancer cell line 4T1, only compounds **5b** and **5f** exhibited better cytotoxicity (IC_{50} of 13.25 and 14.30 μM, respectively) than **CI994** (IC_{50} = 16.74 μM). However, in case of cytotoxicity against murine melanoma cancer cell line B16F10, several compounds (compounds **5a**, **5b**, **5c**, **5i** and **5h**) also yielded better cytotoxicity compared to **CI994** (IC_{50} = 14.34 μM) (**Table 4**). The β-naphthyl derivative (compound **5c**) and pyrazine derivative (compound **5i**) resulted in potent cytotoxicity in B16F10 cell line with an IC_{50} of 9.26 and 9.39 μM, respectively (**Table 2.4**). Again, in case of cytotoxicity in breast cancer cell line, MDA-MB231, compounds **5b**, **5c**, **5d** and **5g** displayed better efficacy than **CI994** (IC_{50} = 15.14 μM) (**Table 2.4**). Among these molecules, compound **5c** was the most cytotoxic one (IC_{50} = 7.92 μM). Interestingly, compound **5b** (IC_{50} values 11.81 μM in MDA-MB-231 and 12.77 μM in B16F10 cells) and compound **5c** (IC_{50} values 7.92 μM in MDA-MB-231 and 9.26 μM in B16F10 cells) exhibited higher IC_{50} values than **CI994** (IC_{50} values 15.14 μM in MDA-MB-231 and 14.34 μM in B16F10 cells) but showed least enzyme inhibitory potency. Though compounds **5e** and **5f** exhibited higher HDAC3 inhibitory potency and selectivity than remaining compounds, they were found to be moderately active against MDA-MB-231, 4T1 and B16F10 cells. All the remaining compounds exhibited comparable IC_{50} values against MDA-MB-231 cells and B16F10 cells (**Figure 2.4A and 2.4C)**. However, in case of 4T1 cells, the IC_{50} values for the remaining compounds were found to be higher than that of the reference compound **CI994** (**Figure 2.4B**).

2.2.2.4. *In vitro* cytotoxicity against normal HEK293 cell lines

Furthermore, the cellular toxicity of all the compounds were tested against normal human embryonic kidney (HEK293) cell line for their IC_{50} determination (**Figure 2.4D)**. The compounds were found to be less cytotoxic towards HEK293. Interestingly, compounds **5e** and **5f** with the IC_{50} values of 1.08 mM and 753.3 µM were found to be significantly less toxic than all the other compounds tested and consequently possessed higher selectivity towards all the cancer cell lines over normal HEK293 cells (**Table 2.4**).

2.2.2.5. Induction of histone hyper acetylation in B16F10 cells: Western blot analysis

The cellular HDAC inhibitory activity of compounds **5e** and **5f** along with reference molecule **CI994** was carried out to find the compounds ability to induce histone acetylation in B16F10 cells by western blot analysis. The histone acetylation level was measured in a dose-dependent manner with compounds **5e** and **5f** on H3K9 and H4K12 as endogenous histone substrates. Treatment of compounds **5e**, **5f** and **CI994** was carried out for 12h at concentrations of 5 µM and 20 µM that induced significant acetylation of H3K9 and H4K12 in a dose-dependent manner (**Figure 2.5 and Figure 2.6**). The upregulation of histone acetylation was in consistent with the *in vitro* HDAC inhibitory activity and also with the cellular antiproliferative activity.

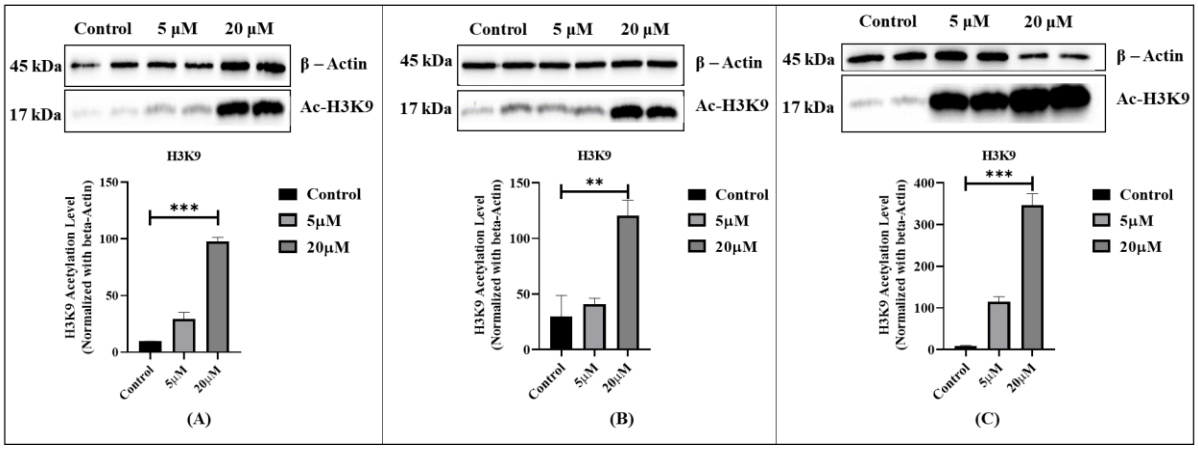

Figure 2.5. Western blot of Ac-H3K9 in whole cell lysates of B16F10 murine melanoma cells after treatment with (A) compound **5e**, (B) compound **5f** and (C) **CI994** at 5 µM and 20 µM for 12h. Results were normalized with respect to β-actin as a housekeeping control.

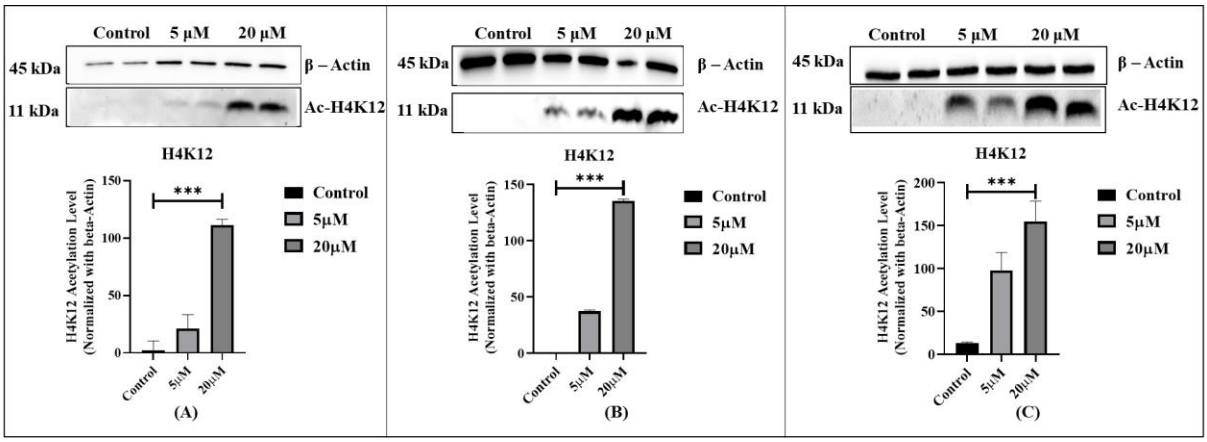

Figure 2.6. Western blot of Ac-H4K12 in whole cell lysates of B16F10 murine melanoma cells after treatment with (A) compound **5e**, (B) compound **5f** and (C) **CI994** at 5 µM and 20 µM for 12h. Results were normalized with respect to β-Actin as housekeeping control.

2.2.2.6. Nuclear staining assay

Further to study the phenotype effect of compounds in cells, nuclear staining assay was performed using DAPI and AO as staining dyes. It was observed that the treatment of B16F10 cells with **5e**, **5f** and **CI994** for 48h has shown distinct difference in cell morphology when compared to the untreated cells as evident from the **Figure 2.7**. These observations indicate nuclear disintegration of treated cells and suggested apoptotic cell death mechanism.

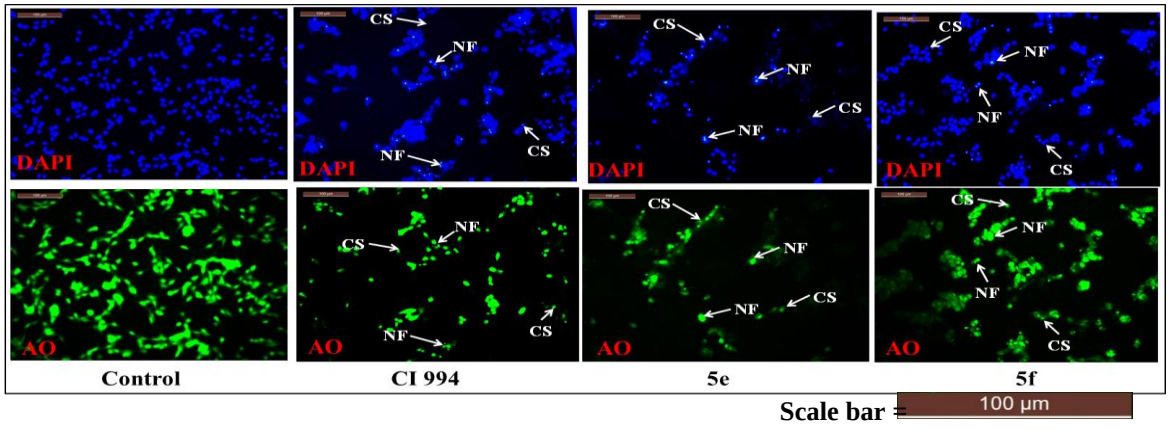

Figure 2.7. Nuclear staining of B16F10 cells using DAPI (4′,6-diamidino-2-phenylindole, a fluorescent stain) and acridine orange (AO) following treatment by (A) Control (B) **CI994** (C) compound **5e** and (D) compound **5f**. The stained nuclei are visualised using fluorescence microscope (Leica microsystems, Germany) on 20x magnification.

2.2.2.7. Apoptosis assay

Several reports have established that HDAC inhibitor-mediated cell death follows apoptotic pathway (J. Zhang & Zhong, 2014a). In order to determine the extent of apoptosis induced by the lead compounds **5e** and **5f**, Annexin-V/FITC–PI apoptotic assay was performed. B16F10 cells were treated with compounds **5e**, **5f** and **CI994** as reference compound for 72h with the concentrations at their respective IC_{50} values. The cells were then processed and the analysis was carried out using flow cytometry analysis. **Figure 2.8** displays the obtained results which suggest a significant enhanced apoptotic activity in treated cells with compounds **5e** and **5f** when compared to **CI994**. Compound **5e** displayed the total apoptotic percentage as 20.65% ± 0.49 (Q2 and Q4), whereas increased apoptotic population was observed for compound **5f** with 35.35% ± 2.89 (Q2 and Q4) when compared to **CI994** with 16.8% ± 0.21 of apoptosis. These results suggest the programmed cell death mechanism induced by compounds **5e** and **5f** leading to significant apoptosis in cancer cells.

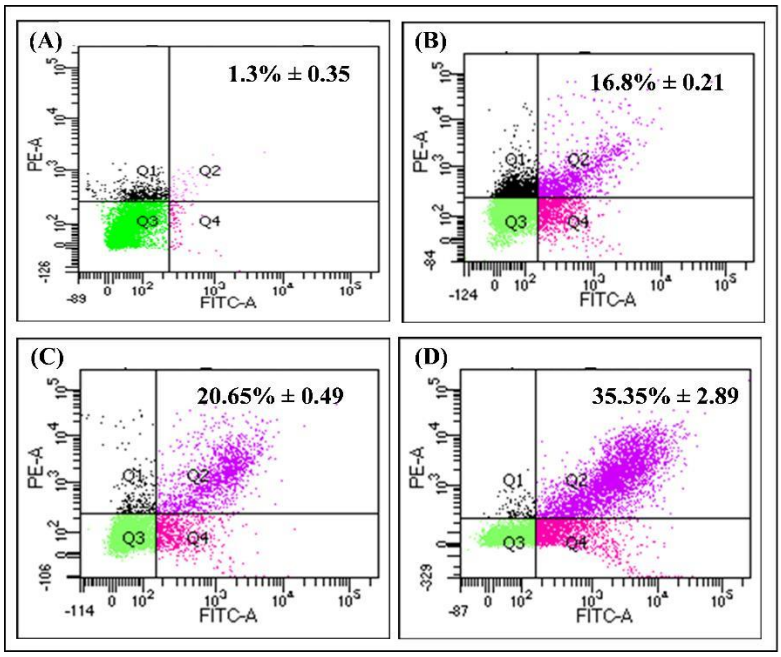

Figure 2.8. Induction of apoptosis in B16F10 cells quantified by Annexin V/PI assay using flow cytometry. (A) Vehicle control (B) CI994 (C) 5e (D) 5f (Q1 – Necrotic cells, Q2 - late apoptosis, Q3 – Live cells, Q4 – early apoptotic cells, X-axis: Annexin V intensity, Y-axis: Propidium iodide intensity).

2.2.2.8. Cell cycle analysis

In continuation to the results obtained in the apoptosis assay, the cell cycle progression was studied with the compounds **5e**, **5f** and **CI994** treatment of B16F10 cells and the cell population at different cell cycle stages was analysed using flow cytometry analysis (**Figure 2.9**).

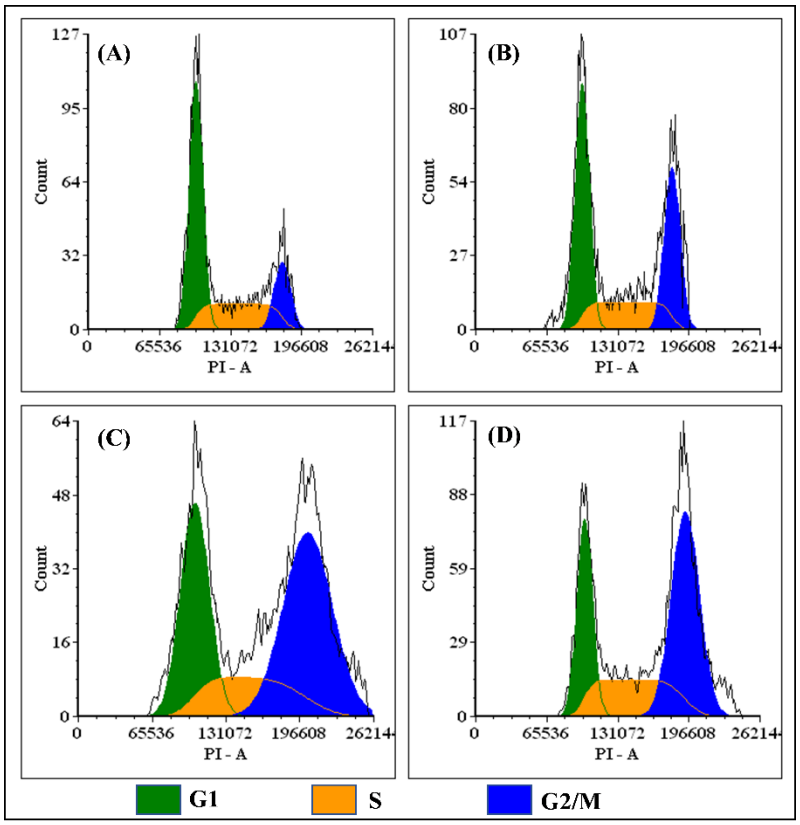

Figure 2.9. Cell cycle arrest induced in murine melanoma cell B16F10 treated with (A) Control (B) CI994 as positive control (C) compound **5e** and (D) compound **5f** for 72h. After the indicated treatment times, cell cycle analysis was performed and analysed by flow cytometry analysis (BD Aria III) ®.

In the cell cycle study, B16F10 cells were treated with compounds **5e** and **5f** and reference compound **CI994** at 15 µM concentration for 72h. These results (**Table 2.5**) indicated the increased cell population in G2/M phase of compound **5e** (45.14%) and compound **5f** (48.66%) when compared to control and a similar tendency was observed with **CI994** (31.74%)

Cell cycle Phase	% Cell population			
	Control	CI994	5e	5f
G1	54.27	43.83	31.11	26.28
S	28.20	24.43	23.75	25.06
G2/M	17.53	31.74	45.14	48.66

Table 2.5. The percentage cell population in different phases of cell cycle. Data was calculated and analysed by FCS express plus software from DNA content histograms.

The study also suggested that the cell cycle arrest at G2/M phase of the cell cycle with increased cell population containing 4n of DNA content. It was observed that compounds **5e** and **5f** showed a decrease in G1 population (31.11% and 26.28%) with no significant change in S phase (23.75% and 25.06%) when compared to reference molecule **CI994** (G1 = 43.83% and S = 24.43%). These results further emphasize the promising anticancer activity of the lead compounds (**5e** and **5f)** which might be guided through cell cycle arrest at G2/M phase. It also supports the apoptotic assay data of programmed cell death.

2.2.3. Molecular docking study

In order to understand the probable binding mode of interactions of the promising HDAC3 inhibitors (compounds **5e** and **5f**) with HDAC3 enzyme (PDB: 4A69), molecular docking studies were performed by using Schrodinger software. The docked structures of these compounds (compounds **5e** and **5f**) along with the reference molecule (**CI994**) are found to be almost superimposed with the each other on the active site of the HDAC3 as depicted in **Figure 2.10**

.

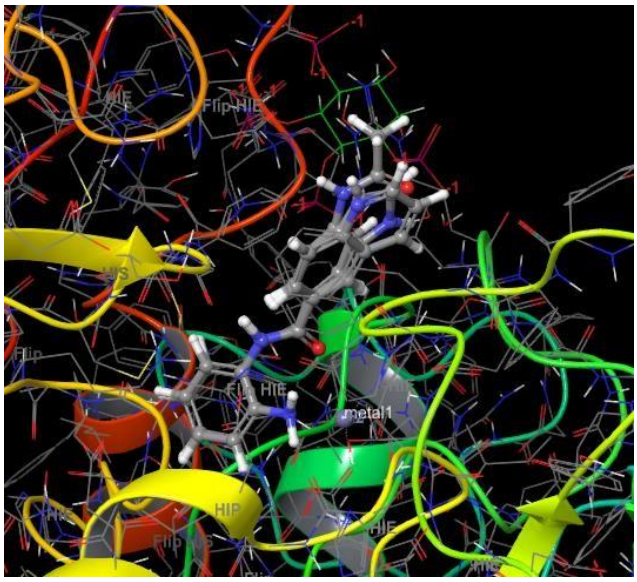

Figure 2.10. The docked conformations of compounds (**5e**, **5f** and **CI994**) superimposed with each other at the active site of HDAC3 (PDB: 4A69).

These inhibitors snugly bind to the binding groove and occupy the pocket as shown in **Figure 2.10** Interestingly, the docking scores are correlated with our *in vitro* HDAC3 assay results of compound 5e (glide score: -6.109; HDAC3 IC_{50} = 0.560 µM), 5f (glide score: -5.652; HDAC3 IC_{50} = 2.077 µM) and reference compound **CI994** (glide score: -5.977; HDAC3 IC_{50} = 0.902 µM). The carbonyl group of both compounds form a hydrogen bonding interaction with Tyr298 of HDAC3 (**Figure 2.11**).

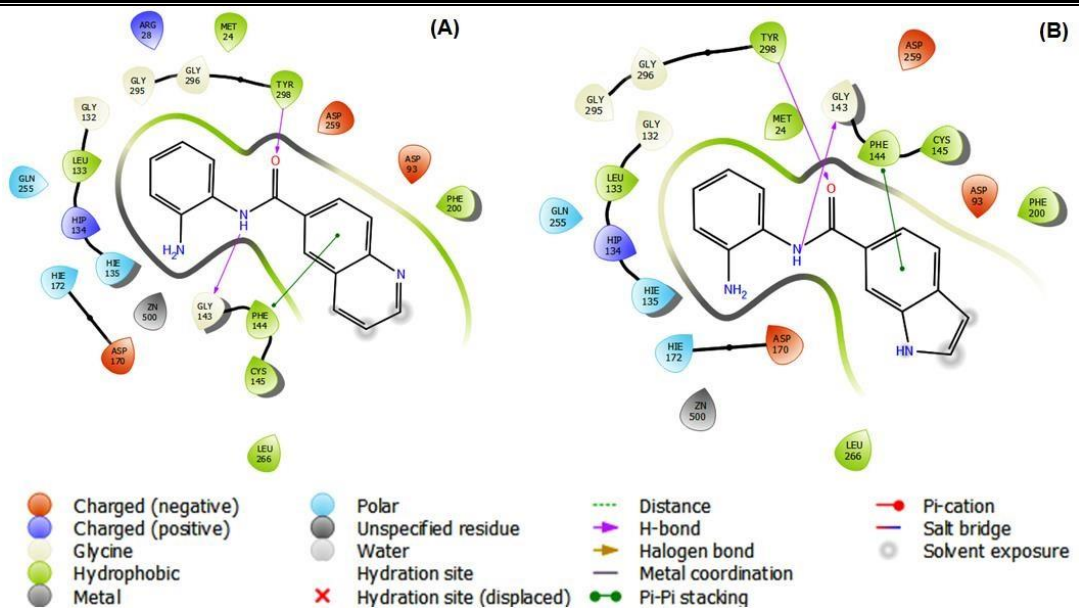

Figure 2.11. Molecular docking interactions of **(A)** compound **5e** and **(B)** compound **5f** with HDAC3 (PDB: 4A69)

Another hydrogen bonding interaction is noticed between the -NH function of benzamide and Gly143 of HDAC3. As seen in **Figure 2.11**, both these inhibitors form a π-π stacking interaction with Phe144. Though there are similar binding modes of interactions of these compounds, the better HDAC3 inhibitory property of compound **5e** over compound **5f** can be explained in terms of binding mode of interactions of these compounds with HDAC3. The orientation of the 6-quinolinyl moiety (compound **5e**) at the HDAC3 active site makes it better suitable for stronger binding interaction compared to the binding orientation of 6-indolyl moiety (compound **5f**). It is important to note that the position or orientation of the heterocyclic nitrogen atom of 6-quinolinyl moiety is more or less, closer to the amide nitrogen of **CI994**. However, it is noticed that the heterocyclic nitrogen atom of 6-indolyl moiety is oriented completely opposite direction of the former ones. Therefore, 6-quinolinyl moiety is favourable than the 6-indolyl scaffold as far as the HDAC3 inhibitory potency and selectivity is concerned.

2.3. Conclusion

A series of linker-less benzamides with different aryl/heteroaryl cap moieties were designed and synthesized as promising HDAC3 inhibitors. All the compounds were studied for their *pan*-HDAC and HDAC3 inhibitory activity. Further, the selected lead compounds **5e** and **5f** were studied for their HDAC 1, 2, 3, 8 and 6 enzyme inhibitory profiles to judge the selectivity towards HDAC3. Two lead compounds **5e** and **5f** were found to be potent and highly selective HDAC3 inhibitors over other Class-I HDACs and HDAC6. Compound **5e** bearing a 6-quinolinyl moiety as the cap group was found to be a highly potent HDAC3 inhibitor (IC_{50} = 560 nM) and displayed 46-fold selectivity for HDAC3 over HDAC2, and 33-fold selectivity for HDAC3 over HDAC1. Moreover, the HDAC3 selectivity of the lead molecules found to be much better than the reference compound **CI994**. All these compounds exhibited effective antiproliferative activity against various cancer cell lines (4T1, B16F10 and MDA-MB-231) with less cytotoxicity against normal cells (HEK293) when compared with reference compound **CI994** and interestingly the most promising molecule (**5e**) showed least toxicity towards normal cells. Further, the acetylation levels of cellular histone (H3K9 and H4K12) were examined and both the lead compounds were able to enhance the acetylation level significantly in a dose-dependent manner in B16F10 cells. Moreover, compounds **5e** and **5f** were found to cause apoptotic cell death and were causing G2/M cell cycle phase arrest in B16F10 cells. The molecular docking study revealed similar binding interactions of the lead molecules and reference compound at the active site of HDAC3. The higher HDAC3 inhibitory potency along with selectivity for HDAC3 of compound **5e** over compound **5f** was also justified by the molecular docking analysis. Based on the findings, it can be inferred that most potent and HDAC3 selective lead molecule **5e** might serve as a potential therapeutic as anticancer agent.

2.4. Experimental

2.4.1. General information on materials and instrumentation

All starting materials, chemicals and reagents were commercially available and were purchased from various chemical suppliers. These were used without further purification. All reactions were monitored by thin layer chromatography (TLC) using precoated plates with Merck 60 F254 silica gel plates purchased from Merck Millipore Co., USA and the reaction components were visualised under ultraviolet light (254 nm). Column chromatography was performed on silica gel (100 – 200 or 230 – 400 mesh size). ^{1}H and ^{13}C NMR spectrum were recorded in deuterated NMR solvents DMSO-d_6 and $CDCl_3$ using Bruker, ASCEND™ 400 MHz spectrometer and the chemical shifts (δ) values are given in parts per million (ppm), and are internally referenced to tetramethylsilane (TMS), residual solvents peak (DMSO-d_6; 2.50 ppm ^{1}H, 39.51 ppm 13C, $CDCl_3$; 7.2 ppm 1H, 77.6 ppm ^{13}C). Peak multiplicities are abbreviated as follows: s (singlet), d (doublet), t (triplet), q (quartet) and m (multiplet) while coupling constants (*J*) are reported in Hz. NMR data were processed using MestReNova Software version 6.0.2-5475.

Three different cell lines were used for the determination of anticancer activity of the novel compounds synthesized. MDA-MB-231 (human breast cancer cell line), 4T1 (murine mammary carcinoma cell line), B16F10 (Murine melanoma cell line) and HEK293 (Human embryonic kidney cell line) were procured from National Centre for Cell Science (NCCS), Pune, India. B16F10, MDA-MB-231 and HEK293 cell lines were cultured in DMEM (high glucose media: AL007S, Dulbecco's modified eagle medium) and 4T1 cell line was cultured in MEM (AT154, Minimum essential medium). All these cell lines were used for cell-culturing with 10% fetal bovine serum (FBS) and 1% antibiotic (Pen strep: A001) and were incubated at 37 °C and 5% CO_2 atmosphere. Dulbecco's phosphate buffered saline (PBS), foetal bovine serum (FBS), antibiotic

solution 100× liquid with 10,000 U penicillin and 10 mg streptomycin/ml, trypsin, 3-(4,5dimethylthiazol-2-yl)-2,5-diphenyl tetrazolium bromide (MTT) were supplied by Himedia Laboratories Pvt. Ltd., (Mumbai, India). HDAC enzyme inhibition assays were performed as per the experimental protocol given in the enzyme kits of *pan*-HDAC (cat# BML-AK501), HDAC1 (cat# BML-AK511), HDAC2 (cat# BML-AK512), HDAC3/NCoR1 (cat# BML-AK531-0001), HDAC8 (cat# BML-AK518) from Enzo life sciences ltd. and HDAC6 (cat# K465-100) from Biovision Ltd. that were purchased from Bionova suppliers, Hyderabad. The absorbance for MTT assay and HDAC enzyme inhibition was measured using a microplate reader (Spectramax™, Molecular Devices).

2.4.2. Chemistry

All starting materials and reagents were commercially available and used without further purification. All reactions were monitored by thin layer chromatography (TLC) using pre-coated plates with silica gel F254 from Merck Millipore Co., USA. ^{1}H and ^{13}C NMR spectrum were recorded in DMSO-d6 and $CDCl_3$ using Bruker-400 MHz and chemical shifts were reported in ppm using tetramethylsilane (TMS) as internal standard. Mass spectroscopy was performed in HRMS (6545 Q-TOF LC/MS, Agilent) at Bits-Pilani, Pilani campus.

2.4.2.1. Preparation of tert-butyl 2-(benzamido) phenyl carbamate (4a).

Compound (**3a**) (100 mg; 0.819 mmol) was dissolved in the solution of dichloromethane and pyridine (1:1) stirred at room temperature in nitrogen environment. To this reaction mixture, 1ethyl-3-dimethyl amino propyl carbodiimide (228 mg; 1.47 mmol) and catalytic amount of 4dimethyl amino pyridine were added. This mixture was stirred at room temperature for 20 min. After 20 min, *tert*-butyl 2-amino phenyl carbamate (187 mg; 0.90 mmol) was added into the

reaction mixture and reaction was continued to 12h. After completion of the reaction, pyridine was then evaporated under vacuum. The mixture was then dissolved in ethyl acetate and washed with sodium bicarbonate. The organic layer was then separated and dried with Na_2SO_4. The dried solvent was evaporated under vacuum. The crude product was then purified using column chromatography (solvent system – hexane and ethyl acetate (70:30)) in silica 230 – 400 mesh to obtain the final compound **4a,** in its pure form (Yield 58%).^{1}H NMR (400 MHz, $CDCl_3$) δ : 9.15 (s, 1H), 7.95 (d, J = 8.4 Hz, 2H), 7.76 (d, J = 7.6 Hz, 1H), 7.59 (t, J = 7.2 Hz, 1H), 7.47 (t, J = 7.6 Hz, 2H), 7.23 (m, 3H), 6.84 (s, 1H), 1.51 (s, 9H). $C_{18}H_{20}N_2O_3$ [M]: 312.36; MS (ESI) *m/z*: $[M+H]^+$: 313.24

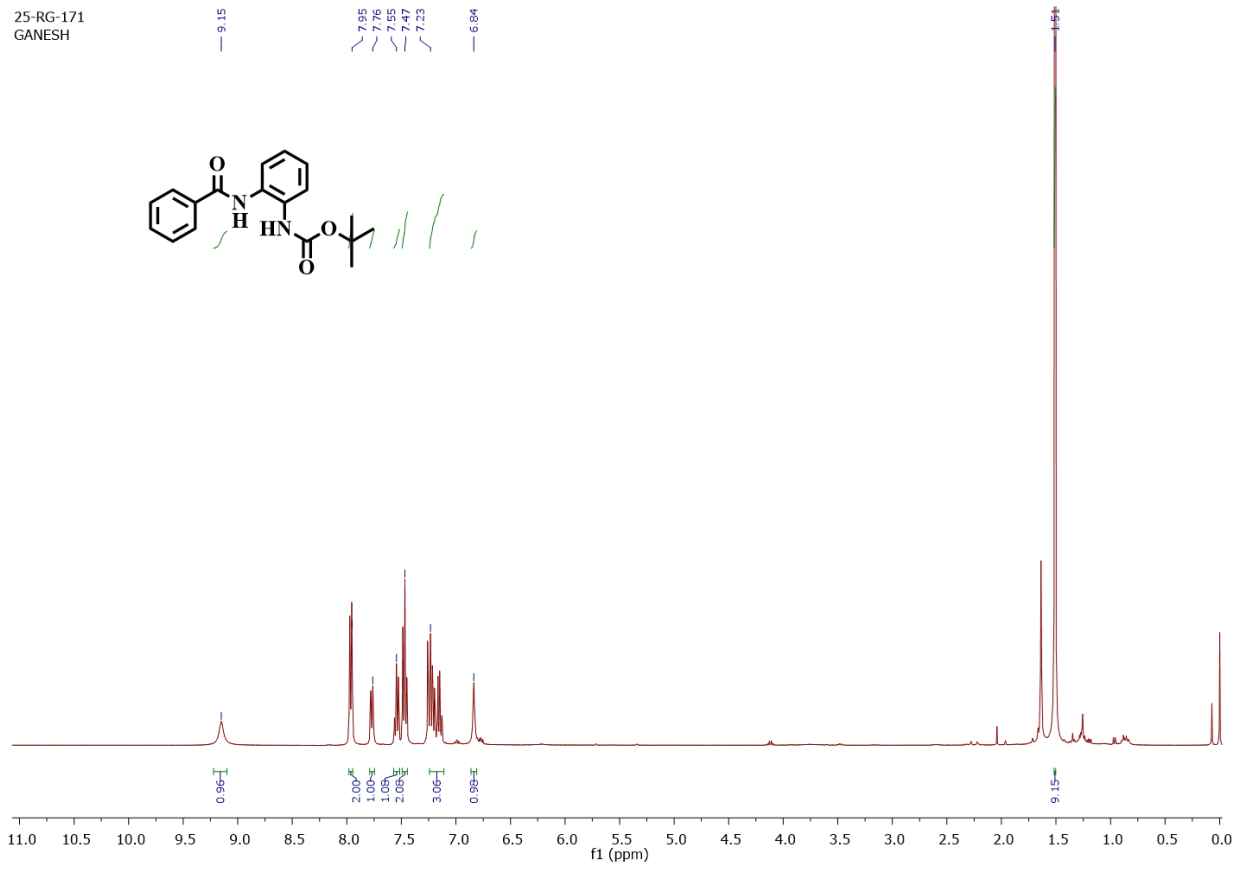

2.4.2.2. Preparation of N-(2-amino phenyl) benzamide (5a).

The compound *tert*-butyl-2-(benzamido) phenyl carbamate (**4a**) (120 mg; 0.384 mmol) was dissolved in dichloromethane (5mL) and the solution of 4M dioxane in HCl was added to it at 0°C. This mixture was then allowed to react under constant stirring at room temperature for 2h. The dioxane was then evaporated under vacuum. The resulting compound was then dissolved in ethyl acetate and washed with water. The organic layer was then separated, dried with Na_2SO_4 and solvent was evaporated under vacuum. The mixture was then washed with pentane to obtain bocdeprotected final compound **5a**. (yield: 87%).^{1}H NMR (400 MHz, $CDCl_3$) δ : 8.01 (s, 1H), 7.88 (d, *J* = 7.88 Hz, 2H), 7.54 (d, *J* = 7.6 Hz, 1H), 7.45 (t, *J* = 7.6 Hz, 2H), 7.28 (d, *J* = 7.6 Hz, 1H), 7.07 (t, *J* = 7.6 Hz, 1H), 6.83 (t, *J* = 5.2 Hz, 2H), 3.69 (s, 2H).^{13}CNMR (101 MHz, $CDCl_3$) δ : 165.87, 140.83, 134.17, 131.93, 128.75, 128.73, 127.32, 127.29, 125.39, 124.72, 119.73, 118.34. ESI-HRMS: calcd for $C_{13}H_{12}N_2O$ m/z: $[M+H]^+$: 213.1015; found $[M+H]^+$: 213.1022.

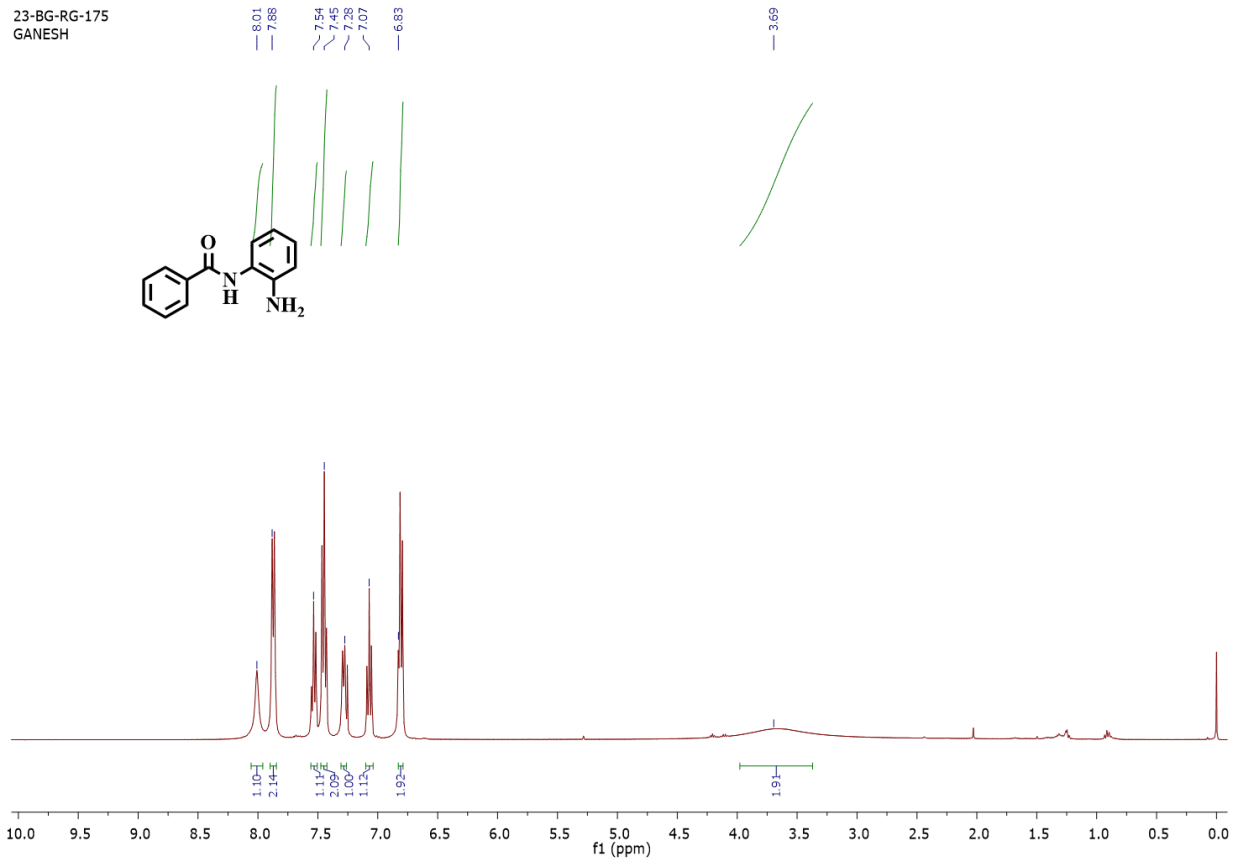
23-BG-RG-175
GANESH
8.01
7.88
7.54
7.45
7.28
7.07
6.83
3.69
O
N
H
NH2
1.10
2.14
1.11
2.09
1.00
1.12
1.92
1.91
10.0
9.5
9.0
8.5
8.0
7.5
7.0
6.5
6.0
5.5
5.0
4.5
4.0
3.5
3.0
2.5
2.0
1.5
1.0
0.5
0.0
f1 (ppm)

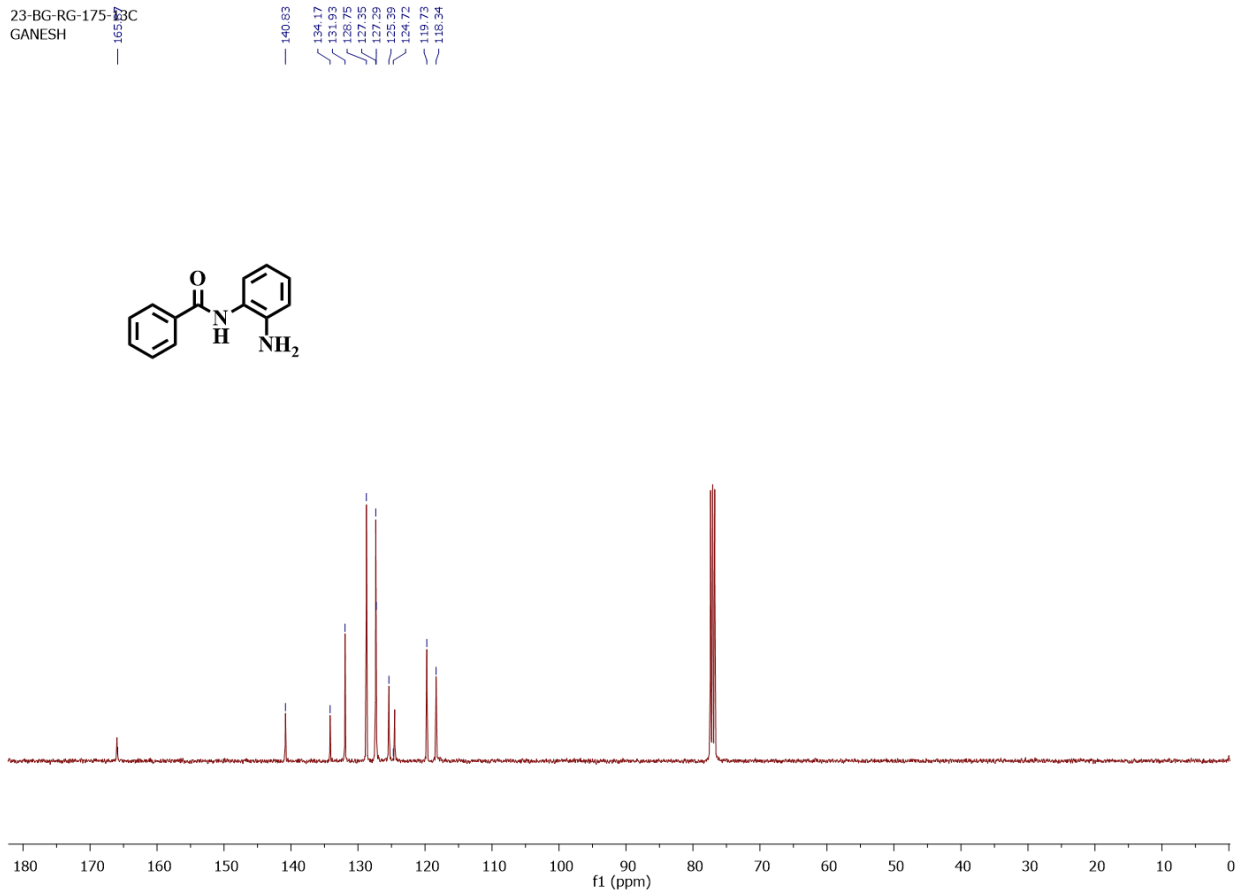
23-BG-RG-175-BC
GANESH
165.57
140.83
134.17
131.93
128.75
127.35
127.29
125.39
124.72
119.73
118.34
O
N
H
NH2
180
170
160
150
140
130
120
110
100
90
80
70
60
50
40
30
20
10
0
f1 (ppm)

HPLC:

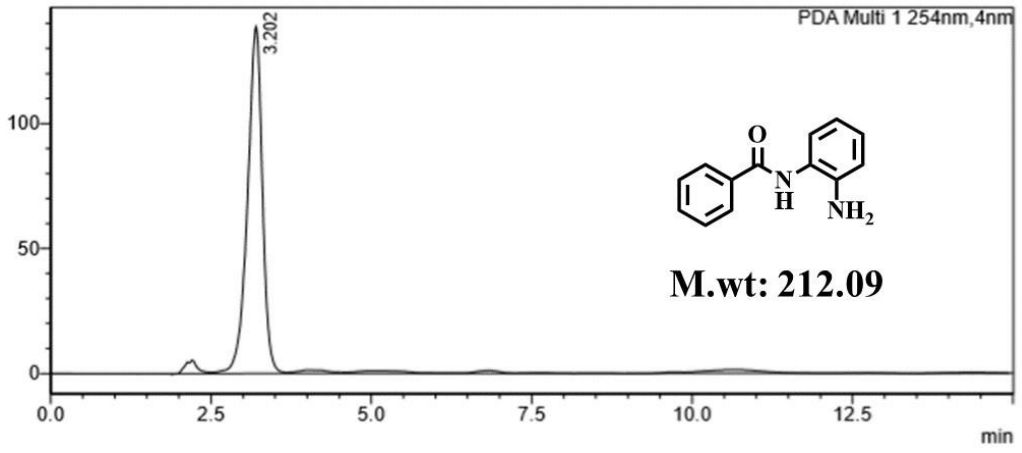
PDA Multi 1 254nm,4nm
3.202
100
50
0
0.0
2.5
5.0
7.5
10.0
12.5
min
O
N
H
NH2
M.wt: 212.09

LCMS:

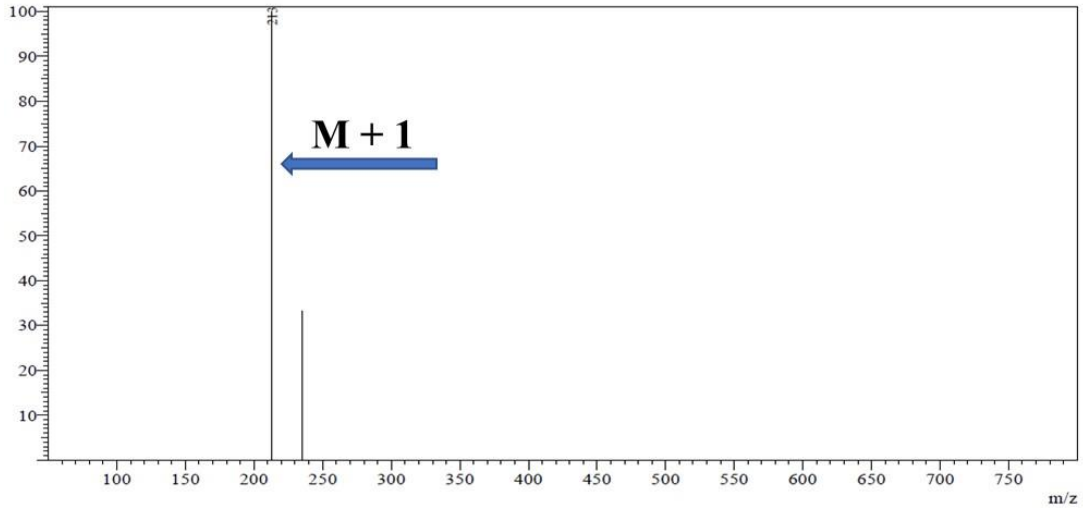

HRMS:

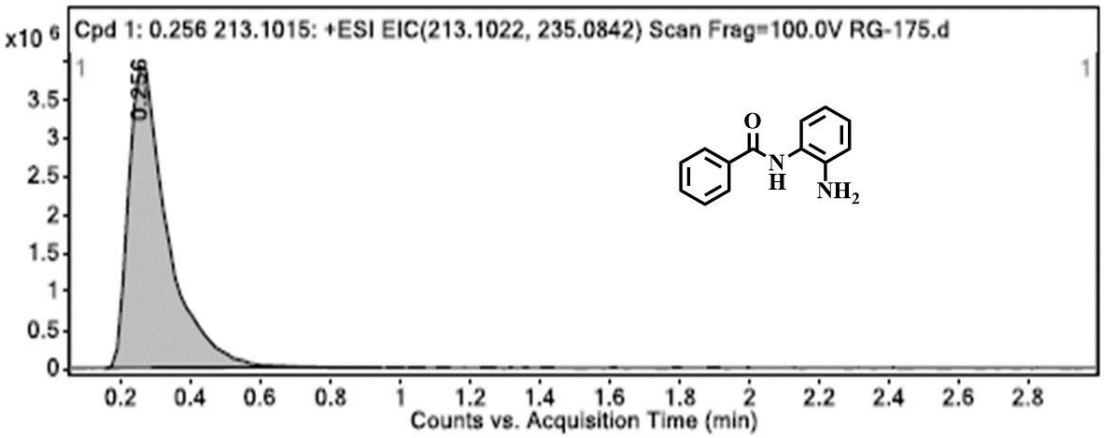

MS Zoomed Spectrum

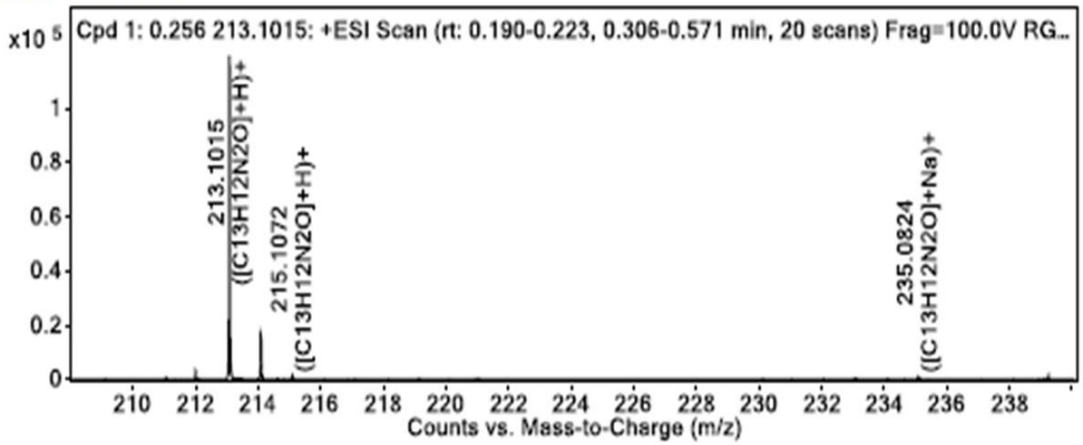

2.4.2.3. Preparation of tert-butyl 2-(1-naphthamido) phenyl carbamate (4b)

1-Naphthoic acid (**3b**) (150 mg; 0.872 mmol) was dissolved in the solution of dichloromethane and pyridine (1:1) followed by the addition of 1-ethyl-3-dimethyl amino propyl carbodiimide (243.28 mg; 1.569 mmol) and catalytic amount of 4-dimethylamino pyridine. The reaction mixture was stirred at room temperature for 20min. After 20min, *tert*-butyl 2-amino phenyl carbamate (199 mg; 0.959 mmol) was added into the reaction mixture and reaction was continued to 12h. The reaction mixture was monitored by TLC. After completion of the reaction, pyridine was then evaporated under vacuum. The mixture was then dissolved in ethyl acetate and washed with sodium bicarbonate. The organic layer was then separated and dried with Na_2SO_4. The dried solvent was evaporated under vacuum that was purified on a silica gel column to give compound as a solid. (yield: 74%).^{1}H NMR (400 MHz, $CDCl_3$) δ : 8.58 (s, 1H), 8.47 (d, J = 8.0 Hz, 1H), 7.95 (d, J = 7.94 Hz, 1H), 7.89 (d, J = 8.8 Hz, 1H), 7.77 (d, J = 6.8 Hz, 2H), 7.57 (m, 2H), 7.48 (t, J = 7.6 Hz, 1H), 7.39 (d, J = 9.2 Hz, 1H), 7.24 (m, 2H), 6.92 (s, 1H), 1.43 (s, 9H). $C_{22}H_{22}N_2O_3$ [M] : 361.43; MS (ESI) *m/z*: $[M+H]^+$:362.24.

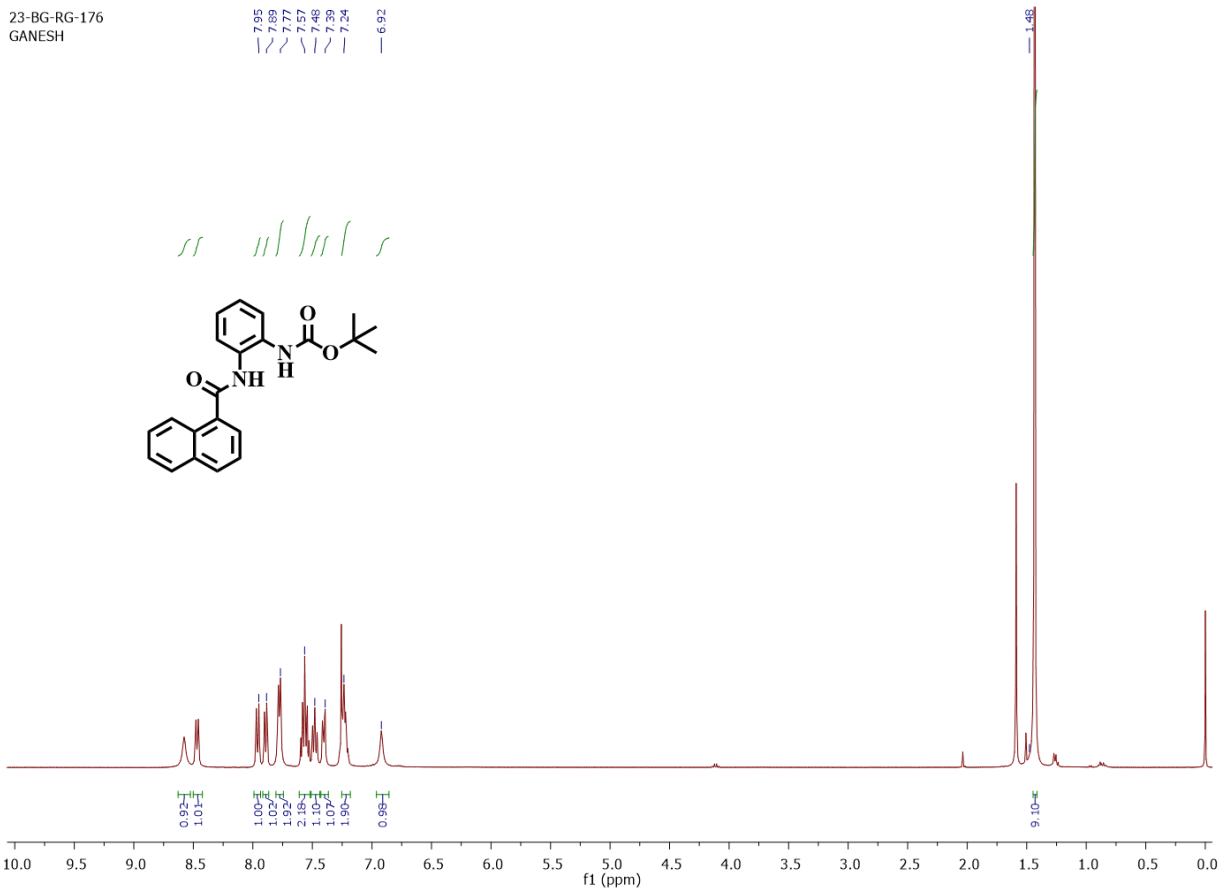

2.4.2.4. Preparation of N-(2-amino phenyl)-1-naphthamide (5b)

The compound *tert*-butyl-2-(1-naphthamido) phenyl carbamate (**4b**) (70 mg; 0.269 mmol) was dissolved in dichloromethane (5 mL). The mixture was stirred at 0°C. To the reaction mixture solution of 4M dioxane in HCl was added to it at same temperature. This mixture was then allowed to react under constant stirring at room temperature for 2h. After completion of the reaction, dioxane was evaporated under vacuum. The resulting compound was quenched with water and extracted with ethyl acetate. The organic layer was then separated, dried with Na_2SO_4 and solvent was evaporated under vacuum. The mixture was then washed with pentane to obtain bocdeprotected final compound **5b**. (yield: 70%).^{1}H NMR (400 MHz, DMSO-d_6) δ : 9.84 (s, 3H), 8.33 (d, J = 7.6 Hz,1H), 8.09 (dd, J = 8.4, 8.8 Hz, 2H), 7.86 (d, J = 6.8 Hz, 1H), 7.62 (m, 3H), 7.38 (d, J = 7.6 Hz,1H), 7.01 (t, J = 7.2 Hz,1H), 6.84 (d, J = 7.6 Hz,1H), 6.68 (t, J = 7.6 Hz,1H),

5.05 (s,2H).^{13}C NMR (101 MHz, DMSO-d6) δ : 167.84, 142.82, 135.16, 133.64, 130.39, 128.75, 127.33, 127.10 – 126.39, 126.16, 126.16, 125.98, 125.50, 123.91, 116.84. ESI-HRMS: calcd for $C_{17}H_{14}N_2O$ m/z: $[M+H]^+$: 263.1168; found $[M+H]^+$:263.1179.

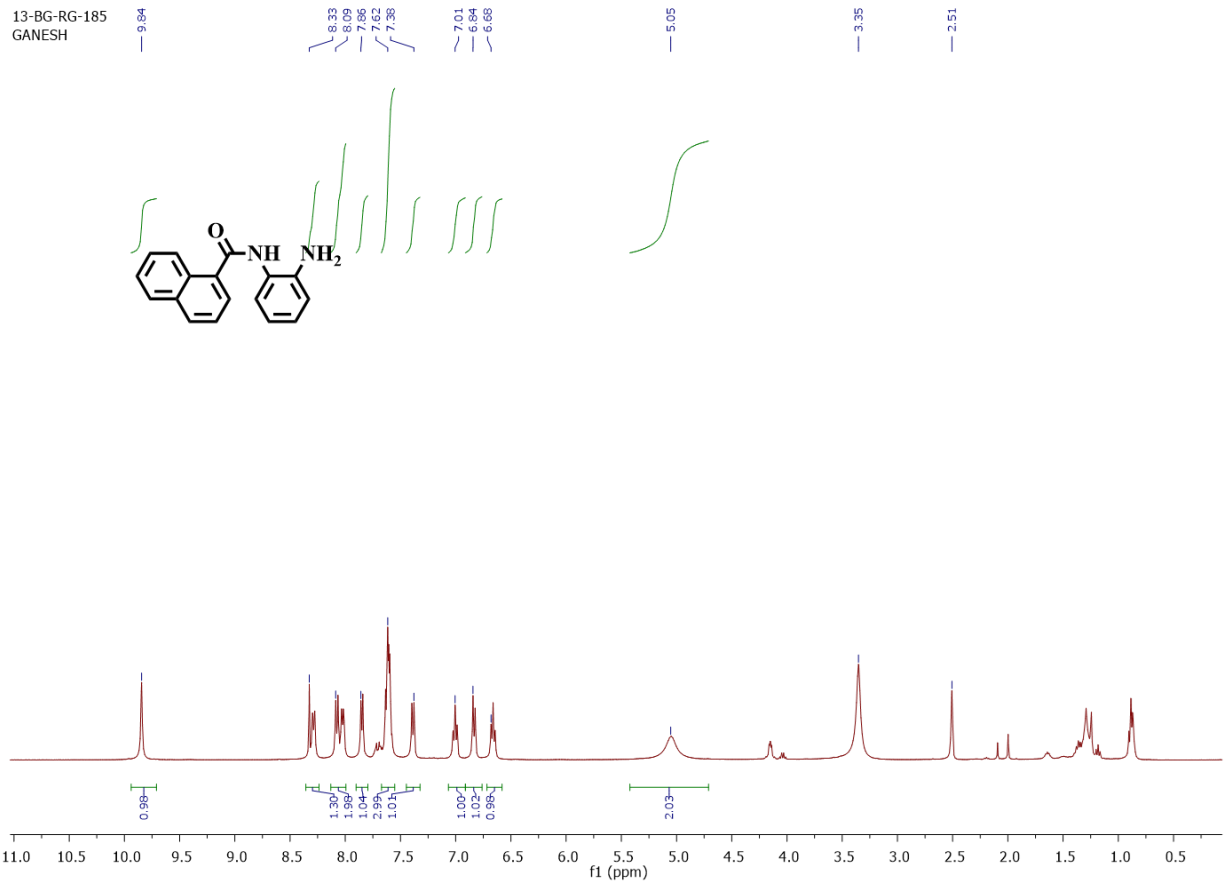

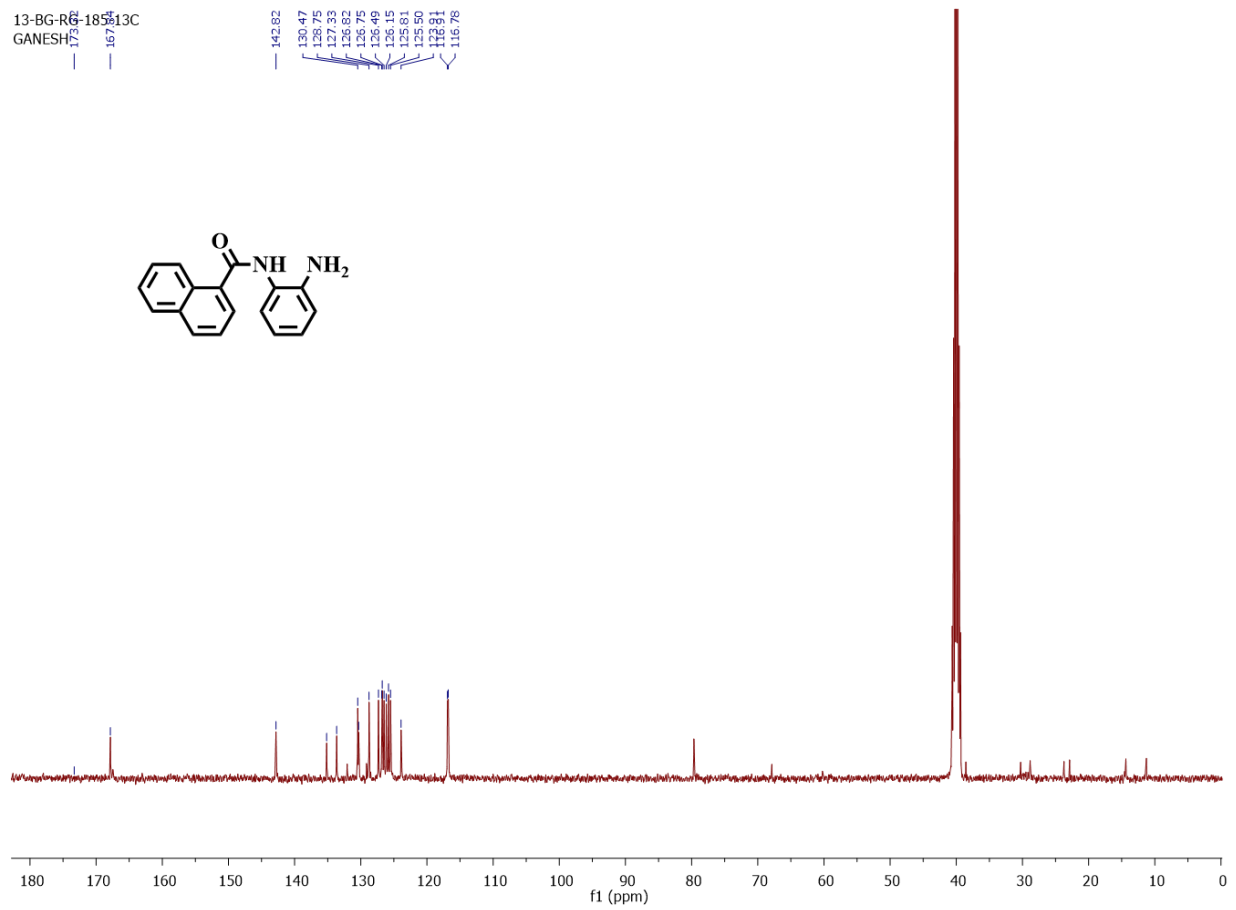
13-BG-RG-185-13C
GANESH
173.22
167.41
142.82
130.47
128.75
127.33
126.82
126.75
126.49
126.15
125.81
125.50
123.91
116.91
116.78
O
NH
NH2
180
170
160
150
140
130
120
110
100
90
80
70
60
50
40
30
20
10
0
f1 (ppm)

HPLC:

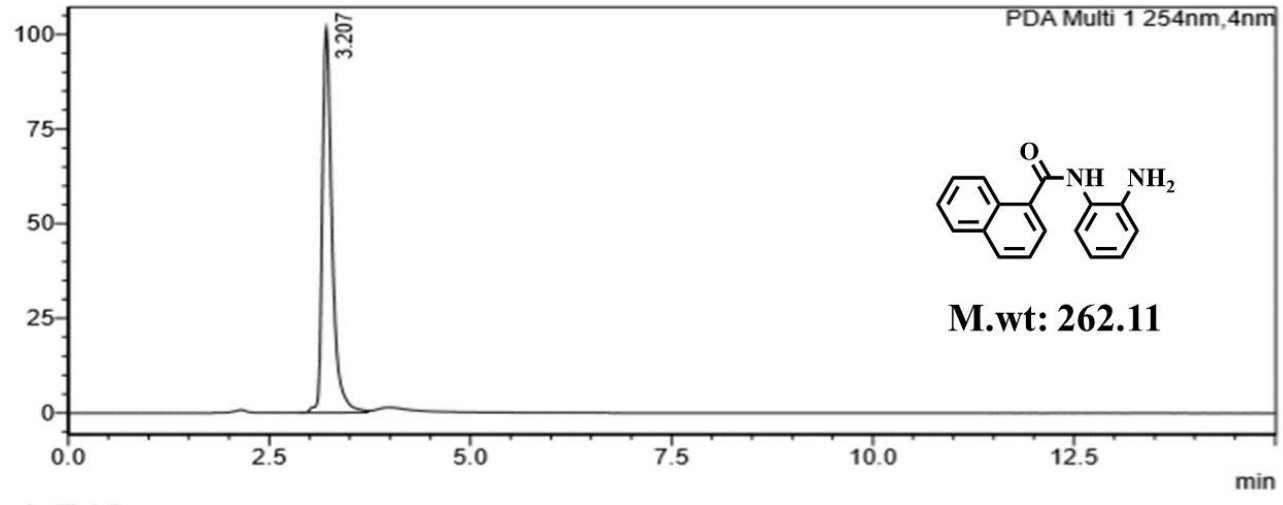
PDA Multi 1 254nm,4nm
3.207
100
75
50
25
0
0.0
2.5
5.0
7.5
10.0
12.5
min
O
NH
NH2
M.wt: 262.11

LCMS:

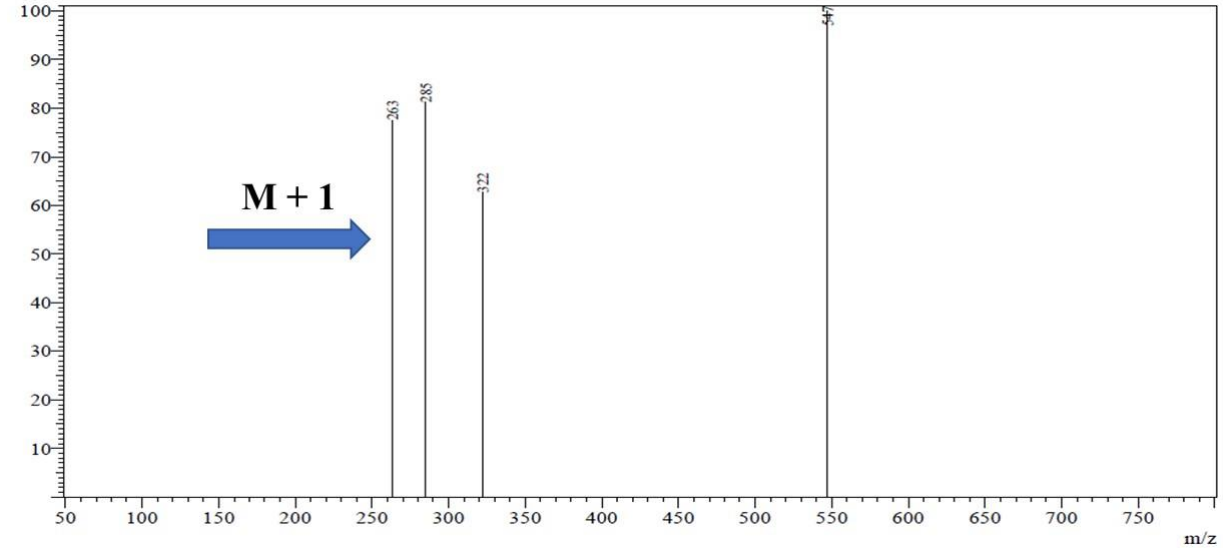
M + 1
263
285
322
547
m/z

HRMS:

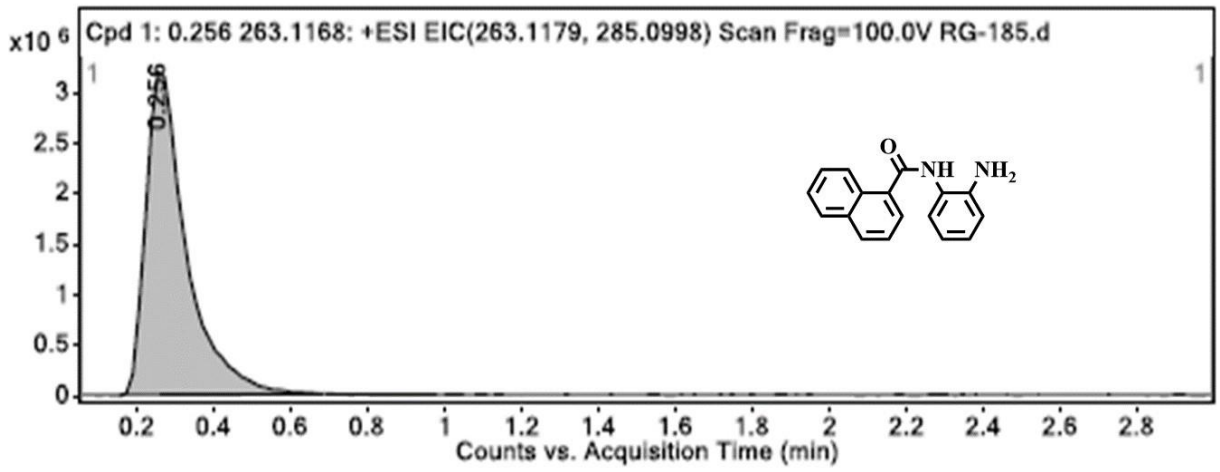
Cpd 1: 0.256 263.1168: +ESI EIC(263.1179, 285.0998) Scan Frag=100.0V RG-185.d
x10 6
0.256
O
NH
NH2
Counts vs. Acquisition Time (min)

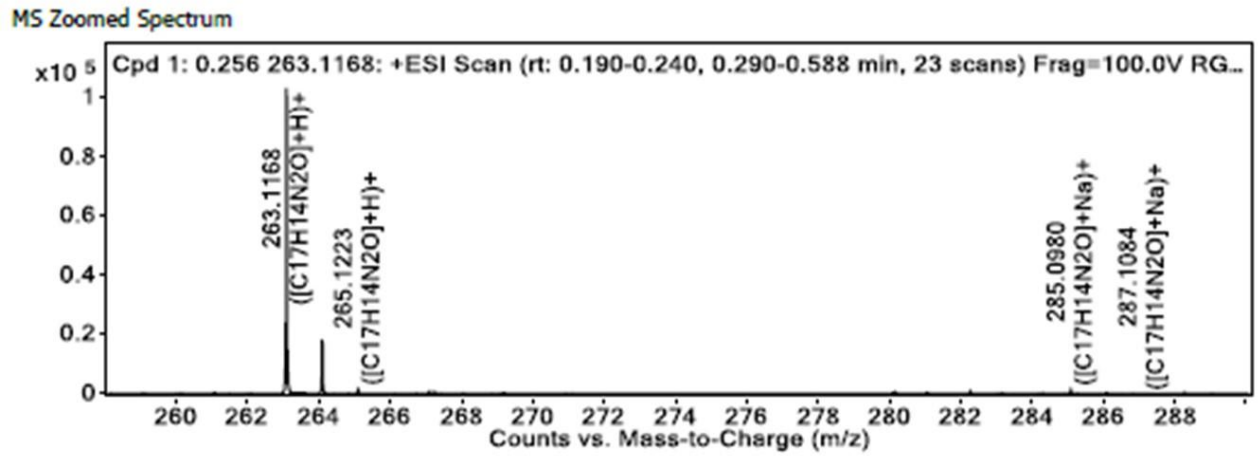

2.4.2.5. Preparation of tert-butyl 2-(2-naphthamido) phenyl carbamate (4c)

To a solution of dichloromethane and pyridine (1:1) was added to 2-naphthoic acid (**3c**) (100 mg; 0.581 mmol) to this reaction mixture 1-ethyl-3-dimethyl amino propyl carbodiimide (243mg; 1.56 mmol) and catalytic amount of 4-di methyl amino pyridine were added in nitrogen environment. The mixture was stirred at room temperature for 15min. After 15min *tert*-butyl 2-amino phenyl carbamate (216.80 mg; 0.955 mmol) was added into the reaction mixture and reaction was continued to 12h. The reaction was monitored with TLC. After completion of the reaction, pyridine was then evaporated under vacuum. The mixture was then dissolved in sodium bicarbonate and extracted with ethylacetate. The organic layer was then separated and dried with Na_2SO_4. The dried solvent was evaporated under vacuum. The crude product was then purified using column chromatography (solvent system – hexane and ethylacetate (50:50)) in silica 230 – 400 mesh to obtain the final compound **4c** in its pure form. (yield: 91%).^{1}H NMR (400 MHz, $CDCl_3$) δ : 9.36 (s, 2H), 8.49 (s, 1H), 8.01 (d, J = 10.0 Hz, 1H), 7.93 (dd, J = 8, 8.8 Hz, 3H), 7.83 (s, 1H), 7.56 (m, 2H), 7.25 (t, J = 4.5 Hz, 2H), 7.16 (m, 1H), 6.99 (t, J = 7.6 Hz, 1H), 6.77 (dd, J = 8.0, 8.4 Hz, 1H), 1.52 (s, 9H). $C_{22}H_{21}FN_2O_3$[M]: 362.42; MS (ESI) *m/z*: $[M+H]^+$: 363.24.

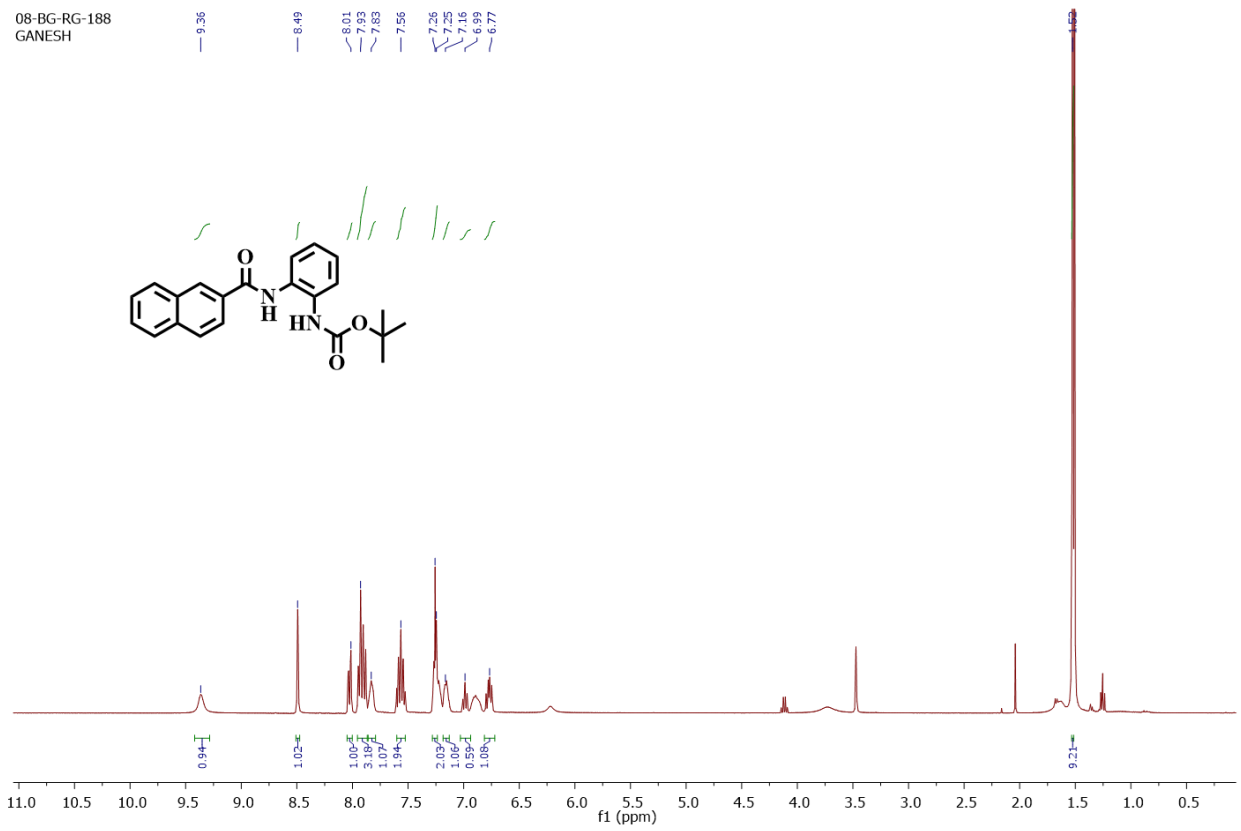

2.4.2.6. Preparation of N-(2-amino phenyl)-2-naphthamide (5c).

The compound *tert*-butyl-2-(2-naphthamido) phenyl carbamate (**4c**) (100 mg; 0.276 mmol) was dissolved in dichloromethane (5mL) and treated with the solution of 4M Dioxane in HCl at 0°C. This mixture was then allowed to react under constant stirring at room temperature for 2h. The reaction completion was monitored by TLC. After completion of the reaction, solvent was then evaporated under vacuum. The resulting compound was then dissolved in water and extracted with ethyl acetate. The organic layer was then separated, dried with Na_2SO_4 and solvent was evaporated under vacuum. The mixture was then washed with pentane to obtain boc-deprotected final compound **5c**. (yield: 71.85%).^{1}H NMR (400 MHz, DMSO-d_6) δ : 9.86 (s, 1H), 8.64 (s, 1H), 8.05 (m, 4H), 7.63 (m, 2H), 7.26 (d, J = 7.6 Hz, 1H), 7.01 (t, J = 8.0 Hz, 1H), 6.84 (d, J = 8.0 Hz, 1H),

6.64 (t, J = 6.8 Hz, 1H), 5.04 (s, 2H). ^{13}C NMR (101 MHz, DMSO-d_6) δ : 165.90, 143.65, 134.70, 132.55, 129.40, 128.60, 128.33 – 127.83, 127.51 – 126.70, 125.11, 123.85, 116.69. ESI-HRMS: calcd for $C_{17}H_{14}N_2O$ m/z: $[M+H]^+$: 263.1171; found $[M+H]^+$: 263.1179.

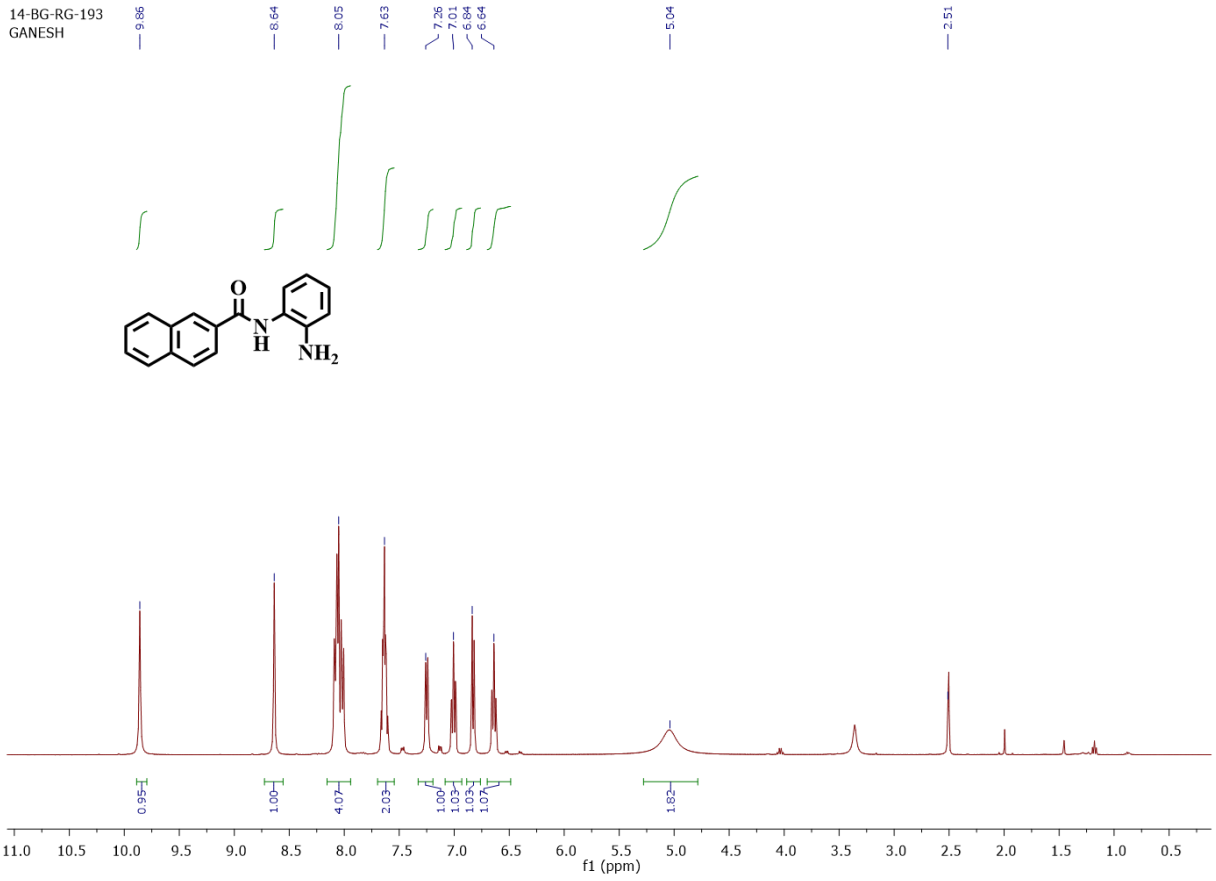

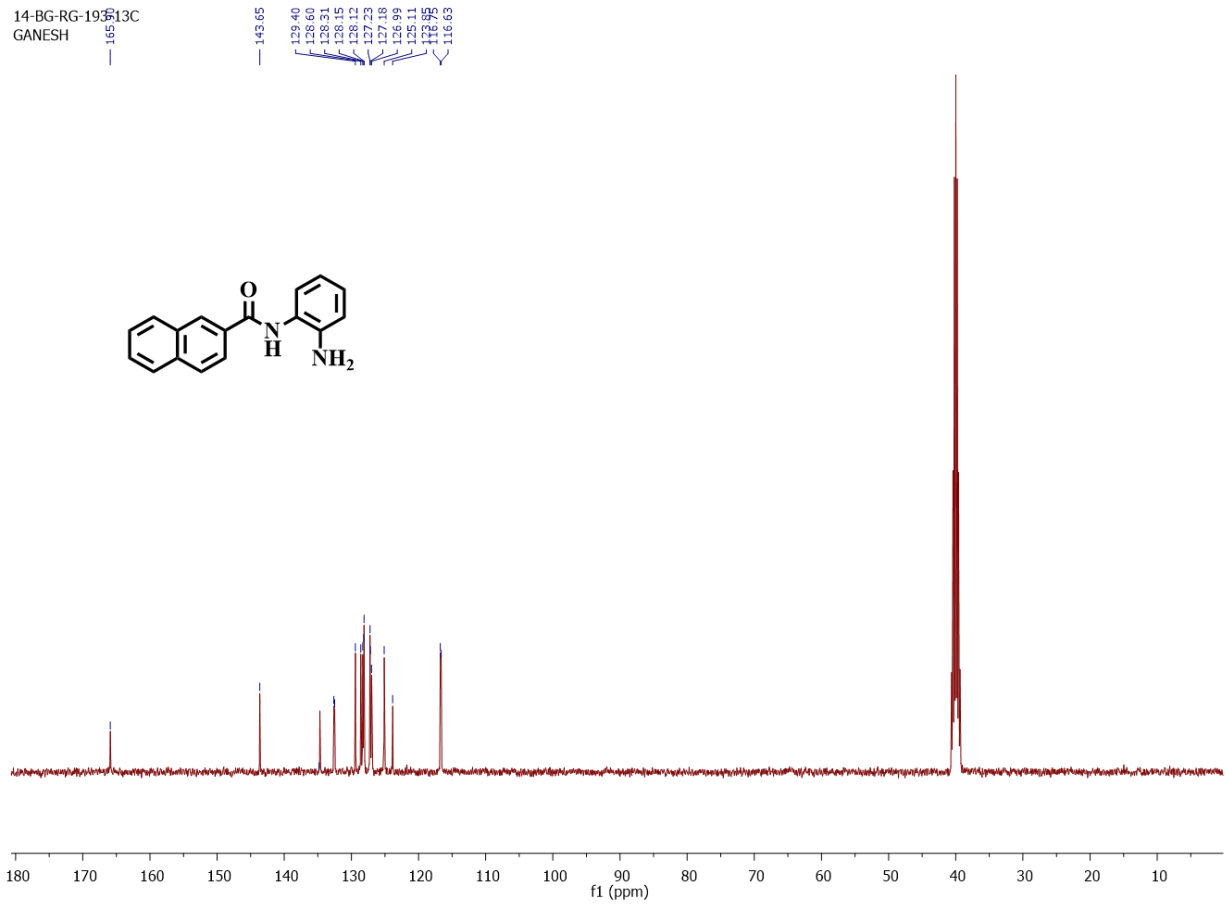
14-BG-RG-193-13C
GANESH
165.50
143.65
129.40
128.60
128.31
128.15
128.12
127.23
127.18
126.99
125.11
116.75
116.63
O
N
H
NH2
180 170 160 150 140 130 120 110 100 90 80 70 60 50 40 30 20 10
f1 (ppm)

HPLC:

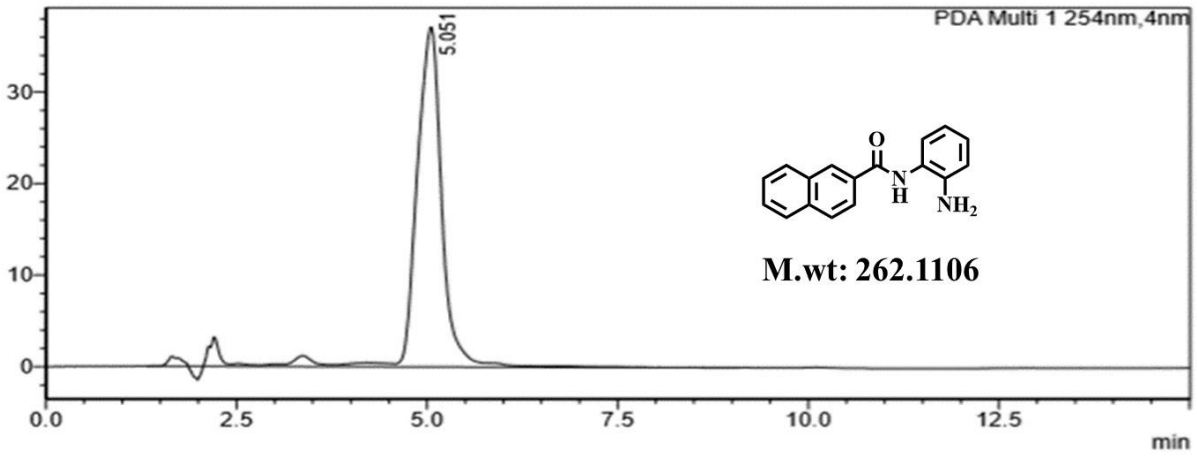
PDA Multi 1 254nm,4nm
5.051
30
20
10
0
0.0
2.5
5.0
7.5
10.0
12.5
min
O
N
H
NH2
M.wt: 262.1106

LCMS:

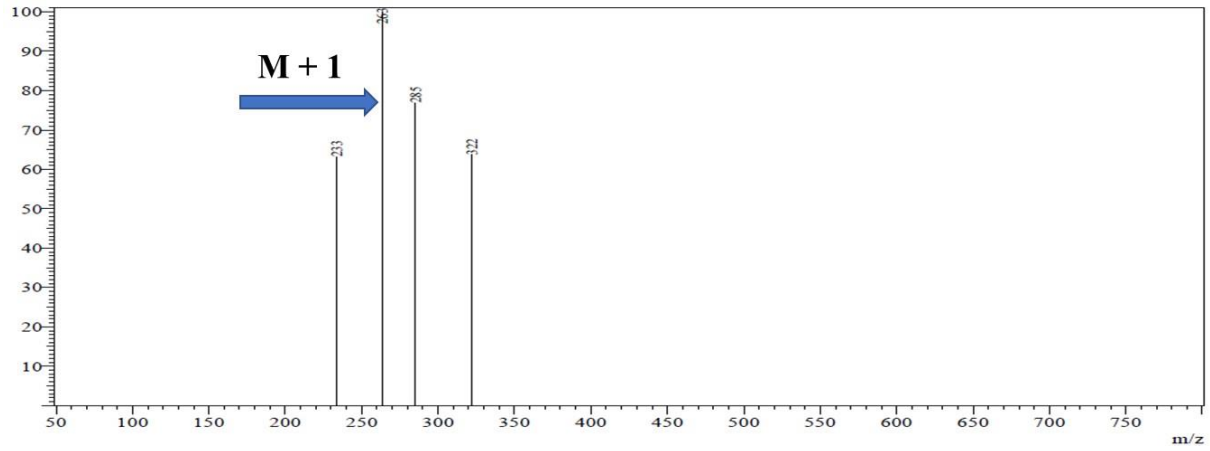
M + 1
263
285
233
322
m/z

HRMS:

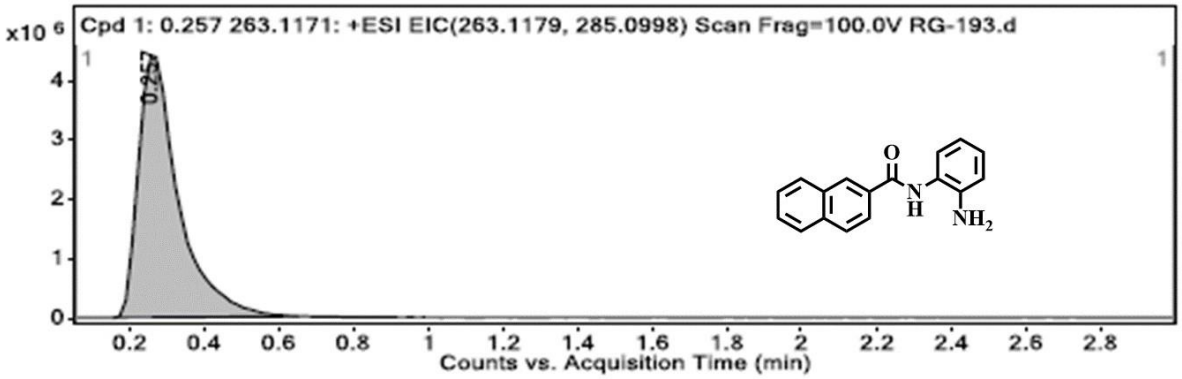
Cpd 1: 0.257 263.1171: +ESI EIC(263.1179, 285.0998) Scan Frag=100.0V RG-193.d
0.257
Counts vs. Acquisition Time (min)

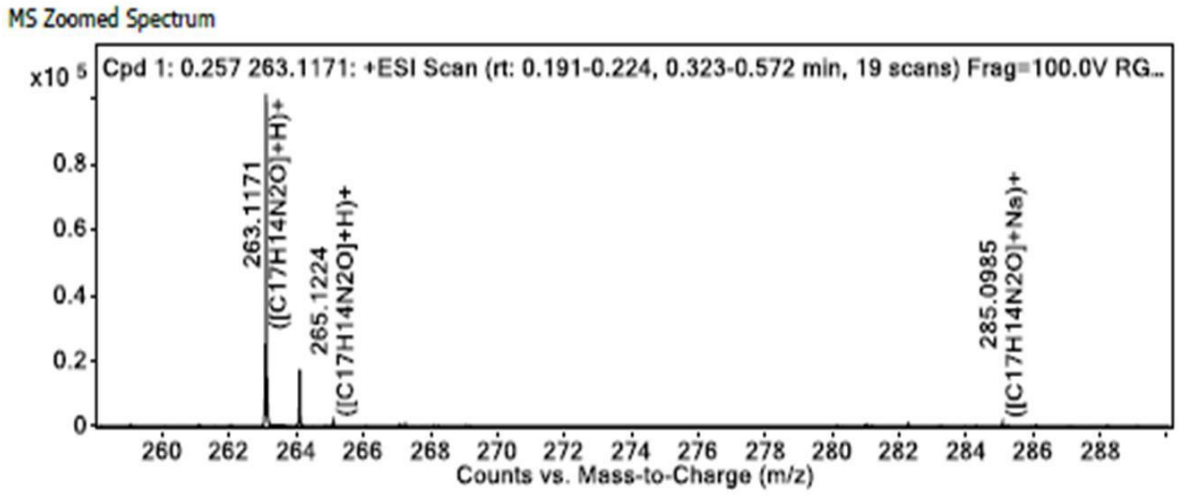
MS Zoomed Spectrum
Cpd 1: 0.257 263.1171: +ESI Scan (rt: 0.191-0.224, 0.323-0.572 min, 19 scans) Frag=100.0V RG...
263.1171
([C17H14N2O]+H)+
265.1224
([C17H14N2O]+H)+
285.0985
([C17H14N2O]+Na)+
Counts vs. Mass-to-Charge (m/z)

2.4.2.7. Preparation of tert-butyl 2-(quinolone-3-carboxamido) phenyl carbamate (4d) 3-Quinoline carboxylic acid (**3d**) (50 mg; 0.289 mmol) was dissolved in dichloromethane and pyridine (5 ml) at 0°C. To this mixture, 1-ethyl-3-dimethylaminopropylcarbodiimide (80 mg; 0.520 mmol) and 3mg of 4-dimethylaminopyridine were added. The mixture was allowed to react under constant stirring for 15min before *tert*-butyl 2-amino phenyl carbamate (65.936 mg; 0.317 mmol) was added into the reaction mixture. This was allowed to react under constant stirring at room temperature for 12h. The pyridine was then evaporated under vacuum. The mixture was then dissolved in ethyl acetate and washed with water. The organic layer was then separated and concentrated under vacuum. The crude product was then purified using column chromatography (solvent system - hexane and ethyl acetate (70: 30)) in silica 60 - 120 mesh to obtain the final compound **4d** in its pure form. (yield 76%). ^{1}H NMR (400 MHz, $CDCl_3$) δ : 9.73 (s, 1H), 9.48 (s, 1H), 8.75 (s, 1H), 8.17 (d, *J = 8.4 Hz*, 1H), 7.92 (m, *J = 8.4 Hz*, 3H), 7.62 (t, *J = 7.2 Hz*, 1H), 7.26 (m, *J = 1.2 Hz*, 3H), 6.95 (s, 1H), 1.26 (s, 9H). $C_{21}H_{21}N_3O_3$ [M]: 363.15; MS (ESI) *m/z*: $[M+H]^+$: 364.245.

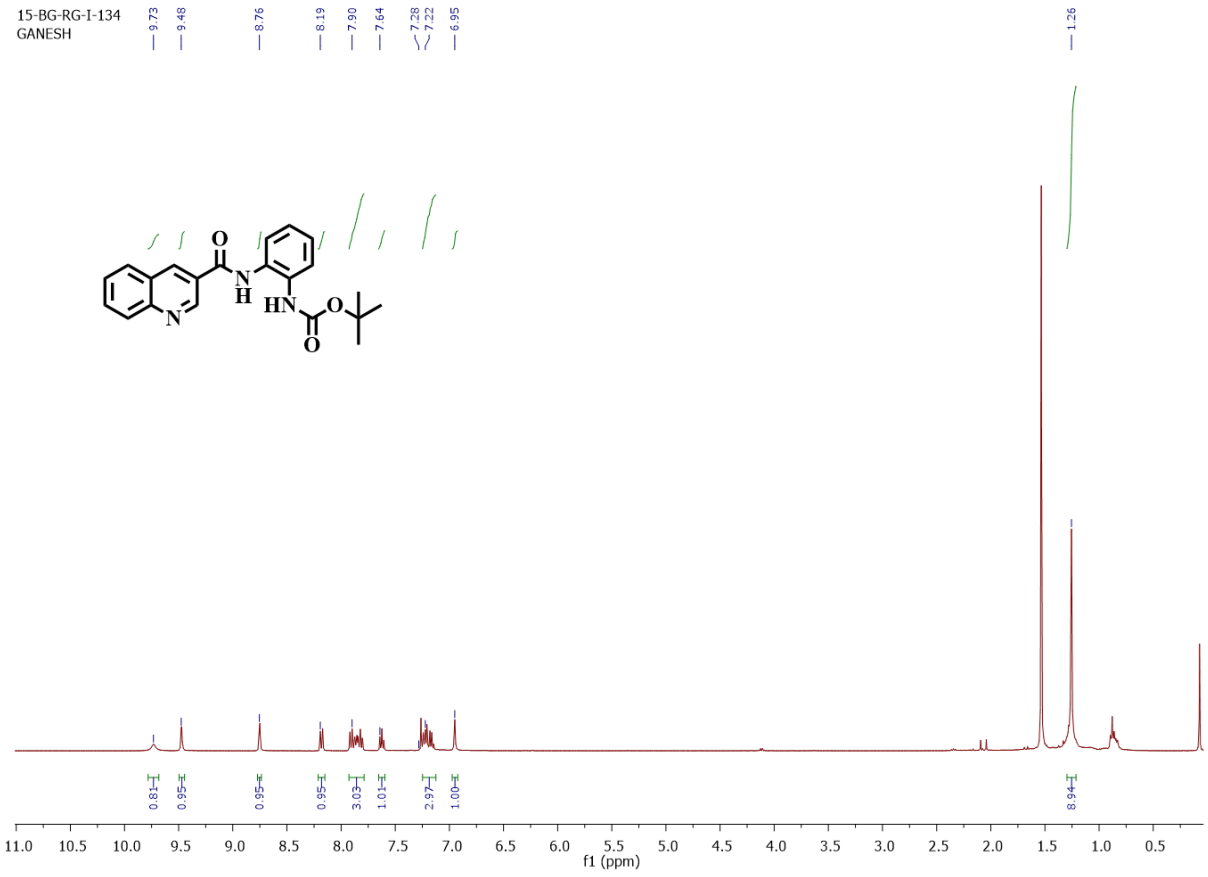

2.4.2.8. Preparation of N-(2-aminophenyl) quinolone-3-carboxamide (5d)

The compound *tert*-butyl 2-(quinolone-3-carboxamido) phenyl carbamate (**4d**) (100 mg; 0.275 mmol) was dissolved in 5ml DCM and 4M dioxane HCl was added to it at 0°C. The mixture was then allowed to react under constant stirring at room temperature for 2h. The dioxane was then evaporated under vacuum. The mixture was then dissolved in ethyl acetate and washed with water. The organic layer was then separated and concentrated under vacuum. The mixture was then washed with pentane to obtain final compound **5d**. (yield 55%) ^{1}H NMR (400 MHz, DMSO-d_6) δ : 10.00 (s, 1H), 9.40 (s, 1H), 9.00 (s, 1H), 8.13 (t, *J = 8.4 Hz* 2H), 7.90 (d, *J = 7.2 Hz*, 1H), 7.74 (s, *J = 7.2 Hz*, 1H), 7.24 (d, *J = 7.2 Hz*, 1H), 7.02 (s, *J = 7.2 Hz*, 1H), 6.83 (d, *J = 7.6 Hz*, 1H),6.64 (s, *J = 7.6 Hz*, 1H).^{13}C NMR (101 MHz, DMSO-d_6) δ : 164.5,149.79,149.02,148.93,143.20,

136.60, 131.70, 129.64, 129.25, 127.89, 127.33 ,127.38,126.99,123.3,116.78, 116.56, 40.19.

ESIHRMS: calcd for $C_{16}H_{13}N_3O$ m/z: $[M+H]^+$: 264.1121; found $[M+H]^{+\cdot}$ 264.1131.

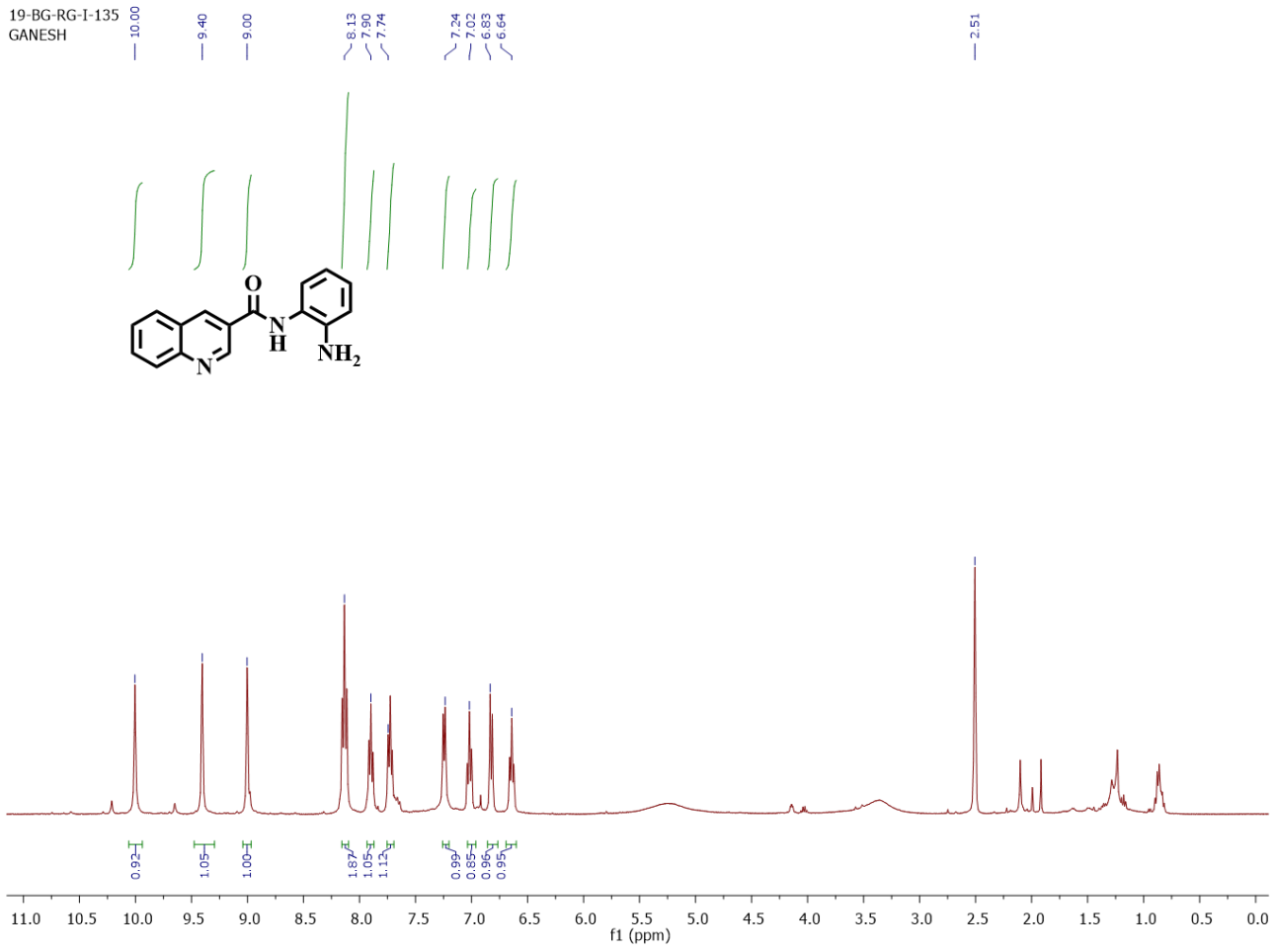

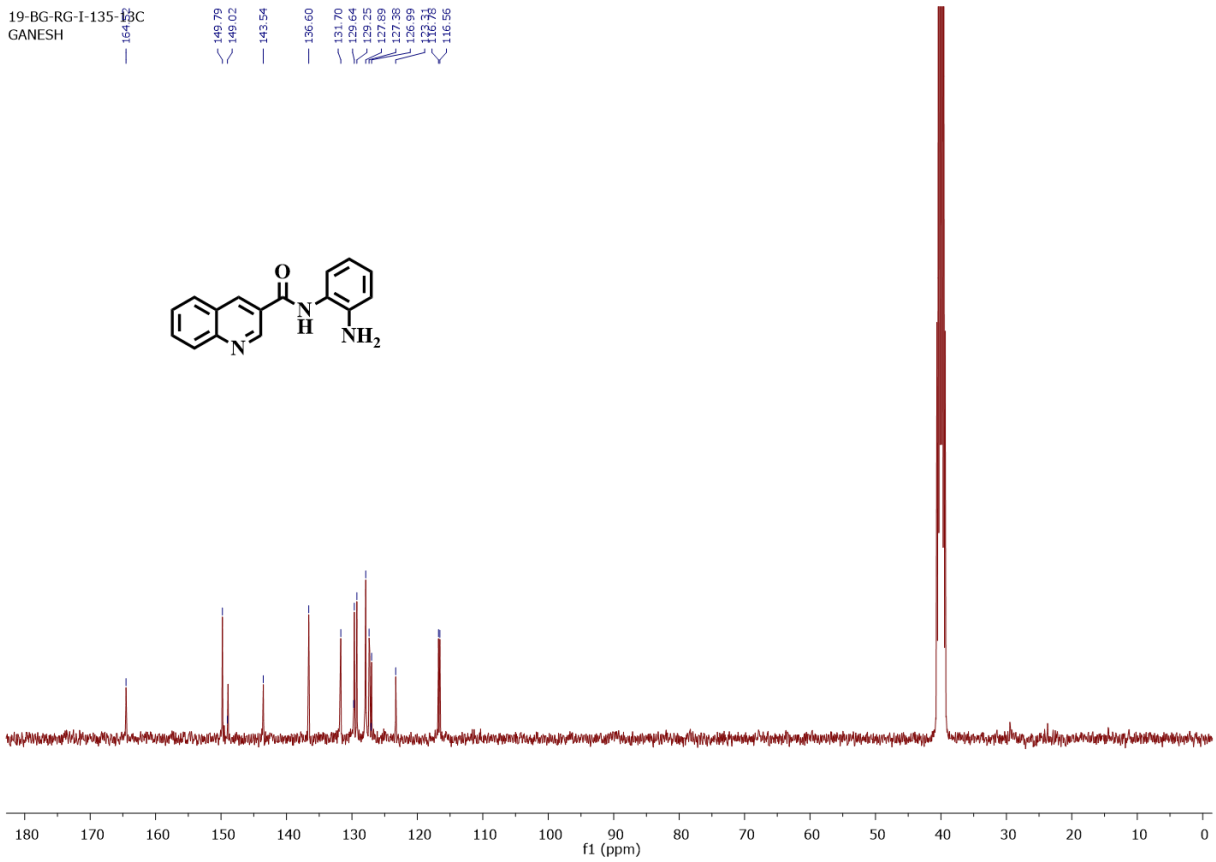
19-BG-RG-I-135-13C
GANESH
164.42
149.79
149.02
143.54
136.60
131.70
129.64
129.25
127.89
127.38
126.99
123.31
118.78
116.56
O
N
H
NH2
N
180 170 160 150 140 130 120 110 100 90 80 70 60 50 40 30 20 10 0
f1 (ppm)

.

HPLC:

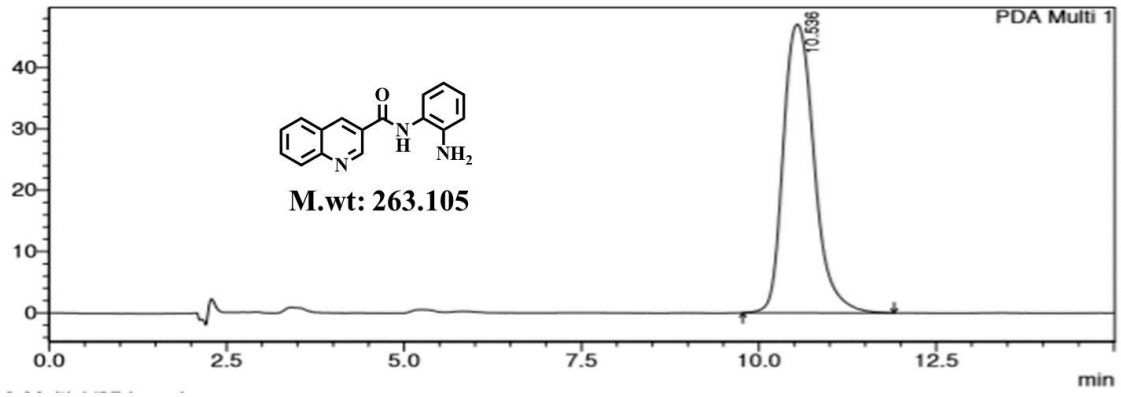
PDA Multi 1
10.536
O
N
H
NH2
N
M.wt: 263.105
40
30
20
10
0
0.0
2.5
5.0
7.5
10.0
12.5
min

LCMS:

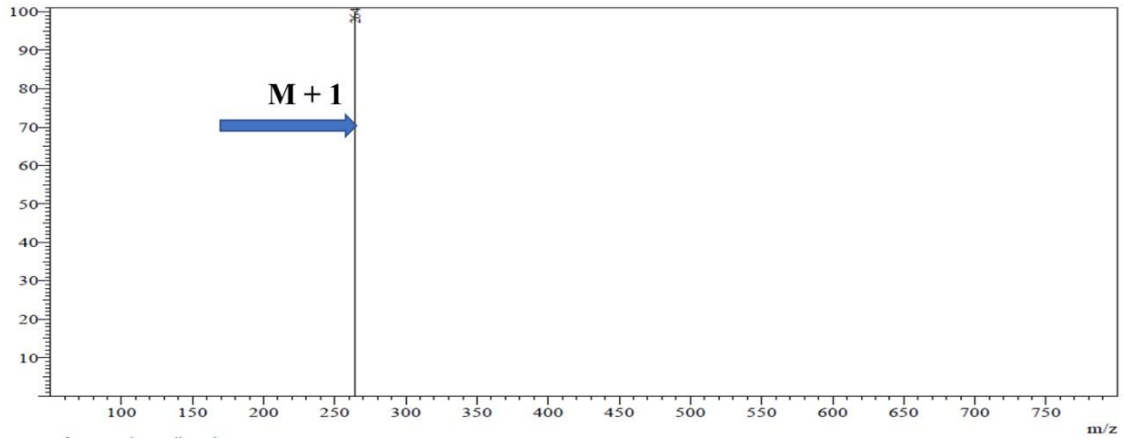

HRMS:

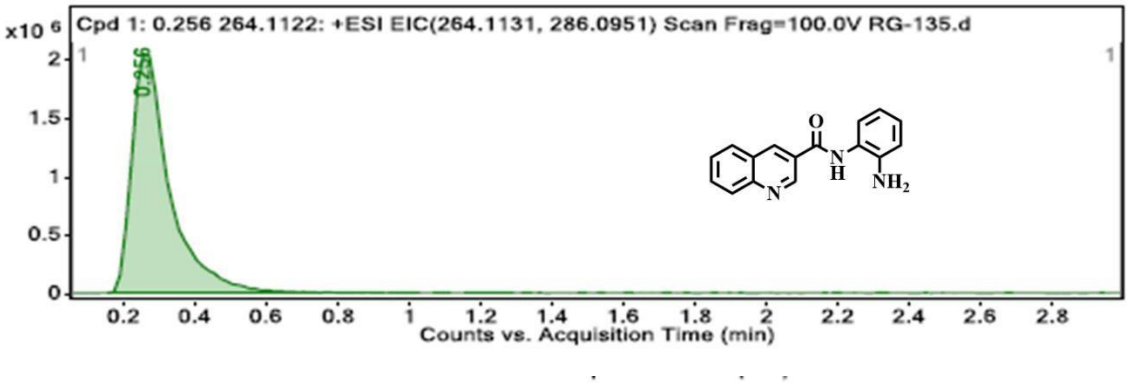

MS Zoomed Spectrum

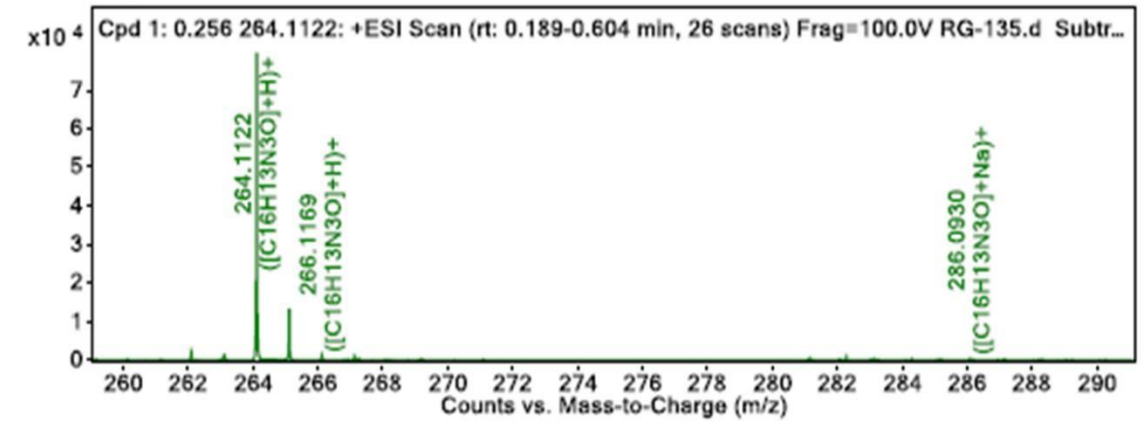

2.4.2.9. Preparation of tert-butyl 2-(quinolone-6-carboxamido) phenyl carbamate (4e)

6-Quinoline carboxylic acid (**3e**) (100 mg; 0.578 mmol) was dissolved in dichloromethane: pyridine in the ratio of 1:1 (5 ml). To this mixture, 1-ethyl-3-dimethyl amino propyl carbo di imide (83.23 mg; 1.04 mmol) and 3 mg of 4-dimethylaminopyridine were added. This mixture was allowed to react under constant stirring for 15min before *tert*-butyl 2-amino phenyl carbamate (132.08 mg; 0.635 mmol) was added into the reaction mixture. This was allowed to react under constant stirring at room temperature overnight. The pyridine was then evaporated under vacuum. The mixture was then dissolved in ethyl acetate and washed with sodium bicarbonate. The organic layer was then separated and the excess solvent was then evaporated under vacuum. The crude product was then purified using column chromatography (solvent system- hexane and ethylacetate (60:40)) in silica 230 - 400 mesh to obtain the final compound **4e** in its pure form. (yield: 45%).^{1}H NMR (400 MHz, $CDCl_3$) δ : 9.49 (s, 1H), 8.94 (d, *J = 2.8 Hz* 1H), 8.44 (s, 1H), 8.18 (d, *J = 8 Hz* 2H), 8.13 (d, *J = 8.8 Hz* 1H), 7.82 (d, *J = 7.6 Hz* 1H), 7.42 (dd, *J= 4.4, 4.2 Hz* 1H), 7.14 (dd, *J= 4.8 ,4.4 Hz* 2H), 6.76 (s, 1H), 1.46 (s, 9H). $C_{21}H_{21}N_3O_3$ [M]: 363.15; MS (ESI) *m/z*: $[M+H]^+$: 364.245.

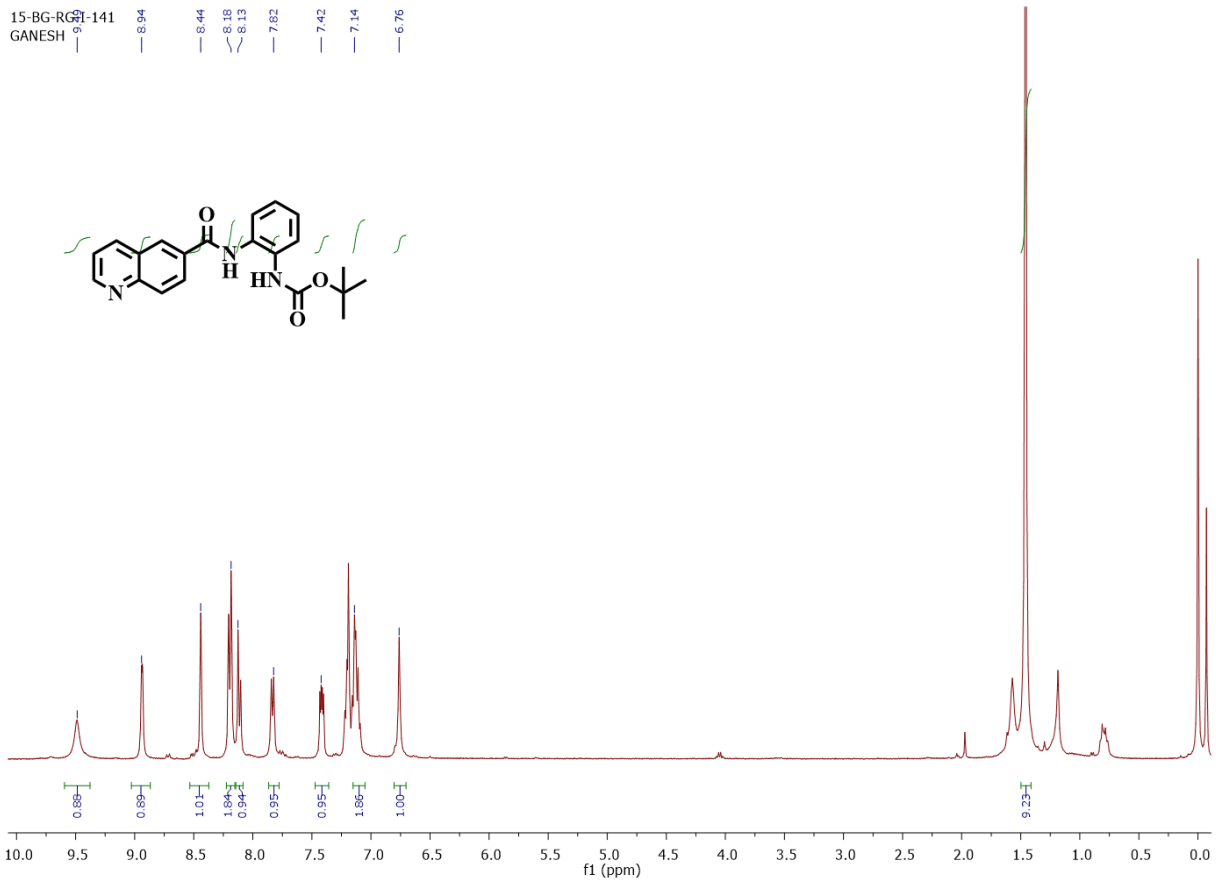

2.4.2.10. Preparation of N-(2-aminophenyl) quinolone-6-carboxamide (5e)

The compound *tert*-butyl 2-(quinolone-6-carboxamido) phenyl carbamate (**4e**) (32 mg; 0.088 mmol) was dissolved in 5ml DCM and 4M dioxane HCl was added to it at 0°C. This mixture was then allowed to react under constant stirring at room temperature for 4h. The dioxane was then evaporated under vacuum. The mixture was then dissolved in ethylacetate and washed with sodium bicarbonate. The organic layer was then separated and the excess solvent was evaporated under vacuum. The mixture was then washed with pentane to obtain boc-deprotected final compound **5e** (yield: 80%).^{1}H NMR (400 MHz, DMSO-d_6) δ : 11.01 (s, 1H), 9.28 (s, 1H), 9.08 (s, 1H), 9.00 (*d, J = 8Hz, 1H*), 8.65 (d, *J = 8.4 Hz*, 1H), 8.42 (d, *J = 8.8 Hz*, 1H), 7.99 (dd, *J = 4.4, 4.4 Hz*, 1H), 7.66 (d, *J = 7.6 Hz*, 1H), 7.56 (d, *J = 7.2 Hz*, 1H), 7.46 (dd, *J = 7.4 ,7.6 Hz*, 2H).^{13}C NMR (101MHz, DMSO-d_6) δ : 165.03, 148.93, 144.78, 142.44, 133.89, 131.84, 130.19, 128.58, 128.12,

127.80, 127.33, 124.66, 123.69, 123.33 – 122.99. ESI-HRMS: calcd for $C_{16}H_{13}N_3O$ m/z: $[M+H]^+$: 264.1121; found $[M+H]^+$: 264.1131.

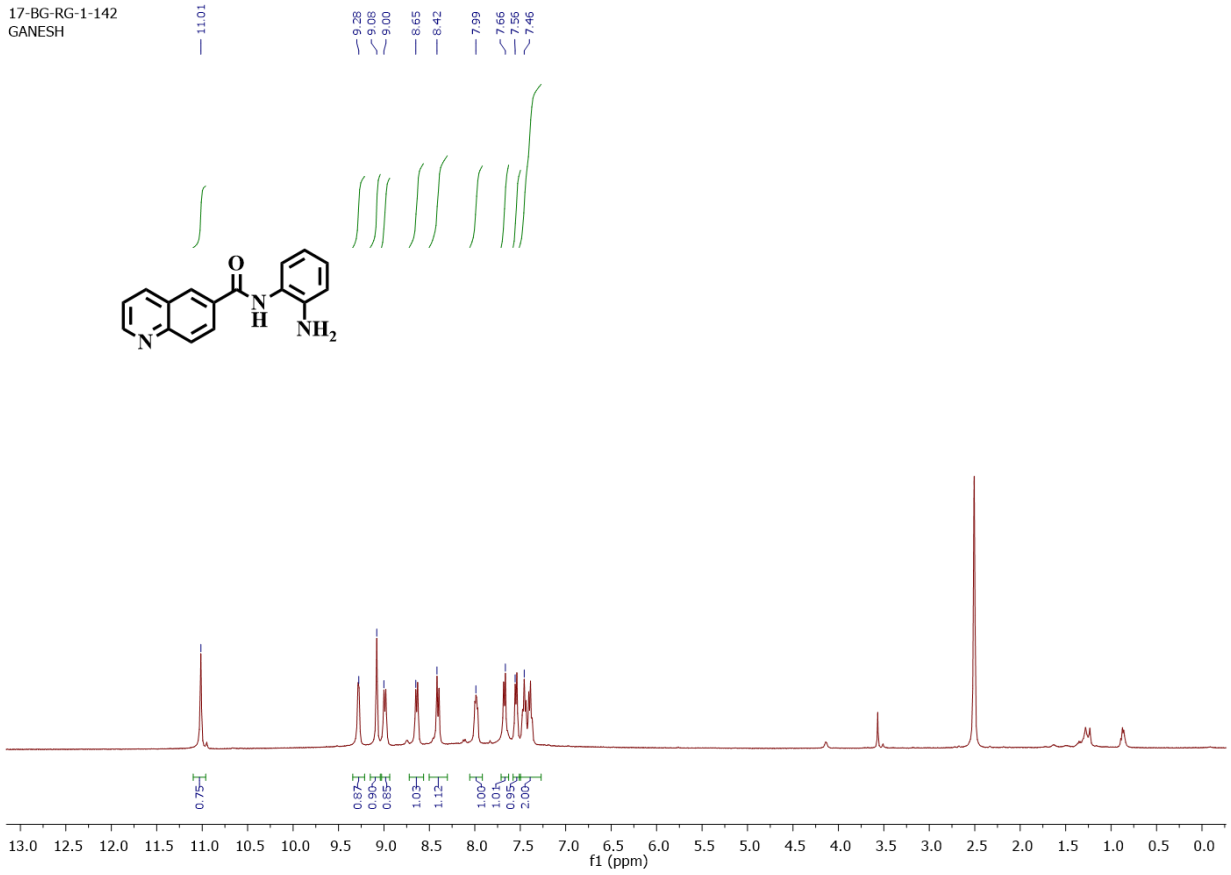

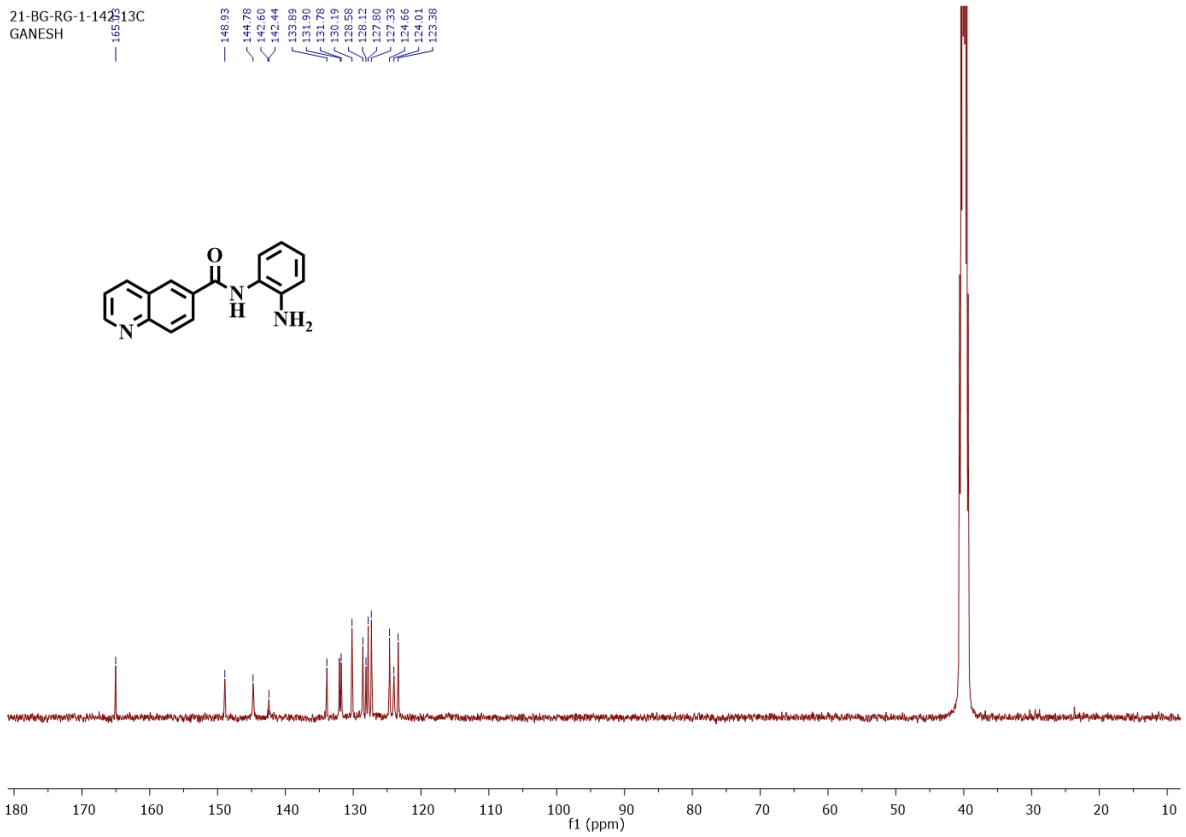
21-BG-RG-1-142 13C
GANESH
165.23
148.93
144.78
142.60
142.44
133.89
131.90
131.78
130.19
128.58
128.12
127.80
127.33
124.66
124.01
123.38
O
N
H
N
NH2
180
170
160
150
140
130
120
110
100
90
80
70
60
50
40
30
20
10
f1 (ppm)

HPLC:

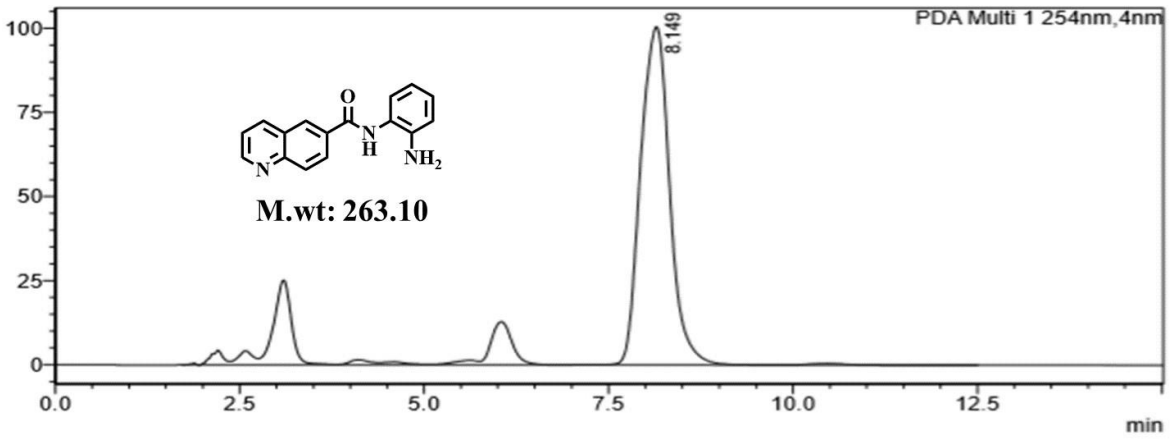
PDA Multi 1 254nm,4nm
8.149
M.wt: 263.10
100
75
50
25
0
0.0
2.5
5.0
7.5
10.0
12.5
min

LCMS:

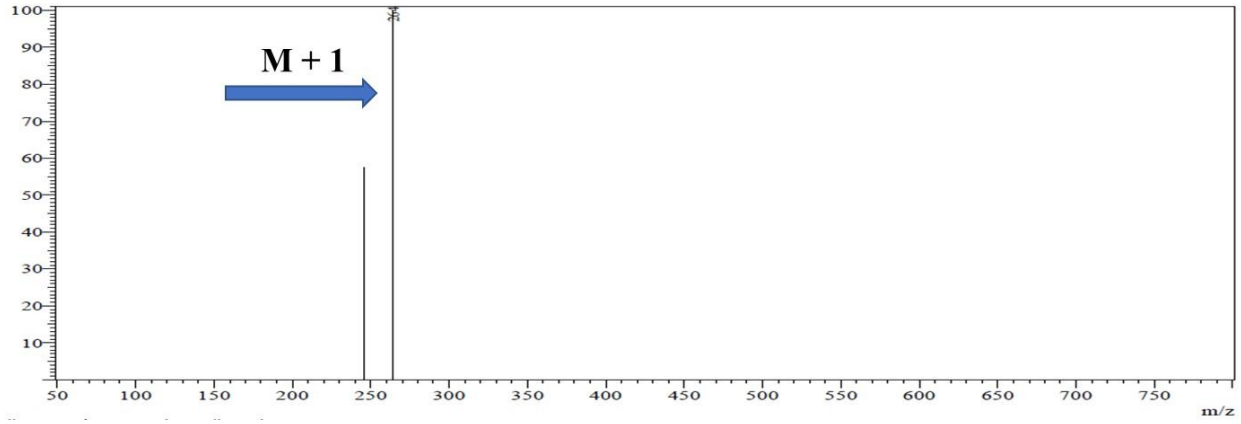

HRMS:

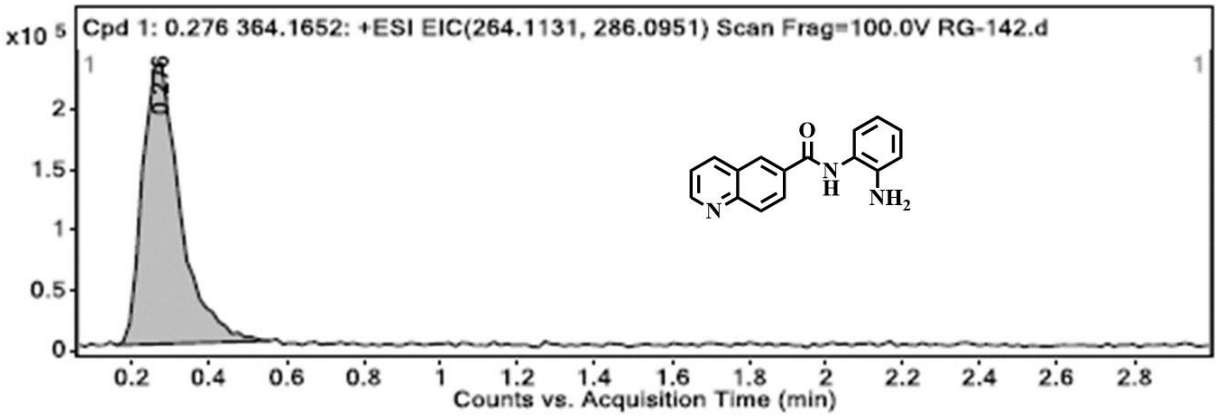

MS Zoomed Spectrum

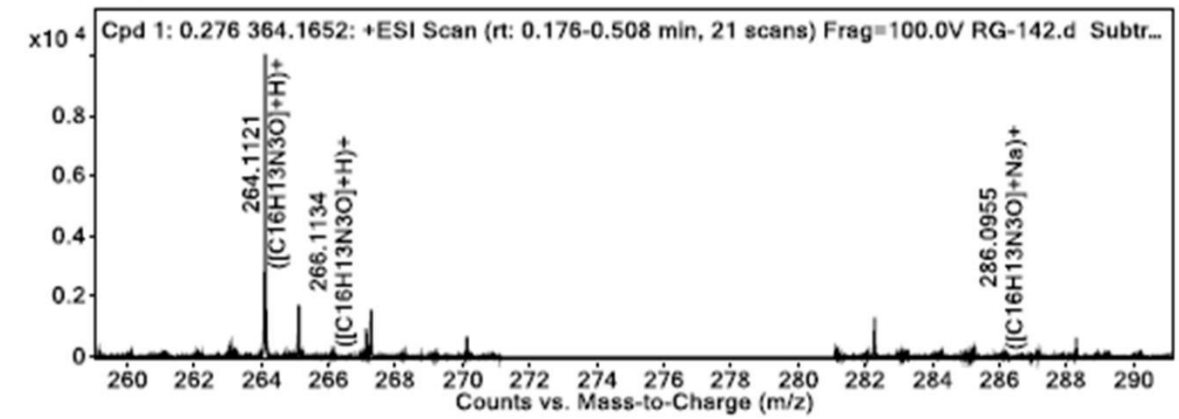

2.4.2.11. Preparation of tert-butyl 2-(1H-indole-6-carboxamido) phenyl carbamate (4f)

Indole-6-carboxylic acid (**3f**) (100 mg; 0.621 mmol) was dissolved in dichloromethane and added Pyridine (5ml) under 0°C. To this mixture, 1-ethyl-3-dimethyl amino propyl carbodiimide (107 mg, 0.690 mmol) and 5mg of 4-dimethyl aminopyridine were added. This mixture was allowed to react under constant stirring for 15min before *tert*-butyl 2-amino phenyl carbamate, (142.08 mg; 0.683 mmol) was added into the reaction mixture. This was allowed to react under constant stirring at room temperature overnight. Pyridine was then evaporated under vacuum. The mixture was then dissolved in ethylacetate and washed with sodium bicarbonate. The organic layer was then separated and the excess solvent was then evaporated under vacuum. The crude product was then purified using column chromatography (solvent system – hexane and ethylacetate (70:30)) in silica 60 – 120 mesh to obtain the final compound **4f** in its pure form. (yield: 84%) ^{1}H NMR (400 MHz, $CDCl_3$) δ : 9.25 (s, 2H), 8.11 (s, 1H), 7.71 (d, 3H), 7.45 (dd, J = 3.6, 3.6 Hz, 1H), 7.33 (dd, J = 3.6, 3.6 Hz, 1H), 7.22 (d, J = 2.4 Hz, 2H), 6.61 (s, 1H), 1.57 (s, 9H).

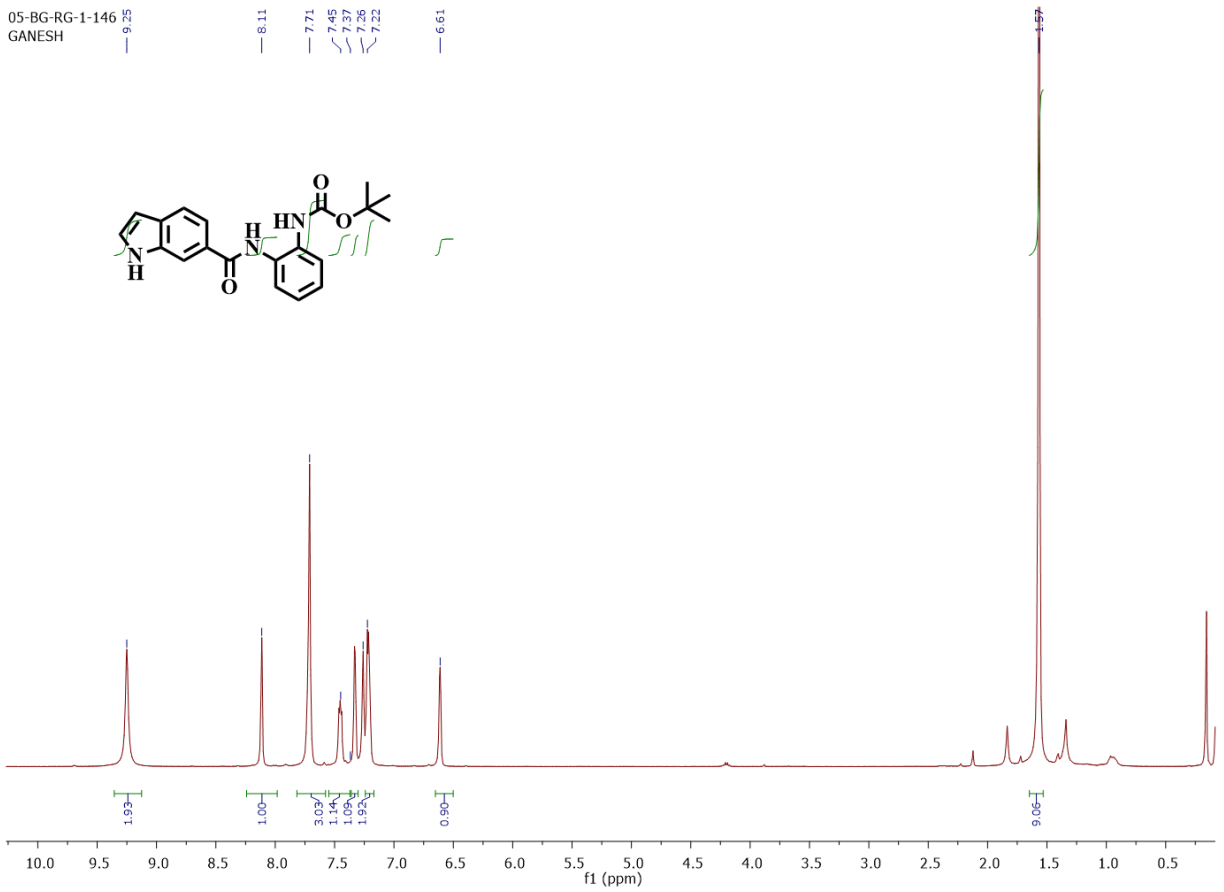

2.4.2.12. Preparation of N-(2-amino phenyl)-1H-indole-6-carboxamide (5f)

The compound *tert*-butyl -2-(1H-indole-6-carboxamido) phenyl carbamate (**4f**) (140 mg; 0.398 mmol) was dissolved in 5ml DCM and 4M dioxane HCl was added to it at 0°C. This mixture was then allowed to react under constant stirring at room temperature for 4h. The dioxane was then evaporated under vacuum. The mixture was then dissolved in ethyl acetate and washed with water. The organic layer was then separated and the excess solvent was evaporated under vacuum. The mixture was then washed with pentane to obtain boc-deprotected final compound. (yield: 70%) ^{1}H NMR (400 MHz, DMSO-d_6) δ : 11.68 (s, 1H), 9.20 (s, 1H), 8.25 (s, 1H), 8.18 (d, 1H), 7.46 (dd, *J* = 3.6,3.6 Hz, 1H), 7.13 (dd, *J* = 2.4, 3.6 Hz, 3H), 6.95 (t, 1H), 6.81 (d, 1H), 6.62 (t, 1H), 4.89 (s, 2H). ^{13}C NMR (101 MHz, DMSO-d_6) δ : 163.74, 143.32, 136.61, 134.79, 129.11, 126.80, 126.23,

124.48, 122.46, 121.53, 120.98, 116.82, 112.34, 110.81. ESI-HRMS: calcd for $C_{15}H_{13}N_3O$ m/z: $[M+H]^+$: 252.1115; found $[M+H]^+$ 252.1131.

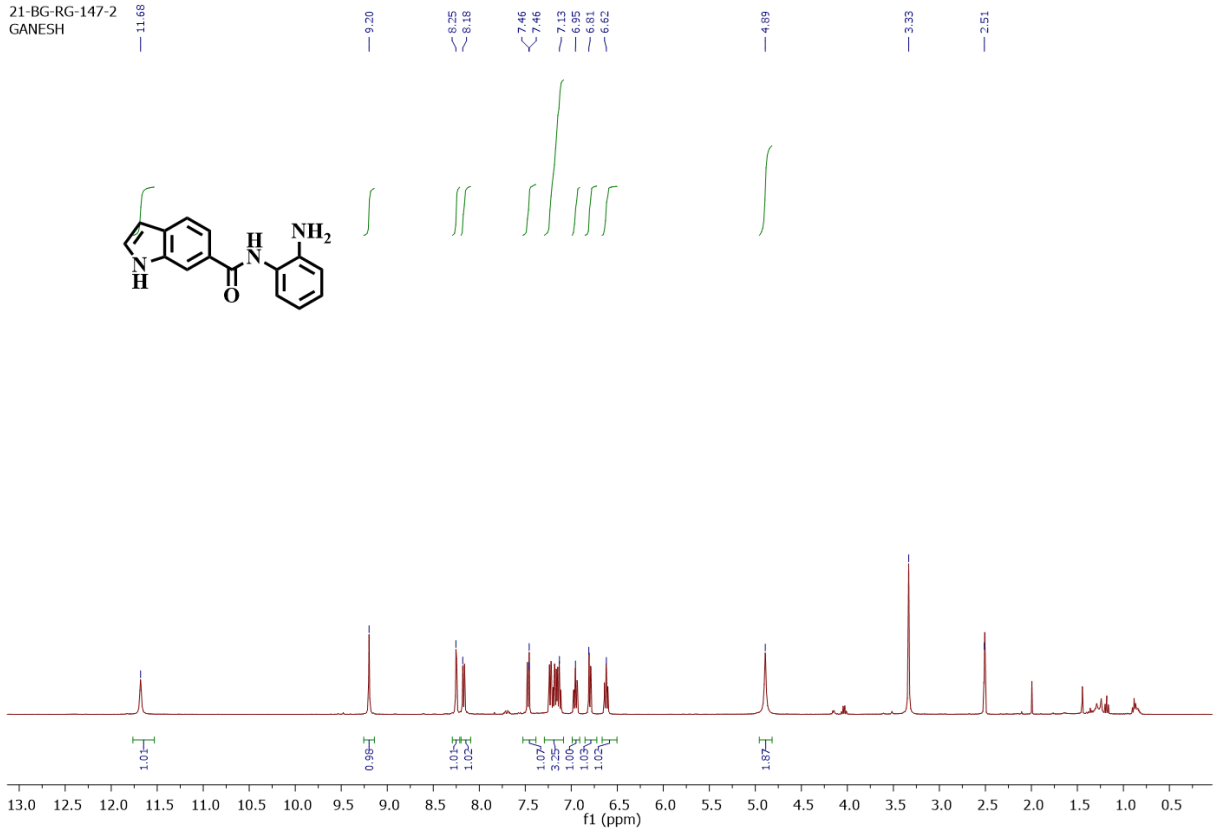

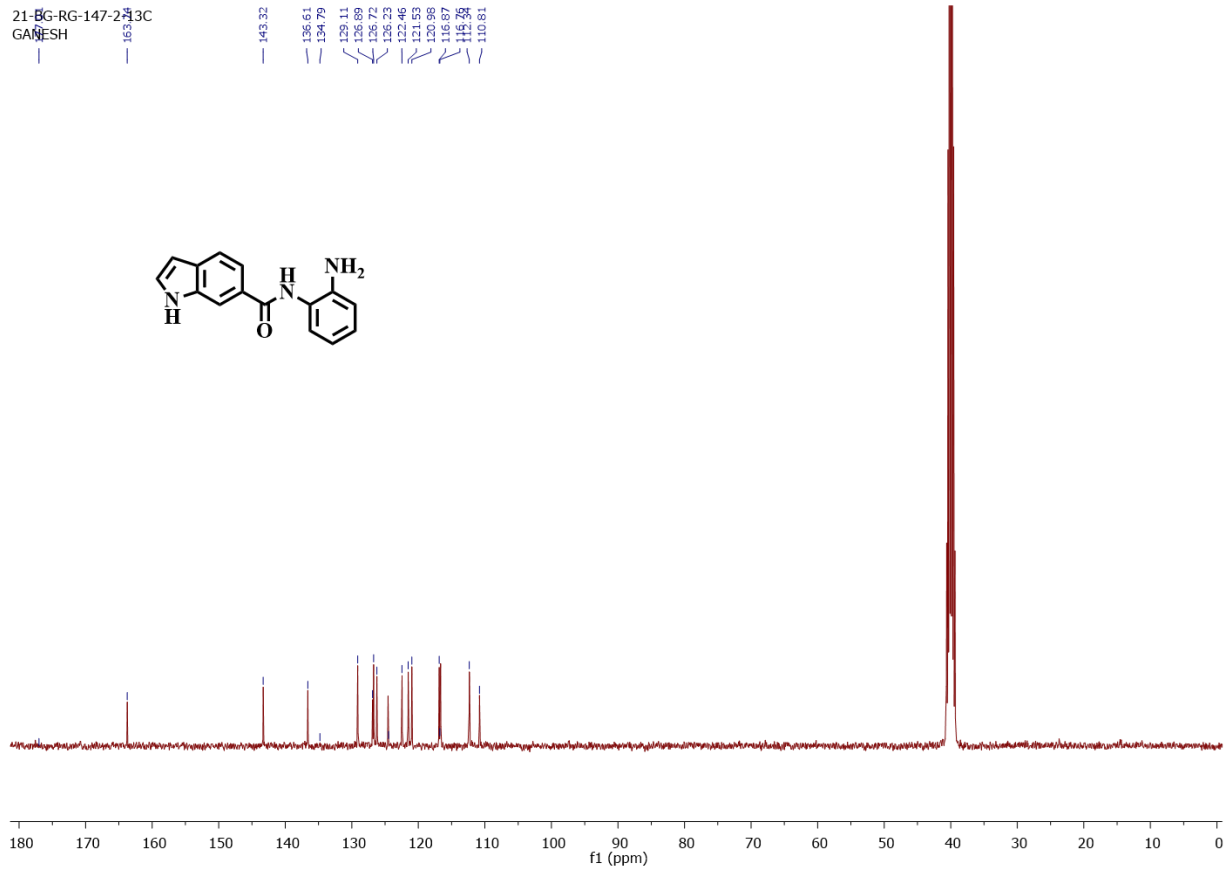
21-BG-RG-147-2-13C
GANESH
143.32
136.61
134.79
129.11
126.89
126.72
126.23
122.46
121.53
120.98
116.87
110.81
NH2
f1 (ppm)

HPLC:

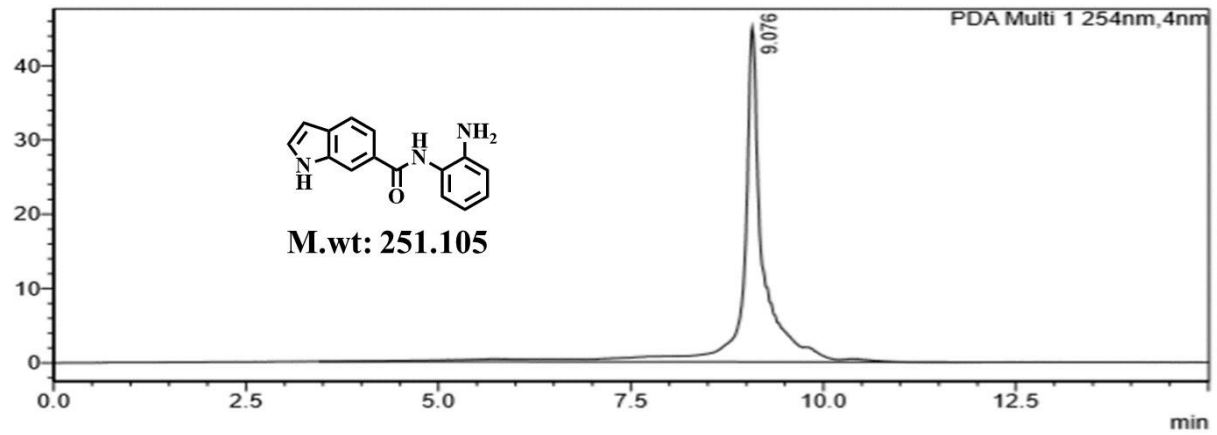
PDA Multi 1 254nm,4nm
9.076
NH2
M.wt: 251.105
min

LCMS:

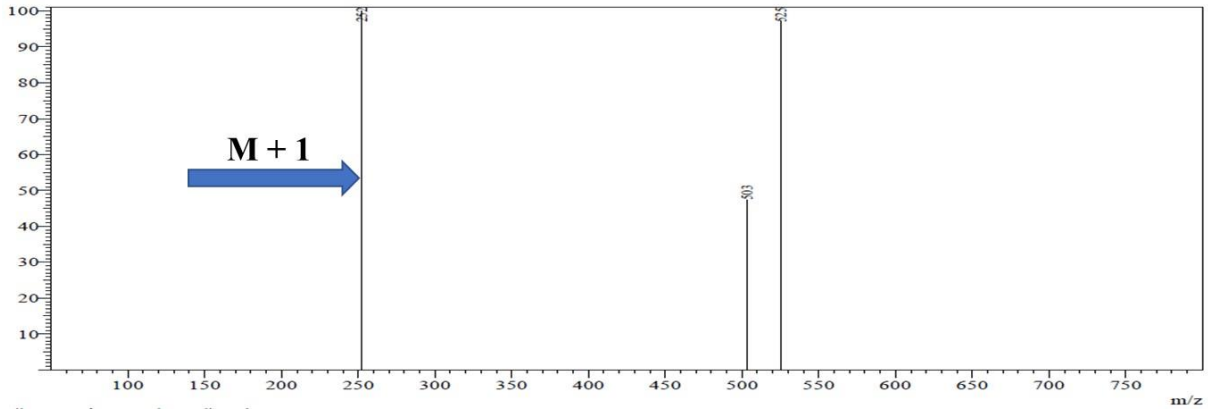

HRMS:

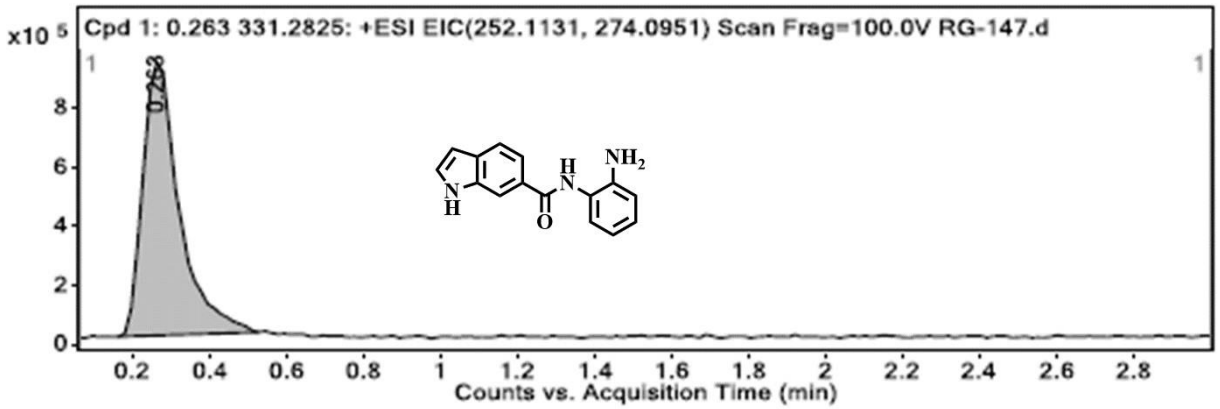

MS Zoomed Spectrum

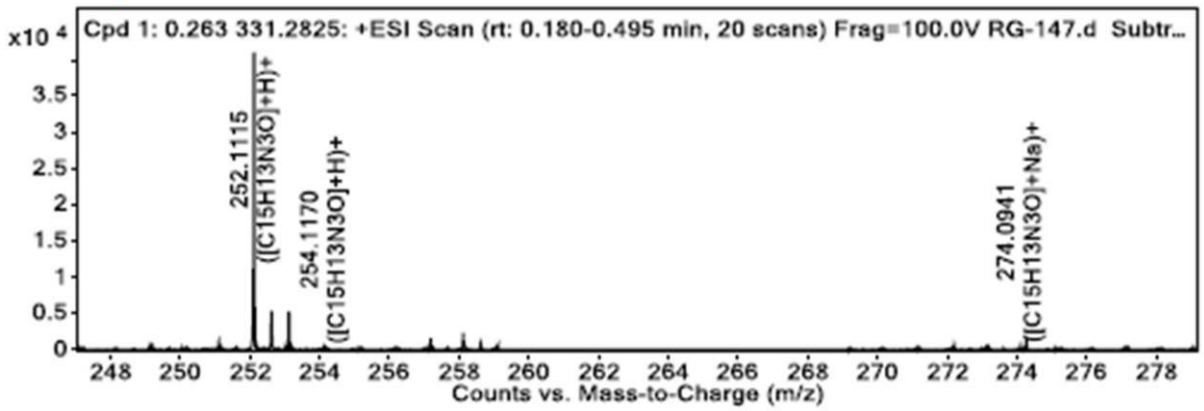

2.4.2.13. Preparation of tert-butyl 2-(1H-indole-3-carboxamido) phenyl carbamate (4g)

Indole-3-carboxylic acid (**3g**) (100 mg; 0.621 mmol) was dissolved in dichloromethane and added Pyridine (5ml) under 0°C. To this mixture, 1-ethyl-3-dimethyl amino propyl carbodiimide, (173.25 mg; 1.11 mmol) and 5mg of 4-dimethyl aminopyridine were added. This mixture was allowed to react under constant stirring for 15min before *tert*-butyl 2-amino phenyl carbamate (142.08 mg; 0.683 mmol) was added into the reaction mixture. This was allowed to react under constant stirring at room temperature overnight. The pyridine was then evaporated under vacuum. The mixture was then dissolved in ethylacetate and washed with sodium bicarbonate. The organic layer was then separated and the excess solvent was then evaporated under vacuum. The crude product was then purified using column chromatography (solvent system – hexane and ethylacetate (70:30)) in silica 230 – 400 mesh to obtain the final compound **4g** in its pure form. (yield: 17%)^{1}H NMR (400 MHz, DMSO-d_6) δ : 11.81 (s, 1H), 9.47 (s, 1H), 8.59 (s, 1H), 8.19 (s, 1H), 8.13 (d, *J = 7.6 Hz*, 1H), 7.57 (dd, *J = 7.2, 7.6 Hz*, 3H), 7.15 (dd, *J = 6.8, 6.8 Hz*, 4H), 1.44 (s, 9H). $C_{20}H_{21}N_3O_3$[M]: 351.15; MS (ESI) *m/z*: $[M-H]^+$: 350.250.

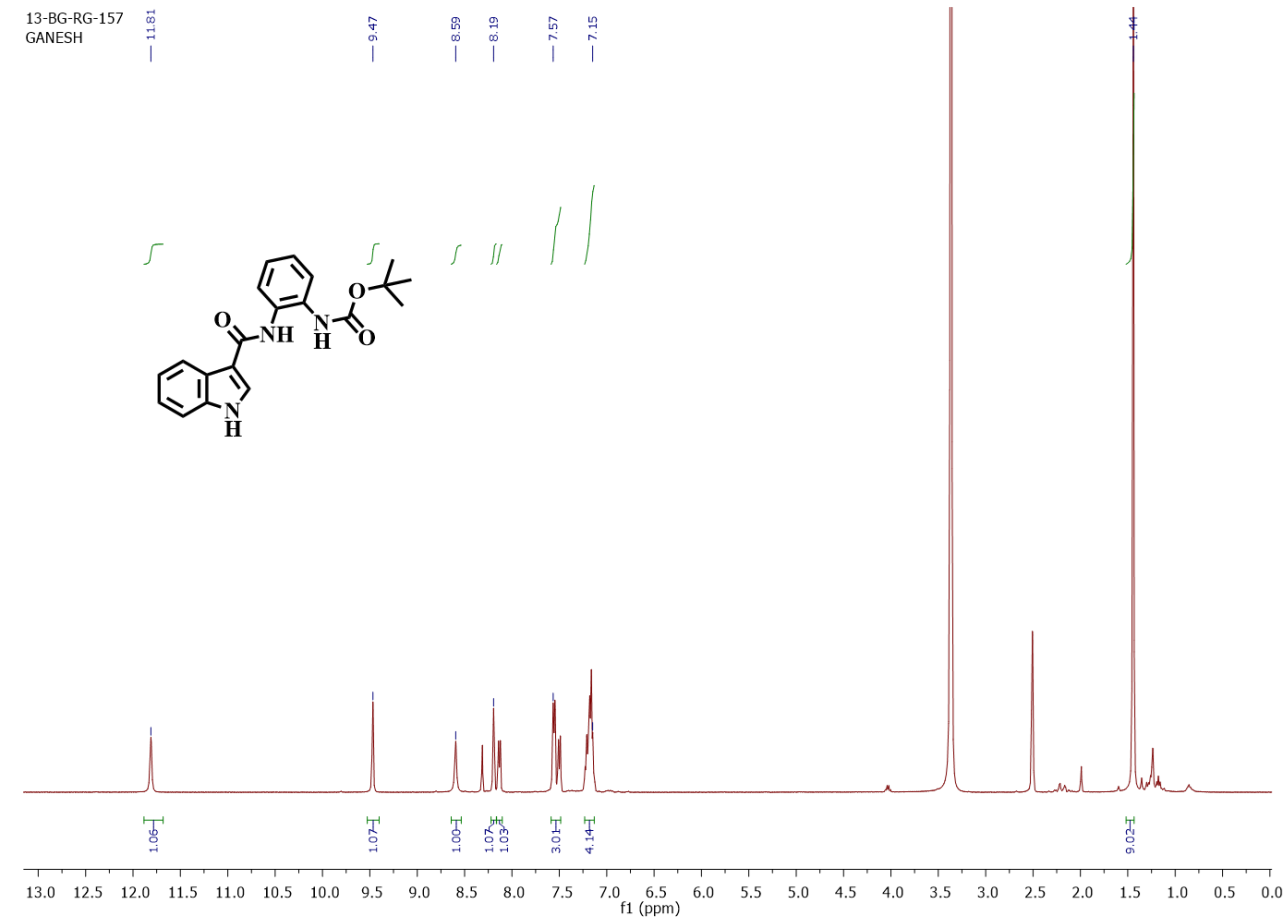

2.4.2.14. Preparation of N-(2-amino phenyl)-1H-indole-3-carboxamide (5g)

The compound *tert*-butyl-2-(1H-indole-6-carboxamido) phenyl carbamate (**4g**) (32 mg; 0.09 mmol) was dissolved in 5ml DCM and 4M dioxane HCl was added to it at 0°C. This mixture was then allowed to react under constant stirring at room temperature for 2h. Dioxane was then evaporated under vacuum. The mixture was then dissolved in ethylacetate and washed with water. The organic layer was then separated and excess solvent was evaporated under vacuum. The mixture was then washed with pentane to obtain boc-deprotected final compound **5g**. (yield: 57.3%).^{1}H NMR (400 MHz, DMSO-d_6) δ : 11.51 (s, 1H), 9.04 (s, 1H), 8.07 (d, *J = 7.1 Hz*, 2H), 7.29 (d, *J =8.0 Hz*,1H), 7.04 (d, *J = 3.8 Hz*, 3H), 6.78 (t, *J = 6.4 Hz*,1H), 6.64 (dd, *J= 1.2, 1.2 Hz*,

1H), 6.47 (dd, *J = 1.6, 1.2 Hz,* 1H), 4.72 (s, 2H).^{13}C NMR (101 MHz, DMSO-d_6) δ : 164.09, 136.61, 128.93, 126.82, 126.37, 124.54, 122.48, 121.52, 121.00, 116.68, 112.35, 111.17 – 110.98. ESI-HRMS: calcd for $C_{15}H_{13}N_3O$ m/z: $[M+H]^+$: 252.1121; found $[M+H]^+$: 252.1131.

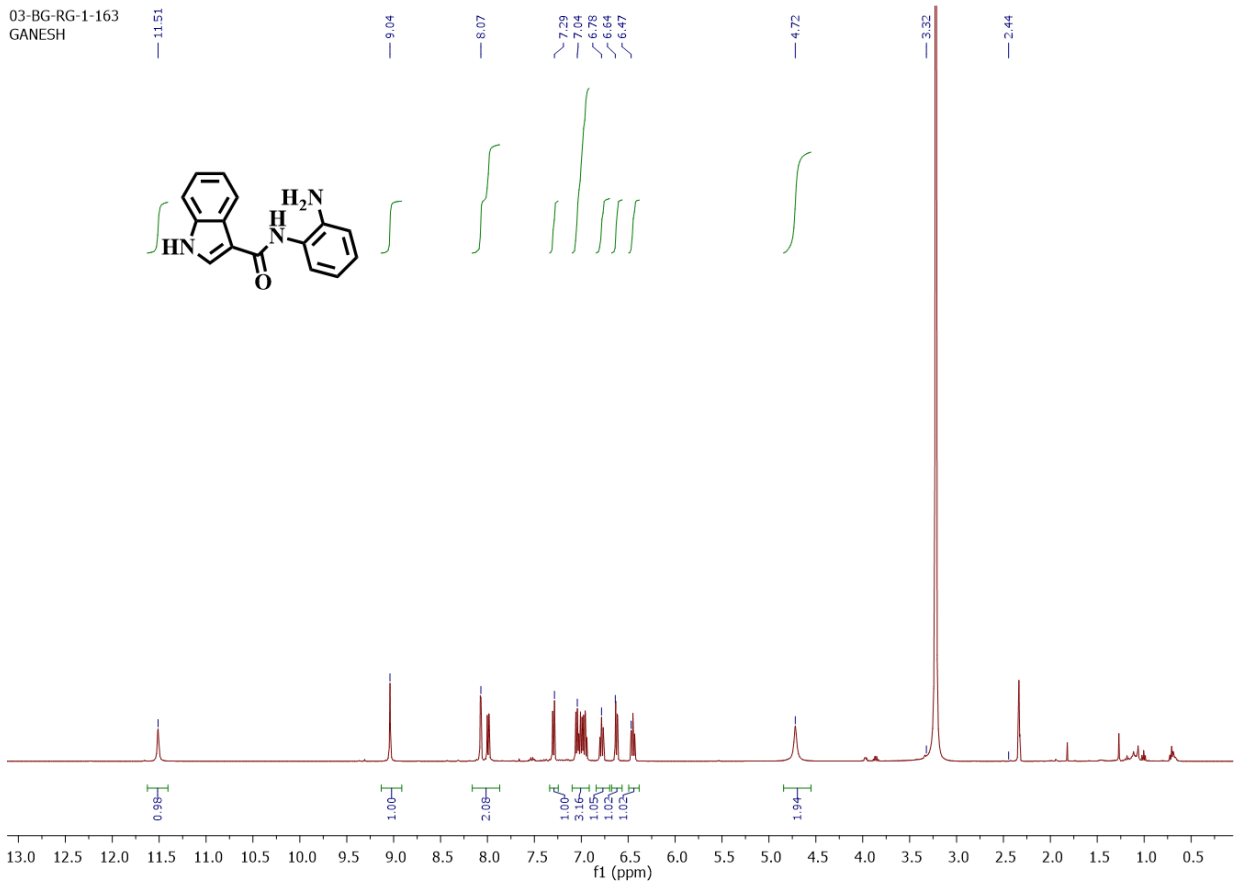

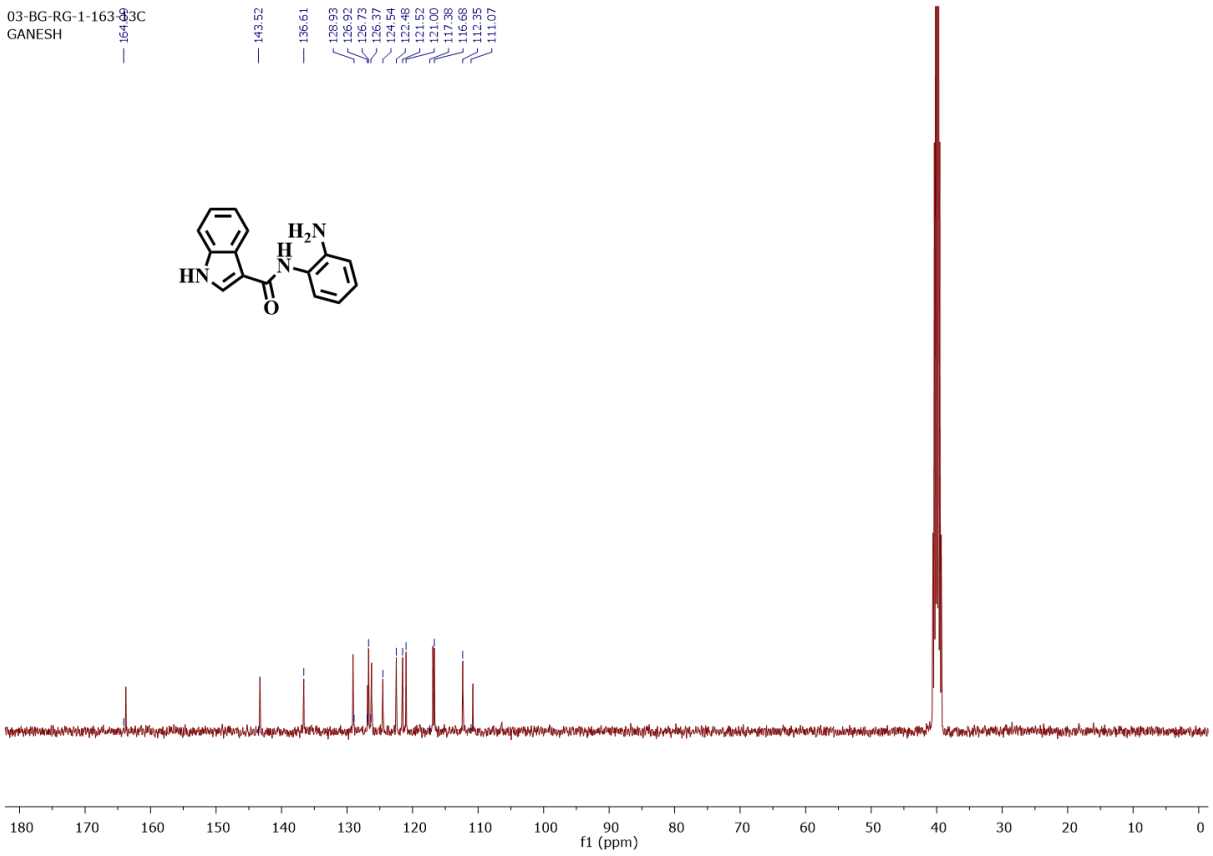
03-BG-RG-1-163-13C
GANESH
164.00
143.52
136.61
128.93
126.92
126.73
126.37
124.54
122.48
121.52
121.00
117.38
116.68
112.35
111.07
H2N
H
N
HN
O
180 170 160 150 140 130 120 110 100 90 80 70 60 50 40 30 20 10 0
f1 (ppm)

HPLC:

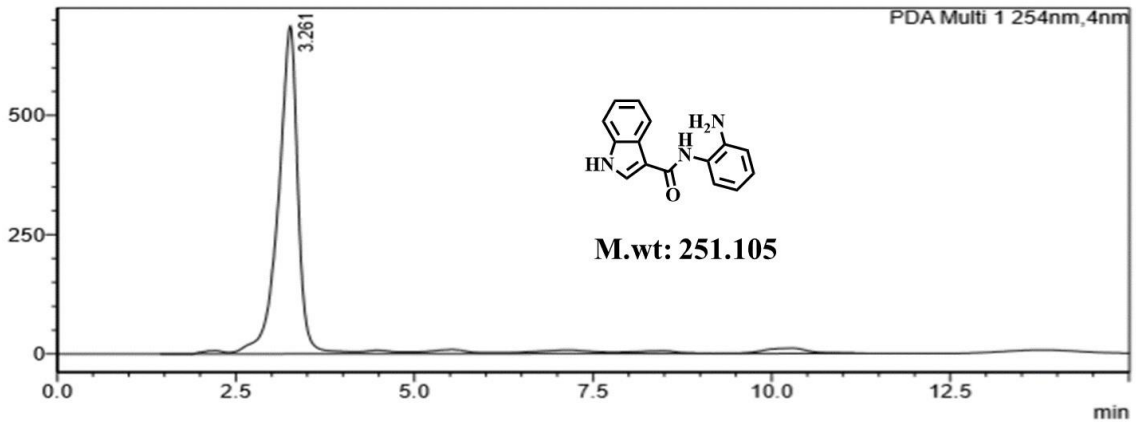
PDA Multi 1 254nm,4nm
3.261
500
250
0
0.0 2.5 5.0 7.5 10.0 12.5
min
H2N
H
N
HN
O
M.wt: 251.105

LCMS:

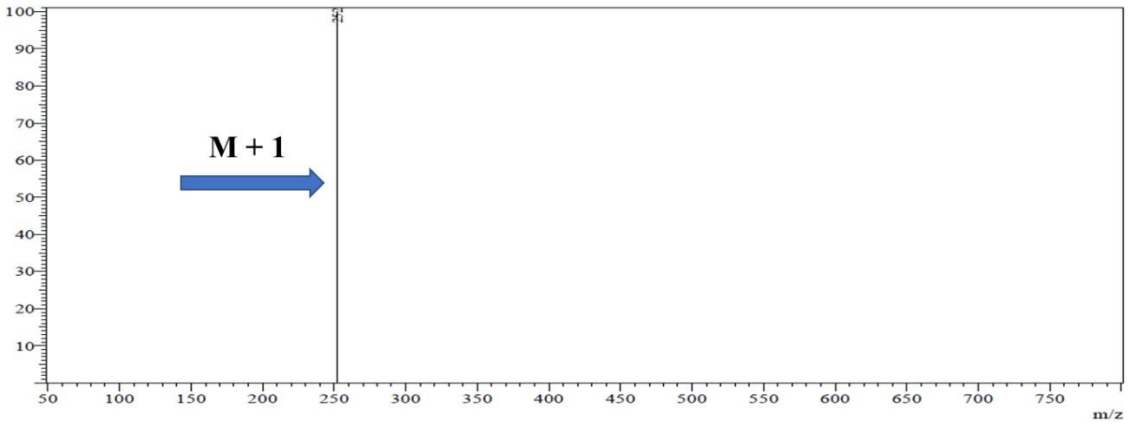

HRMS:

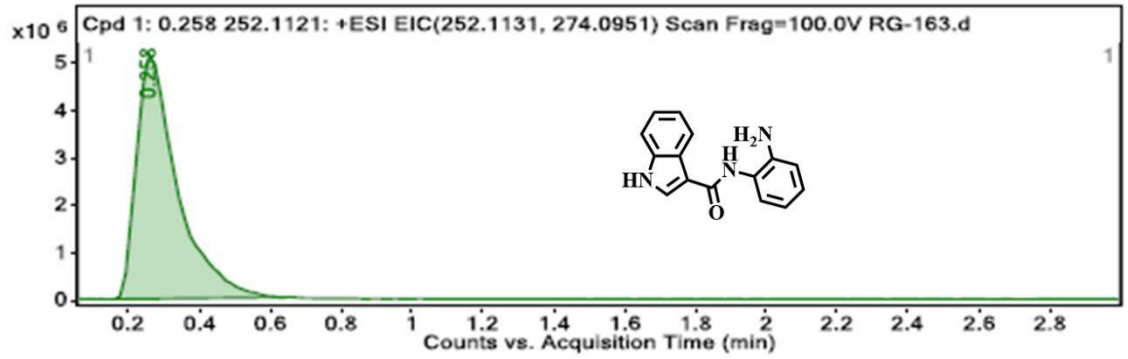

MS Zoomed Spectrum

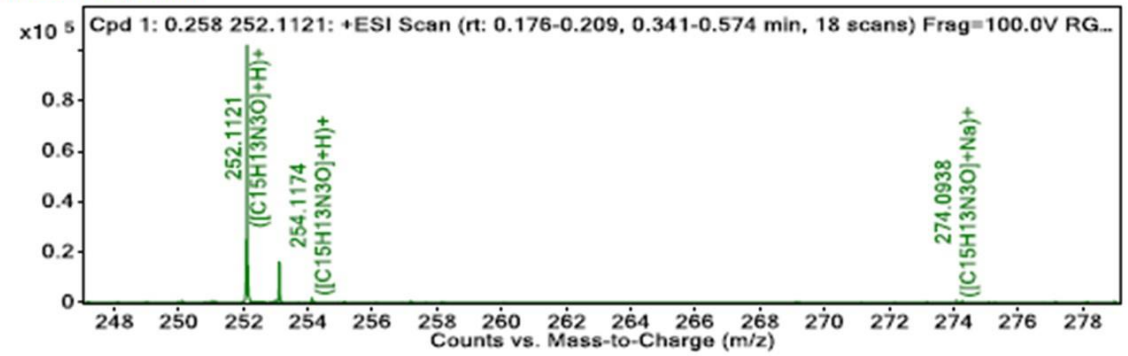

2.4.2.15. Preparation of tert-butyl 2-(thiophene-3-carboxamido) phenyl carbamate (4h)

Thiophene-3-carboxylic acid (**3h**) (100 mg; 0.900 mmol) was dissolved in dichloromethane and added pyridine (5ml) at 0°C. To this mixture, 1-ethyl-3-dimethyl amino propyl carbo di imide, (251 mg; 1.62 mmol) and 5 mg of 4-dimethylamino pyridine were added. This mixture was allowed to react under constant stirring for 15min before *tert*-butyl 2-amino phenyl carbamate (206 mg; 0.990 mmol) was added into the reaction mixture. This was allowed to react under constant stirring at room temperature overnight. Pyridine was then evaporated under vacuum. The mixture was then dissolved in ethylacetate and washed with sodium bicarbonate. The organic layer was then separated and excess solvent was then evaporated under vacuum. The crude product was then purified using column chromatography (solvent system – DCM and ethylacetate (5:95)) in silica 230 – 400 mesh to obtain the final compound **4h** in its pure form. (yield: 43%)^{1}H NMR (400 MHz, $CDCl_3$) δ : 9.12 (s, 1H), 8.05 (s, 1H), 7.72 (d, *J = 8 Hz*, 1H), 7.57 (d, *J = 1.2 Hz*, 1H), 7.38 (dd, *J = 2.8, 2.8 Hz*, 1H), 7.21 (dd, *J = 1.2, 1.6 Hz*, 3H), 6.84 (s, 1H), 1.52 (s, 9H). $C_{16}H_{20}N_2O_3S$ [M]: 318.10; MS (ESI) *m/z* : $[M-H]^+$: 317.200.

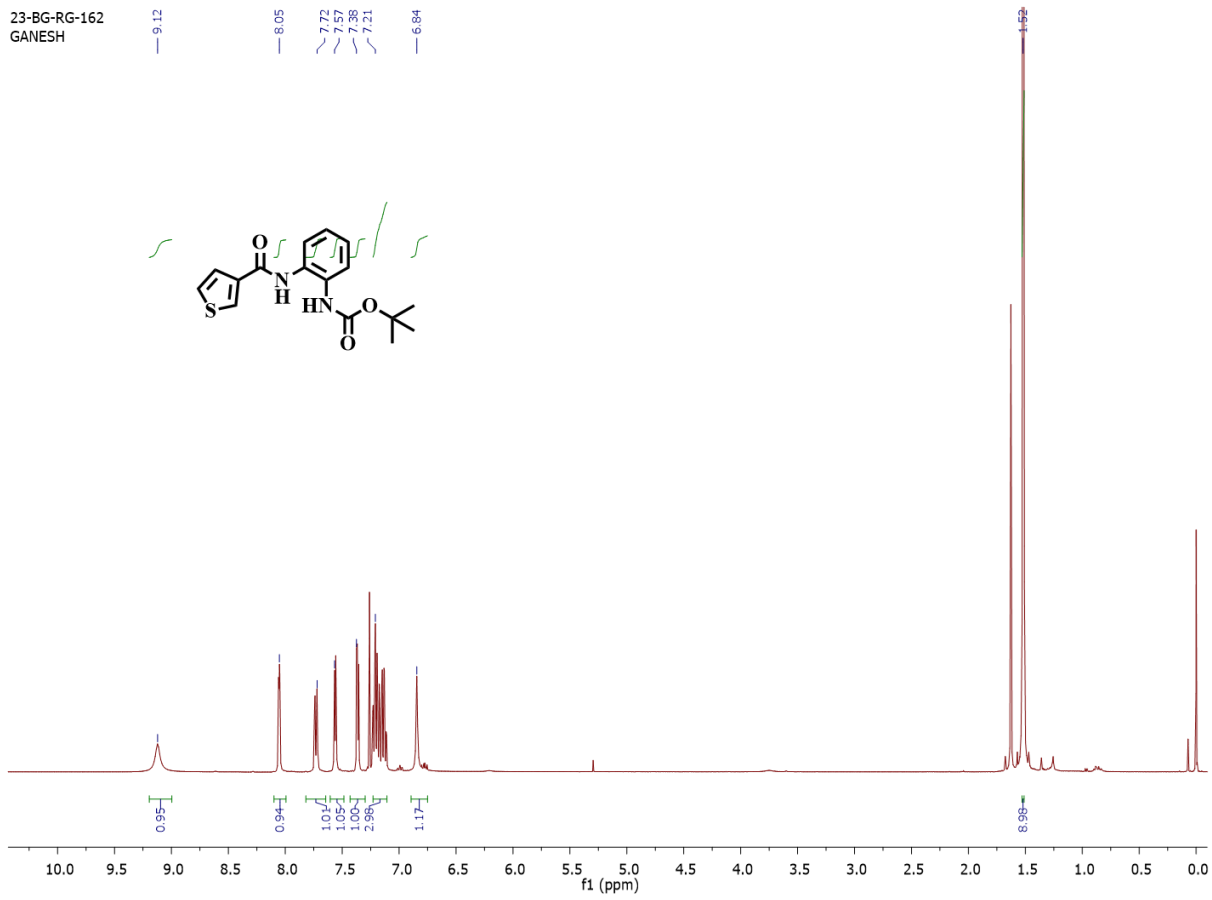

2.4.2.16. Preparation of N-(2-amino phenyl)-thiophene-3-carboxamide: (5h)

The compound *tert*-butyl-2-(thiophene-3-carboxamido) phenyl carbamate (**4h**) (100 mg; 0.314 mmol) was dissolved in 5ml DCM and 4M dioxane HCl was added to it at 0°C. This mixture was then allowed to react under constant stirring at room temperature for 2h. Dioxane was then evaporated under vacuum. The mixture was then dissolved in ethylacetate and washed with water. The organic layer was then separated and excess solvent was evaporated under vacuum. The mixture was then washed with pentane to obtain boc-deprotected final compound **5h**. (yield: 86%).^{1}H NMR (400 MHz, DMSO-d_6) δ : 9.58 (s, 1H), 8.37 (s, 1H), 7.68 (d, *J = 2.0 Hz*, 2H), 7.18 (d, *J = 0.8 Hz*, 1H), 7.03 (t, *J = 1.6 Hz*, 1H), 6.85 (d, *J = 1.2 Hz*, 1H), 6.67 (t, *J = 0.8 Hz*, 1H), 4.94 (s, 2H).^{13}C NMR (101 MHz, DMSO-d_6) δ : 161.46, 143.96, 138.18, 129.97, 127.77,

127.260,127.14,127.01,126.72, 123.49, 116.64. ESI-HRMS: calcd for $C_{16}H_{18}N_2O_3S$ m/z: $[M+H]^+$: 219.0575; found $[M+H]^+$: 219.0587.

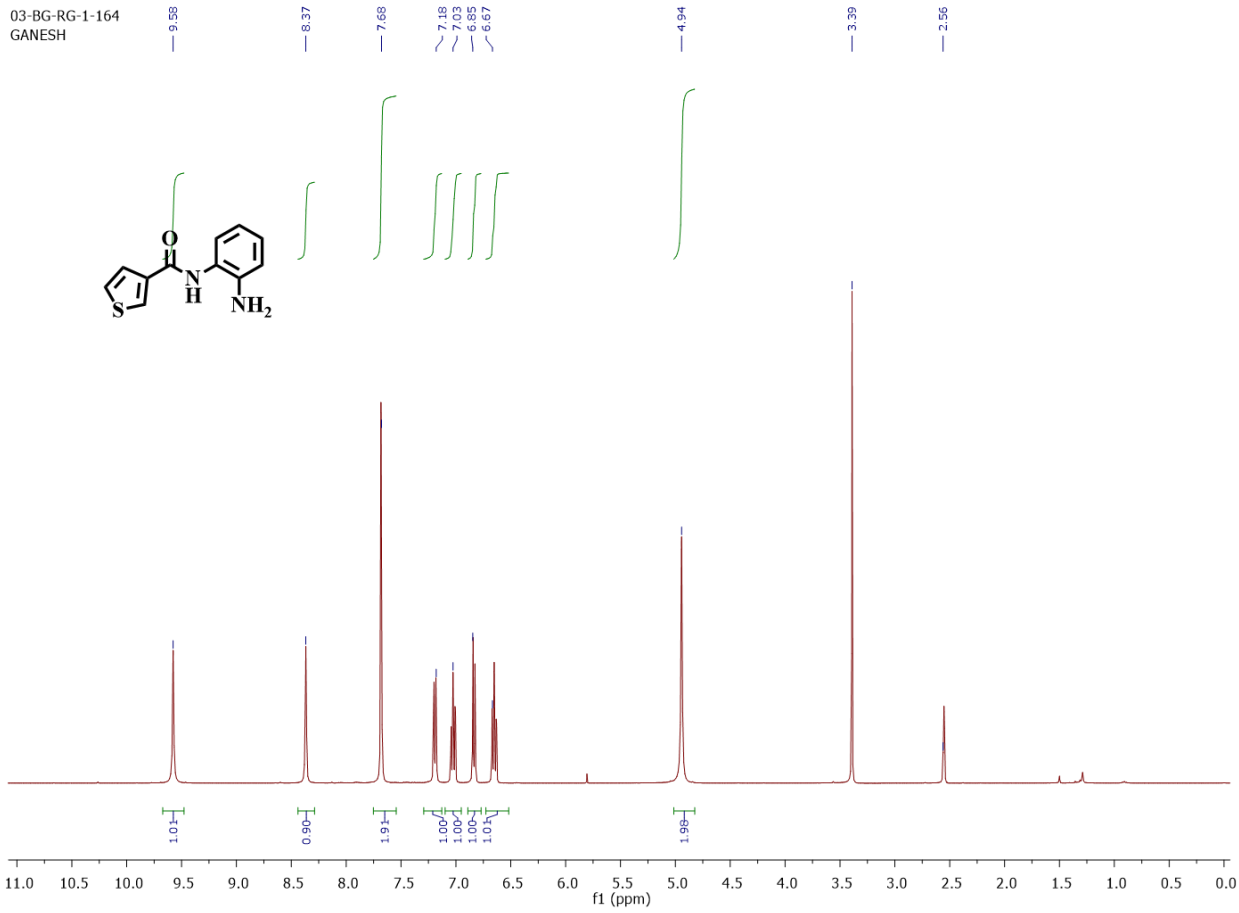

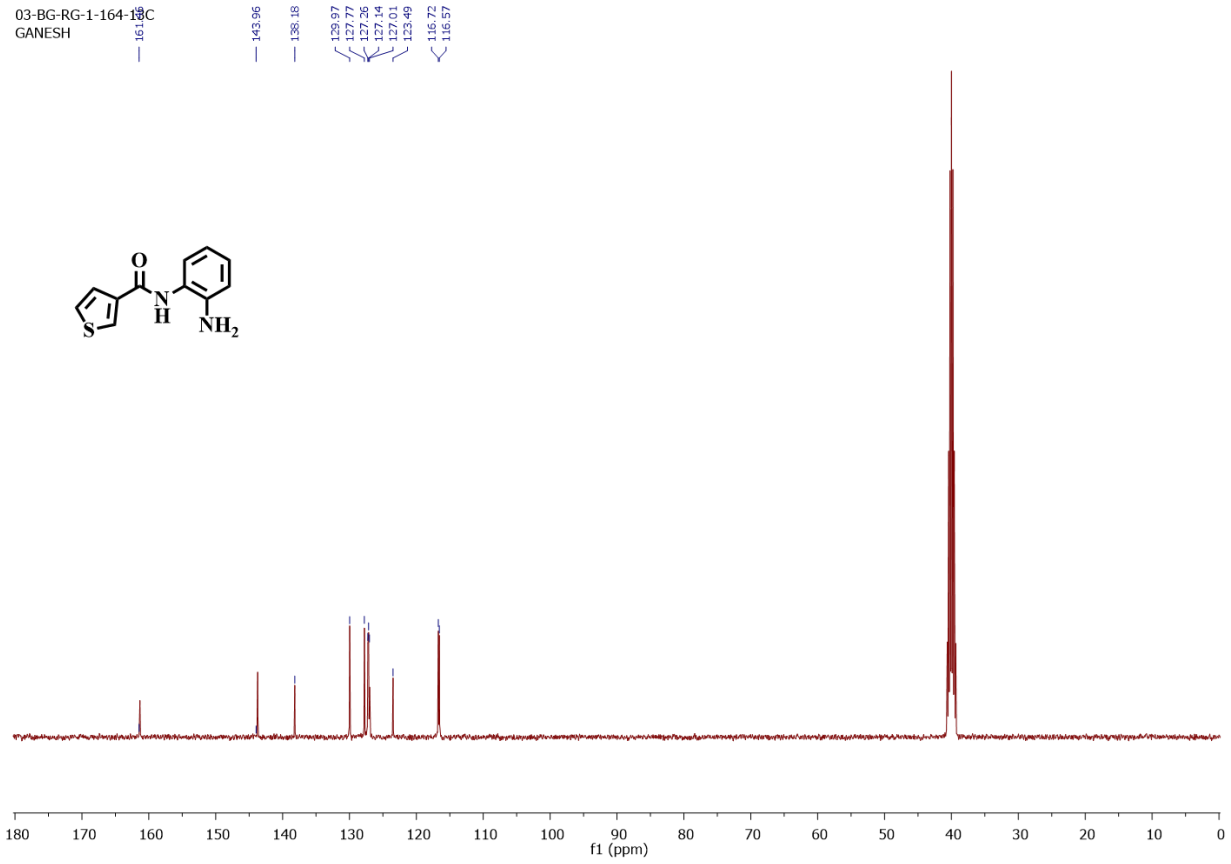
03-BG-RG-1-164-13C
GANESH
161.15
143.96
138.18
129.97
127.77
127.36
127.14
127.01
123.49
116.72
116.57
O
N
H
S
NH2
180 170 160 150 140 130 120 110 100 90 80 70 60 50 40 30 20 10 0
f1 (ppm)

HPLC:

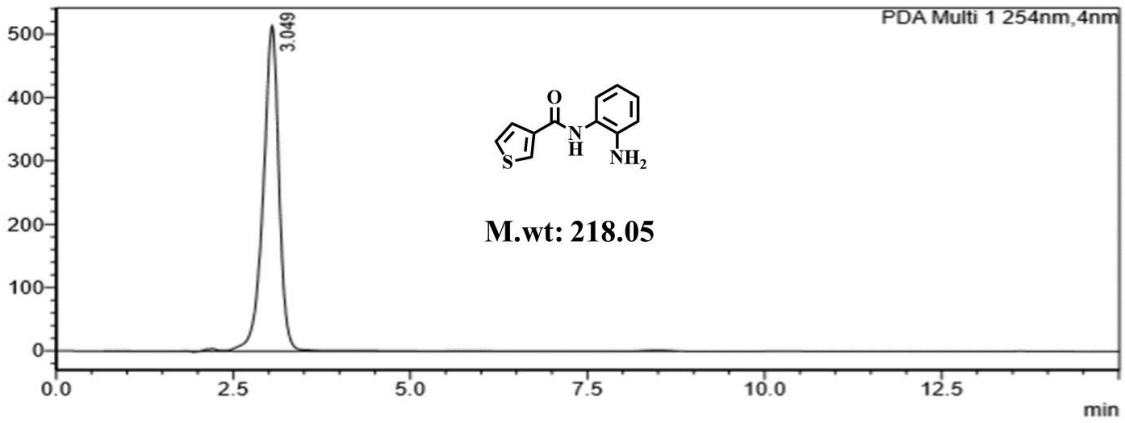
PDA Multi 1 254nm,4nm
3.049
500
400
300
200
100
0
0.0 2.5 5.0 7.5 10.0 12.5
min
O
N
H
S
NH2
M.wt: 218.05

LCMS:

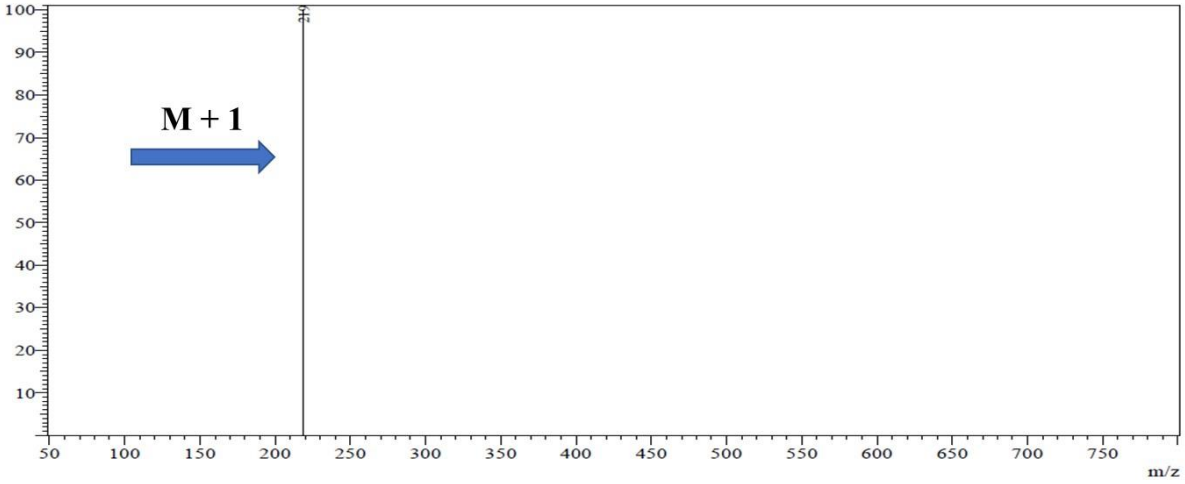
M + 1
m/z

HRMS:

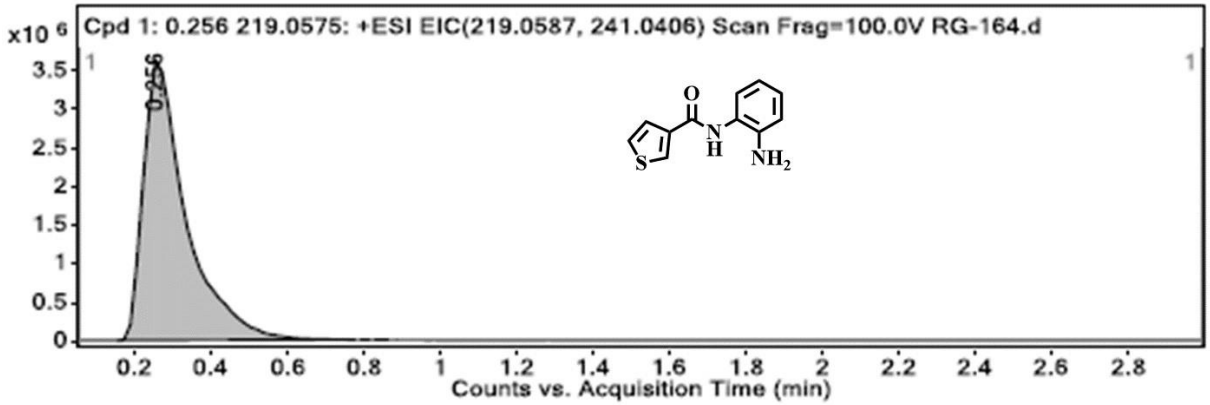
Cpd 1: 0.256 219.0575: +ESI EIC(219.0587, 241.0406) Scan Frag=100.0V RG-164.d
0.256
Counts vs. Acquisition Time (min)

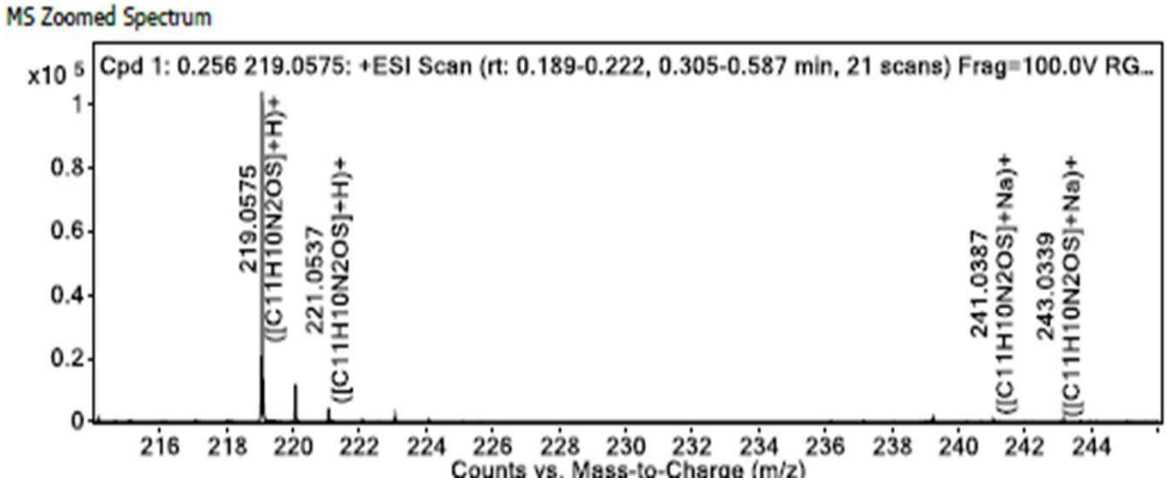
MS Zoomed Spectrum
Cpd 1: 0.256 219.0575: +ESI Scan (rt: 0.189-0.222, 0.305-0.587 min, 21 scans) Frag=100.0V RG...
219.0575 ([C11H10N2OS]+H)+
221.0537 ([C11H10N2OS]+H)+
241.0387 ([C11H10N2OS]+Na)+
243.0339 ([C11H10N2OS]+Na)+
Counts vs. Mass-to-Charge (m/z)

2.4.2.17. Preparation of N-phenyl-6-(phenyl amino) pyrazine-2-carboxamide (2i):

Aniline was added to a solution of methyl 6-chloro pyrazine-2-carboxylate (**1i**) in *N*methylpyrrolidine at 0°C. To the reaction mixture diisopropyl amine was added at the same temperature and the reaction was heated to 160°C for 20h. The completion of the reaction was monitored by TLC. Water was added to the reaction mixture and the crude compound was extracted with ethyl acetate, dried using anhydrous sodium sulphate, solvent was evaporated using rota evaporator. The obtained crude product was purified by column chromatography. ^{1}H NMR (400 MHz, DMSO -d_6) δ : 10.08 (s, 1H), 9.89 (s, 1H), 8.56 (s, 1H), 8.49 (s, 1H), 7.80 (d, *J = 9.8 Hz*, 4H), 7.47 (dd, *J* = 5.2, 5.2 *Hz*, 4H), 7.20 (t, *J* = 8.0 Hz, 1H),7.12 (t, *J = 6.4 Hz*, 1H). $C_{17}H_{14}FN_4O$ [M]: 290.32; MS (ESI) *m/z*: $[M+H]^+$: 291.07.

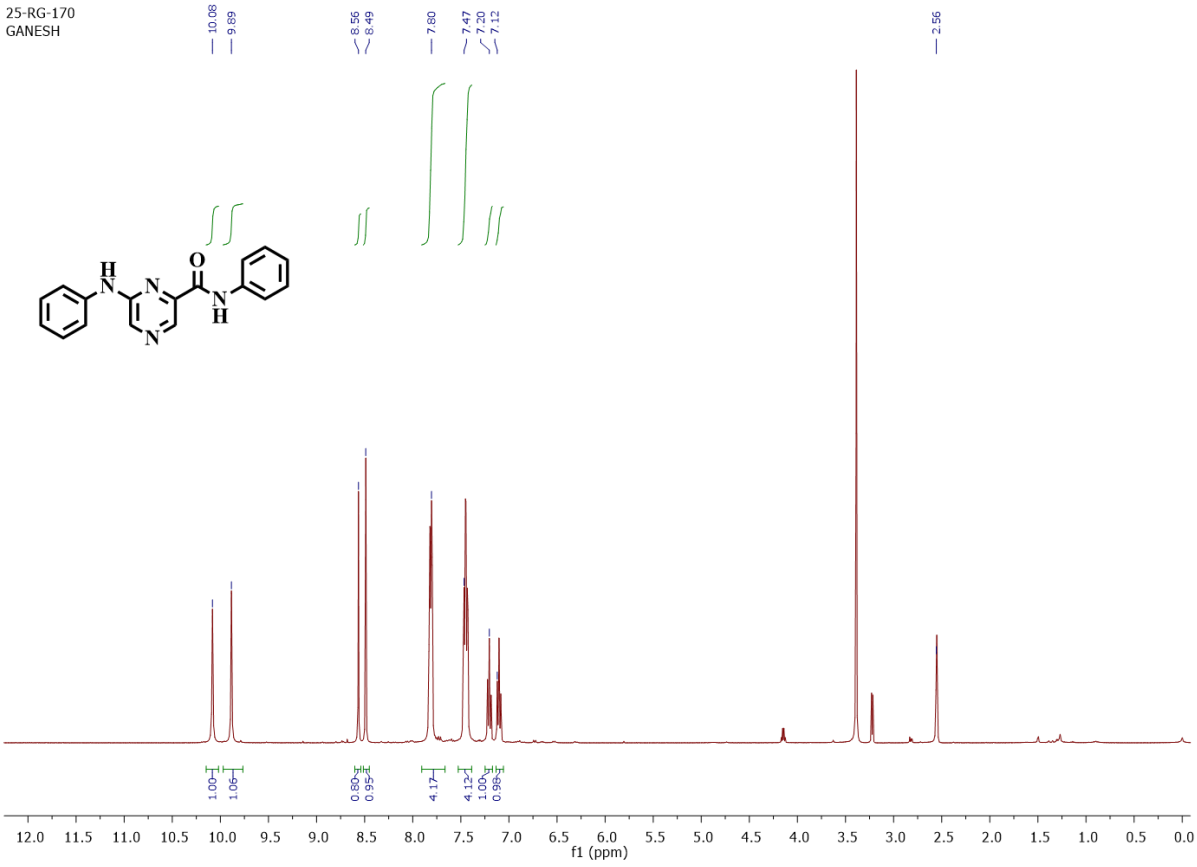

2.4.2.18. Preparation of 6-(phenyl amino) pyrazine-2-carboxylic acid (3i):

N-phenyl-6-(phenyl amino) pyrazine-2-carboxamide (**2i**) was dissolved in methanol and aqueous sodium hydroxide was added to the reaction mixture and the reaction was stirred at 80°C for 1h. The reaction was cooled at room temperature, added ice-cold water and neutralised with 1N HCl. The compound was extracted with ethylacetate, dried using sodium sulphate and the excess solvent was evaporated using rota evaporator. The obtained crude mixture was purified by column chromatography (solvent system – dichloromethane and methanol (7:3)). ^{1}H NMR (400 MHz, DMSO-d_6) δ : 9.79 (s, 1H), 8.47 (s, 2H), 7.71 (d, *J = 6.0 Hz*, 2H), 7.34 (t, 2H), 7.03 (t, 1H). $C_{11}H_9N_3O_2$[M]: 215.21; MS (ESI) *m/z*: $[M+H]^+$: 216.18.

***2.4.2.19. Preparation of tert-butyl 2- (amino phenyl)-6-phenylamino pyrazine-2-carbamate (4i)*:**

To a solution of dichloromethane and pyridine (1:1) was added to 6-(phenyl amino) pyrazine -2carboxylic acid (**3i**) (50 mg; 0.232 mmol). To this reaction mixture, 1-ethyl-3-dimethyl amino propyl carbo di imide (64.72 mg; 0.417 mmol) and catalytic amount of 4-dimethylamino pyridine were added in nitrogen environment. The mixture was stirred at room temperature for 15min. After 15min, *tert*-butyl 2-amino phenyl carbamate (53.209 mg; 0.255 mmol) was added into the reaction mixture and reaction was continued for 12h. The reaction was monitored with TLC. After completion of the reaction, pyridine was then evaporated under vacuum. The mixture was then dissolved in sodium bicarbonate and extracted with ethyl acetate. The organic layer was then separated and dried with Na_2SO_4. The dried solvent was evaporated under vacuum. The crude product was then purified using column chromatography (solvent system – hexane and ethylacetate (50:50)) in silica 230 – 400 mesh to obtain the final compound **4i** in its pure form. (Yield: 89%). ^{1}H NMR (400 MHz, DMSO-d_6) δ : 9.86 (s, 2H), 9.04 (s, 1H), 8.56 (s, 1H), 8.45 (s, 1H), 7.96 (d, *J* = 7.6 Hz, 1H), 7.77 (d, *J* = 8.0 Hz, 2H), 7.42 (t, *J* = 7.6 Hz, 2H), 7.29 (dd, *J* = 7.6,7.6 Hz, 2H),

7.18 (t, *J* = 6.4 Hz, 1H), 7.02 (t, *J* = 7.6 Hz, 1H), 1.20 (s, 9H). $C_{22}H_{23}N_5O_3$ [M]: 405.45; MS (ESI) m/z: $[M+H]^+$: 406.57

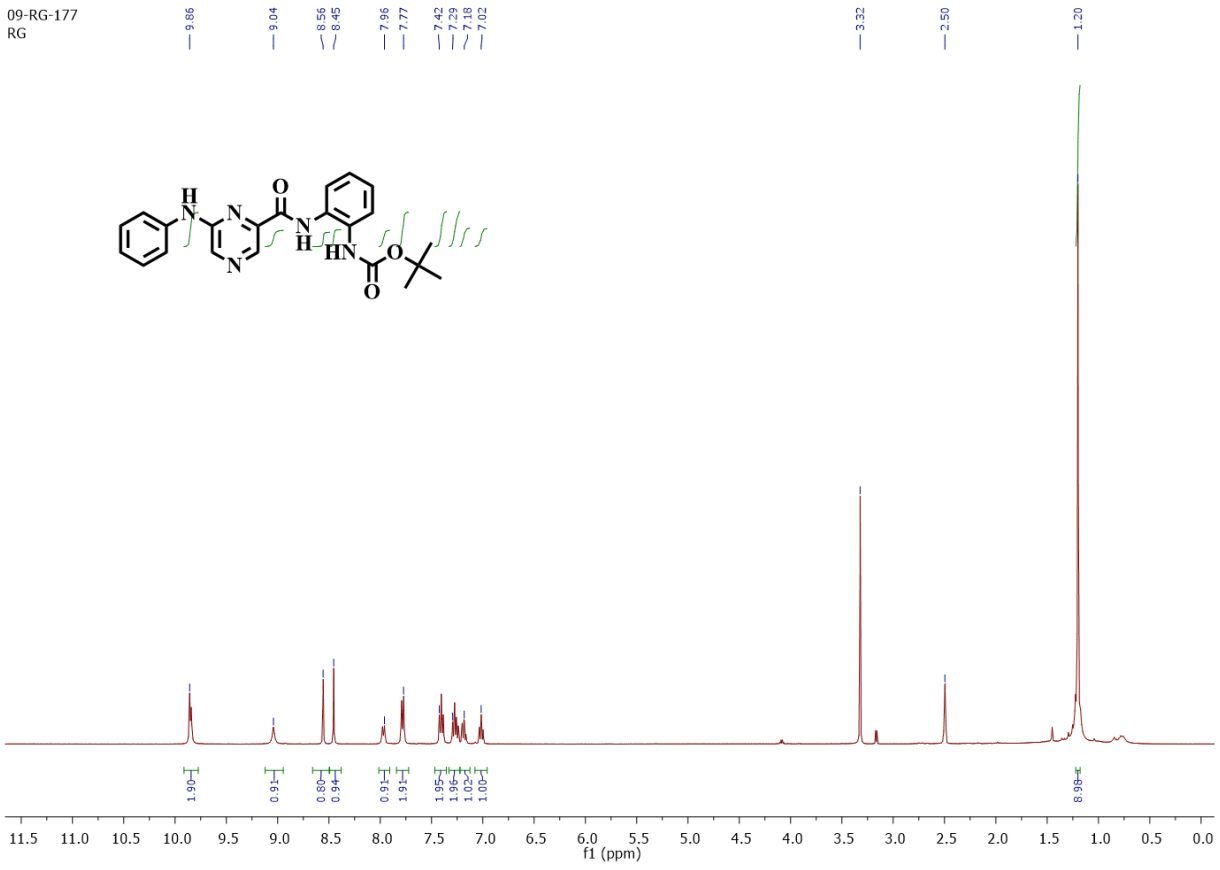

2.4.2.20. Preparation of N-(2-aminophenyl)-6-phenylamino pyrazine-2-carboxamide (5i)

The compound *tert*-butyl 2-(amino phenyl)-6-phenylamino pyrazine-2-carbamate (**4i**) (100 mg; 0.276 mmol) was dissolved in dichloromethane (5mL) and treated with the solution of 4M dioxane in HCl at 0°C. This mixture was then allowed to react under constant stirring at room temperature for 2h. The reaction was monitored by TLC. After completion of the reaction, solvent was then evaporated under vacuum. The resulting compound was then dissolved in water and extracted with ethyl acetate. The organic layer was then separated, dried with Na_2SO_4 and excess solvent was evaporated under vacuum. The mixture was then washed with pentane to obtain boc-deprotected

final compound (Yield: 88.88%). ^{1}H NMR (400 MHz, $CDCl_3$) δ : 9.42 (s, 1H), 8.87 (s, 1H), 8.40 (s, 1H), 7.54 (d, J = 7.6 Hz 1H), 7.43 (m, 4H), 7.18 (t , J = 6.8 Hz, 1H), 7.09 (t, J = 7.2 Hz, 1H), 6.87 (dd, J = 11.5, 7.8 Hz, 2H), 6.77 (s, 1H), 3.95 (s, 2H). ^{13}C NMR (101 MHz, $CDCl_3$) δ : 161.12, 150.14, 141.22, 139.82, 138.40, 136.30, 134.25, 129.56, 126.88, 124.54, 124.13, 121.03, 119.95, 118.29. ESI-HRMS: calcd for $C_{17}H_{15}N_5O$ m/z: $[M+H]^+$: 306.1335; found $[M+H]^+$: 306.1349.

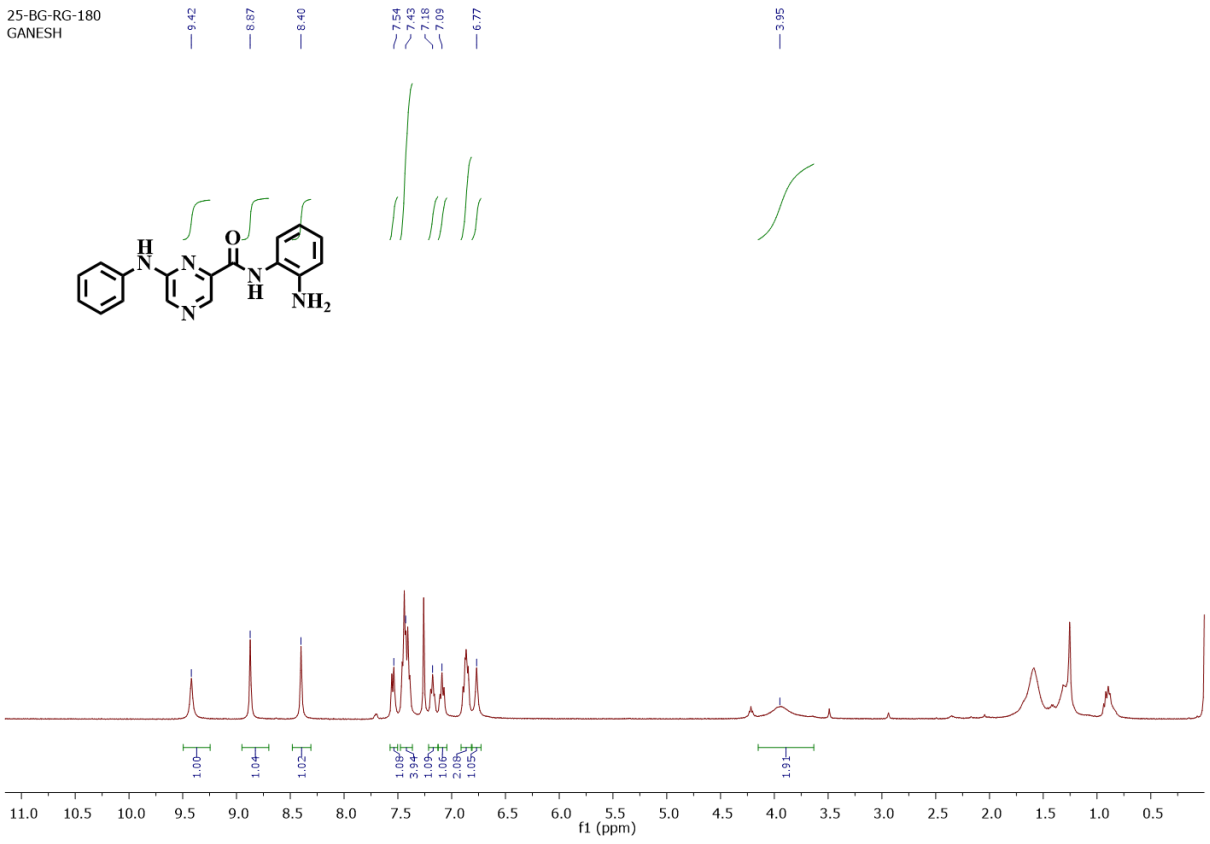

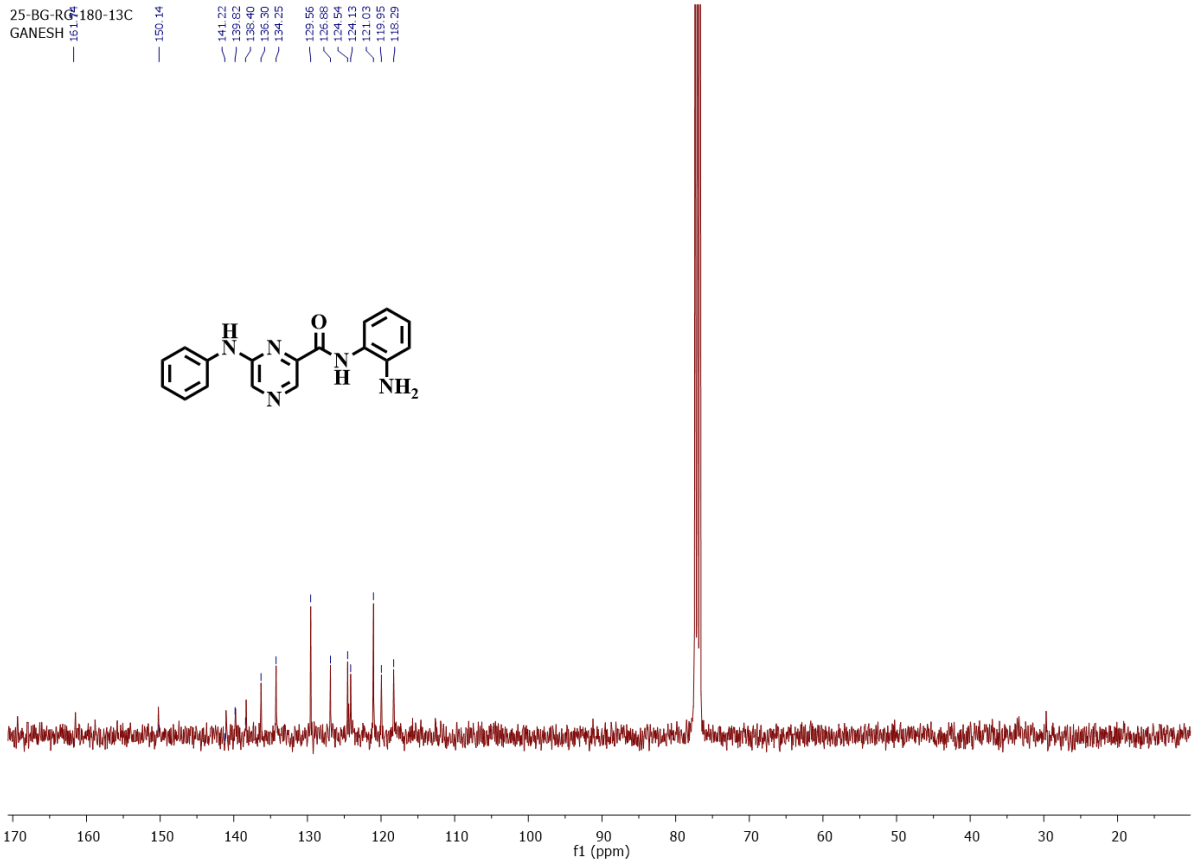
25-BG-RG-180-13C
GANESH
161.74
150.14
141.22
139.82
138.40
136.30
134.25
129.56
126.88
124.54
124.13
121.03
119.95
118.29
170
160
150
140
130
120
110
100
90
80
70
60
50
40
30
20
f1 (ppm)

HPLC:

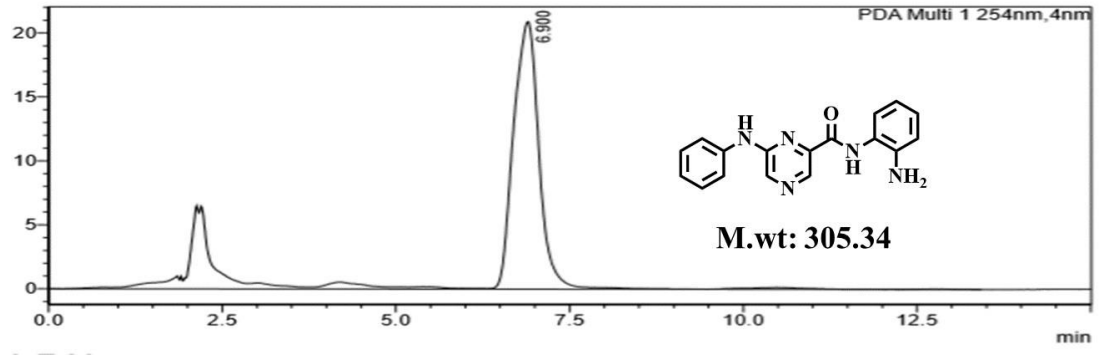
PDA Multi 1 254nm,4nm
6.900
M.wt: 305.34
20
15
10
5
0
0.0
2.5
5.0
7.5
10.0
12.5
min

LCMS:

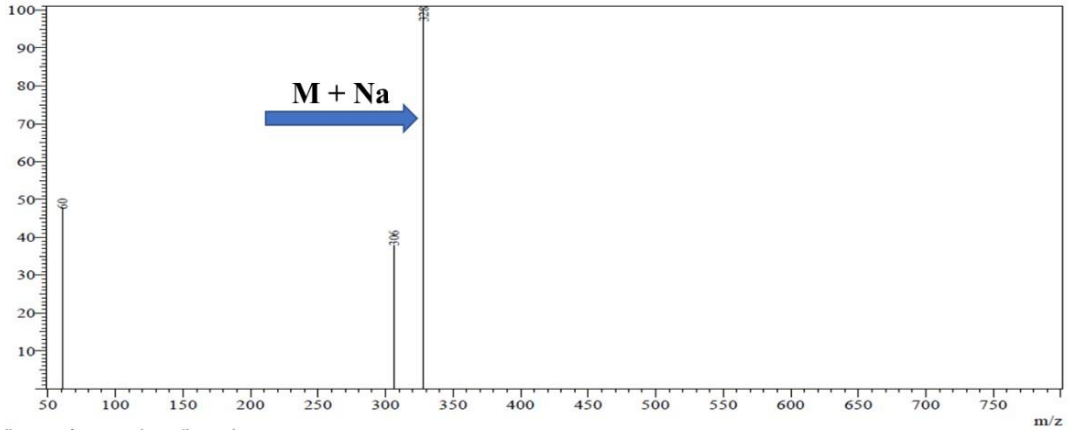
M + Na
m/z

HRMS:

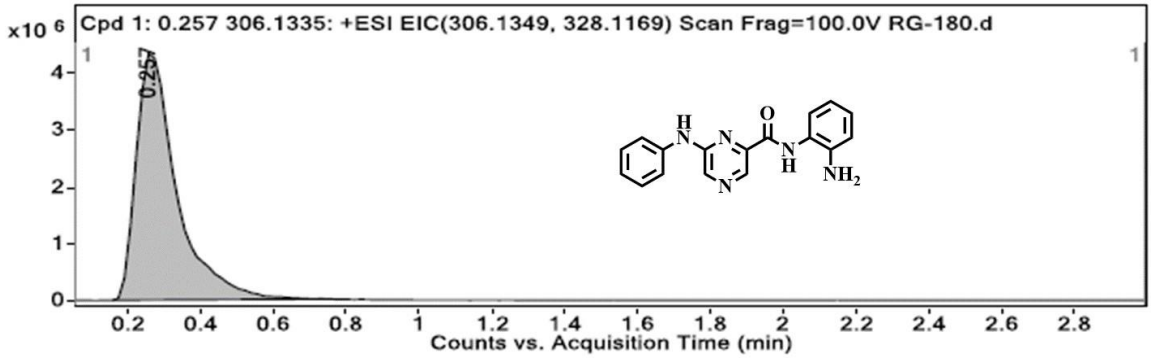
Cpd 1: 0.257 306.1335: +ESI EIC(306.1349, 328.1169) Scan Frag=100.0V RG-180.d
0.257
Counts vs. Acquisition Time (min)

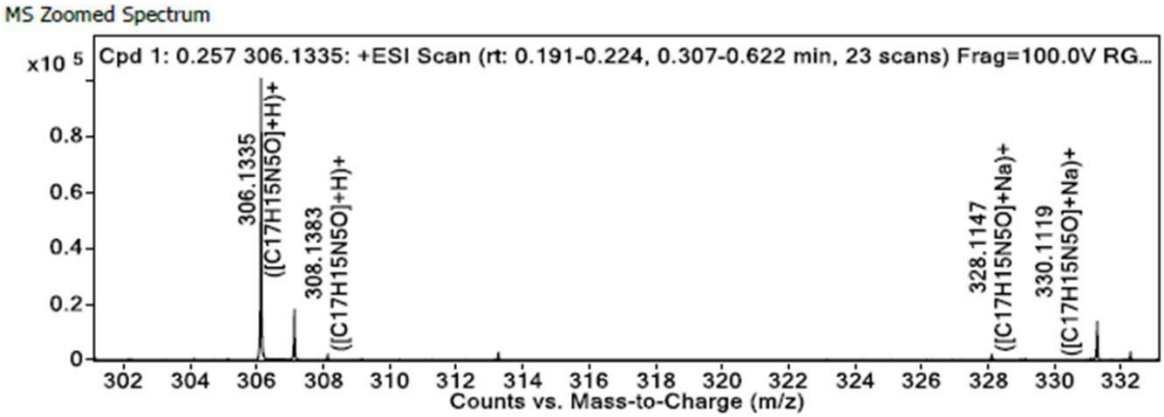
MS Zoomed Spectrum
Cpd 1: 0.257 306.1335: +ESI Scan (rt: 0.191-0.224, 0.307-0.622 min, 23 scans) Frag=100.0V RG...
306.1335 ([C17H15N5O]+H)+
308.1383 ([C17H15N5O]+H)+
328.1147 ([C17H15N5O]+Na)+
330.1119 ([C17H15N5O]+Na)+
Counts vs. Mass-to-Charge (m/z)

2.4.3. Biology

2.4.3.1. Cell culture

Three different cell lines were used for the determination of anticancer activity of the novel compounds synthesized. For the purpose, MTT assay was carried out on Mouse breast cancer cell line (4T1), Murine melanoma cancer cell line (B16F10) and human breast cancer (MDA-MB-231) cell line that were procured from National Centre for Cell Science (NCCS, Pune, India). B16F10 and MDA-MB-231 cell lines were cultured in DMEM (high glucose media: AL007S, Dulbecco's modified eagle medium) and 4T1 cell line was cultured in MEM (AT154, Minimum essential medium) with 10% fetal bovine serum (FBS) and 1% antibiotic (Pen strep: A001) and were incubated at 37 °C and 5% CO_2 atmosphere. MTT [3-(4,5-dimethylthiazol-2-yl)-2,5diphenyltetrazolium bromide], a yellow dye was used for the assay. All reagents were purchased from Hi media Laboratories Pvt. Ltd., Mumbai, India.

2.*4.3.2. Chemicals and anti-bodies*

All the compounds were synthesized as described above. The compounds were dissolved in DMSO stock solution and were stored in -20°C. Primary antibodies - Rabbit mAb H3K9 acetylated histone H3 (catalogue #9649), Rabbit mAb H4K12 acetylated histone H4 (catalogue #13944), mouse mAb beta-Actin primary antibodies (catalogue #58169) and secondary antibodies – antirabbit HRP linked antibody and anti - mouse IgG HRP-Linked antibody were purchased from cell signalling technology. DAPI (4′,6-diamidino-2- phenylindole) and acridine orange, propidium iodide and RNase were purchased from Sigma. TACs Annexin-V/FITC – PI assay kit was purchased from Bio legend and was used as per the protocol given.

2.4.3.3. MTT Assays

As per the protocol, 96 well plate was seeded with 100 µL/well of cell suspension with the cell density of 1×10^4 per well and were incubated for overnight. Subsequently, the medium was aspirated, and the cells were treated with the synthesized novel compounds along with **CI994** as positive control at a concentration of 100 µM and 10 µM in 150 µL of their respective media in duplicate and further incubated for 72h. Following incubation, the culture medium was aspirated and subsequently, 50 µl of 5 mg/ml concentrated solution of MTT (3-(4,5-dimethylthiazol-2-yl)2,5-diphenyltetrazolium bromide) in phenol red free DMEM media was prepared and added in each well and further incubated for 3h for the formation of formazan crystals that are formed as a result of cellular enzymatic activity. Subsequently, 150 µl of DMSO was added to the culture after aspirating media in the wells to dissolve the formazan crystals and the absorbance was measured using multi-well plate reader Spectramax (Molecular Devices, USA) at two different wavelengths of 570 nm and 650 nm. The % cell viability was calculated as a fraction of absorbance obtained from the treated cells from the absorbance of untreated control cells. The same procedure was followed for all the three cell lines. For the IC_{50} measurement of all the compounds in the series along with **CI994**, the same procedure was followed as described above. The DMSO solutions of the selected compounds were prepared and they were further diluted to 200 µM, 100 µM, 50 µM, 25 µM, 12.5 µM, 6.25 µM, 3.125 µM, 1.562 µM and 0.781 µM with the DMEM complete media and MEM media respectively for the determination of IC_{50} values along with a blank control containing DMSO in medium and **CI994** as positive control and were incubated for 72h. The experiment was repeated following the same protocol on all the 3 cell lines and the cell viability was measured by MTT assay as discussed. IC_{50} determination was also performed for the selected

compounds to evaluate their cytotoxicity using Human embryonic kidney (HEK293) cell line subcultured in DMEM (high glucose media: AL007S, Dulbecco's modified eagle medium) with 10% fetal bovine serum (FBS) and 1% antibiotic (Pen strep: A001) and were incubated at 37°C and 5% CO_2 atmosphere. MTT [3-(4,5-dimethylthiazol-2-yl)-2,5 diphenyltetrazolium bromide], a yellow dye was used for the assay. All reagents were purchased from Himedia Laboratories Pvt. Ltd., Mumbai, India. Cytotoxicity assay was performed to study their selectivity over cancer cell lines. The DMSO solutions of the selected compounds were prepared and they were further diluted to 2 mM, 1 mM, 500 μM, 250 μM, 125 μM, 62.5 μM, 31.25 μM, 15.62 μM and 7.81 μM with the DMEM complete media for the determination of IC_{50} values along with a blank control containing DMSO in medium and were incubated for 72h.

2.4.3.4. HDAC Inhibition Assays

2.4.3.4.1. HDAC inhibition assay

The enzyme inhibition assay was performed using HDAC colorimetric assay kit (BML-AK501, ENZO life sciences). Briefly, 5 μL of HeLa nuclear extract (BML-KI137–0500), 10 μL of assay buffer (BMLKI143–0020), 10 μL of sample solution was added per well in amicrotiter plate. The reaction was started with addition of 25 μL Colorde Lys® substrate solution (BML-KI138–0050). The reaction was then incubated for 30min at 37°C, which was terminated by addition of a 50 μl mixture of developer (BML-KI139-0300) plus stop solution. The plate was incubated for 15min at 37°C and absorbance was measured at 405 nm. All synthesized compounds were screened at 10 μM concentration in duplicate.

2.4.3.4.2. HDAC1 inhibition assay

The HDAC 1 enzyme inhibition assay was performed using HDAC 1 fluorimetric drug discovery assay kit (BML-AK511, ENZO life sciences). To the 96 well microtiter plate provided in the kit,

10 µL of test sample solution and 15 µL diluted HDAC1 complex solution (BML-SE456-0050) were added per well and 25 µL Fluor de Lys® substrate solution (BML-KI177-0005) was added. The plate was incubated for 15min at 37°C for the reaction to occur. To terminate the reaction, 50 µL of mixture of Fluor de Lys® developer II (BML-KI176-1250) and Trichostatin A ((BMLGR309-9090) was added per well and incubated for 45 min at 37 °C as per the protocol given in the kit. The fluorescence intensity was measured at Excitation wavelength 360 nm, Emission wavelength 460 nm using Spectra max M4 (Molecular Devices, USA). Initially, all the selected promising compounds **5e** and **5f** along with **CI994** were screened at 10 µM concentration in duplicate. Further, all the compound sat the concentration range of 1.25 µM – 80 µM were tested in duplicate to find out the IC_{50} values following the same procedure as described above. The IC_{50} values of these compounds were calculated using nonlinear regression analysis method using Graph Pad Prism 5.

2.4.3.4.3. HDAC2 inhibition assay

The HDAC 2 enzyme inhibition assay was performed using HDAC 2 fluorimetric drug discovery assay kit (BML-AK512, ENZO life sciences). To the 96 well microtiter plate provided in the kit, 10 µL of test sample solution and 15 µL diluted HDAC2 complex solution (BML-KI575-0030) were added per well and 25 µL Fluor de Lys substrate solution (BML-KI572-0050) was added. The plate was incubated for 30min at 37°C for the reaction to occur. To terminate the reaction, 50 µL of mixture of Fluor de Lys developer II (BML-KI105-0300) and Trichostatin A ((BMLGR309-9090) was added per well and incubated for 15min at 37°C as per the protocol given in the kit. The fluorescence intensity was measured at Excitation wavelength 485 nm, Emission wavelength 530 nm using Spectra max M4 (Molecular Devices, USA). Initially, all the selected promising compounds **5e** and **5f** along with **CI994** were screened at 10 µM concentration in duplicate.

Further, all the compounds at the concentration range of 0.625 μM – 80 μM were tested in duplicate to find out the IC_{50} values following the same procedure as described above. The IC_{50} values of these compounds were calculated using nonlinear regression analysis method using Graph Pad Prism 5.

2.4.3.4.4. HDAC3/NCOR1 inhibition assay

The HDAC 3 enzyme inhibition assay was performed using HDAC3/NCOR1 fluorimetric drug discovery assay kit (BML-AK531-0001, ENZO life sciences). To the 96 well microtiter plate provided in the kit, 10 μL of test sample solution and 15 μL diluted HDAC3/NCOR1 complex solution (BMLKI574-0030) were added per well and 25 μL Fluor de Lys® substrate solution (BML-KI177-0005) was added. The plate was incubated for 15min at 37°C for the reaction to occur. To terminate the reaction, 50 μL of mixture of Fluor de Lys® developer II (BML-KI1761250) and Trichostatin A ((BML-GR309-9090) was added per well and incubated for 45min at 37°C as per the protocol given in the kit. The fluorescence intensity was measured at Excitation wavelength 360 nm, Emission wavelength 460 nm using Spectra max M4 (Molecular Devices, USA). Initially, all the synthesized compounds along with **CI994** were screened at 1 μM concentration in duplicate. The promising test compounds **5e and 5f** along with **CI994** as positive control at the concentration range of 0.25 μM – 8 μM were tested in duplicate to find out the IC_{50} values following the same procedure as described above. The IC_{50} values of these compounds were calculated using nonlinear regression analysis method using Graph Pad Prism 5.

2.4.3.4.5. HDAC6 inhibition assay

The HDAC 6 enzyme inhibition assay was performed using HDAC 6 fluorimetric inhibitor screening kit (K465-100, Biovision). To the 96 well microtiter plate provided in the kit, 2 μL of test sample solution and 50 μL diluted HDAC2 complex solution (K465-100-2) were added per

well and incubated for 15min at 37°C. To this 48 µL Fluor de Lys® substrate solution (K465-1003) was added. The plate was incubated for 30min at 37°C for the reaction to occur. To terminate the reaction, 10 µL of developer II (K465-100-4) was added per well and incubated for 10min at 37°C as per the protocol given in the kit. The fluorescence intensity was measured at Excitation wavelength 380 nm, Emission wavelength 490 nm using Spectra max M4 (Molecular Devices, USA). Initially, all the selected promising compounds **5e, 5f** and **CI994** were screened at 20 µM concentration in duplicate. Further, all the compounds at the concentration range of 10 µM – 320 µM were tested in duplicate to find out the IC_{50} values following the same procedure as described above. The IC_{50} values of these compounds were calculated using nonlinear regression analysis method using Graph Pad Prism 5.

2.4.3.4.6. HDAC8 inhibition assay

The HDAC 8 enzyme inhibition assay was performed using HDAC 8 fluorimetric drug discovery assay kit (BML-AK518, ENZO life sciences). To the 96 well microtiter plate provided in the kit, 10 µL of test sample solution and 15 µL diluted HDAC8 complex solution (BML-SE145-0100) were added per well and 25 µL Fluor de Lys® substrate solution (BML-KI178-0005) was added. The plate was incubated for 10min at 37°C for the reaction to occur. To terminate the reaction, 50 µL of mixture of Fluor de Lys® developer II (BML-KI176-1250) and Trichostatin A ((BMLGR309-9090) was added per well and incubated for 45min at 37°C as per the protocol given in the kit. The fluorescence intensity was measured at Excitation wavelength 360 nm, Emission wavelength 460 nm using Spectramax M4 (Molecular Devices, USA). Initially, all the selected promising compounds **5e** and **5f** along with **CI994** were screened at 5 µM concentration in duplicate. Further, all the compounds at the concentration range of 0.625 µM – 40 µM were tested in duplicate to find out the IC_{50} values following the same procedure as described above. The IC_{50}

values of these compounds were calculated using nonlinear regression analysis method using Graph Pad Prism 5.

2.4.3.5. Western blot analysis

For western blotting of acetylated Histone H3(H3K9) and acetylated Histone H4 (H4K12) B16F10 murine melanoma cells were plated in flat bottom 96 well plate and allow to grow overnight, and then they treated with the **5e**, **5f** and **CI994** at 5 μM, 20 μM final concentrations for 12h. After the treatment, the cells were harvested by Trypsinization and centrifuge at 1250 rpm for 5min. The cells pallet was washed by ice cold PBS, and the total protein was extracted using 100 μL, 1X RIPA lysis buffer (Millipore, Billerica, MA, USA), supplemented with 0.5 mM phenyl methyl sulfonyl fluoride (PMSF) and protease inhibitor. After lysing, the suspension was vertex and centrifuged at 14000 rpm for 15min at 4°C. The whole-cell lysates 20 μL and 5 μL of loading buffer (4X) was heated at 95°C for 5min and subjected to sodium dodecyl sulphate-polyacrylamide gel electrophoresis on 15% Bis-Tris 10-well gels at 60V for approximately 180min in SDS Running Buffer. Gels were transferred to the polyvinylidene fluoride membranes (Bio-Rad, Laboratones, Inc.) and run at 60V for 80min. Membranes were blocked in 5% non-fat skimmed milk (Bio-Rad, Laboratones, Inc.) in tris-buffered saline with 1% Tween 20 (TBST), and incubated with Rabbit mAb H3K9 acetylated histone H3, Rabbit mAb H4K12 acetylated histone H4 and Mouse mAb beta-Actin primary antibodies overnight at 4°C, which were diluted up-to 1:7000 in 5% (w/v) milk. The membranes were then incubated with Horseradish peroxidase (HRP)conjugated anti-rabbit secondary antibody and anti-mouse secondary antibody and then visualized with a chemiluminescence kit (Bio-Rad, Laboratories, Inc.) and exposed using a Fusion plus 6 Imaging System (Vilber Lour mat, France). Beta-Actin was used as an internal control.

2.4.3.6. Nuclear staining assay

The Nuclear staining were performed to investigate the status of nuclear disintegration of cancerous cells after treatment of **5e**, **5f** and **CI994** as standard by staining with DAPI (4′,6diamidino-2- phenylindole) and acridine orange. For nuclear staining, B16F10 murine melanoma cells were plated in flat bottom 12 well plate and allow to grow overnight, and then they treated with the **5e** (17.89 µM), **5f** (26.40 µM) and **CI994** (14.59 µM) concentrations and incubate for 48h. After 48h of the treatment, control and compounds **5e, 5f** and **CI994** treated group were fixed with 4% paraformaldehyde solution, thereafter both control and compounds treated cells were stained with DAPI and acridine orange. The nuclear staining of both control and treated cells was visualized under fluorescence microscope (Leica microsystems, Germany) on 20x Magnification.

2.4.3.7. Apoptosis assay

B16F10 cells were seeded with the cell density of 0.5×10^6/well in 12 well tissue culture plates and left overnight. Next day cells were treated with **5e** (17.89 µM), **5f** (26.40 µM) and **CI994** (14.59 µM) for 72h and the cells were incubated at 37°C in CO_2 incubator to assess the apoptosis. The study was carried out as per the manufacturer's protocol (Bio Legend, US). The cells were washed with ice cold PBS, trypsinized and centrifuged to get cell pellet. The pellet was resuspended in 100 µL reagent containing AnnexinV buffer, FITC (1 µL) and PI (10 µL) and kept for incubation for 30min at room temperature. AnnexinV binding buffer, 1X (400 µl) was added to each sample and characterized by flow cytometer (BDAria^{TM} III). The cells with no treatment were considered as controls. FITC versus PI with quadrant gating was done as dot plot which represents (Q1 – Necrotic cells, Q2 - late apoptosis, Q3 – Live cells, Q4 – early apoptotic cells). To determine the extent of apoptosis, early and late apoptotic events were taken.

2.4.3.8. Cell cycle analysis

The cell cycle analysis was performed by using flow cytometry. The cells B16F10 cells were seeded with density of 0.5×10^6 cells per well. After overnight incubation, 15 µM dose of **5e**, **5f** and **CI994** were added to cells and incubated for another 48h. Then the cells were harvested with trypsin and the cell pellet was washed with ice cold PBS. The cells were fixed with 70% ethanol by dropwise addition into the cell suspension under gentle vortex. The clumping of cell was avoided and single cell fixation was visualized under microscope for cross-verification. The samples were kept in -20°C for overnight. The next day fixed samples were centrifuged at 1000 rpm, 4°C for 7min to obtain cell pellet. Finally, the cells were re-suspended in 500 µL of PI and RNAse staining solution. The staining solution was prepared by addition of 20 % w/v RNAse and 2% w/v PI in 0.1% v/v of Triton X-100 solution in PBS. The samples were incubated in dark for 30min at room temperature and analyzed by flow cytometry (BDAria^{TM} III). The dot plot of PI width against PI area was recorded and histogram of PI area on X axis and counts on Y axis was plotted. The percentage of cells in each phase of the cell cycle was evaluated using the FCS express software.

2.4.4. Molecular docking

Molecular docking study was performed to predict binding interactions of promising HDAC3 inhibitors with the HDAC3 enzyme using the Glide module of Schrodinger Maestro software (Life at Schrödinger | Schrödinger) The protein structure (PDB: 4A69) was selected (Watson *et al*., 2012) and prepared by using the Glide module of Maestro software (Life at Schrödinger | Schrödinger, n.d.). On the other hand, ligands were prepared as per our earlier mentioned protocol

(Watson *et al.,* 2012). A grid box was created on the centroid of the HDAC3 binding site. Finally, the prepared ligands and the protein were used to execute the extra precision (XP) docking (Watson *et al*., 2012; Baidya *et al*., 2019).

Chapter - 3

Design, synthesis, and binding mode of interaction of novel small molecule o-hydroxy benzamides as HDAC3selective inhibitors with promising antitumor effects in 4T1-Luc breast cancer Xenograft model

ABSTRACT

Histone deacetylase 3 (HDAC3) is one of the most promising targets to develop anticancer therapeutics. In continuation of our quest for selective HDAC3 inhibitors, a series of small molecules having o-hydroxy benzamide as the novel zinc binding group (ZBG) has been introduced for the first time that can be able to produce good HDAC3-selectivity over other HDACs. The most promising HDAC3 inhibitors, 11a and 12b, displayed promising in vitro anticancer activities with less toxicity to normal kidney cells. These compounds significantly upregulate histone acetylation and induce apoptosis with a G2/M phase arrest in B16F10 cells. Compound 11a exhibited potent antitumor efficacy in 4T1-Luc breast cancer xenograft mouse model in female Balb/c mice. It also showed significant tumor growth suppression with no general toxicity and extended survival rates post tumor resection. It significantly induced higher ROS generation, leading to apoptosis. No considerable toxicity was noticed in major organs isolated from the compound 11a-treated mice. Compound 11a also induced the upregulation of acH3K9, acH4K12, caspase-3 and caspase-7 as analyzed by immunoblotting with treated tumor tissue. Overall, HDAC3 selective inhibitor 11a might be a potential lead for the clinical translation as an emerging drug candidate.

3.1 Introduction

Cancer has been emerging as the second most death-causing disease, next to cardiovascular diseases worldwide. About 13.1 million deaths due to cancer are predicted by 2030 (Yun *et al*., 2019). It is well established that epigenetic alterations of the activity of tumor suppressor genes and oncogenes lead to the development of cancer (Sadikovic *et al.*, 2008b). The acetylation of histone proteins is the most widely studied epigenetic phenomena (Timmermann *et al.*, 2001), and two types of enzymes namely histone acetyltransferases (HATs) and histone deacetylases (HDAC) are mainly responsible for causing the hyperacetylation and hypoacetylation, respectively on lysine residues of histones. The disparity between the activity of HATs and HDACs leads to abnormal gene expression

(Legube & Trouche, 2003) and is supposed to be the key reason for cancer progression. The classical HDACs are zinc-dependent metalloenzymes, which are known to take part crucially in cell migration, invasion etc. The HDAC inhibitors have also been studied widely in various biological activities such as autophagy, DNA repair, accelerating apoptosis and programmed cell death, cell cycle arrest; thus, they are considered anticancer agents (Marks *et al*., 2000; Y. Li & Seto, 2016b; Gong *et al.,* 2019; J. Zhang & Zhong, 2014b). Different types of cancers are developed due to the overexpression of abnormally expressed *HDAC* genes (Adhikari *et al*., 2018b). There are 18 different HDAC isoforms reported so far and are grouped into four different classes considering their sequence homology as well as the organization of domains with the yeast original enzymes. HDAC1, HDAC2, HDAC3 and HDAC8 belong to class I HDACs, whereas class II HDACs are grouped into class IIa (containing HDAC4, HDAC5, HDAC7 and HDAC9) and class IIb (consisting of HDAC6 and HDAC10). However, the sirtuins (SIRT 1-7) are categorized into class III, and class IV HDAC consists of one isoform, i.e., HDAC11. These class I, II and IV HDACs contain zinc metal ion at their active catalytic site, whereas class III HDAC has NAD^+ in the active site for the catalytic activity of these enzymes (de Ruijter *et al.,* 2003). Among these class I HDACs, HDAC3 is proven to be as a promising therapeutic target of cancer due to its overexpression in various cancers (Adhikari *et al.,* 2018b; Spurling *et al.,* 2008b; Ma *et al*., 2015b; Minami *et al*., 2014b; Hsieh *et al.*, 2017b) . HDAC3 deacetylates histone proteins and plays a vital role in cell cycle progression, and known to take part crucial roles in DNA damage and repair, apoptosis and in the modulation of transcriptional activity (Bhaskara *et al*., 2010). Recently, we have reviewed the extensive and diverse roles of HDAC3 in multiple disease conditions including various cancers, neurodegeneration, diabetes, obesity, cardiovascular diseases, inflammatory diseases and viral diseases (Adhikari *et al*., 2021). Consequently, a number of studies performed earlier clearly pointed out the diverse

mechanisms of HDAC3 in the progression of various cancers such as breast carcinoma (Cui *et al*., 2018), colon cancer Spurling *et al*., 2008b;, pancreatic cancer (Hu *et al*., 2019), prostate cancer (McLeod *et al*., 2018) , colorectal cancer (P. He *et al.,* 2018), lymphoma (Wells *et al.,* 2013; Gupta *et al*., 2012), myeloma Minami *et al.,* 2014b; Harada *et al*., 2017), leukemia (Long *et al.,* 2017), melanoma and glioma (Liu *et al.,* 2015), human maxillary cancer (Narita *et al*., 2005), Ewing's sarcoma (Ma *et al.,* 2019), cholangiocarcinoma (Yin *et al*., 2017), etc. Therefore, in this context, it should be well established that HDAC3 might be targeted to design and discover novel and selective small molecule inhibitors for newer anticancer therapeutics.

Exploiting the structural differences between HDAC3 with other class I HDAC isoforms, several inhibitors have been designed and studied towards isoform specificity of HDAC3 so far (Sarkar *et al*., 2020b). Most HDAC inhibitors possess a general pharmacophore feature containing a catalytic Zn^{+2} binding group (ZBG), a cap function interacting with the surface binding region, and a linker region that interacts with the hydrophobic grove and also with the adjacent internal cavity (Miller *et al.,* 2003b). Based on the presence of zinc-binding groups, the HDAC inhibitors have been grouped into different chemical classes namely hydroxamates, short-chain fatty acids, benzamides, thiols, hydrazides and cyclic tetrapeptides (Sarkar *et al*., 2020b). Though a plethora of HDAC inhibitors reported in the literature, only a few are clinically approved. To date, the clinically approved HDAC inhibitor molecules, such as vorinostat/SAHA, belinostat, panobinostat, and pracinostat are from hydroxamate class, romidepsin from cyclic tetrapeptide class, and Chidamide from benzamide class. Moreover, all of them are approved for the treatment of different cancers (Dokmanovic *et al.,* 2007b; Pulya, Amin, *et al*., 2021b). Benzamides possess a moderate affinity towards Zn^{2+}, and in particular, they are promising class I HDAC selective inhibitors (Zhou *et al.,* 2008; Hirata *et al.,* 2018; Nepali *et al*., 2020; Y. Li *et al*., 2015; Marson *et*

al., 2015a; Abdizadeh *et al.*, 2017). To name a few, MS-275 (Entinostat, **1**) (Knipstein & Gore, 2011b) and CI-994 (Tacedinaline, **2**) (Riva *et al.*, 2000) are *o*-aminobenzamides with class I HDAC selectivity (**Figure 1**).

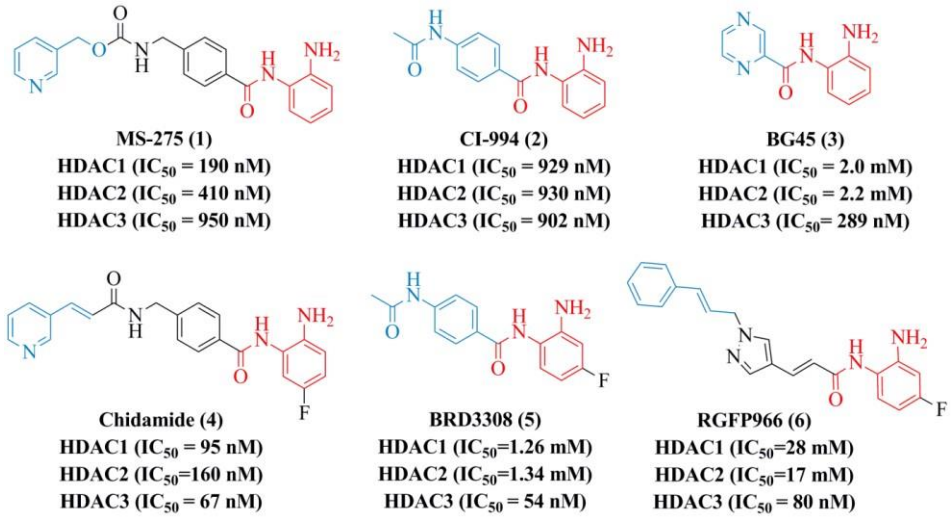

Figure 3.1. Structures of reported reference class I HDAC selective benzamides (Cap group: Indigo; Linker function: Black; ZBG: Red).

Similarly, BG45 (**3**, **Figure 3.1**), a small molecule linker less benzamide with pyrazine as cap a group, has shown to be more specific towards HDAC3 over HDAC1 and HDAC2 Minami *et al.*, 2014b;. Apart from cap group modifications, several other changes on the benzamide moiety also showed an increase in the selectivity and potency towards HDAC3 as in the case of chidamide (**4**, **Figure 3.1** (Knipstein & Gore, 2011b), BRD3308 (**5**, **Figure 3.1**) (Lundh *et al.*, 2015; Dirice *et al.*, 2017) and RGFP966 (**6**, **Figure 3.1**) (Yu *et al.*, 2020; Malvaez *et al.*, 2013). It was reported that the appearance of a fluorine atom at the *para* position of benzamide scaffold took part in the HDAC3 selectivity compared to other class I HDACs Hsieh *et al.*, 2017b). A number of research has been performed in the recent decade taking into account the benzamide class of compounds as potent and HDAC3-selective inhibitors along with significant antitumor activity *in vivo* (Ning *et al.*,

2012;Y. Chen *et al.*, 2020; Hubeek *et al*., 2008; LoRusso *et al*., 1996; Fournel *et al.*, 2008). Chidamide (**4**) is an approved benzamide derivative by Chinese Food and Drug Administration (CFDA) as a potent and HDAC3-selective molecule for treating recurrent or refractory peripheral T-cell lymphoma (PTCL) (Lu *et al*., 2016c).

Our group has been working extensively for designing and synthesizing small-molecule HDAC3 specific inhibitors by incorporating several modifications on the cap group and benzamide ZBG with/without a linker (Adhikari *et al*., 2018b; Sarkar *et al*., 2020b; Trivedi *et al*., 2018b; Hamoud *et al.*, 2020b; Amin, Adhikari, Kotagiri, *et al*., 2019b; Amin, Adhikari, Jha, *et al*., 2019; Pulya, Mahale, *et al*., 2021b). Recently, we have reported a series of small molecules with different aromatic or heteroaromatic cap groups with *o*-aminobenzamide as ZBG. The molecules exhibited excellent selectivity towards HDAC3 compared to CI-994. (Routholla *et al*., 2021). In continuation of our earlier observation, herein we report a series of HDAC inhibitors with further delineated benzamide scaffold and modified cap region with various aromatic or heteroaromatic substituents.

We have further demonstrated their detailed synthetic schemes and chemical characterization, HDAC inhibitory activity studies along with detailed *in vitro* biological characterization. We have also reported *in vivo* therapeutic potential of the lead compound of the series in 4T1-Luc breast cancer xenograft model.

3.2 Results and discussion

3.2.1 Chemistry

3.2.1.1 Design and synthesis of HDAC3 inhibitors

In this communication, some novel substituted benzamides have been designed with modifications on the ZBG with different cap groups based on our recent report (Routholla *et al*., 2021). Here in, we introduced the hydroxy group in the *ortho*-position to the anilide moiety in place of the amine

group on a series of molecules containing various aryl (namely phenyl and naphthyl) as well as heteroaryl (namely quinolinyl, indolyl, thienyl and pyrazinyl-aminophenyl) cap functions. To study the influence of the fluorine atom at *para* position to the anilide group, here we incorporated fluorine on amine/hydroxy containing benzamides (**Figure 3.2**).

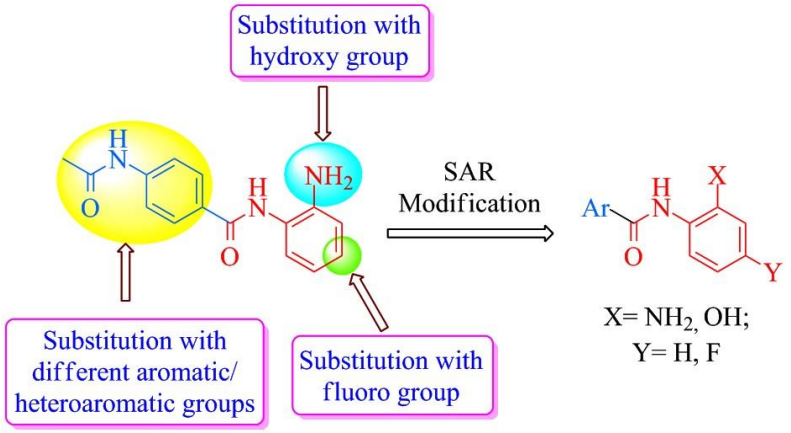

Figure 3.2. Design of aryl or heteroaryl cap containing benzamide and modified benzamide derivatives.

As far as the synthesis is concerned, **Scheme 1** represents the detailed synthetic routes of making novel benzamides (**10a – 14a and 10b – 14b**). All the aromatic or heteroaromatic carboxylic acids (**5 - 9**) were procured from commercial vendors, and were coupled with 2aminophenol or 2-amino-5-fluorophenol with the help of 1-Ethyl-3-(3-dimethylaminopropyl) carbodiimide **(**EDC) as a coupling agent under general acid–amine coupling reaction condition using 4-Dimethylaminopyridine (DMAP) as a catalyst and dichloromethane [DCM: pyridine (1:1)] as solvent to obtain the final compounds **10a – 14a and 10b – 14b**. **Scheme 1**. Synthesis of target compounds and analogues **10** – **14**.[a]

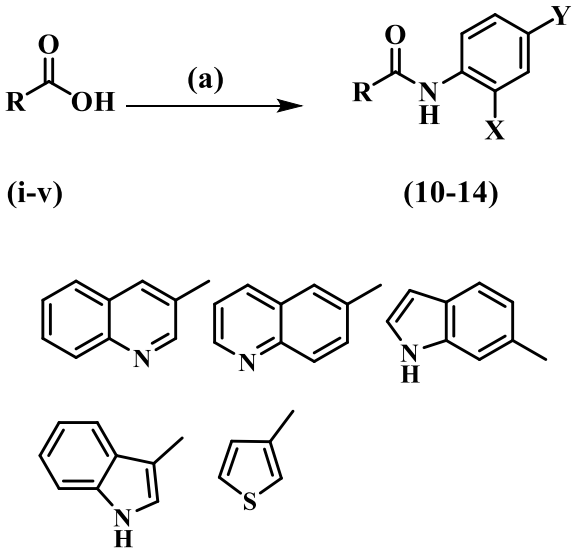

10a,11a,12a,13a,14a : X = OH; Y= H
10b,11b,12b,13b,14b: X = OH; Y= F

[a]Chemical reagents and reaction conditions: (a) Substituted 2-aminophenol, EDC, DMAP, DCM: pyridine (1:1), RT, 6 h.

Scheme 2 displays the synthetic procedure of the target compounds **17a – 17c**. All the aryl or heteroaryl carboxylic acids (**15a – 15c**) were coupled with *tert*-butyl 2-amino 5-fluoro phenyl carbamate according to the previously reported protocol (Routholla *et al*., 2021), following the general acid-amine coupling conditions with the help of EDC as a coupling reagent to produce respective intermediate amino ester compounds (**16a – 16c**). These amino esters upon deprotection of the carbamate moiety in an acidic condition yielded the final compounds (**17a – 17c**).

Scheme 2. Synthesis of target compounds **17a** – **17c**.[a]

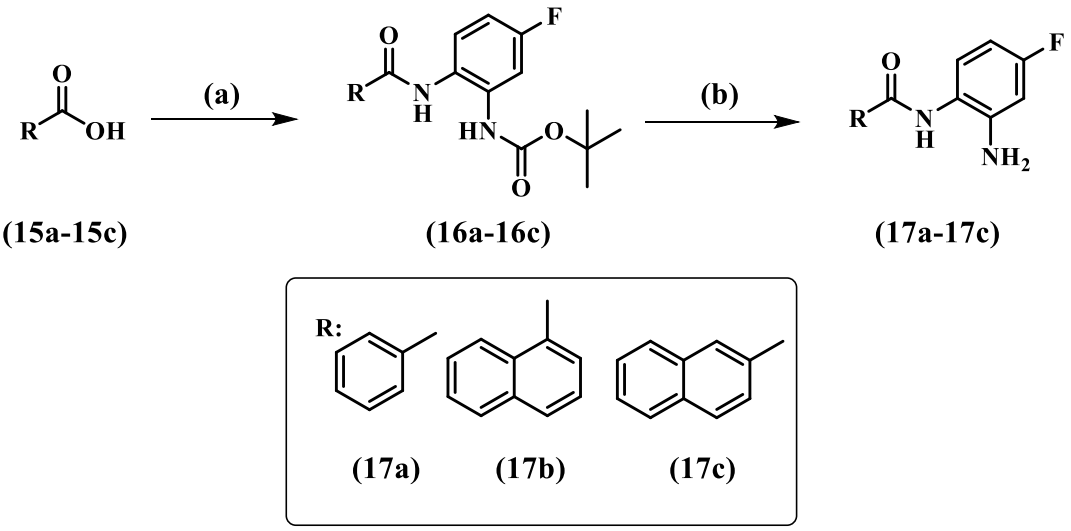

[a]Chemical reagents and reaction conditions: (a) *tert*-butyl 2-amino 5-fluoro phenyl carbamate, EDC, DMAP, DCM: pyridine (1:1), RT, 12 h. (b) 4M dioxane in HCl, 0 °C, 2h.

The target molecule **22** was synthesized by the route described in **Scheme 3**. Commercially available methyl 6-chloropyrazine-2-carboxylate (**18**) was transformed to methyl 6-(phenylamino) pyrazine-2-carboxylate (**19**) by reacting with aniline in the presence of *N*-methyl 2-pyrrolidone (NMP) as a solvent and *N*, *N*-Diisopropylethylamine (DIPEA) as a Hunig's base. Therefore, the 6-(phenylamino) pyrazine-2-carboxylic acid (**20**) was produced by base hydrolysis of the ester compound (**19**). The acid compound (**20**) was then coupled with *tert*-butyl 2-amino 5-fluoro phenyl carbamate (**4**), and was prepared as per our earlier report (Routholla *et al*., 2021), under acid-amine coupling condition with the help of EDC as a coupling agent to produce an intermediate compound **21**. The carbamate group of compound **21** was deprotected under the acidic conditions, afforded the final compound **22**.

Scheme 3. Synthesis of target compound **22**.[a]

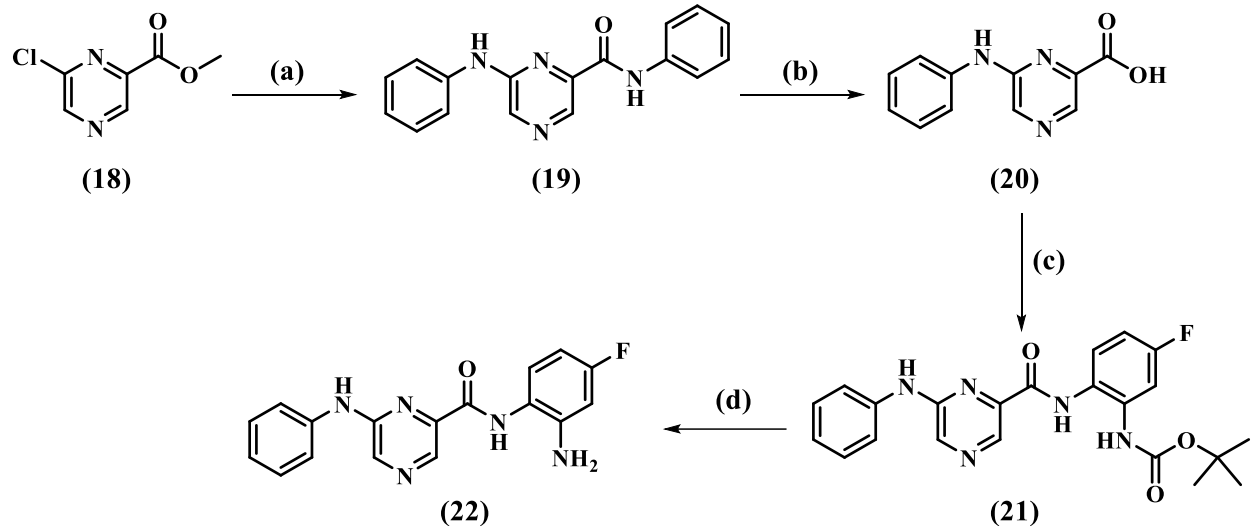

[a]Chemical reagents and reaction conditions: (a) Aniline, NMP, DIPEA, 160 °C, 20 h, reflux (b) NaOH, MeOH, H_2O, 1 h (c) *tert*-butyl 2-amino phenyl carbamate, EDC, DMAP, DCM: pyridine (1:1), RT (d) 4 M HCl in dioxane, 0 °C, 2 h.

The chemical structures of the final synthesized compounds (**compounds 10a-b**, **11a-b**, **12a-b**, **13a-b**, **14a-b**, **17a-c**, **22**) including their % yields as well as physicochemical properties are represented in **Table 3.1**. The purity of the final compounds was estimated with the help of ^{1}H NMR, ^{13}C NMR and HRMS analysis. The spectral data of these final molecules are presented in the supporting information section (**Supporting spectra S1 – S46**).

Table 3.1. Structures of the designed and synthesized compounds including their % yield and calculated physicochemical properties

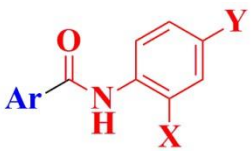

X= NH_2, OH; Y= H, F

Cpd*a*	Ar	X	Y	%yield	*HBD*	*HBA*	*Log P*
10a	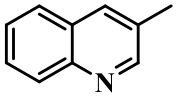	OH	H	56	2	3	2.534
10b	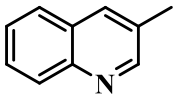	OH	F	50	2	4	2.692
11a	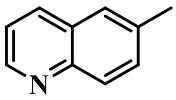	OH	H	46	2	3	2.534
11b	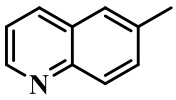	OH	F	55	2	4	2.692
12a	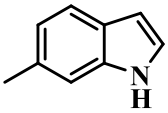	OH	H	46	3	3	1.991
12b	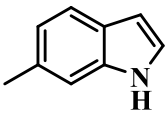	OH	F	42	3	4	2.149
13a	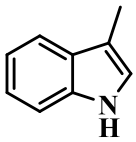	OH	H	30	3	3	1.991
13b	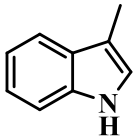	OH	F	48	3	4	2.149
14a	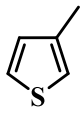	OH	H	52	2	2	2.376
14b	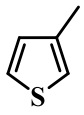	OH	F	45	2	3	2.534
17a	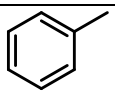	NH_2	F	82	2	3	1.894

17b	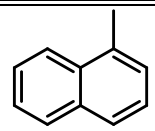	NH_2	F	66.66	2	3	3.192
17c	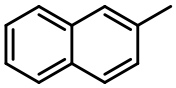	NH_2	F	61.78	2	3	3.192
22	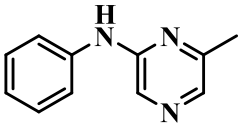	NH_2	F	62.28	3	6	2.125

[a]Compound number; HBD = Hydrogen bond donor; HBA = Hydrogen bond acceptor; LogP = Hydrophobicity

3.2.2 Biological evaluation

3.2.2.1 Pan-HDAC and HDAC3 inhibition

Initially, all these synthesised final molecules (**compounds 10a-b**, **11a-b**, **12a-b**, **13a-b**, **14a-b**,**17a-c**, **22**) were subjected to evaluation for their enzyme inhibitory activities against pan-HDAC (HeLa Nuclear extract) as well as HDAC3 enzymes (**Supplementary Figure S1 and S2**) following the protocol as described in **4.2.4.1** and **4.2.4.4** sections. Interestingly, all of them exhibited moderate pan-HDAC and HDAC3 enzyme inhibition at 10 μM and 1 μM in duplicate, respectively (**Table 3.2)**.

Cpd[a]	*Pan*-HDAC % Inhibition[b]	HDAC3 % Inhibition[c]
10a	22.17 ± 1.98	13.15 ± 3.35
10b	27.87 ± 5.12	21.54 ± 4.56
11a	23.80 ± 0.46	27.07 ± 0.79
11b	23.55 ± 3.75	26.01 ± 0.49
12a	15.59 ± 5.82	10.39 ± 4.78
12b	23.21 ± 0.85	23.79 ± 4.22
13a	18.17 ± 0.26	14.44 ± 3.77
13b	16.56 ± 1.24	11.74 ± 1.41

14a	28.38 ± 1.64	14.47 ± 4.57
14b	26.01 ± 6.47	15.88 ± 3.86
17a	24.57 ± 1.05	19.06 ± 1.36
17b	18.00 ± 0.14	7.38 ± 1.99
17c	25.73 ± 3.45	19.62 ± 1.49
22	18.19 ± 1.62	3.88 ± 4.96
CI-994	53.80 ± 1.60	53.65 ± 1.82

[a]Compound number; [b]Inhibition at 10 μM; [c]Inhibition at 1 μM; Data represents mean ± SD (n = 2).

Table 3.2. Percentage (%) inhibition of the synthesized compounds using CI994 as a reference standard against *pan*-HDAC and HDAC3 enzymes.

All these compounds exhibited lower HDAC3 inhibitory potency compared to the reference molecule CI-994 (53.8% pan-HDAC inhibition at 10 μM and 53.65% HDAC3 inhibition at 1 μM). Apart from the variation of the aryl/heteroaryl group at R position, most of the studied compounds in this communication (compounds **10a-10b**, **11a-11b**, **12a-12b**, **13a-13b** and **14a-14b**) possess a hydroxyl group at X position in place of amino group of CI-994. As all these compounds are less potent compared to CI-994, it may be assumed that the amino group is more preferable at the X position compared to hydroxyl group regarding HDAC3 inhibitory activity. Thus, it may be conferred that *o*-amino aniline group is a better Zn^{2+} chelator than the corresponding *o*-hydroxy aniline moiety. Moreover, it was also noticed that compounds possessing the *o*-amino aniline/benzamide moiety (compounds **17a**-**17c**, **22**) were less effective compared to CI-994 as not only the benzamide ZBG is crucial but also the terminal aryl cap group is also important as far as higher HDAC inhibition is concerned. However, it was also noticed that many of these compounds exhibited a pattern of HDAC3 selectivity (compounds **10b**, **11a-11b**, **12a-12b**, **13a-13b**, **17a**, **17c**) over *pan*-HDAC (HDAC3 % inhibition at 1 μM is more or less similar to the *pan*-HDAC % inhibition at 10 μM). Compounds **11a**, **11b** and **12b** have displayed similar inhibitory potency of

27.07%, 26.01% and 23.79% towards HDAC3. Interestingly, compounds containing quinoline (compound **11a** and **11b**), indole moiety (compound **12b**) as cap groups exhibited better HDAC3 inhibitory potency compared to the corresponding derivatives reported earlier (Routholla *et al.*, 2021). Compounds either 3-quinolinyl (compound **10b**) or 6quinolinyl (compound **11a**-**11b**) substitutions resulted in good efficacy against both *pan*-HDAC and HDAC3. However, the compound with 6-indolyl group (compound **12b**) was better than the corresponding compounds with 3-indolyl function (compounds **13a** and **13b**). It is interesting to observe that the benzamide derivative with pyrazine moiety (compound **22**) neither exhibited *pan*-HDAC inhibition nor HDAC3 inhibition effectively compared to other compounds. Among these benzamides, we have further explored compounds **11a**, **12b** with different aromatic moieties as cap groups to find better potency and selectivity towards HDAC3.

3.2.2.2 Determination of IC_{50} of potent and selective derivatives in different HDACs

Among these compounds tested for % inhibition against *pan*-HDAC and HDAC3, three effective compounds (compounds **11a, 11b** and **12b**) were selected further for the evaluation of IC_{50} against HDAC3 depending on the results obtained in the initial screening of HDAC inhibition taking into account, using CI-994 as a positive control. The IC_{50} values against HDAC3 were found to be 1.586, 3.386 and 2.685 µM for compounds **11a, 11b** and **12b**, respectively (**supplementary Figure S3**). It is noteworthy that these molecules contain 6-quinolinyl (compound **11a** and **11b**) and 6-indolyl (compound **12b**) group in the cap region. Of these three compounds, those containing *o*-hydroxyl benzamide (compound **11a**) or fluoro substituted *o*-hydroxy benzamide (compound **12b**) ZBG groups with more potency against HDAC3 were further explored for their IC_{50} determination against other human recombinant HDAC isoforms such as HDAC1, HDAC2, HDAC6 and HDAC8 to get their more precise selectivity profile towards HDAC3. The results are tabulated in **Table 3.3** and the

sigmoidal dose response graphs generated for the determination of IC_{50} are depicted in the **supplementary Figure S4**.

Cpd[a]	IC_{50} (μM)					Selectivity factor for HDAC3			
	HDAC1	HDAC2	HDAC3	HDAC8	HDAC6	HDAC 1/3	HDAC 2/3	HDAC 8/3	HDAC 6/3
11a	26.63 ± 2.20	32.35 ± 2.97	1.586 ± 0.120	46.11 ± 3.41	49.89 ± 2.76	16.79	20.39	29.07	31.46
12b	30.67 ± 1.97	32.82 ± 3.54	2.685 ± 0.471	45.77 ± 4.12	62.9 ± 3.9	11.42	12.22	17.05	23.42
CI-994	0.929 ± 0.060	0.93 ± 0.09	0.902 ± 0.140	19.57 ± 2.10	40.58 ± 3.21	1.03	1.03	21.7	44.99

[a]Compound number; Data represents mean ± SD (n = 2); CI-994 is a positive control

Table 3.3. IC_{50} values of **11a** and **12b** evaluated on human recombinant HDAC1, 2, 3, 8 and 6 including their HDAC3-selectivity profile over these HDACs.

For the determination of IC_{50}, these compounds were evaluated in the 0.061 – 80 μM concentration range in duplicate according to the protocol of HDAC enzyme assay provided in the enzyme assay kits. The IC_{50} values of these molecules were estimated by means of the nonlinear regression analysis method of the Graph Pad Prism 5 software.

The IC_{50} profiles in the form of the dose-response curve of these selected compounds (compounds **11a** and **12b**) have been shown in **supplementary Figure S4**. Compound **11a** was found to be the most selective for HDAC3 with 16.79, 20.39, 29.07, and 31.46-fold HDAC3 selectivity over HDAC1, HDAC2, HDAC8 and HDAC6, respectively. However, for compound **12b**, it was also found to be a good HDAC3-selective compound over other HDACs but HDAC3 selectivity was less compared to compound **11a**. Compound **12b** exhibited 11.42, 12.22, 17.05 and 23.42-fold selectivity towards HDAC3 compared to other HDACs tested, i.e., HDAC1, HDAC2, HDAC8 and HDAC6, respectively. It is noteworthy that compared to **CI-994** both these compounds (compound **11a** and **12b**) displayed better HDAC3 selectivity over all other HDACs tested (**Table 3**).

3.2.2.3 *Antiproliferative assay against different cancer cell lines*

All the synthesized molecules including the reference standard CI-994 were subjected to evaluation for their anticancer activity by using MTT assay against human triple-negative breast cancer (TNBC) cell line (MDA-MB-231), mouse breast cancer cell line (4T1) as well as murine melanoma cancer cells (B16F10). Initially, all these final molecules were evaluated in duplicate at two different concentrations (100 and 10 μM) (**supplementary Figure S5 – S8**). Further, all these compounds were evaluated for their IC_{50} determination with a wide range of concentrations following the protocol detailed in **4.2.3**. This result implies that the antiproliferative activity conferred by these molecules against all the cell lines was comparable to the standard molecule CI-994 (**Table 4**). The highest antiproliferative activity was observed for compound **17a** (IC_{50} = 7.19 μM), compound **17b** (IC_{50} = 11.14 μM) and compound **22** (IC_{50} = 7.53 μM) in B16F10 cells and for the rest of the compounds, the values were in the range of 14 μM – 50 μM that are comparable to CI-994 (IC_{50} =14.34 μM) (**Table 4**). The dose response curves of the compounds in the series including lead compounds, **11a** and **12b** against MDA-MB-231, 4T1 and B16F10 are represented in the form of sigmoidal curves for reference in the **supplementary figure S9A – S9C**.

Cpd*a*	**IC_{50} in μM**				**Selectivity for cancer cells**		
	4T1	**B16F10**	**MDA-MB-231**	**HEK-293**	**4T1**	**B16F10**	**MDA-MB-231**
10a	16.25 ± 1.29	48.73 ± 1.69	22.70 ± 1.22	313.6 ± 8.98	19.30	6.44	13.81
10b	22.76 ± 2.87	19.67 ± 2.98	31.87 ± 2.68	586.9 ± 7.89	25.79	29.84	18.42
11a	10.29 ± 3.58	18.55 ± 1.54	13.87 ± 1.29	449.7 ± 6.98	43.70	24.24	32.42

11b	11.84 ± 1.04	37.44 ± 3.69	17.83 ± 1.05	992 ± 11.25	83.78	26.50	55.64
12a	13.10 ± 1.16	24.04 ± 2.76	11.57 ± 1.28	876.6 ± 9.58	66.92	36.46	75.76
12b	12.80 ± 0.98	40.71 ± 5.06	19.60 ± 2.95	500.3 ± 6.87	39.09	12.29	25.53
13a	7.38 ± 0.78	40.42 ± 4.98	13.04 ± 0.88	716.2 ± 5.76	97.05	17.72	54.92
13b	9.23 ± 1.24	30.1 ± 3.67	14.85 ± 0.69	618.9 ± 6.79	67.05	20.56	41.68
14a	27.19 ± 2.98	22.2 ± 2.98	20.63 ± 2.98	169.7 ± 2.99	6.24	7.64	8.23
14b	9.74 ± 1.09	14.03 ± 0.68	11.76 ± 1.17	507.3 ± 8.64	52.08	36.16	43.14
17a	26.93 ± 2.65	7.19 ± 0.48	21.82 ± 2.48	254 ± 5.44	9.43	35.33	11.64
17b	17.07 ± 0.87	11.14 ± 0.29	21.39 ± 3.67	327 ± 6.78	19.16	29.35	15.29
17c	19.99 ± 1.19	29 ± 1.08	8.21 ± 0.99	237.4 ± 9.33	11.88	8.19	28.92
22	38.76 ± 1.20	7.53 ± 1.19	6.53 ± 0.26	630.5 ± 8.77	16.27	83.73	96.55
CI-994	16.74 ± 0.87	14.34 ± 1.68	15.14 ± 0.36	216.2 ± 4.69	12.92	15.08	14.28

Table 3.4. IC_{50} (μM) of the novel compounds against 4T1, B16F10 and MDA-MB-231 cancer cell lines and the *in vitro* cytotoxicity (IC_{50}) of the compounds against normal HEK 293 cell line along with their selectivity profile towards these cancer cell lines compared to normal cell line HEK-293.

Compounds **11a** and **12b** exhibited highest enzymatic potency and selectivity than remaining compounds, but their antiproliferative activities were found to be moderate and they did not show the highest potency in the antiproliferative assay. The IC_{50} values of compounds **11a** and **12b** are 13.87 and 19.60 μM against MDA-MB-231; 10.29 and 12.80 μM against 4T1; and 18.55 and 40.71 μM against B16F10 cell line, respectively (**Table 3.4**).

3.2.2.4. Evaluation of in vitro cytotoxicity against HEK-293 cell lines

The cytotoxicity of these molecules was judged against the normal human embryonic kidney cell line (HEK - 293) and the precise effect was determined in the form of IC_{50} values (**supplementary Figure S9D)**. As expected, the most selective compounds are found to be the least cytotoxic towards normal cells (HEK-293). The compounds **11a** and **12b** with higher potency and selectivity among all the compounds tested exhibited the IC_{50} values of 449.7 μM, and 500.3 μM revealed to be the least cytotoxic towards normal cells (**Table 3.4**).

3.2.2.5. HDAC inhibitory activity in B16F10 murine melanoma cell line (Western blot analysis)

HDACs act by deacetylating both histone and non-histone proteins *in vitro*. In this regard, class-I HDACs were known to deacetylate the lysine residues of histones such as H3 (ac-H3K9) and H4 (ac-H4 K5/K8/K12/K16) (Seto & Yoshida, 2014). The cellular histone deacetylase inhibitory activity of the selected compounds **11a** and **12b** including the reference compound CI-994 were measured by determining the histone acetylation level in B16F10 cells with the help of western blot analysis technique. The histone acetylation level was determined in a dose-dependent fashion for these compounds using anti-ac-H3K9 and anti-ac-H4K12 antibody. Treatment with compounds **11a**, **12b** and **CI-994** was conducted for 12 h at a concentration of 5 and 20 μM. The increase of acetylation on H3K9 and H4K12 was found significantly in a dose-dependent manner (**Figure 3.3**

and Figure 3.4). This upregulation of acetylation on both the histone substrates was in accordance with the *in vitro* HDAC inhibitory activity of these compounds.

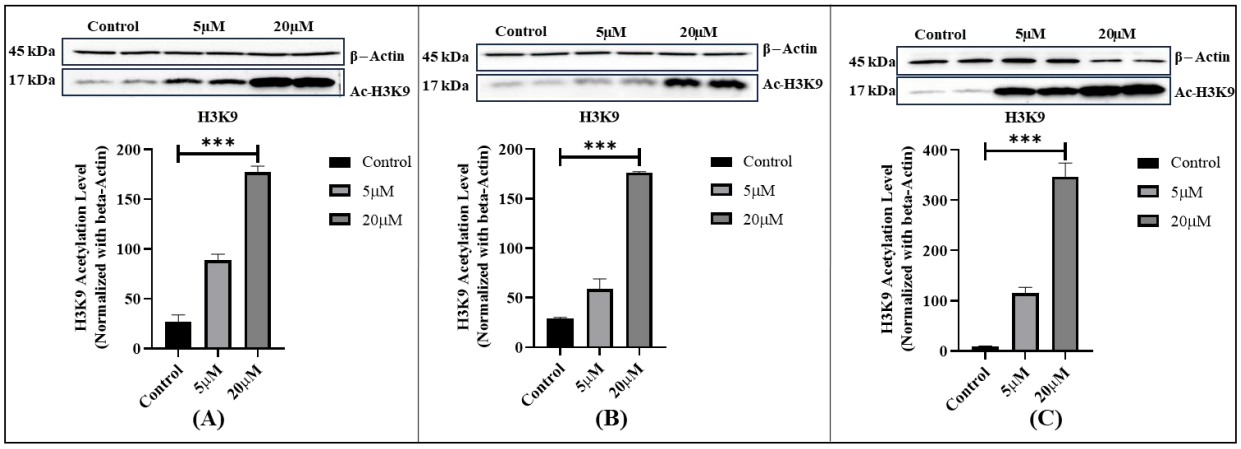

Figure 3.3. Western blot analysis of Ac-H3K9 in whole-cell lysates of B16F10 cells after treatment with (A) **11a** (B) **12b** and (C) **CI-994** at 5 and 20 μM after 12 h treatment of the cells with the compounds. Results normalized with β-actin as housekeeping control.

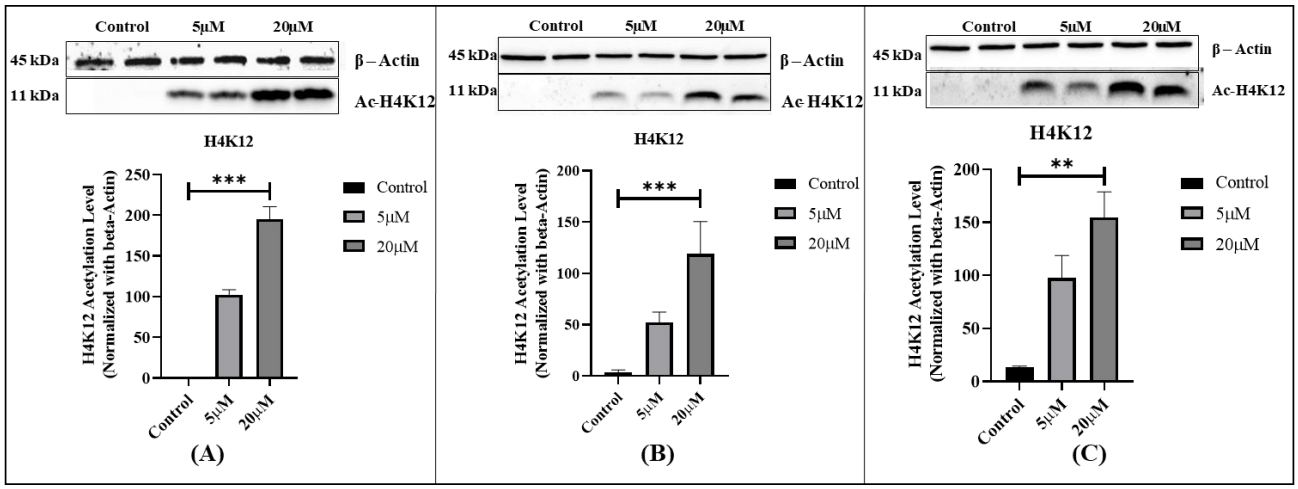

Figure 3.4. Western blot analysis of Ac-H4K12 in whole cell lysates of B16F10 cells after treatment with (A) **11a** (B) **12b** and (C) **CI-994** at 5 and 20 μM for 12 h. Results were normalized with β-actin as housekeeping control.

3.2.2.6 Nuclear staining assay

Nuclear staining assay was conducted in B16F10 cells using compounds **11a** and **12b** to evaluate the impact of these compounds in the form of change in cell morphology and based on the extent

of staining using DAPI (4′,6-diamidino-2-phenylindole) and AO (acridine orange) as staining dyes. It was noticed that after the treatment of B16F10 cells with compounds **11a**, **12b** and **CI-994** for 48 h, there was a clear difference in cellular morphology with the untreated cells (**Figure 3.5**). These results indicate the nuclear disintegration of treated cells and suggest a clear mechanism of programmed cell death.

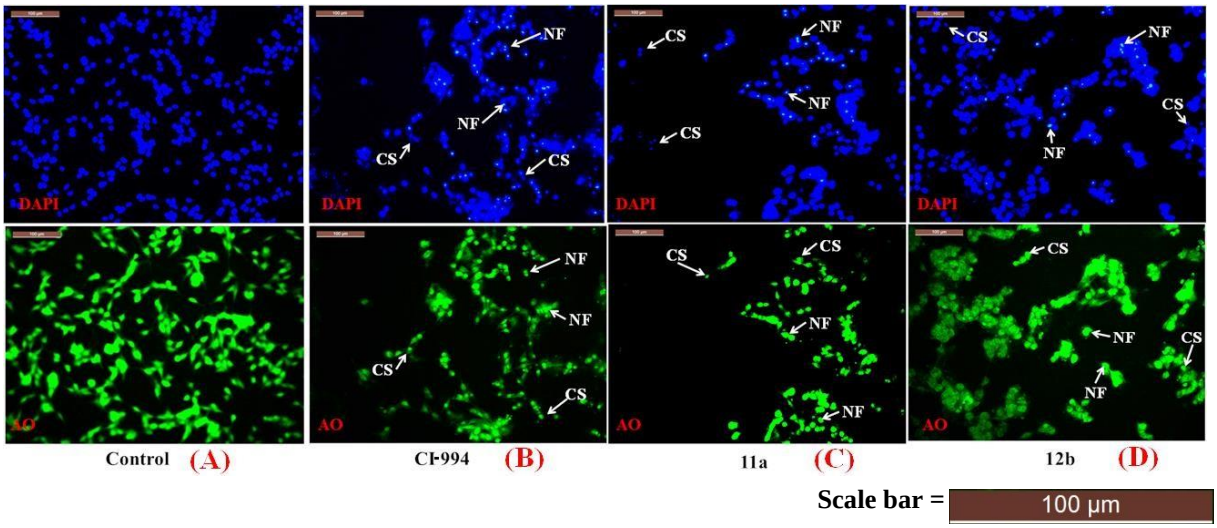

Figure 3.5. Nuclear staining of B16F10 cells using DAPI and AO following treatment: (A) **Control** (B) **CI-994** (C) **11a** and (D) **12b**. The stained nuclei were visualised with the help of a fluorescence microscope (Leica microsystems, Germany) on 20x Magnification.

3.2.2.7 *Annexin-V/FITC apoptosis assay in B16F10 cells*

HDAC inhibitor-mediated cell death through apoptosis leading to anticancer activity has already been well established (Gong et al., 2019; J. Zhang & Zhong, 2014a). The Annexin-V/FITC – PI apoptotic assay was carried out to estimate the extent of apoptosis caused by **11a** and **12b**. B16F10 cells were treated with compounds **11a**, **12b** and **CI-994** for 72 h with the compound IC_{50} concentrations. The cells were then processed as per the protocol described in the **4.2.7**. The analysis was then conducted by using the flow cytometry analysis. The results suggested an

increased apoptotic activity in treated cells with compounds **11a** and **12b** when compared to **CI994** (**Figure 3.6**). Compound **11a** showed the total apoptotic percentage of 26.45% ± 1.62 (Q2 and Q4), whereas the increased apoptotic population of compound **12b** was 39.15% ± 0.71 (Q2 and Q4) while compared to **CI-994** with 16.5% ± 0.25 apoptotic cells. The results suggested that the mechanism of programmed cell death was triggered by compounds **11a** and **12b** leading to apoptosis significantly in B16F10 cells.

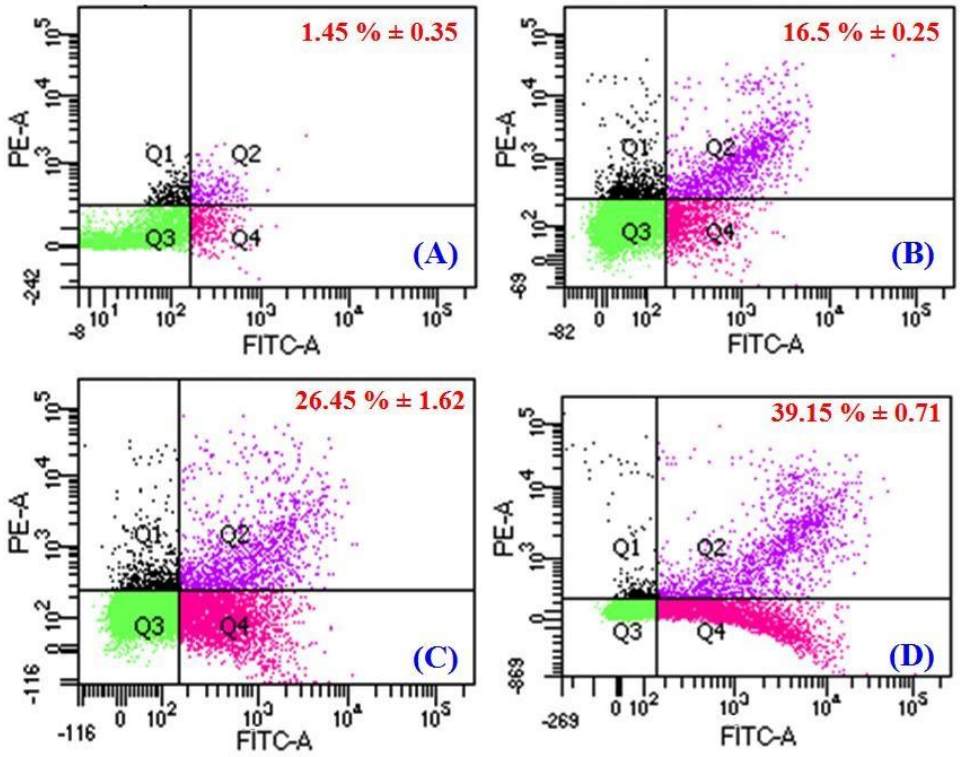

Figure 3.6. Apoptosis induction in B16F10 cells quantified by Annexin V/PI assay with the help of flow cytometry. (A) **Control** (B) **CI-994** (C) **11a** (D) **12b** (Q1 – Necrotic cells, Q2 - late apoptosis, Q3 – Live cells, Q4 – early apoptotic cells, X-axis: Annexin V intensity, Y-axis: Propidium iodide intensity).

3.2.2.8. Cell cycle in G2/M phase arrest in treated cells

The results different experiments so far indicated, compounds **11a** and **12b** possess significant potency and HDAC3 selectivity over other HDAC isoforms and also were found to be enhancing

the cellular histone acetylation levels, causing nuclear disintegration resulting in apoptosisinduced cell death in B16F10 cells *in vitro*. In this regard, we further studied the cell cycle analysis to find out the %cell population at various stages of cell cycle upon treatment of compounds **11a and 12b** using flow cytometry (**Figure 3.7**).

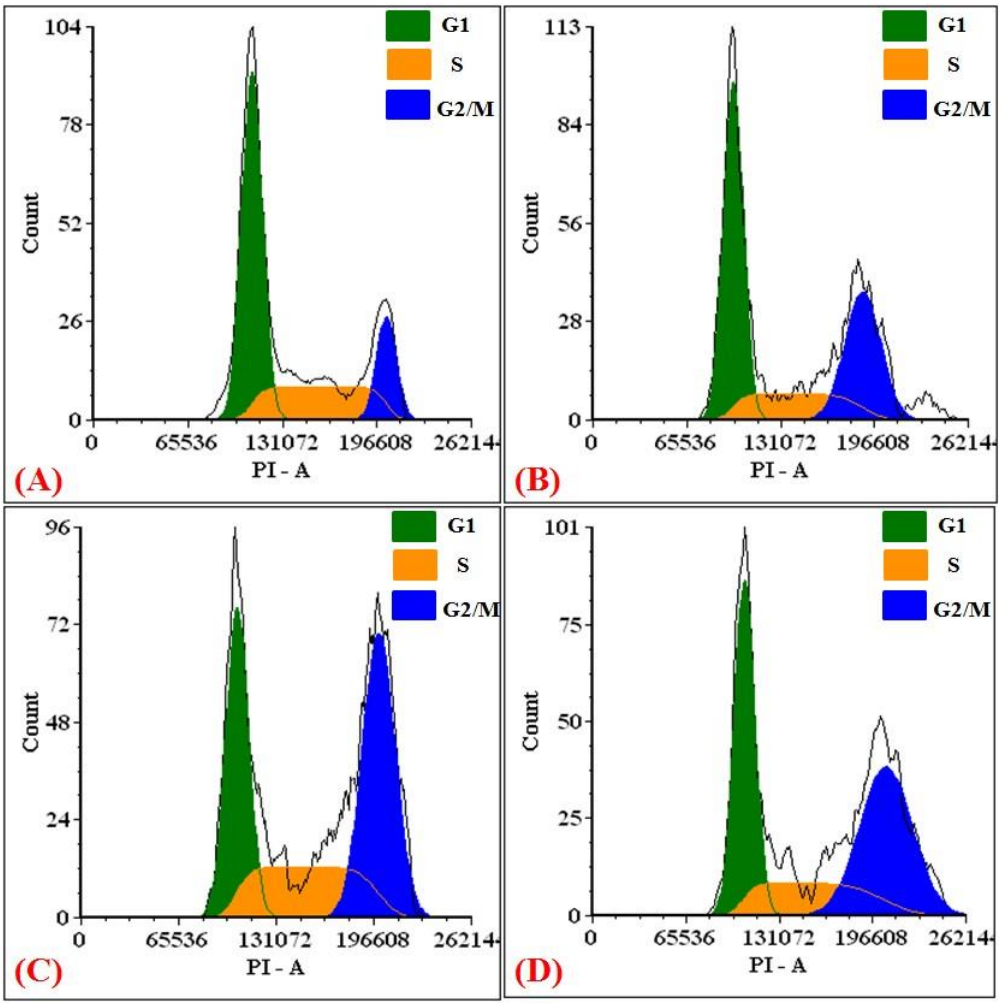

Figure 3.7. Cell cycle arrest induced in B16F10 melanoma cells treated with (A) Control, (B) CI994 as a positive control, (C) **11a** and (D) **12b** after treatment for 72 h. Cell cycle analysis was conducted and analysed by Flow cytometry (BD Aria III) ®.

In this study, B16F10 cells were subjected to the treatment at 15 µM of compounds **11a** and **12b** and the reference compound **CI-994**, for 48 h as per the protocol described in **4.2.8**. Results were

tabulated in **Table 3.5** that depicted the enhanced cell population in G2/M phase for compound **11a** (42.10 %) and compound **12b** (42.48 %) while compared to that of the standard **CI-994** (32.75 %), suggesting the cell cycle arrest at the G2/M cell cycle stage with an increased cell population with 4n of DNA content.

Cell cycle Phase	**% Cell population**			
	Control	**CI-994**	**11a**	**12b**
G1	56.51	48.28	32.32	37.87
S	27.50	18.97	25.59	19.65
G2/M	15.99	32.75	42.10	42.48

Table 3.5. The % cell population in different phases of cell cycle. Data was calculated and analysed by FCS express plus software from DNA content histograms.

It was noticed that compounds **11a** and **12b** resulted in a decrease in the G1 population (32.32% and 37.87%) and no significant change was noticed in the S phase (25.59 % and 19.65 %) when compared to **CI-994** (G1= 48.28% and S=18.97%). These results further point out strongly that the anticancer activity conferred by the lead compounds **11a** and **12b** might be following the cell cycle arrest at G2/M phase with increased population and also supports the apoptotic assay results leading to the programmed cell death.

3.2.2.9 Antitumor efficacy of compound 11a in 4T1-Luc breast cancer xenograft model

With the promising findings of highly selective HDAC3 inhibitor, **11a** in hand, and obtained antiproliferative activities against different cancer cell line including 4T1 cell line *in vitro*, we evaluated compound **11a** for *in vivo* efficacy against "4T1-Luc breast cancer cells tumor xenograft model" in female Balb/c mice. Literature findings from different groups, including our group,

demonstrated the prolonged administration with lower drug doses were more effective. The maximum tolerated dose for previously reported compounds of benzamide chemotype such as **CI994**, **MS-275**, **BG45** were kept between 40 mg/kg/injection to 60 mg/kg/injection and were reported as well tolerated with no gross toxicity (Minami *et al.,* 2014; LoRusso *et al*., 1996; Saito *et al*., 1999b; Santo *et al*., 2012; Hess-Stumpp *et al.,* 2007). In our adopted protocol, 4T1-Luc tumor implanted mice were categorized into three groups having 4 mice belonging to each group. Mice were treated with vehicle alone, 25 mg/kg and 50 mg/kg dose of compound **11a** as described in section **4.3.1**. The tumor volumes were measured once in three days, and the graph was plotted as tumor volume *vs* days of treatment. The tumor volume growth curve is represented in **Figure 3.8A**.

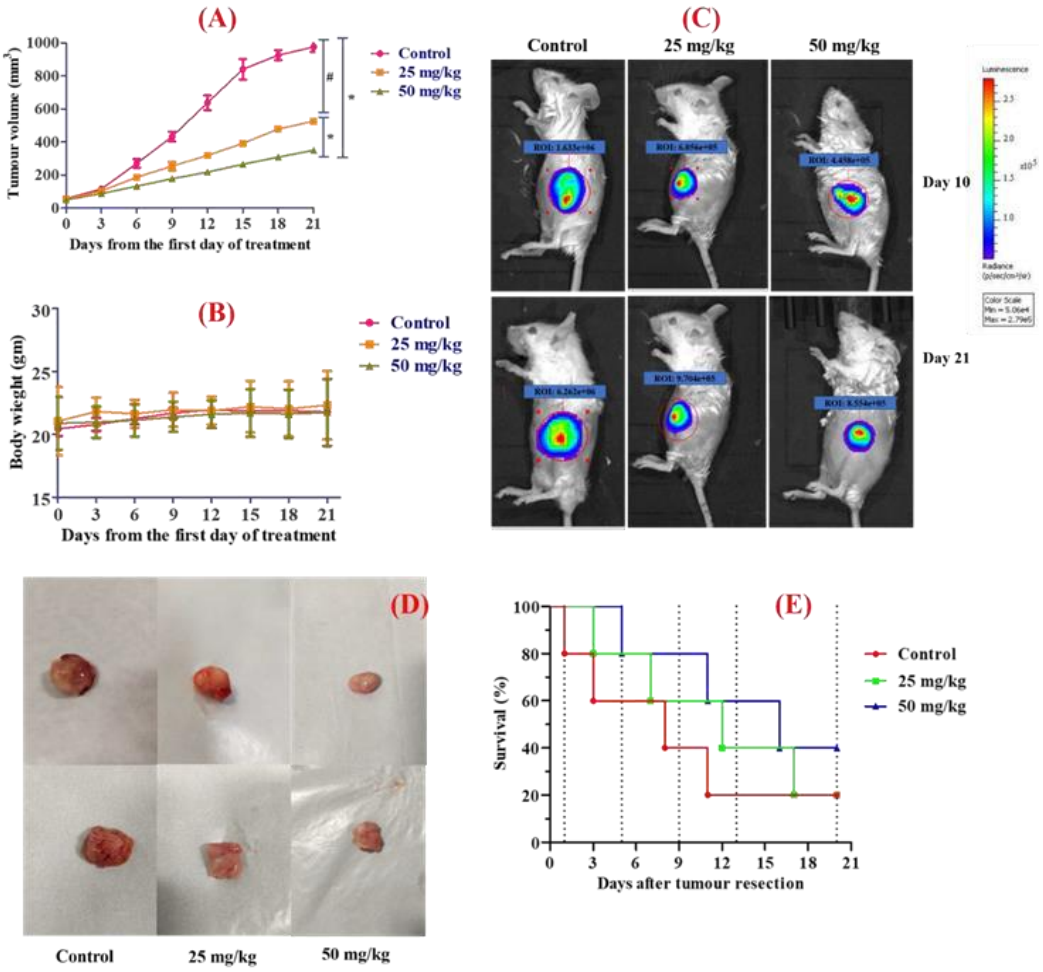

Figure 3.8. Evaluation of *in vivo* therapeutic efficacy in 4T1 Luc tumor bearing Balb/C female mice treated with vehicle Control, 25 mg/kg, and 50 mg/kg of **11a** (n=4). **(A)** Graph representing the tumor volume reduction over days of treatment. **(B)** Measurement of body weight over days of treatment. **(C)** *In vivo* real-time bioluminescence imaging on day 10 and 21, treated with **11a** (Dose:25 mg/kg and 50 mg/kg) in 4T1 Luc tumor-bearing mice. Whole-body NIRF images of mice after Intraperitoneal injection of D-luciferin (IVIS-LUMINA-III). **(D)** Representative tumors isolated from mice post-treatment (n=2). **(E)** Kaplan-Meier survival graph of the treated mice post tumor resection for 21 days. Data represent mean ± SEM, n =4. *p < 0.05, #p = 0.11.

For a period of over 21 days, the average tumor volume of the control group (no treatment) increased rapidly from 56.75 mm^3 to 975.25 mm^3, whereas the average tumor volume for the group treated with a 25 mg/kg dose of compound **11a** was enhanced from 53.50 mm^3 to 526.50 mm^3 and interestingly, for the group treated with a higher dose of 50 mg/kg of compound **11a,** the average volume raised from 50.25 mm^3 to 350 mm^3 only. The inhibition of tumor growth indicated the significant antitumor activity of the lead compound **11a** in 4T1-Luc breast cancer xenograft model. The animal body weight change for each treatment group is shown in **Figure 3.8B,** which showed that the body weights of mice were found to be consistent during the study suggesting no general toxicity in all the treatment groups. Further, we have performed bioluminescence imaging (BLI) by injecting Luciferin D (100 µl) intraperitoneally into one mouse randomly selected from each group on day 10 and day 21 and live imaging experiments were done using IVIS-LUMINA-III **(Figure 3.8C)**. Tumors from the control group showed the highest BLI intensity when compared to the treated groups. The results showed a gradual increase in tumor volume in all the groups, whereas the increase in the control group was at a much higher rate compared to the treated groups correlating with the tumor volume inhibition experiment **(Figure 3.8D)**. The survival study was also performed post-resection of the tumor for 21 days **(section 4.3.1)**. The mice treated with the higher dose of 50 mg/kg lived significantly longer than the lower dose (25 mg/kg) treated animals, while the lowest survival data was obtained for untreated/control animals. The percentage survival of the treated and control group mice was represented with Kaplan-Meier curve in **Figure 3.8E**. These results indicated that the treatment with compound **11a** not only significantly reduced tumor growth but also improved the survival duration of the treated mice at three weeks post tumor resection. Overall, the new potent and selective HDAC3 inhibitor, compound **11a,** exhibited significant *in vivo* anticancer therapeutic activity.

3.2.2.10. Study of compound 11a induced ROS-dependant apoptosis in 4T1-Luc implanted mice

With the *in vitro* apoptosis data in promise, we further investigated the generation of reactive oxygen species (ROS) in 4T1-Luc tumor implanted mice. At the end of 21 days treatment regime, two mice from each group were randomly selected and were injected with DCFH-DA fluorescence probe as per the protocol described in section **4.3.4.2**. The mice were then imaged with IVIS Lumina-III 10 mins after the injection of the probe. **Figure 3.9A** represents the florescence signals indicating the ROS generation induced by compound **11a** treatment of mice and compared to control group mice.

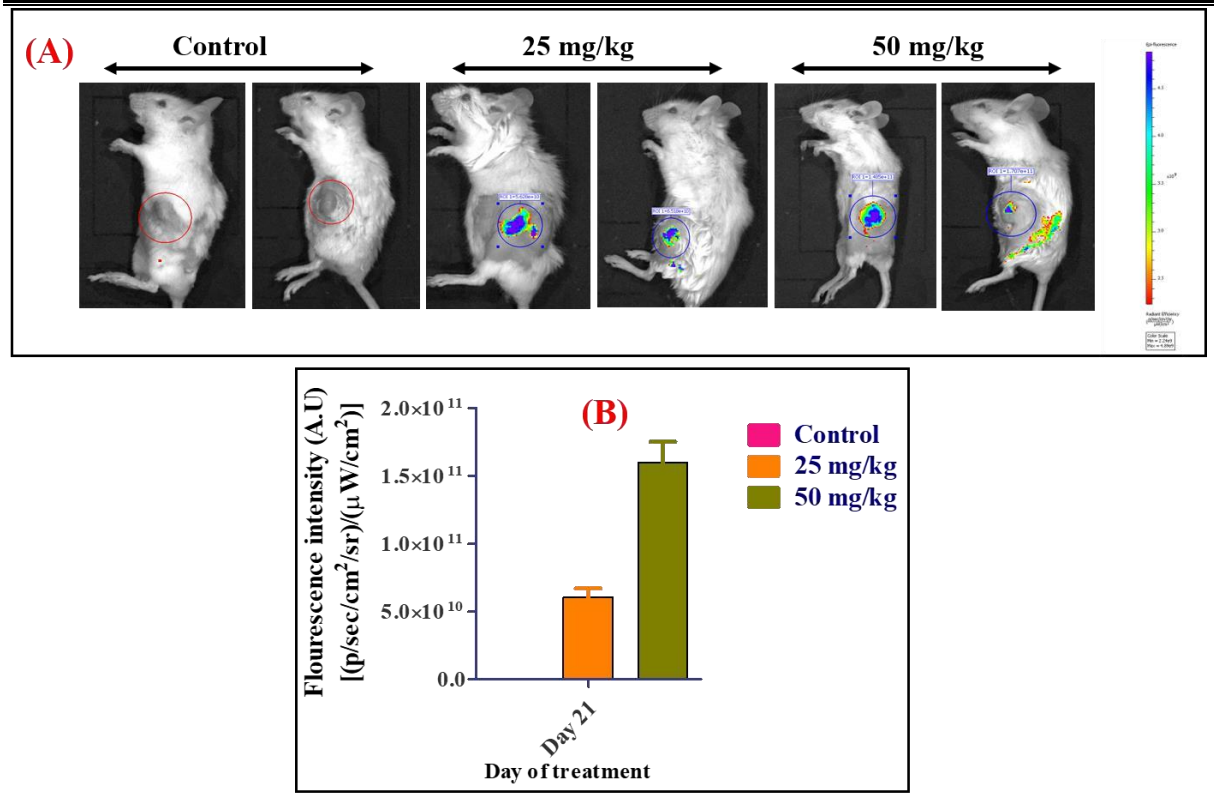

Figure 3.9. **(A)** *In vivo* real-time bioluminescence imaging for ROS generation on day 21, treated with Control and **11a** (Dose:25 mg/kg and 50 mg/kg) in 4T1 Luc tumor-bearing mice (n=2). Whole-body NIRF images of mice after intra tumoral administration of DCFDA. **(B)** Graphical representation of florescence intensity of the tumors on 21st day.

The extent of ROS generation was quantified in terms of fluorescence intensity [(p/sec/cm^2/sr)/µW/cm^2] and is represented as graph in **Figure 3.9B**. The results represented in the graph shows a significant increase in the ROS generation in mice treated with 50 mg/kg than 25 mg/kg with no signals in the control group. Further, the mice were sacrificed after 30 mins of DCFH-DA treatment, and the tumors were collected. The tumors were cryo-sliced into 5 µm thick slices and were stained with DAPI and observed under a florescence microscope (green filter).

Figure 3.10A indicates the images obtained correlated with the *in vivo* imaging confirming further the extent of ROS generation in the order 50 mg/kg > 25 mg/kg. These results suggest that compound **11a** is capable of inducing ROS dependant apoptosis in 4T1-Luc implanted mice.

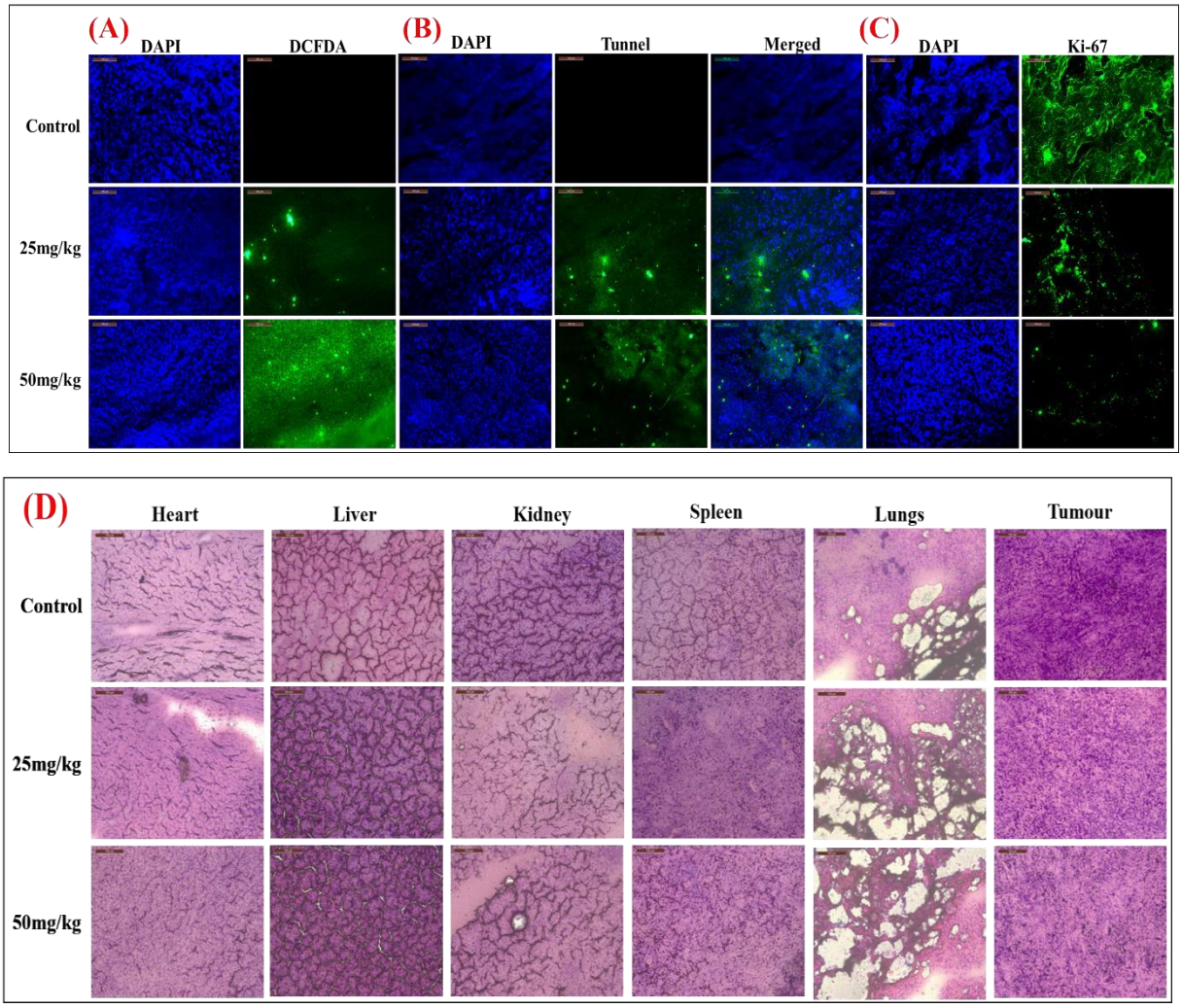

Figure 3.10. Representative images of tumor sections treated with vehicle (Control) and compound **11a** (25 mg/kg, 50 mg/kg) **(A)** photographs of tumor sections representing intra-tumoral ROS levels **(B)** TUNEL staining **(C)** fluorescent images of immune-histochemical analysis of Ki67 **(D)** Representative images of H & E staining for histopathological analysis of various organs and tumor isolated from treated mice. (Scale bar is 20 μm).

3.2.2.11. *TUNEL assay on tumor cryosections*

TUNEL assay was performed on tumor cryosections sliced into 5 µm thickness as per the protocol described in section **4.3.4.1**. TUNEL assay is based on the principle of nuclear DNA fragmentation by nucleases, thus inducing cell death. **Figure 3.10B** represents the images obtained under a florescence microscope indicating the presence of apoptotic cells as indicated by green dots (TUNEL +ve cells) in case of 25 mg/kg and 50 mg/kg treated tumor tissue sections and compared with no indication in control group tumor sections. These results further indicate that **11a** induces apoptosis leading to cell death *in vivo*.

3.2.2.12. *Immunohistochemistry of tumor sections and H&E staining*

To characterise the effect of compound **11a** on cell proliferation, tumor cryosections were sliced into 5 µm thickness as per the protocol described in section **4.3.4.3**. The tumor microarray slides were immune-stained with the Ki-67 antibody overnight, as Ki67 protein is a proliferation marker and the slides were further incubated with secondary antibody and were observed under the fluorescence microscope (**Figure 3.10C**). In untreated tissue sections, the percentage of positively stained cells for Ki-67 was higher when compared to the treated cells. Among the treated cells, those treated with 50 mg/kg had shown far less positive staining when compared to 25 mg/kg treated cells. These results indicate the decrease in the extent of cell proliferation in tumors treated with compound **11a**. The histopathological analysis of various organ and tumor sections was performed as per the protocol described in section **4.3.4.4.** The bright-field images were captured under the fluorescence microscope (**Figure 3.10D**). The images indicate no induced toxicity or damage to major organs in the treated mice, and they were similar to control mice. Whereas the images of the tumor section indicated, the tissue damage occurred in treated tissue sections

compared to the control group tissue sections, further suggesting apoptosis induced by the compound.

3.2.2.13. Analysis of histone acetylation level in the tumor tissue of control and compound 11a treated mice by immunoblotting technique

We further investigated the ability of compound **11a** to modulate the histone acetylation level following a dose-dependent fashion with the biomarkers associated with HDAC inhibition and apoptotic pathway (Shao *et al*., 2004) such as ac-H3K9, ac-H4K12, caspase-3 and caspase-7 through immunoblotting analysis (**Figure 3.11)**.

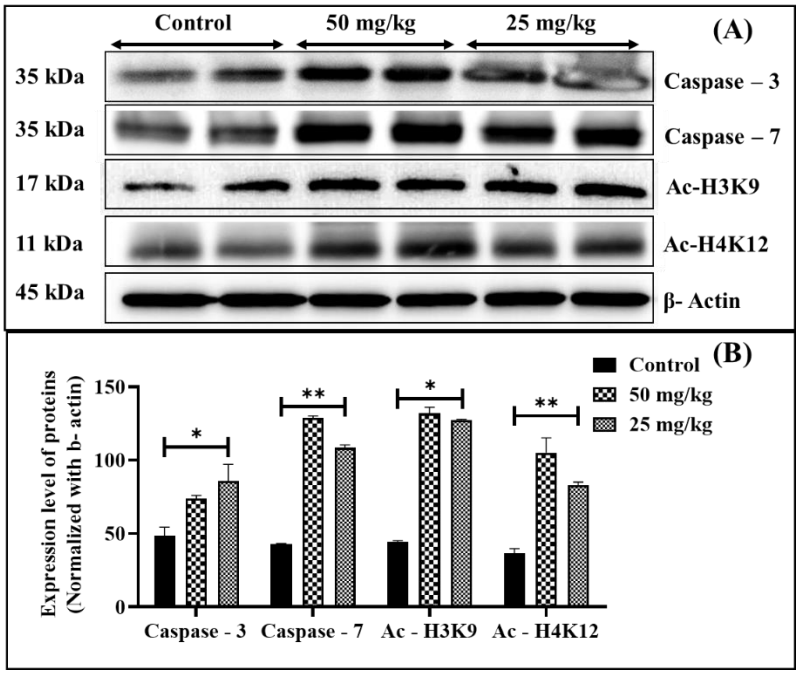

Figure 3.11. **(A)** Western blot of Caspase-3, Caspase-7, Ac-H3K9, Ac-H4K12 in tumor tissue after treatment with control, 25 mg/kg, 50 mg/kg of compound **11a**. **(B)** Results were normalized with respect to β-actin as housekeeping protein in respective controls. Quantification was done using ImageJ software. Each column represents the mean ± SEM of protein expression as indicated.

The tumour tissues were collected from the control group and treated mice and then were homogenized and lysed as per the protocol described in section **4.3.3**. The obtained cell lysates were exposed to western blot analysis. It was noticed that HDAC3 inhibition by compound **11a** leads to the increased level of H3K9 and H4K12 acetylation levels *in vivo* along with the upregulation of Caspase-3 and Caspase-7, indicating the apoptotic pathway in 4T1-Luc tumors *in vivo* (**Figure 3.11**).

3.2.3 Molecular docking-based binding mode of compounds 11a and 12b with HDAC3 active site

The synthesized compounds were docked to the binding pocket of HDAC3 (PDB: 4A69), and most of these showed the same orientation in the binding pocket (**Figure 3.12**).

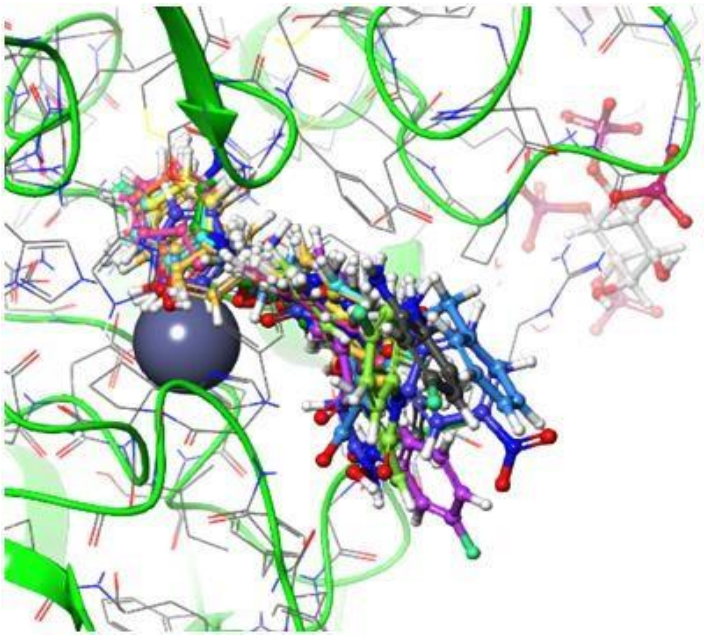

Figure 3.12. The docked conformations of designed compounds at HDAC3 active site (PDB: 4A69).

Most of these compounds formed hydrogen bonding with Gly143 and π-π stacking with Phe144 at HDAC3 active site. These amino acids were found to be crucial in interacting with the reported

inhibitors. The hydroxyl group at phenyl ring interacts with the Zn^{2+} ion at the HDAC3 active site. Hence, the molecular docking of these molecules in the active site of HDAC3 provided good fit and docking scores. Not surprisingly, the docking scores correlate well with the HDAC3 inhibitory outcomes of compound **11a** (glide score: -9.630; HDAC3 IC_{50} = 1.586 μM), compound **12b** (glide score: -7.941; HDAC3 IC_{50} = 2.685 μM) and reference standard CI-994 (glide score: -5.977; HDAC3 IC_{50} = 0.902 μM). This observation is in agreement with the results of our earlier observation (Routholla *et al*., 2021). The binding pattern of interactions of these two effective molecules **11a** and **12b** are displayed in **Figure 3.13**.

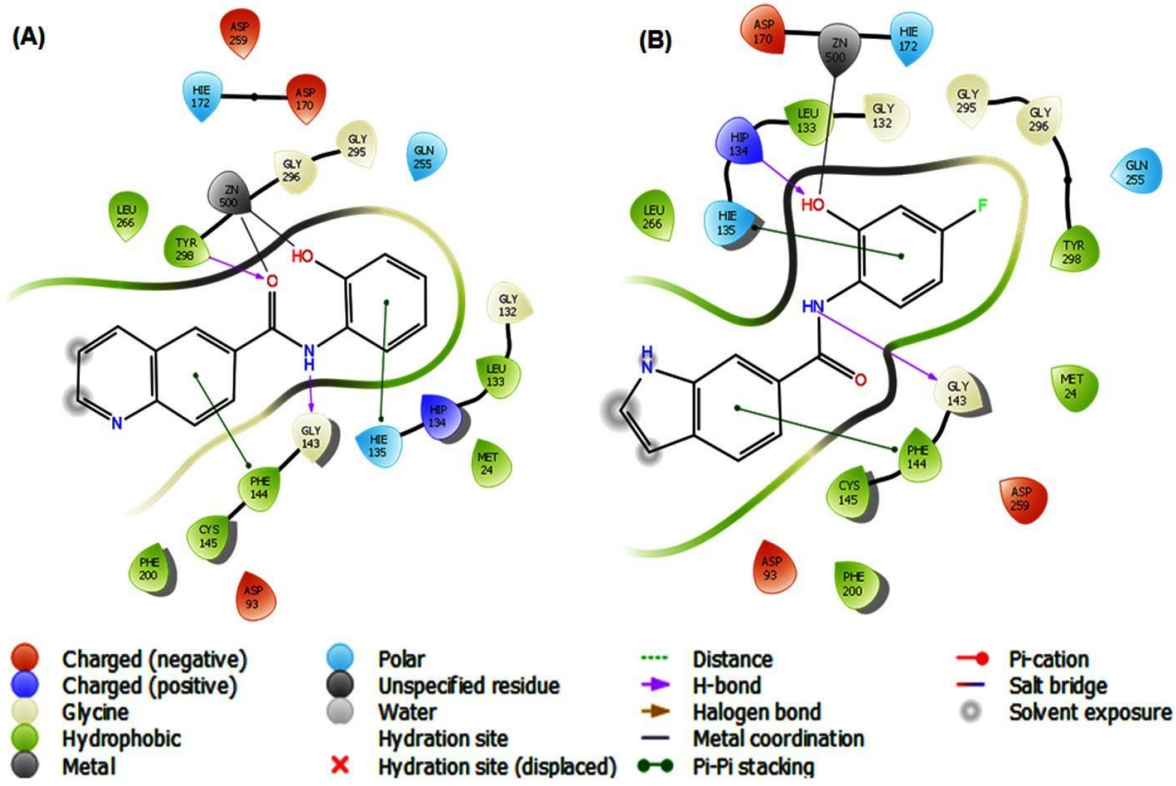

Figure 3.13. Binding mode of interactions of **(A)** Compound **11a** and **(B)** Compound **12b** with active site of HDAC3 (PDB: 4A69)

It was observed that the hydroxyl function of the ZBG of both these molecules formed Zn^{2+} ion coordination (**Figure 3.13**). It was interesting to note that for compound **11a**, the carbonyl oxygen adjacent to the amide group also involved Zn^{2+} ion coordination. However, in case of compound **12b**, the same carbonyl group moved completely opposite direction without forming any metal coordination. Again, the carbonyl moiety of compound **11a** also formed hydrogen bonding interaction with Tyr298 which was not observed for compound **12b**. Again, the spatial arrangement of the 6-quinolinyl function (compound **11a**) at the HDAC3 active site was completely opposite to the respective orientation of 6-indolyl function (compound **12b**) that made compound **11a** better than compound **12b** as far as the stronger binding interaction was concerned. This may be the probable reason behind the better docking score as well as better HDAC3 inhibition conferred by compound **11a** compared to compound **12b**. This observation was again in agreement with our earlier observation (Routholla *et al*., 2021). The amide group of both these molecules formed a hydrogen bonding interaction with Gly143. In addition, a potential π-π stacking interaction also appeared between His135 of the active site and that of the phenyl ring of both of these molecules. Apart from that, His134 was noticed to form a hydrogen bonding interaction with hydroxyl group of compound **12b**. Noticeably, the molecular docking study of these compounds against HDAC6, HDAC8 and HDAC10 were not so encouraging, and therefore, further validated the biological outcomes. Since the selectivity issue is one of the bottlenecks in contemporary HDAC drug discovery, the insight obtained from this study could aid in further designing novel small molecules with enhanced receptor discrimination. This current analysis for the individual models may be able to generate a preliminary idea about the structural requirement of such type of HDAC3 inhibitors.

3.3 Conclusion

In this study, a series of novel substituted benzamides consisting of various aryl and heteroaryl cap groups with *o*-hydroxy and *p*-fluoro substituted benzamides as effective ZBG were designed and synthesized. These compounds were studied as potential and selective HDAC3 inhibitors possessing effective anticancer activities. These novel compounds were screened against cancer cell lines 4T1, B16F10 and MCF-7 and are found to possess significant antiproliferative activity when compared to class-I selective HDAC inhibitor **CI-994** as a reference molecule. These molecules were also relatively nontoxic to the normal cell line HEK-293. Among the series, compounds **11a** and **12b** were the most potent and HDAC3-selective over other Class-I HDACs and HDAC6. Compound **11a** possessing a 6-quinolyl scaffold in the cap region and hydroxyl function substituted at the *ortho* position of the benzamide scaffold was found to be the most promising with over 20 and 16-fold HDAC3 selectivity over HDAC2 and HDAC1, respectively. Compounds **11a** and **12b** were found to induce significant upregulation of acetylated H3K9 and H4K12 in B16F10 cells in a dose-dependent fashion *in vitro*. Molecular docking analysis with compounds **11a** and **12b** at the HDAC3 active site were found to be a good fit with the docking scores correlating the *in vitro* HDAC3 inhibitory assay results. They were found to induce apoptosis and cause the cell cycle arrest in G2/M phase as evidenced in B16F10 cells. The *in vivo* antitumor efficacy studies in 4T1-Luc breast cancer xenograft model in female Balb/c mice indicated that the compound **11a** (25 mg/kg and 50 mg/kg) exhibited a significant reduction in tumor volume compared to control group mice which are treated with vehicle alone. No change in body weights during the treatment period suggested no general toxicity of the compound **11a** even at 50 mg/kg dose. TUNEL assay results indicated the extent of apoptosis increased with 50 mg/kg when compared to 25 mg/kg dose treatment with a greater number of TUNEL (+ve) staining in

the tissue of 50 mg/kg. Compound **11a** also significantly induced ROS generation leading to apoptosis. Moreover, a decrease in cell proliferation has been indicated by the significant reduction in Ki-67 positive stained tumor tissue as in the case of treated tumor tissue sections when compared to control group tumor tissues. No significant toxicity was found in major organs, as evidenced by H&E staining of various organs of compound **11a** treated mice. Western blot analysis of tumor tissues of compound **11a** treated mice also showed the upregulation of acetylated H3K9 and H4K12 levels along with the upregulation of apoptotic markers such as caspase-3 and caspase-7 levels further indicating the significant apoptotic activity through enhanced histone acetylation due to the inhibition of HDAC3 enzyme *in vivo*. Altogether, the results obtained from the *in vitro* and *in vivo* antitumor experiments pointed out that compound **11a** from the series of HDAC3 specific inhibitors might be promising anticancer therapeutics and can be taken further for the clinical translation as an emerging anticancer drug candidate.

3.4 Experimental section

3.4.1 Chemicals and analysis techniques

All the chemicals and reagents required for the study were bought from several chemical suppliers. Thin layer chromatography (TLC) was used to monitor all the reactions with the help of precoated plates of Merck 60 F254 silica gel plates were bought from Merck Millipore Co., USA and the plates were visualised under ultraviolet light (254 nm). Column chromatography was done on silica gel (100 – 200 or 230 – 400 mesh size). ^{1}H and ^{13}C NMR spectrum were obtained in deuterated NMR solvents DMSO-d_6 and $CDCl_3$ with the help of Bruker, ASCEND™ 400 MHz spectrometer. The chemical shifts (δ) are provided in parts per million (ppm), and are internally referenced to tetramethylsilane (TMS), residual solvents peak (DMSO-d_6; 2.50 ppm ^{1}H, 39.51 ppm ^{13}C, $CDCl_3$; 7.2 ppm ^{1}H, 77.6 ppm ^{13}C). Peak multiplicities are abbreviated as s (singlet), d

(doublet), t (triplet), q (quartet) and m (multiplet), while coupling constants (*J*) are reported in Hz. NMR data were recorded with the help of MestReNova Software version 6.0.2-5475. Mass spectroscopy was conducted with the help of HRMS (6545 Q-TOF LC/MS, Agilent) at IIT-Jammu, Central facility.

3.4.1.1. Preparation of N-(2-hydroxyphenyl) quinolone-3-carboxamide (10a)

3-Quinoline carboxylic acid (**5**) (50 mg; 0.289 mmol) was dissolved in dichloromethane and added pyridine (5 ml) under 0 °C. To this mixture, 1-ethyl-3-dimethyl amino propyl carbo di imide, (80 mg, 0.520 mmol) and 3 mg of 4-dimethylaminopyridine were added. This mixture was subjected to allow for the reaction under continuous stirring for 15 mins before 2-Hydroxy aniline (34.5 mg; 0.317 mmol) was added into the reaction mixture. This was also subjected to react under continuous stirring at room temperature for 6 h. After that, pyridine was evaporated under vacuum and the mixture was dissolved in ethyl acetate and thoroughly washed with water. The organic portion was then isolated and excess solvent was dried up under vacuum. The crude compound was then purified with the help of column chromatography (Solvent system- hexane and ethyl acetate (80: 20)) in silica 60 - 120 mesh to finally obtain the final compound in its pure form. (Yield 56%). ^{1}H NMR (400 MHz, DMSO-*d6*) δ : 9.94 (s, 1H), 9.74 (s, 1H), 9.38 (s, 1H), 8.99 (s, 1H), 8.11 (dd, *J* = 8.0, 8.8 Hz, 2H), 7.91 (t, *J* = 7.6 Hz, 1H), 7.73 (td, *J* = 7.6, 7.6 Hz, 2H), 7.09 (t, *J* = 8.0 Hz, 1H), 6.97 (d, *J* = 7.6 Hz, 1H), 6.87 (t, *J* = 7.2 Hz, 1H).^{13}C NMR (101 MHz, DMSO*d6*) δ : 164.53, 150.43, 149.56, 149.00, 136.49, 131.82, 129.73, 129.25, 127.94, 127.73, 126.96, 126.66, 125.88, 125.48, 119.46, 116.52. HRMS (AP-ESI) *m/z* calcd for $C_{16}H_{12}N_2O_2$ $[M+H]^+$ 265.0932, found 265.0988 $[M+H]^+$.

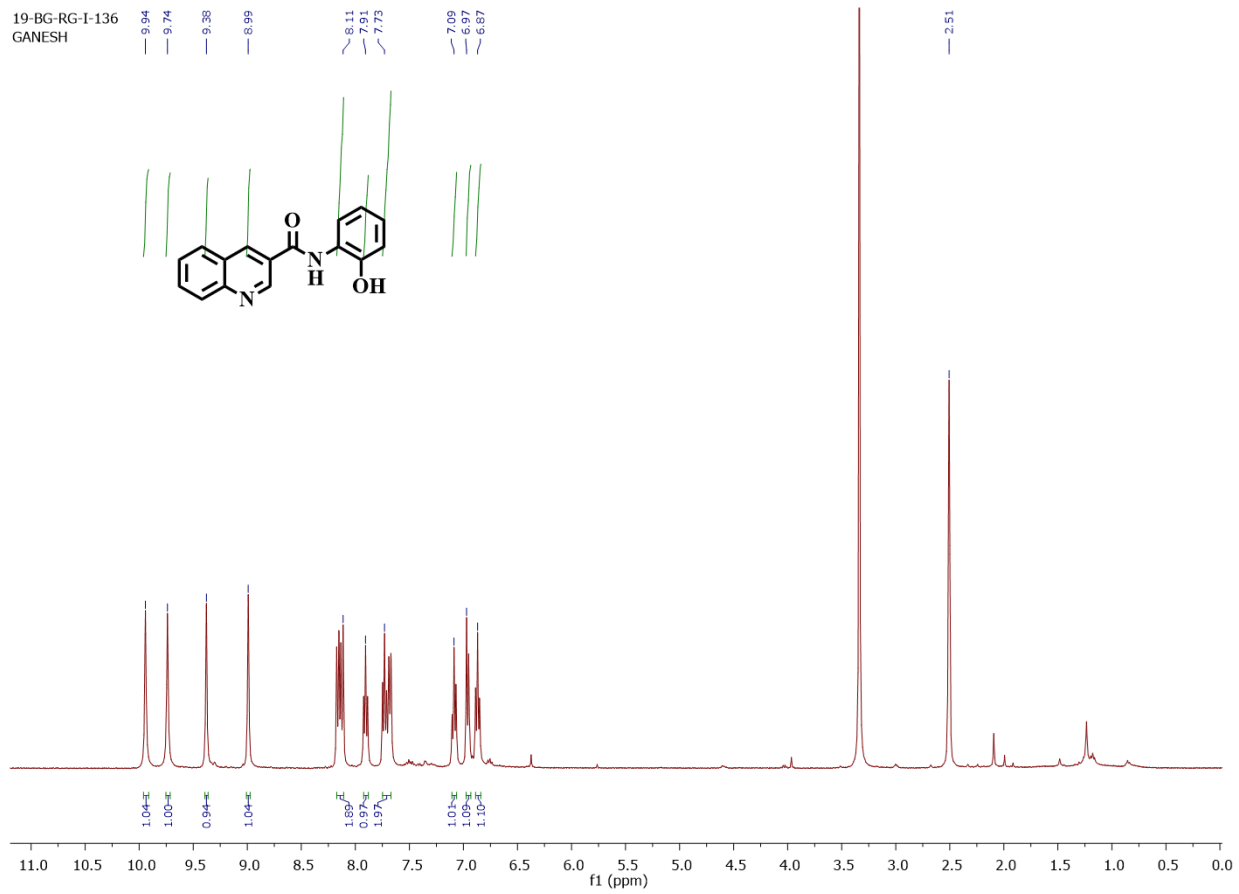
19-BG-RG-I-136
GANESH
9.94
9.74
9.38
8.99
8.11
7.91
7.73
7.09
6.97
6.87
2.51
O
N
H
OH
N
1.04
1.00
0.94
1.04
1.89
0.97
1.97
1.01
1.09
1.10
11.0 10.5 10.0 9.5 9.0 8.5 8.0 7.5 7.0 6.5 6.0 5.5 5.0 4.5 4.0 3.5 3.0 2.5 2.0 1.5 1.0 0.5 0.0
f1 (ppm)

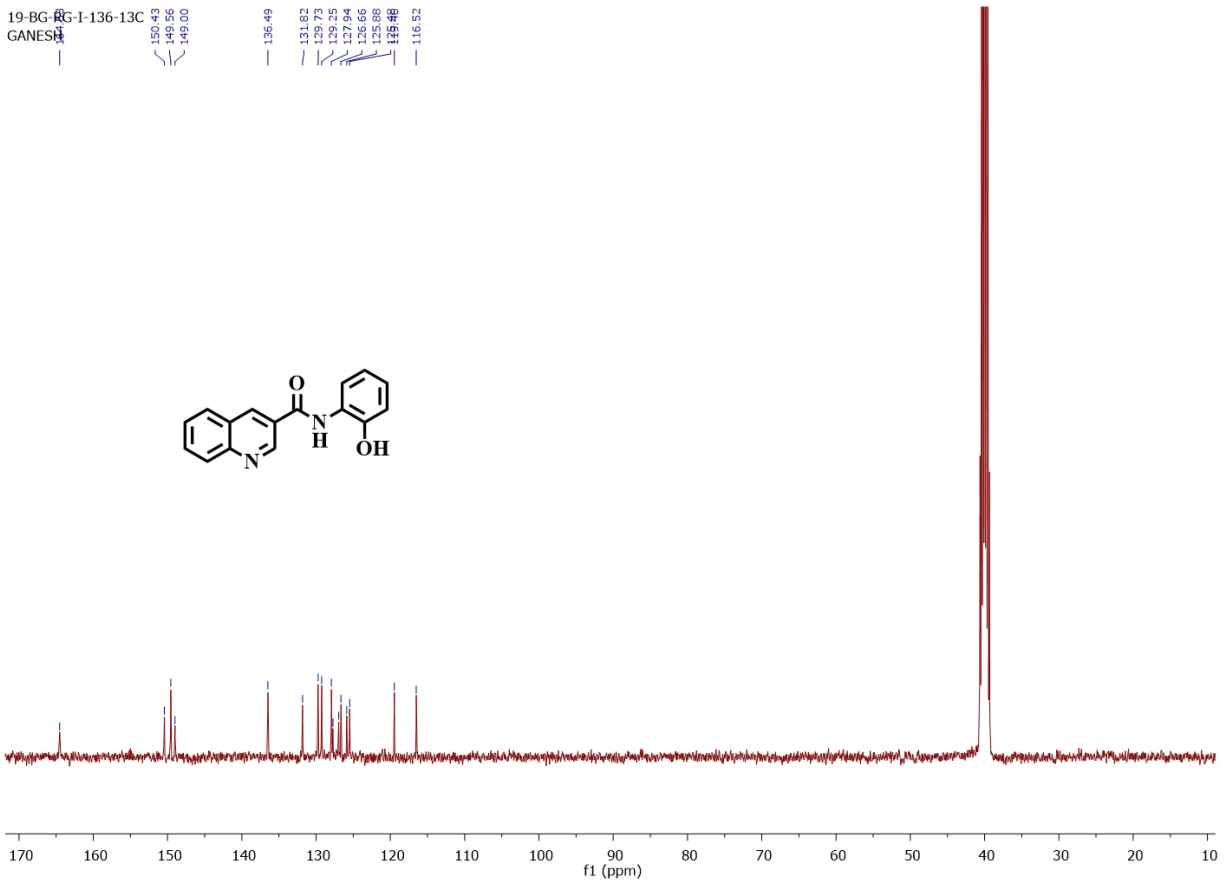
19-BG-RG-I-136-13C
GANESH
150.43
149.56
149.00
136.49
131.82
129.73
129.25
127.94
126.66
125.88
116.52
O
N
H
OH
N
170
160
150
140
130
120
110
100
90
80
70
60
50
40
30
20
10
f1 (ppm)

HPLC:

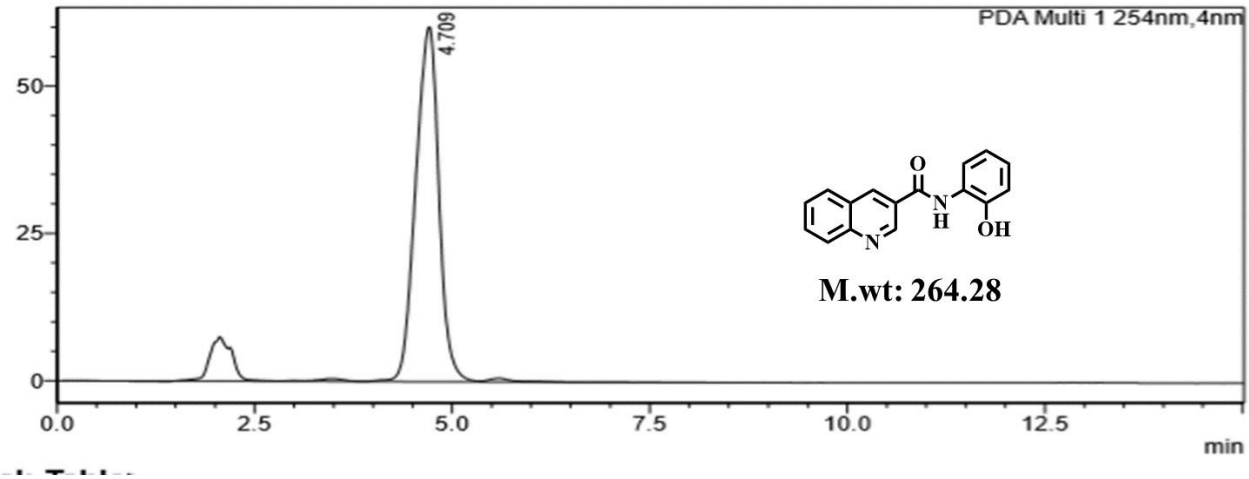
PDA Multi 1 254nm,4nm
4.709
50
25
0
0.0
2.5
5.0
7.5
10.0
12.5
min
O
N
H
OH
N
M.wt: 264.28

LCMS:

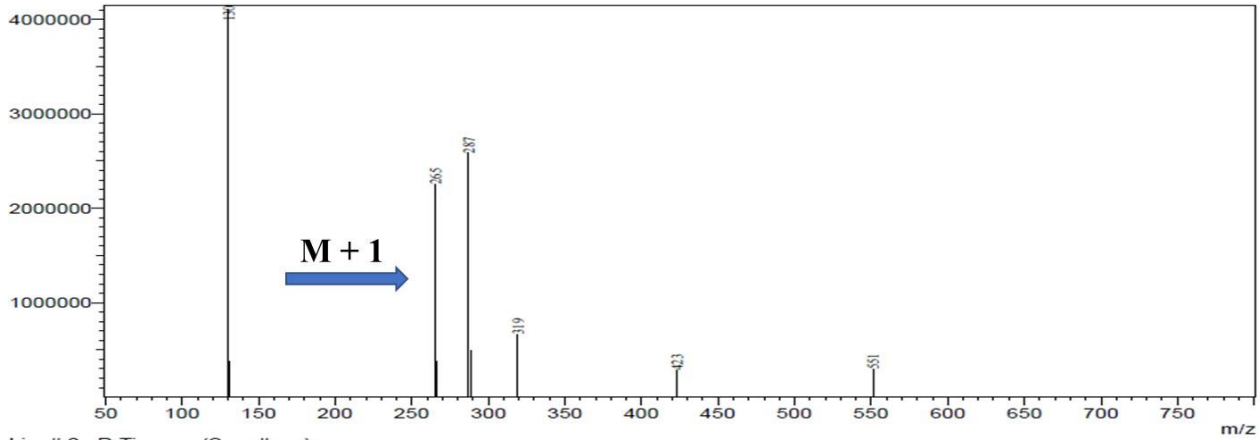
4000000
3000000
2000000
1000000
M + 1
265
287
319
423
551
50
100
150
200
250
300
350
400
450
500
550
600
650
700
750
m/z

HRMS:

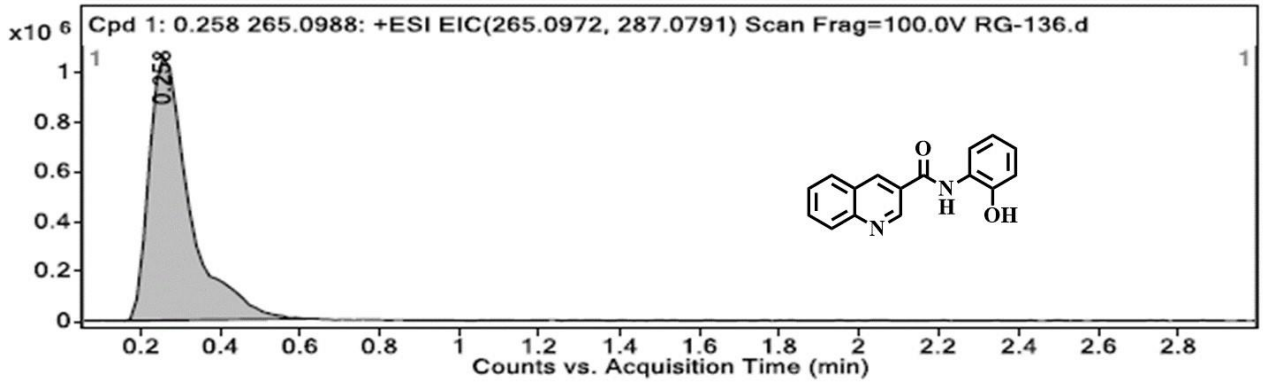
x10 6
Cpd 1: 0.258 265.0988: +ESI EIC(265.0972, 287.0791) Scan Frag=100.0V RG-136.d
0.258
1
0.8
0.6
0.4
0.2
0
0.2
0.4
0.6
0.8
1
1.2
1.4
1.6
1.8
2
2.2
2.4
2.6
2.8
Counts vs. Acquisition Time (min)
O
N
H
OH
N

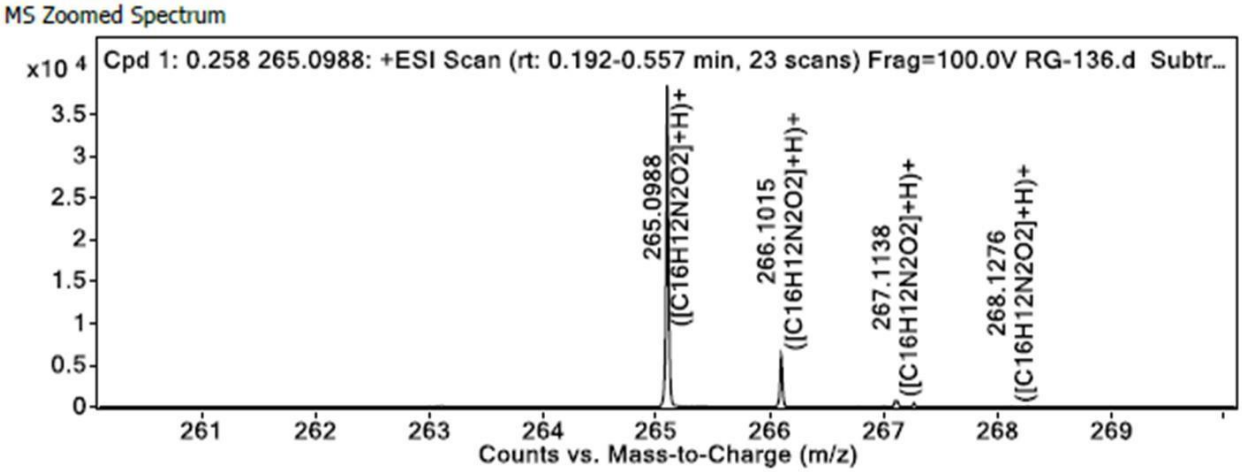
MS Zoomed Spectrum
x10 4
Cpd 1: 0.258 265.0988: +ESI Scan (rt: 0.192-0.557 min, 23 scans) Frag=100.0V RG-136.d Subtr...
265.0988
([C16H12N2O2]+H)+
266.1015
([C16H12N2O2]+H)+
267.1138
([C16H12N2O2]+H)+
268.1276
([C16H12N2O2]+H)+
3.5
3
2.5
2
1.5
1
0.5
0
261
262
263
264
265
266
267
268
269
Counts vs. Mass-to-Charge (m/z)

3.4.1.2. Preparation of N-(2-hydroxy-5-floro-phenyl) quinolone-3-carboxamide (10b)

3-Quinoline carboxylic acid (**5**) (50 mg; 0.289 mmol) was dissolved in dichloromethane and added Pyridine (5ml) under 0 °C. To this mixture, 1-ethyl-3-dimethyl amino propyl carbo di imide (40.37 mg, 0.317 mmol) and 3mg of 4-dimethylaminopyridine were added. This mixture was reacted for 15 mins with continuous stirring before 2-amino-5-fluoro phenol (40.2 mg; 0.317 mmol) was included to the reaction mixture. This was allowed to react under constant stirring at room temperature for 7h. Under vacuum condition, pyridine was evaporated. After that, the mixture was dissolved in ethyl acetate and thoroughly washed with water. The organic portion was then collected and excess solvent was evaporated under vacuum. The crude compound was then purified using column chromatography (Solvent system - hexane and ethyl acetate (50:50)) in silica 60 - 120 mesh to finally obtain the final compound in its pure form. (Yield 50%). ^{1}H NMR (400 MHz, DMSO-*d6*) δ : 10.27 (s, 1H), 10.01 (s, 1H), 9.43 (s, 1H), 9.04 (s, 1H), 8.16 (dd, *J =8.0,* 8.4 Hz, 2H), 7.95 (dd, *J* = 1.6, 1.6 Hz, 1H), 7.78 (t, *J* = 1.2 Hz, 1H), 7.67 (t, *J* = 6.4 Hz, 1H), 6.78 (dd, *J* = 2.8, 2.8 Hz, 1H).^{13}C NMR (101 MHz, DMSO-*d6*) δ : 64.64, 161.83, 159.43, 152.46, 149.58, 149.00, 136.53, 131.81, 129.70, 129.25, 127.93, 126.84, 122.25, 105.87, 103.67. HRMS (AP-ESI) *m/z* calcd for $C_{16}H_{11}FN_2O_2$ $[M+H]^+$: 283.0838 $[M+H]^+$ found 283.0895.

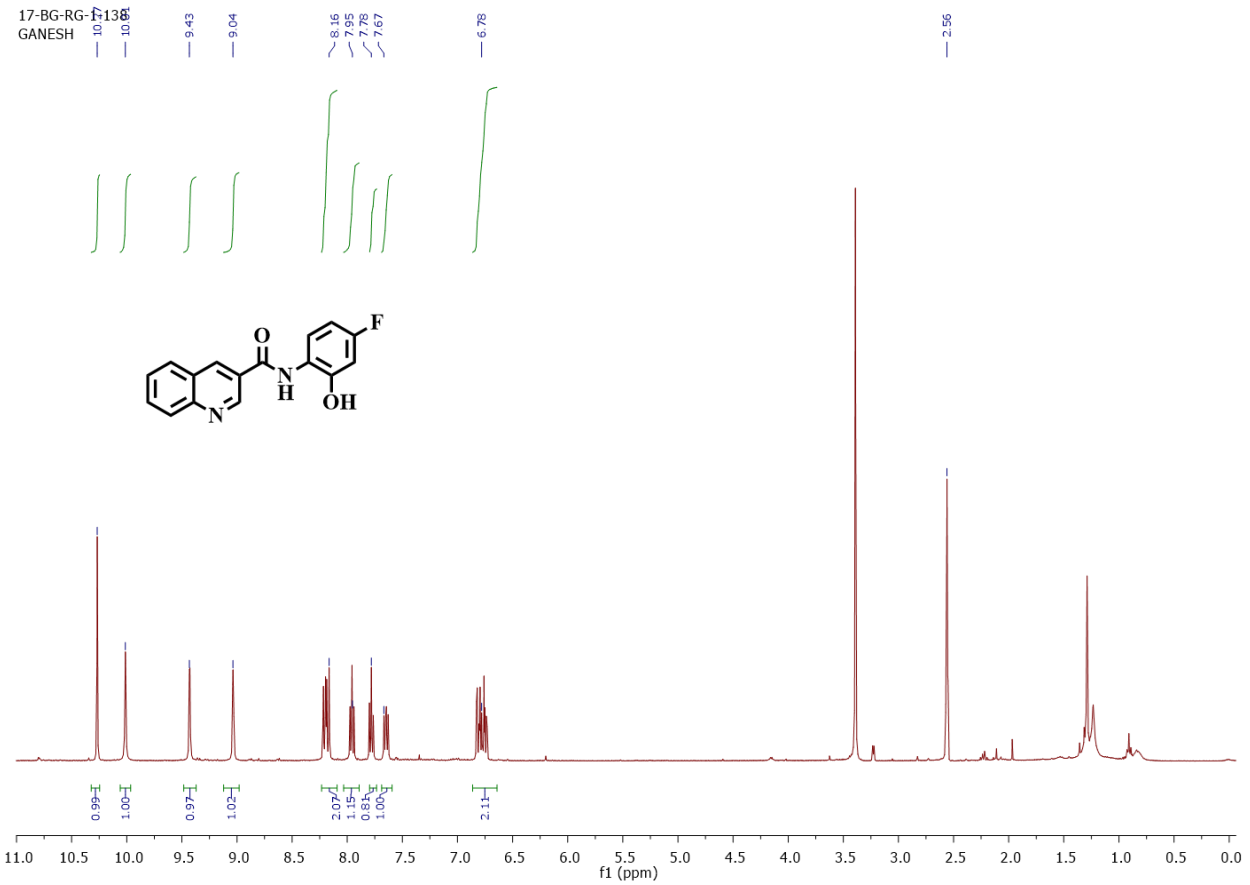
17-BG-RG-I-138
GANESH
10.17
10.04
9.43
9.04
8.16
7.95
7.78
7.67
6.78
2.56
O
N
H
F
OH
N
0.99
1.00
0.97
1.02
2.07
1.15
0.81
1.00
2.11
11.0 10.5 10.0 9.5 9.0 8.5 8.0 7.5 7.0 6.5 6.0 5.5 5.0 4.5 4.0 3.5 3.0 2.5 2.0 1.5 1.0 0.5 0.0
f1 (ppm)

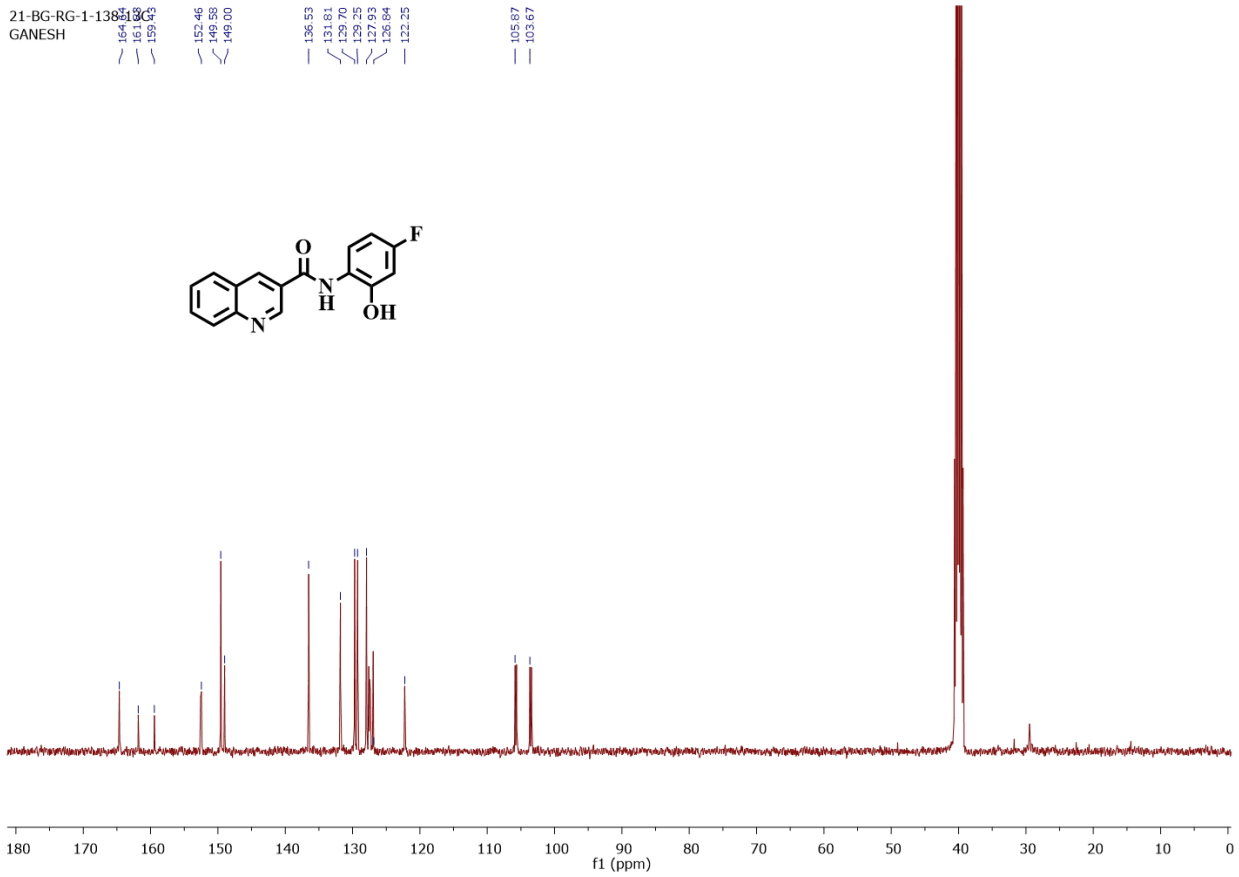
21-BG-RG-1-138-13C
GANESH
164.64
161.68
159.43
152.46
149.58
149.00
136.53
131.81
129.70
129.25
127.93
126.84
122.25
105.87
103.67
O
N
H
OH
F
180
170
160
150
140
130
120
110
100
90
80
70
60
50
40
30
20
10
0
f1 (ppm)

HPLC:

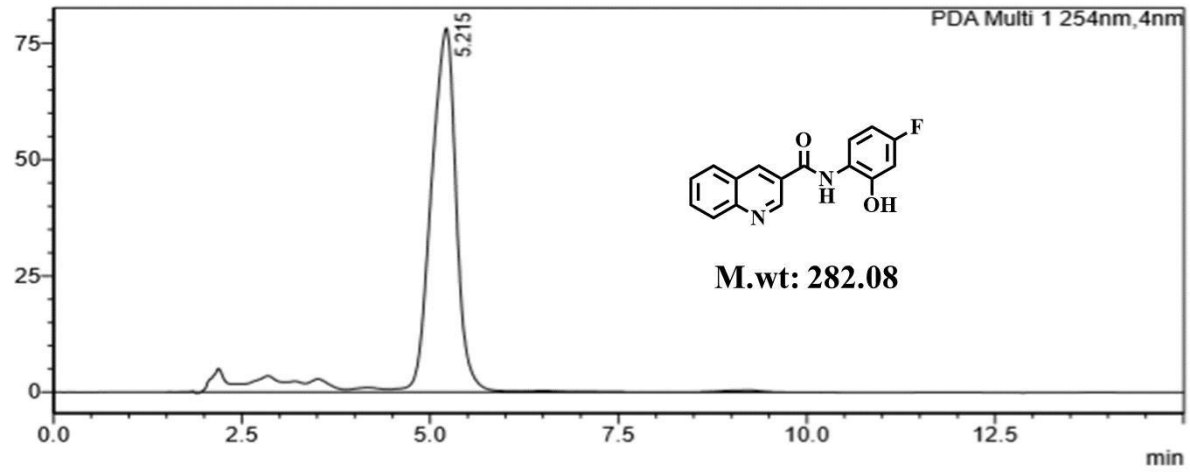
PDA Multi 1 254nm,4nm
5.215
75
50
25
0
0.0
2.5
5.0
7.5
10.0
12.5
min
O
N
H
OH
F
M.wt: 282.08

LCMS:

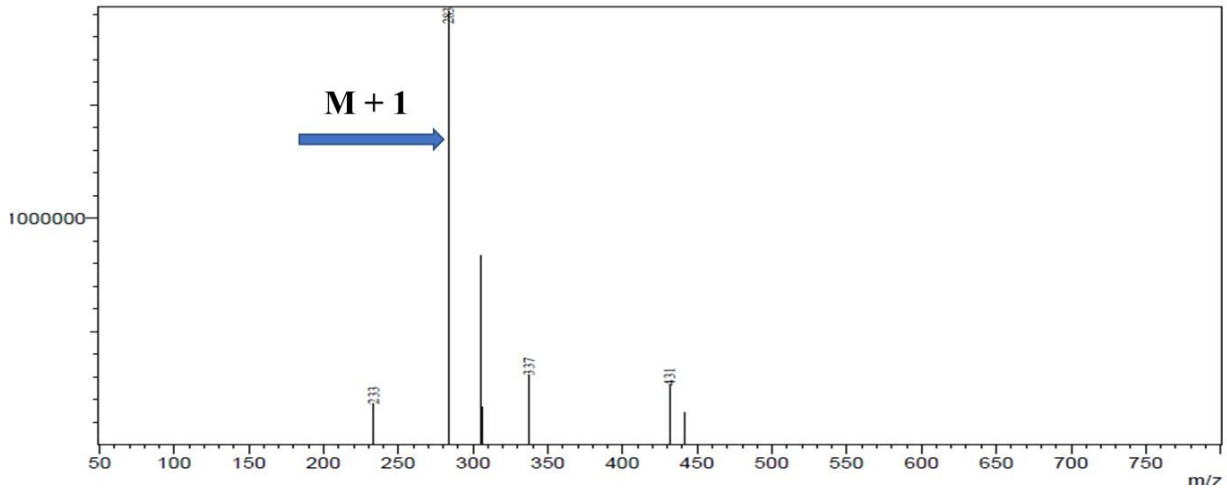
M + 1
1000000
283
233
337
431
50 100 150 200 250 300 350 400 450 500 550 600 650 700 750
m/z

HRMS:

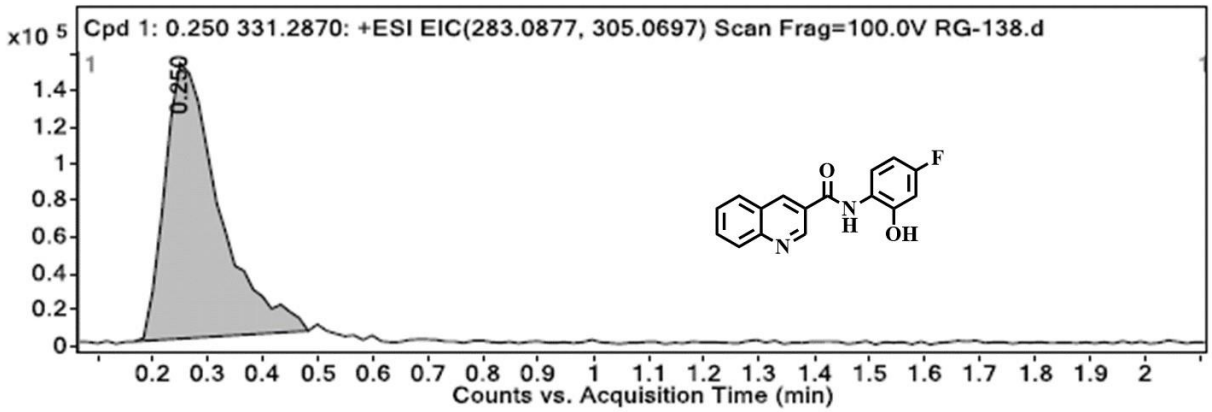
x10 5
Cpd 1: 0.250 331.2870: +ESI EIC(283.0877, 305.0697) Scan Frag=100.0V RG-138.d
1
0.250
1.4
1.2
1
0.8
0.6
0.4
0.2
0
0.2 0.3 0.4 0.5 0.6 0.7 0.8 0.9 1 1.1 1.2 1.3 1.4 1.5 1.6 1.7 1.8 1.9 2
Counts vs. Acquisition Time (min)
O
N
H
F
OH
N

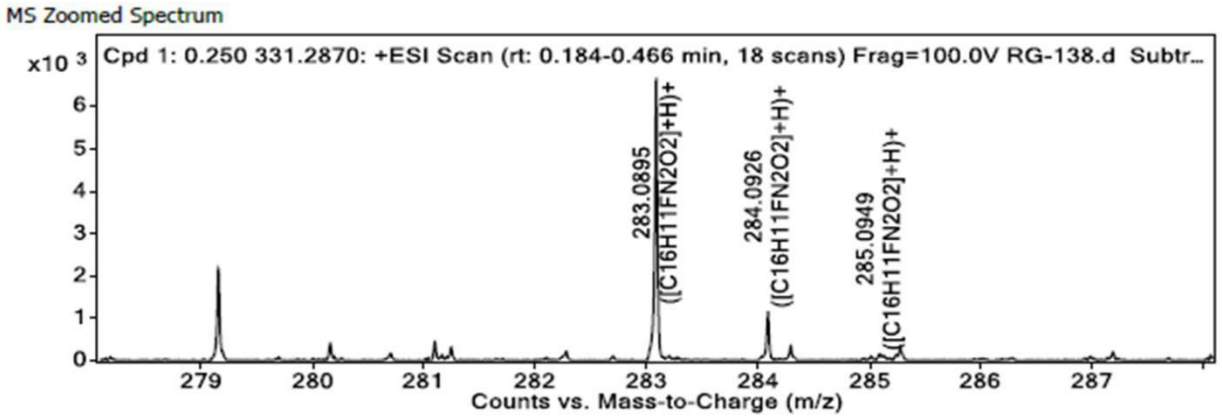

3.4.1.3. Preparation of N-(2-hydroxyphenyl) quinoline-6-carboxamide (11a)

6-Quinoline carboxylic acid (**6**) (100 mg; 0.578 mmol) was dissolved into dichloromethane: pyridine (5 ml: 5 ml). To this mixture, 1-ethyl-3-dimethyl amino propyl carbo di imide (161 mg; 1.04 mmol) and 3mg of 4-dimethylaminopyridine were added. This mixture was subjected to react along with constant stirring for 15 mins before 2-amino phenol (31.5 mg; 0.289 mmol) was added. The reaction was then continued for 9 h at room temperature with continuous stirring. After removal of pyridine under vacuum condition, the mixture was dissolved in ethyl acetate and washed with sodium bicarbonate. The organic part was isolated and excess solvent was evaporated under vacuum. The crude compound was purified using column chromatography (Solvent system – hexane and ethyl acetate (60:40)) in silica 60 - 120 mesh to obtain the final compound in its pure form. (Yield: 46 %). 1H NMR (400 MHz, DMSO-*d6*) δ : 9.79 (s, 2H), 9.02 (d, J = 2.4 Hz, 1H), 8.68 (s, 1H), 8.56 (d, J = 8.0 Hz, 1H), 8.28 (d, J = 8.4 Hz, 1H), 8.15 (d, J = 8.8 Hz, 1H), 7.74 (m, 2H), 7.08 (t, J = 7.2 Hz, 1H), 6.97 (d, J = 8 Hz, 1H) 6.89 (t, J = 7.6 Hz, 1H). 13C NMR (101 MHz, DMSO-*d6*) δ : 165.33, 152.74, 150.08, 149.25, 137.71, 132.73, 129.65, 128.91, 128.37, 127.61,126.21, 124.84, 122.74, 119.51, 116.47. HRMS (AP-ESI) *m/z* calcd for $C_{16}H_{12}N_2O_2$ $[M+H]^+$ 265.0932 $[M+H]^+$ found 265.0983.

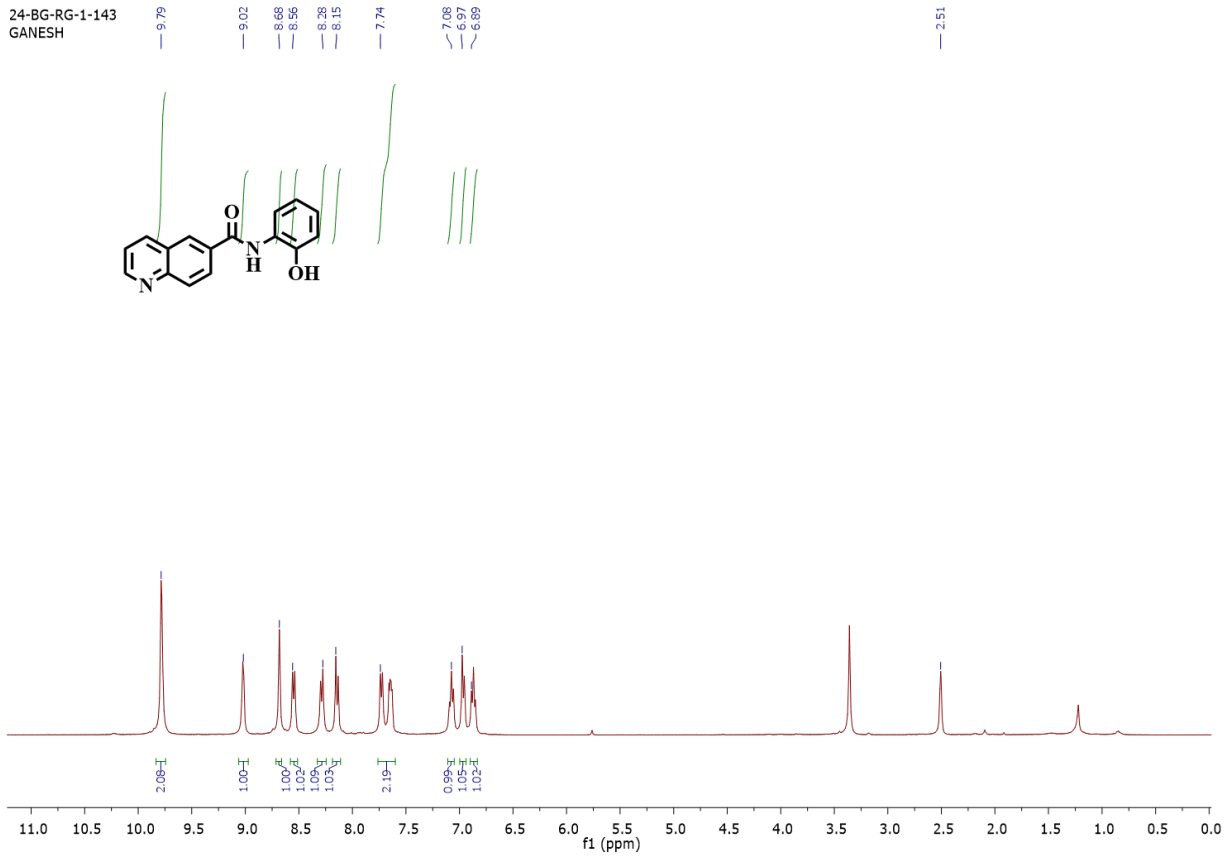
24-BG-RG-1-143
GANESH
9.79
9.02
8.68
8.56
8.28
8.15
7.74
7.08
6.97
6.89
2.51
O
N
H
OH
N
2.08
1.00
1.00
1.02
1.09
1.03
2.19
0.99
1.05
1.02
11.0 10.5 10.0 9.5 9.0 8.5 8.0 7.5 7.0 6.5 6.0 5.5 5.0 4.5 4.0 3.5 3.0 2.5 2.0 1.5 1.0 0.5 0.0
f1 (ppm)

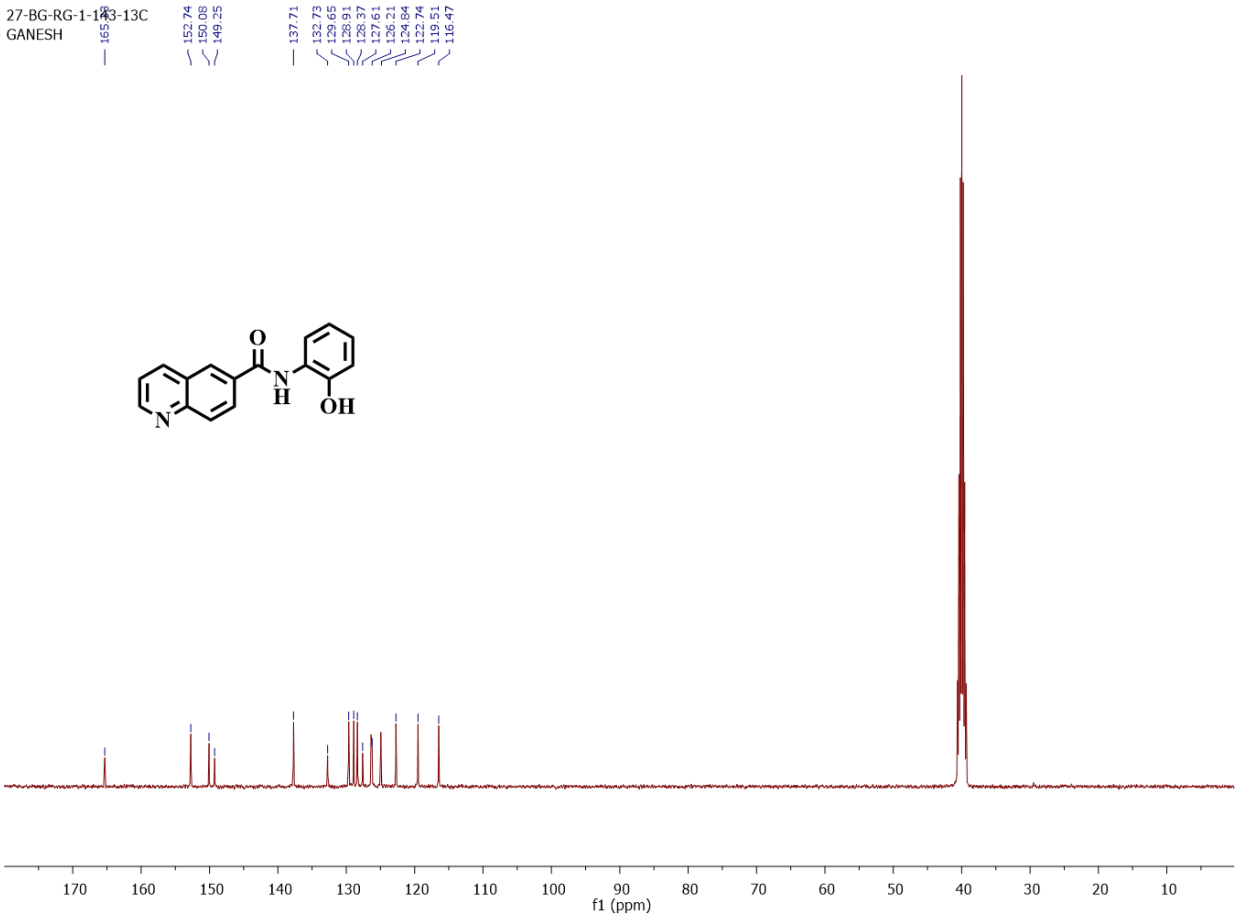
27-BG-RG-1-143-13C
GANESH
165.48
152.74
150.08
149.25
137.71
132.73
129.65
128.91
128.37
127.61
126.21
124.84
122.74
119.51
116.47
O
N
H
OH
N
170
160
150
140
130
120
110
100
90
80
70
60
50
40
30
20
10
f1 (ppm)

HPLC:

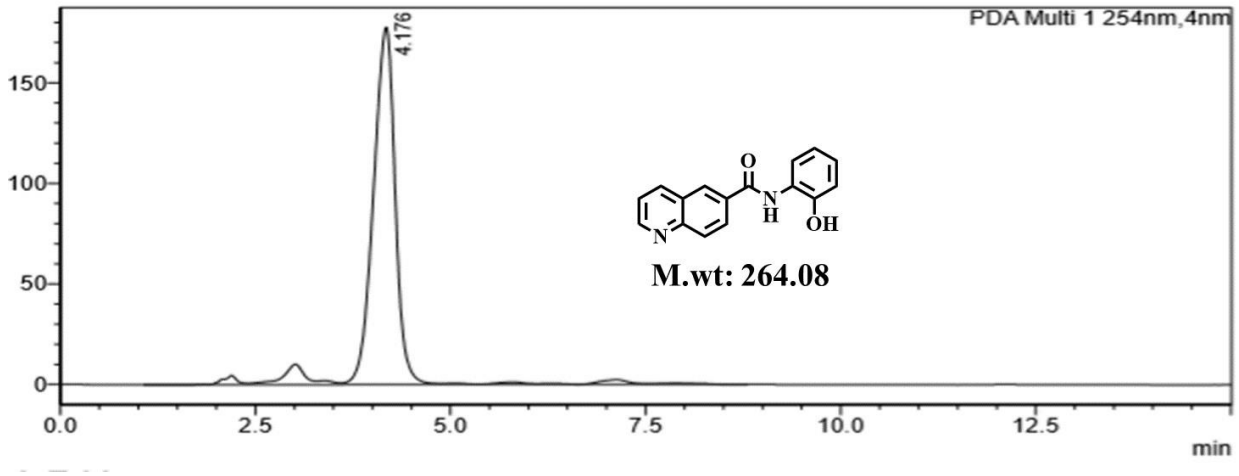
PDA Multi 1 254nm,4nm
4.176
150
100
50
0
0.0
2.5
5.0
7.5
10.0
12.5
min
O
N
H
OH
N
M.wt: 264.08

LCMS:

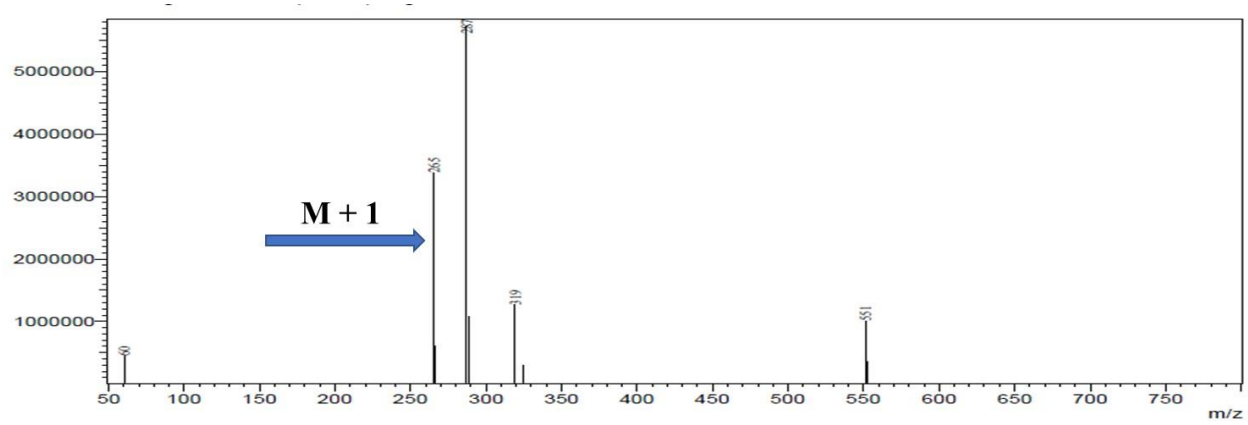
M + 1
5000000
4000000
3000000
2000000
1000000
50
100
150
200
250
300
350
400
450
500
550
600
650
700
750
m/z

HRMS:

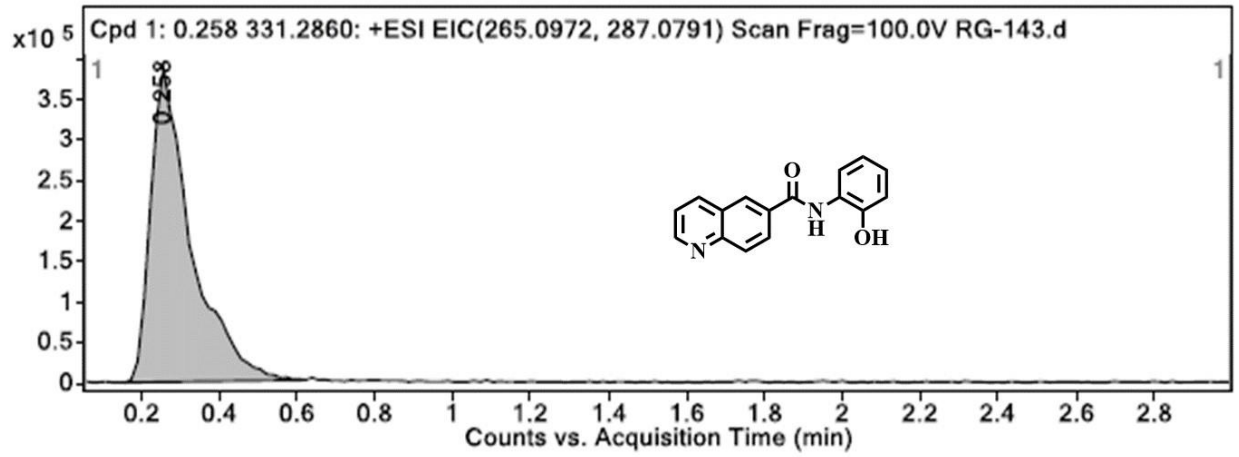
x10 5
Cpd 1: 0.258 331.2860: +ESI EIC(265.0972, 287.0791) Scan Frag=100.0V RG-143.d
0.258
3.5
3
2.5
2
1.5
1
0.5
0
0.2
0.4
0.6
0.8
1
1.2
1.4
1.6
1.8
2
2.2
2.4
2.6
2.8
Counts vs. Acquisition Time (min)
O
N
H
OH
N

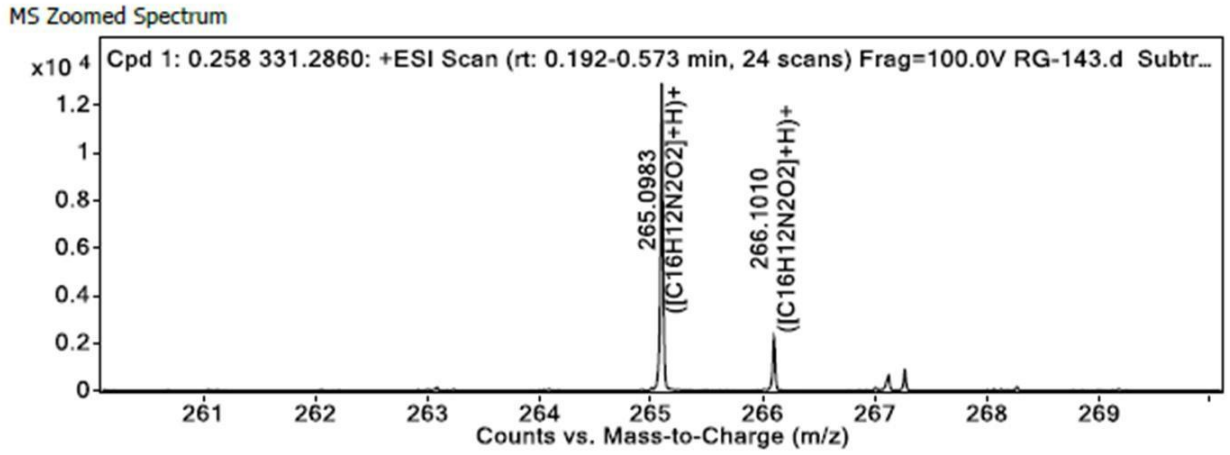

3.4.1.4. Preparation of N-(2-hydroxy-5-floro-phenyl) quinolone-6-carboxamide (11b)

6 - Quinoline carboxylic acid (**6**) (100 mg; 0.578mmol) was dissolved into dichloromethane: pyridine (5 ml: 5 ml). To this mixture, 1-ethyl-3-dimethyl amino propyl carbo di imide (161 mg; 1.04 mmol) and 5mg of 4-dimethylaminopyridine were added. This mixture was settled to react for 15 mins with continuous stirring before 2-amino, 5-fluorophenol (80.75 mg; 0.635 mmol) was added. This reaction was continued with constant stirring at room temperature for 6 h. Finally, pyridine was evaporated under vacuum and the reaction mixture was dissolved in ethyl acetate and washed thoroughly with sodium bicarbonate. The organic portion was collected and excess solvent was removed under vacuum. The crude compound was then purified using column chromatography (Solvent system – hexane and ethyl acetate (70:30)) in silica 60 - 120 mesh to obtain the final compound in its pure form. (Yield: 55%). 1H NMR (400 MHz, DMSO-d_6) δ : 10.25 (s, 1H), 9.80 (s, 1H), 9.01 (dd, J = 1.6, 1.6 Hz, 1H), 8.68 (s, 1H), 8.52 (s, 1H), 8.27 (dd, J = 1.6, 1.6 Hz, 1H), 8.15 (d, J = 8.8 Hz, 1H), 7.62 (dd, J = 4.4 Hz, 4.0 Hz, 2H), 6.73 (dd, J = 2.8, 2.8 Hz, 2H).^{13}C NMR (101 MHz, DMSO-d_6) δ : 165.45, 161.68, 159.28, 152.72, 149.35, 137.69, 132.62, 129.58, 128.97, 128.42, 127.58, 127.06, 122.83, 105.84, 103.40. HRMS (AP-ESI) *m/z* calcd for $C_{16}H_{11}FN_2O_2$ $[M+H]^+$: 283.0838 $[M+H]^+$ found 283.0891.

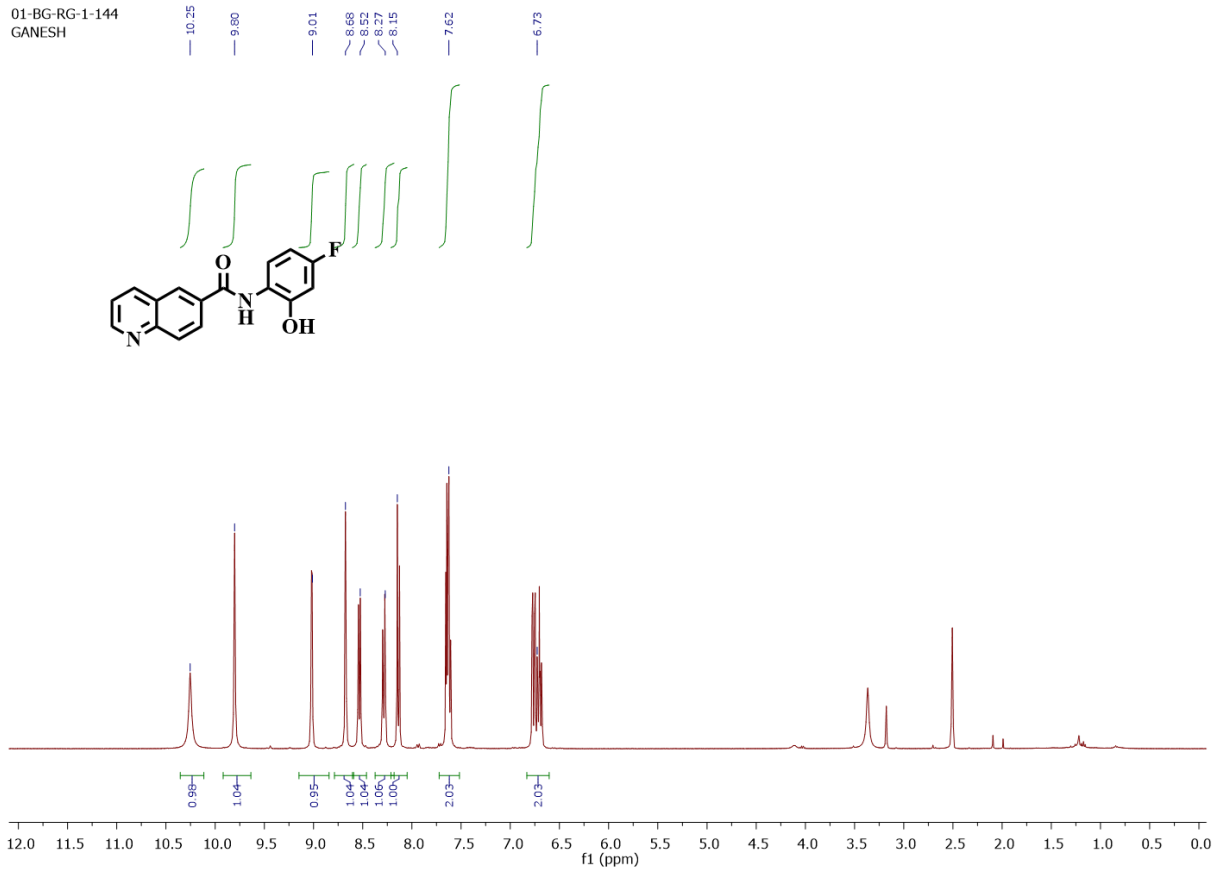
01-BG-RG-1-144
GANESH
10.25
9.80
9.01
8.68
8.52
8.27
8.15
7.62
6.73
O
N
H
F
OH
N
0.98
1.04
0.95
1.04
1.04
1.06
1.00
2.03
2.03
12.0 11.5 11.0 10.5 10.0 9.5 9.0 8.5 8.0 7.5 7.0 6.5 6.0 5.5 5.0 4.5 4.0 3.5 3.0 2.5 2.0 1.5 1.0 0.5 0.0
f1 (ppm)

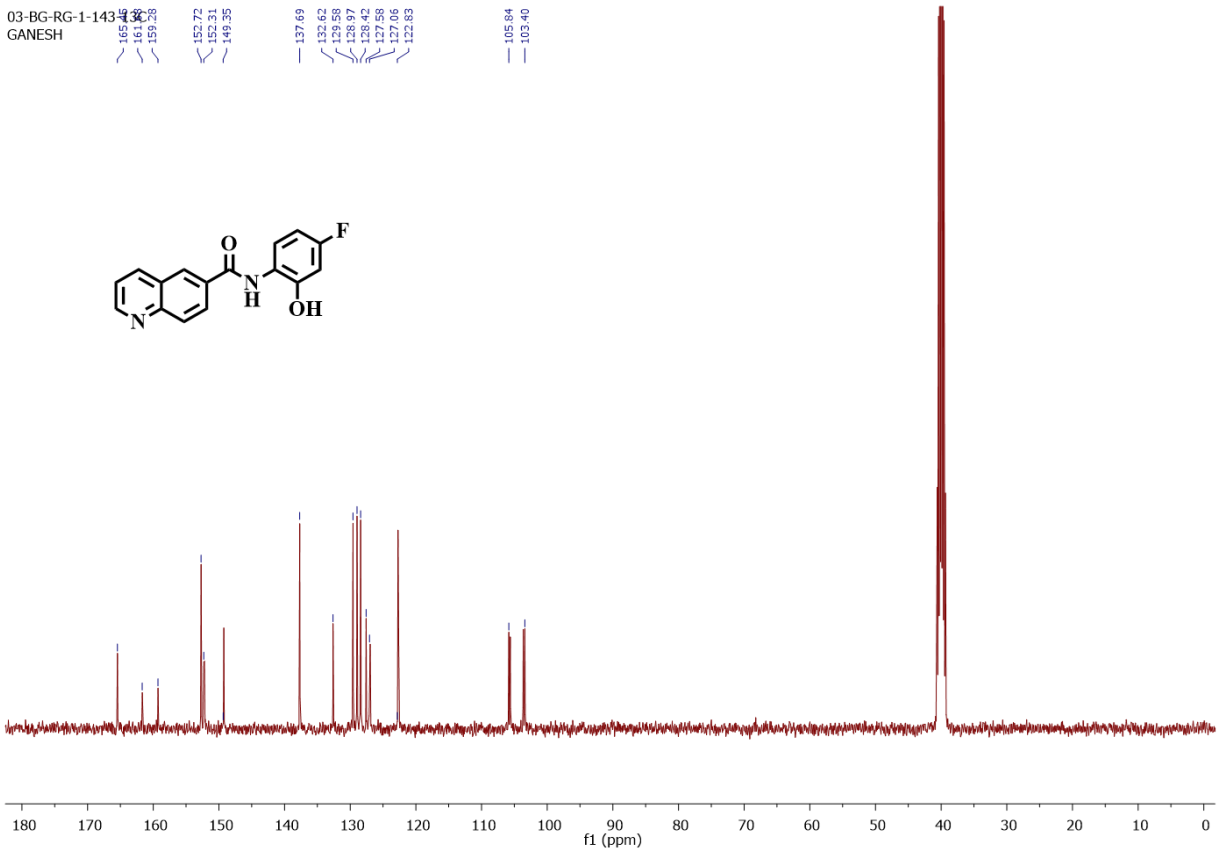
03-BG-RG-1-143-13C
GANESH
165.15
161.32
159.28
152.72
152.31
149.35
137.69
132.62
129.58
128.97
128.42
127.58
127.06
122.83
105.84
103.40
O
N
H
F
OH
N
180
170
160
150
140
130
120
110
100
90
80
70
60
50
40
30
20
10
0
f1 (ppm)

HPLC:

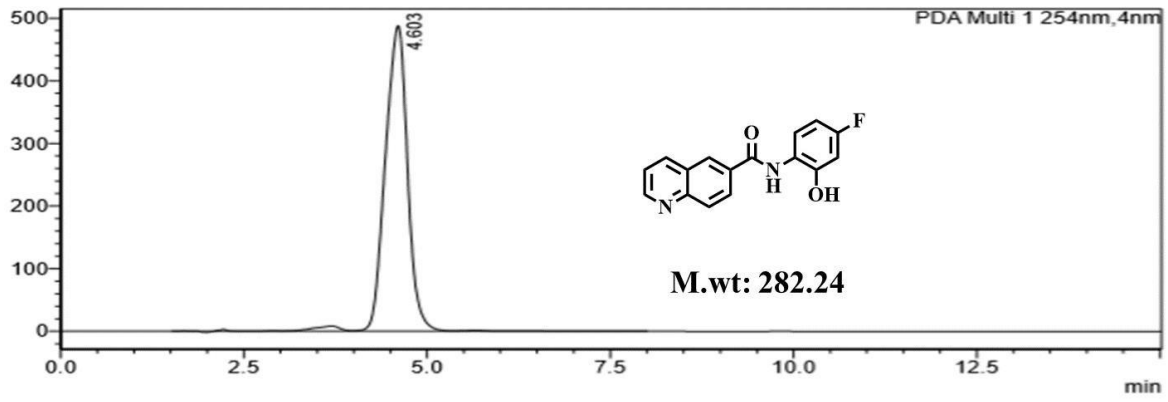
PDA Multi 1 254nm,4nm
4.603
500
400
300
200
100
0
0.0
2.5
5.0
7.5
10.0
12.5
min
O
N
H
F
OH
N
M.wt: 282.24

LCMS:

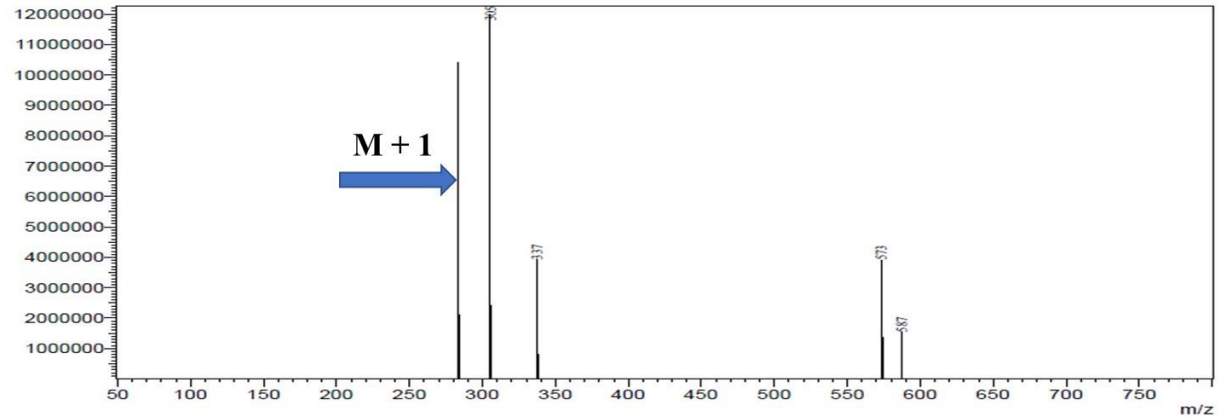
M + 1
12000000
11000000
10000000
9000000
8000000
7000000
6000000
5000000
4000000
3000000
2000000
1000000
50
100
150
200
250
300
350
400
450
500
550
600
650
700
750
m/z

HRMS:

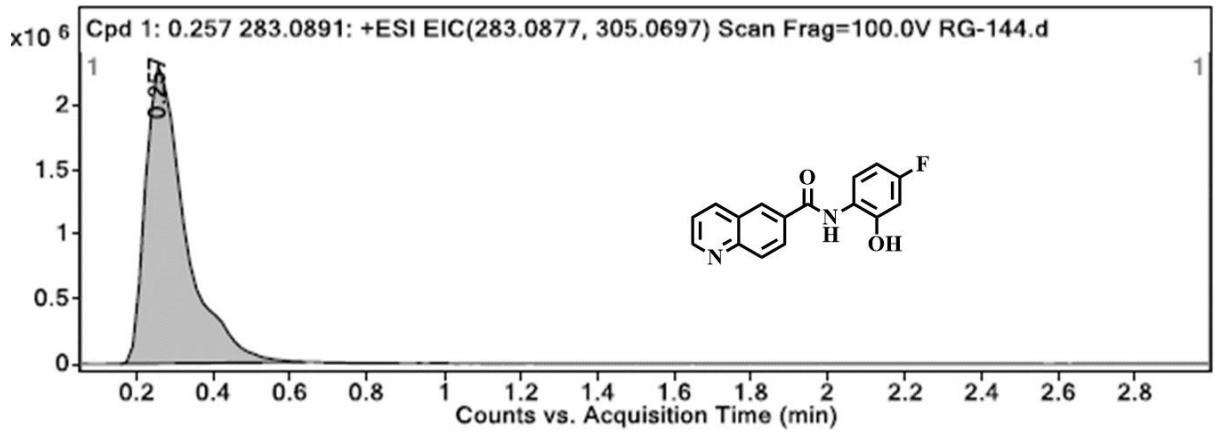
Cpd 1: 0.257 283.0891: +ESI EIC(283.0877, 305.0697) Scan Frag=100.0V RG-144.d
x10 6
2
1.5
1
0.5
0
0.257
O
N
H
F
OH
N
0.2
0.4
0.6
0.8
1
1.2
1.4
1.6
1.8
2
2.2
2.4
2.6
2.8
Counts vs. Acquisition Time (min)

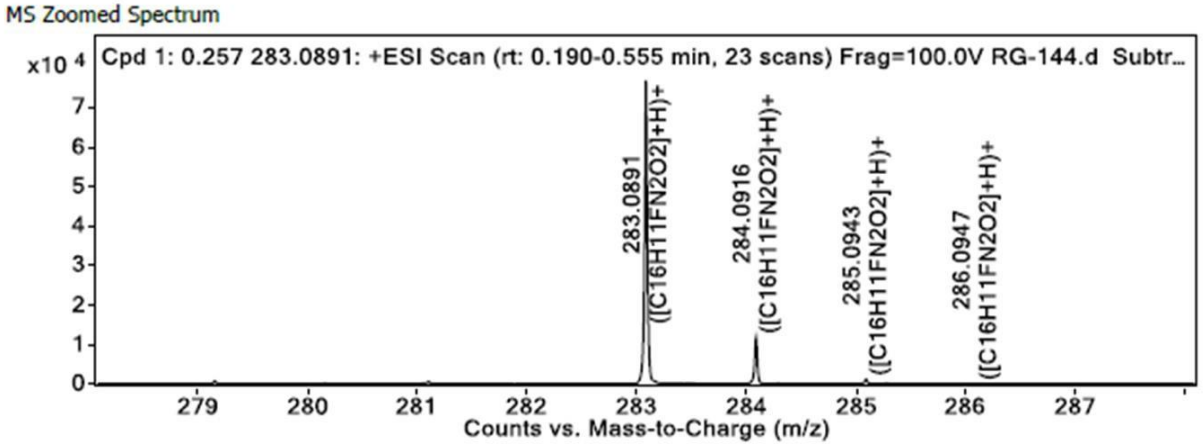

3.4.1.5. Preparation of N-(2-hydroxy phenyl)-1H-indole-6-carboxamide (12a)

Indole-6-carboxylic acid (**7**) (150 mg; 0.931 mmoles) was dissolved in dichloromethane and added Pyridine (5 ml) under 0 °C. To this mixture, 1-ethyl-3-dimethyl amino propyl carbo di imide,(259.74 mg; 1.675 mmol) and 5 mg of 4-dimethylaminopyridine, were added. This mixture was subjected to react with constant stirring for 15 mins before the addition of 2-amino phenol (111.6 mg; 1.0241 mmol) into the reaction mixture. This reaction was continued with constant stirring at room temperature for 6 h. Finally, pyridine was evaporated and the mixture was dissolved in ethyl acetate and washed with water. The organic part was then separated and subsequently, excess solvent was evaporated under vacuum. The crude compound was then purified by using column chromatography (Solvent system – hexane and ethyl acetate (60: 40)) in silica 60 – 120 mesh to obtain the final compound in its pure form. (Yield: 46%). ^{1}H NMR (400 MHz, DMSO-*d6*) δ : 11.48 (s, 1H), 9.86 (s, 1H), 9.49 (s, 1H), 8.09 (s, 1H), 7.80 (dd, *J* = 1.2, 1.6 Hz, 1H), 7.68 (dd, *J* =1.6,1.2 Hz, 2H), 7.57 (t, *J* = 2.8 Hz, 1H), 7.03 (m, 1H), 6.96 (dd, *J* = 1.6, 1.6 Hz, 1H), 6.86 (dd, *J*= 1.6, 1.2 Hz, 1H), 6.55 (t, *J* = 2.0 Hz, 1H). ^{13}C NMR (101 MHz, DMSO-*d6*) δ : 166.74, 149.15,135.75, 130.77, 129.03, 127.28, 127.05, 125.73, 123.58, 120.27, 119.63,

118.51, 116.57, 112.04, 101.87. HRMS (AP-ESI) *m/z* calcd for $C_{15}H_{12}N_2O_2$ $[M+H]^+$ 253.0932 $[M+H]^+$ found 253.0984.

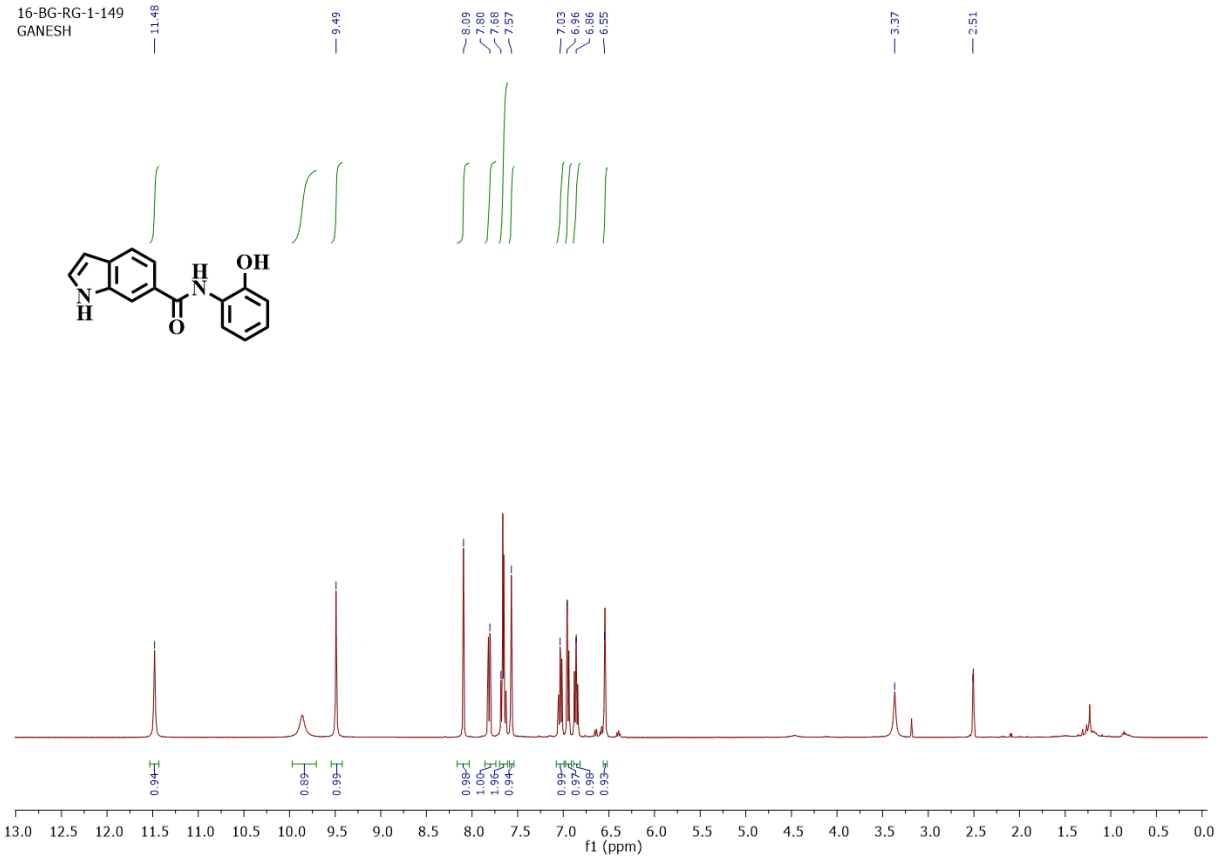

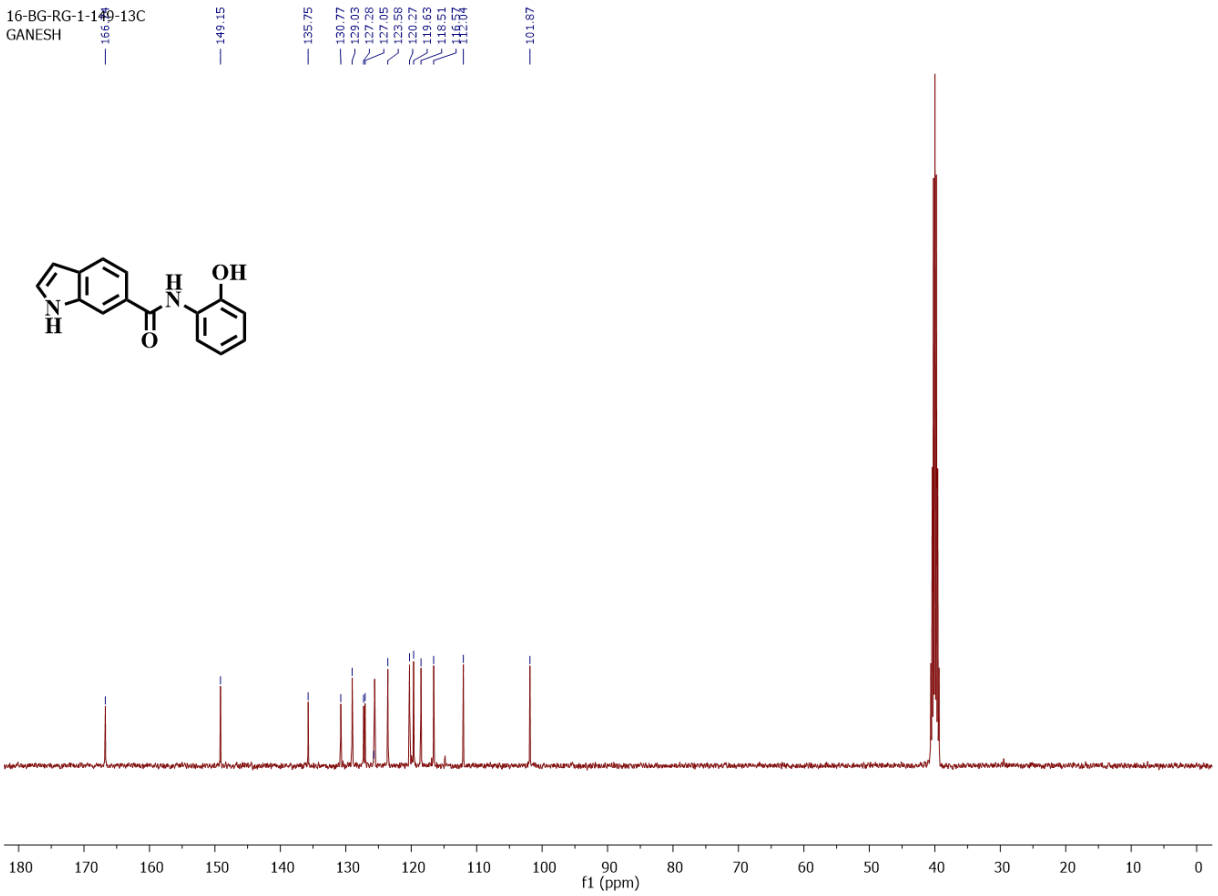
16-BG-RG-1-149-13C
GANESH
166.47
149.15
135.75
130.77
129.03
127.28
127.05
123.58
120.27
119.63
118.51
116.54
101.87
OH
H
N
N
H
O
180
170
160
150
140
130
120
110
100
90
80
70
60
50
40
30
20
10
0
f1 (ppm)

HPLC:

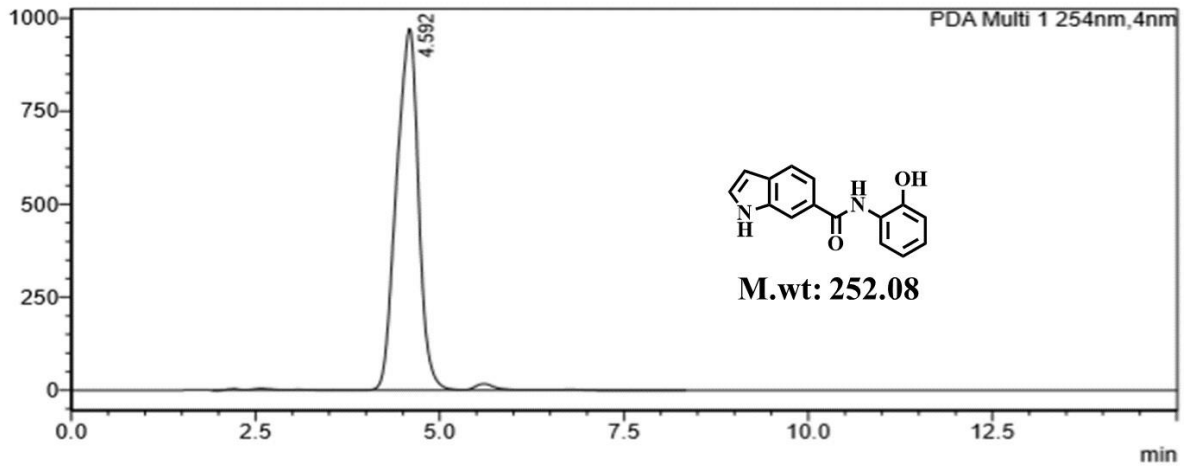
PDA Multi 1 254nm,4nm
4.592
1000
750
500
250
0
0.0
2.5
5.0
7.5
10.0
12.5
min
OH
H
N
N
H
O
M.wt: 252.08

LCMS:

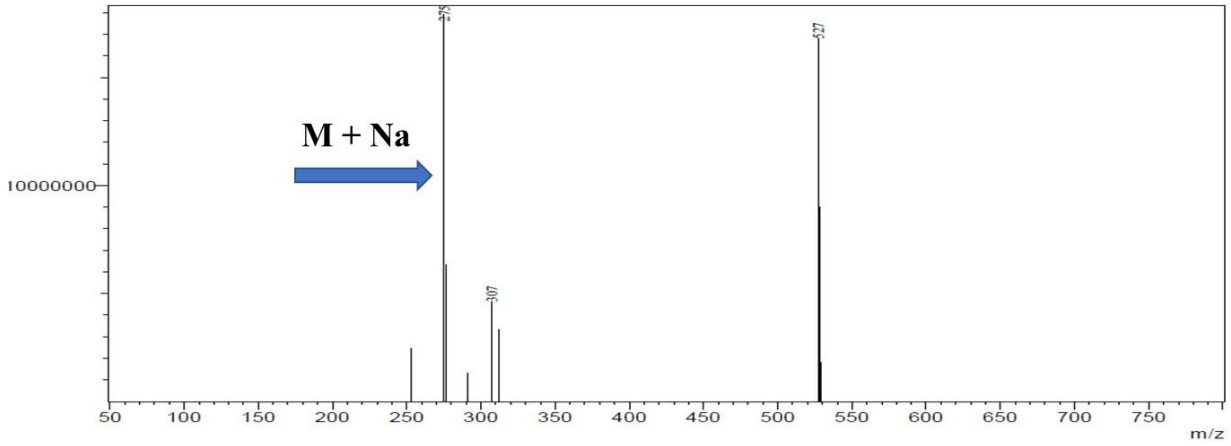
M + Na
10000000
275
527
307
50 100 150 200 250 300 350 400 450 500 550 600 650 700 750
m/z

HRMS:

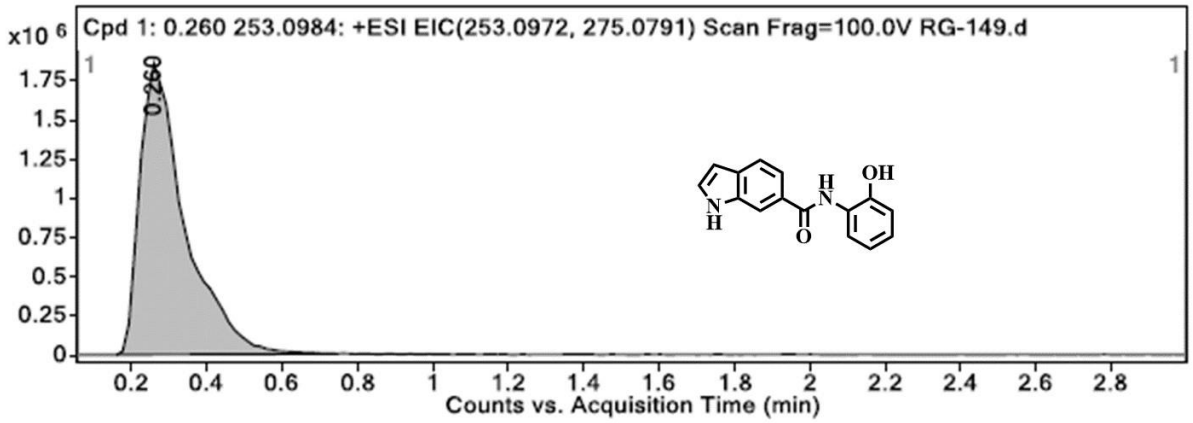
x10 6
Cpd 1: 0.260 253.0984: +ESI EIC(253.0972, 275.0791) Scan Frag=100.0V RG-149.d
0.260
1.75
1.5
1.25
1
0.75
0.5
0.25
0
0.2 0.4 0.6 0.8 1 1.2 1.4 1.6 1.8 2 2.2 2.4 2.6 2.8
Counts vs. Acquisition Time (min)
OH
N
H
H
N
O

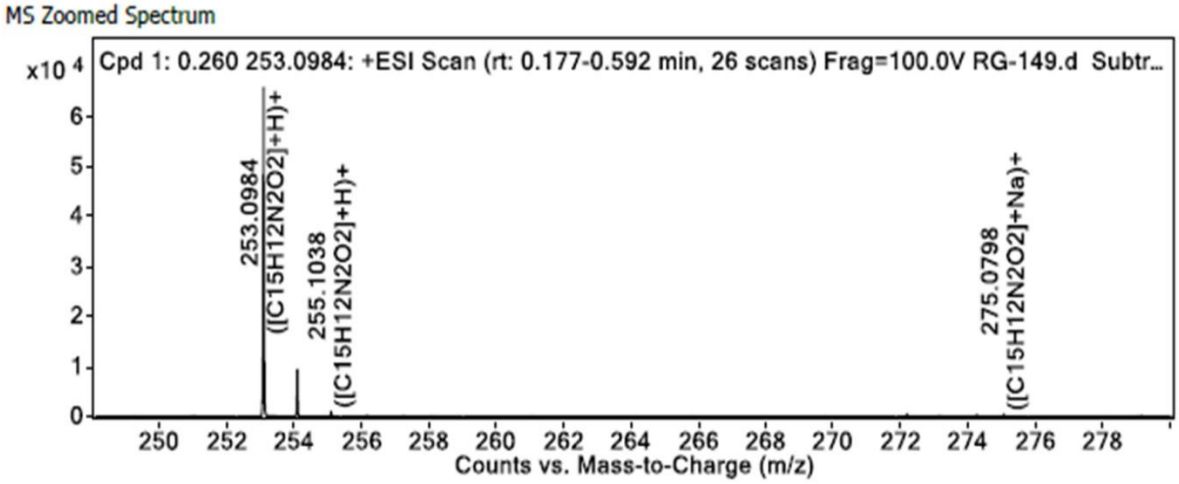
MS Zoomed Spectrum
x10 4
Cpd 1: 0.260 253.0984: +ESI Scan (rt: 0.177-0.592 min, 26 scans) Frag=100.0V RG-149.d Subtr...
253.0984
([C15H12N2O2]+H)+
255.1038
([C15H12N2O2]+H)+
275.0798
([C15H12N2O2]+Na)+
6
5
4
3
2
1
0
250 252 254 256 258 260 262 264 266 268 270 272 274 276 278
Counts vs. Mass-to-Charge (m/z)

3.4.1.6. Preparation of N-(4-fluoro-2-hydroxyl phenyl)-1-H-Indole-6-Carboxamide (12b)

Indole-6-carboxylic acid (**7**) (100 mg; 0.621 mmol) was dissolved in dichloromethane and added Pyridine (5 ml) under 0 °C. To this mixture, 1-ethyl-3-dimethyl amino propyl carbo di imide (173.25 mg; 1.117 mmol) and 5 mg of 4-dimethylaminopyridine were added with continuous stirring for 15 mins before 2-amino-5-fluoro phenol (86.77 mg; 0.683 mmol) was added into the reaction mixture. This reaction was carried out under continuous stirring at room temperature for 6 h. After that, pyridine was evaporated and the mixture was dissolved in ethyl acetate and washed thoroughly with water. The organic portion was then isolated and excess solvent was evaporated under vacuum. Finally, the crude compound obtained was purified by using column chromatography (Solvent system – hexane and ethyl acetate (65:35)) in silica 60 – 120 mesh to obtain N-(4-fluoro-2-hydroxyl phenyl)-1-H-Indole-6-Carboxamide in its pure form. (Yield: 42%). 1H NMR (400 MHz, DMSO-*d6*) δ : 11.46 (s, 1H), 10.29 (s, 1H), 9.47 (s, 1H), 8.08 (s, 1H), 7.65 (dd, J = 2.4, 0.8 Hz, 3H), 7.56 (t, J = 2.8 Hz,1H), 6.73 (dd, J = 2.8, 2.8 Hz, 2H), 6.53 (t, J = 1.6 Hz, 1H). ^{13}C NMR (101 MHz, DMSO-d_6) δ : 166.85, 151.28, 135.71, 130.73, 128.96, 127.19, 125.62, 123.43, 120.16, 118.60, 112.11, 105.85, 105.63, 103.62, 101.84. HRMS (AP-ESI) *m/z* calcd for $C_{15}H_{11}FN_2O_2$ $[M+H]^+$ 271.0838 $[M+H]^+$ found 271.0878 $[M+H]^+$.

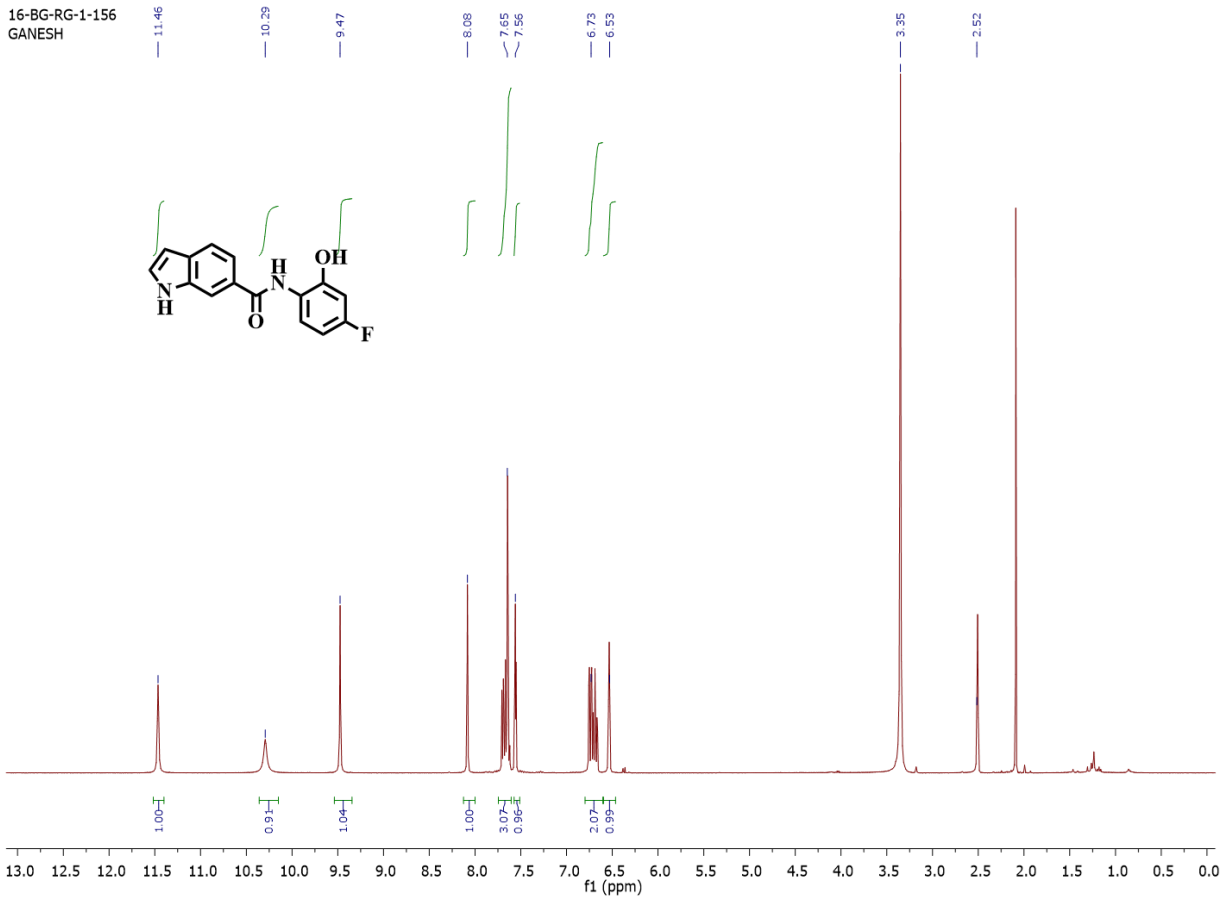
16-BG-RG-1-156
GANESH
11.46
10.29
9.47
8.08
7.65
7.56
6.73
6.53
3.35
2.52
OH
H
N
N
H
O
F
1.00
0.91
1.04
1.00
3.07
0.96
2.07
0.99
13.0 12.5 12.0 11.5 11.0 10.5 10.0 9.5 9.0 8.5 8.0 7.5 7.0 6.5 6.0 5.5 5.0 4.5 4.0 3.5 3.0 2.5 2.0 1.5 1.0 0.5 0.0
f1 (ppm)

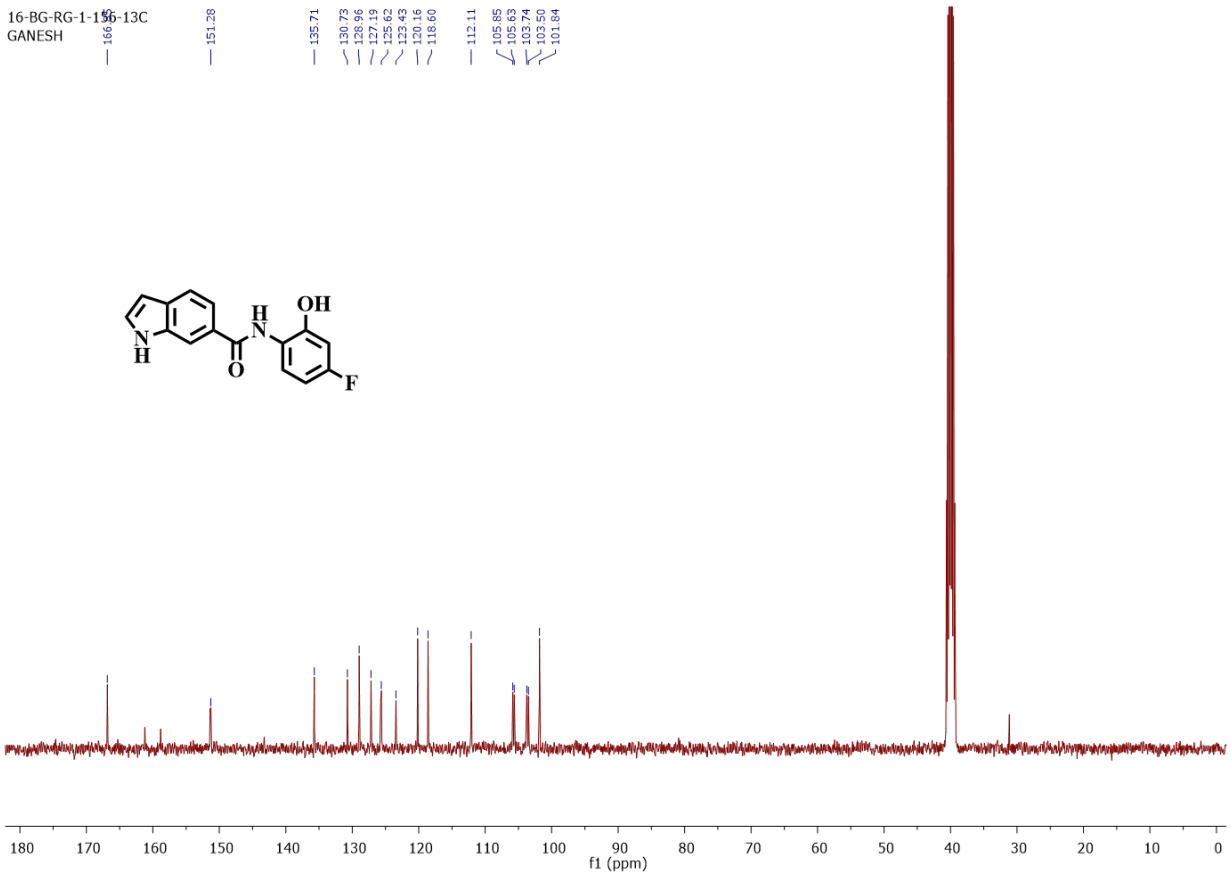
16-BG-RG-1-156-13C
GANESH
166.42
151.28
135.71
130.73
128.96
127.19
125.62
123.43
120.16
118.60
112.11
105.85
105.63
103.74
103.50
101.84
OH
H
N
N
H
O
F
180
170
160
150
140
130
120
110
100
90
80
70
60
50
40
30
20
10
0
f1 (ppm)

.

HPLC:

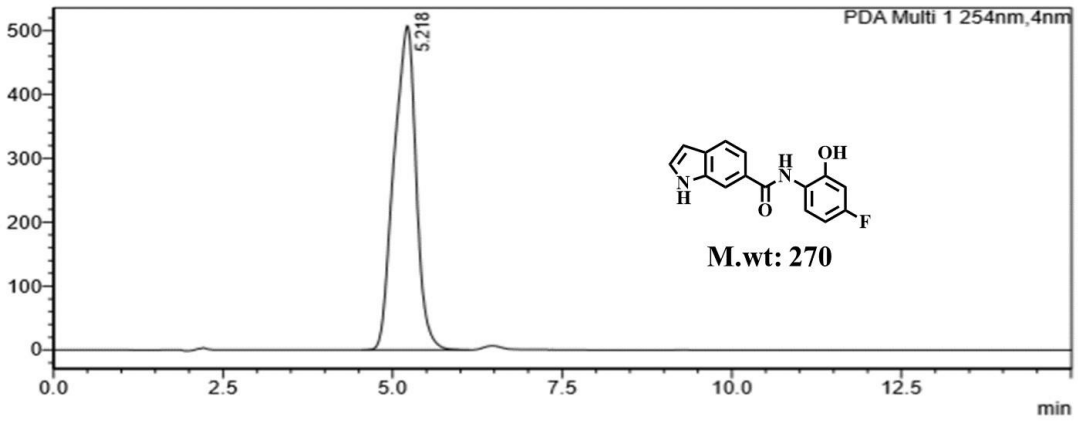

LCMS:

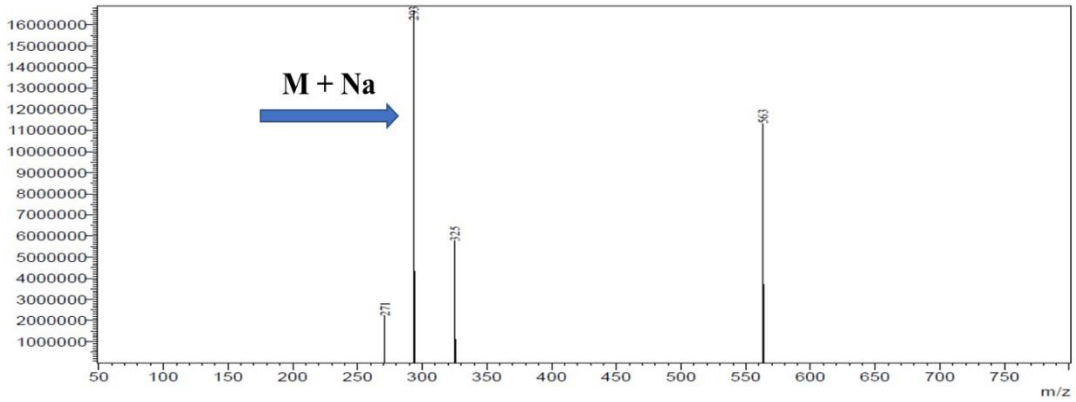

HRMS:

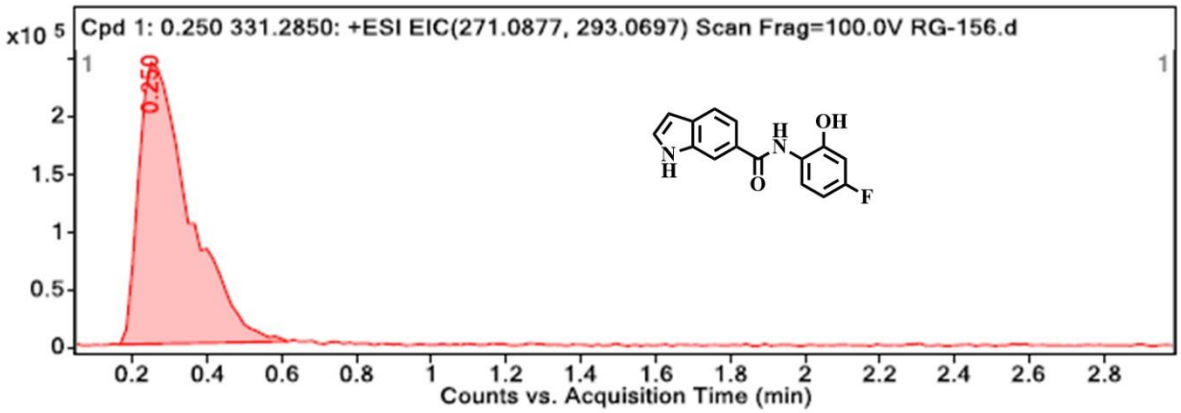

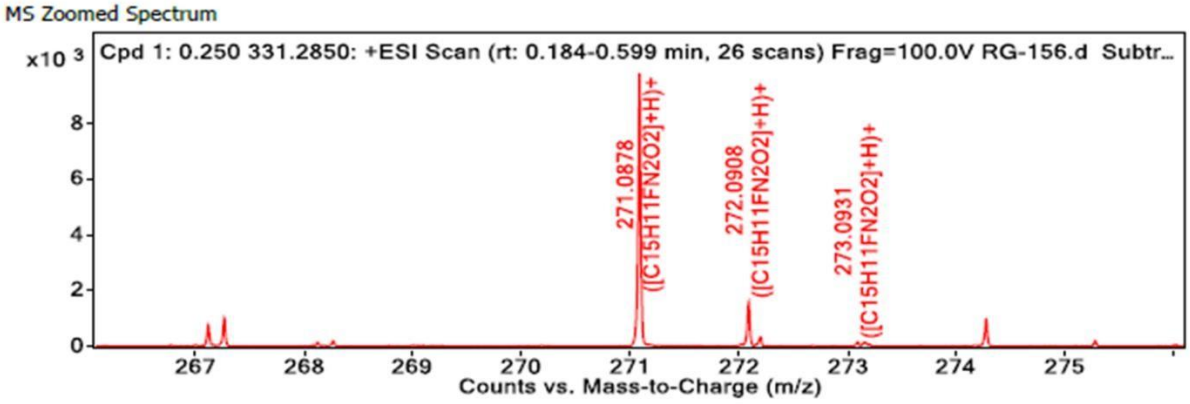

3.4.1.7. Preparation of N-(2-hydroxy phenyl)-1H-indole-3-carboxamide (13a)

Indole-3-carboxylic acid (8) (100 mg; 0.621 mmol) was dissolved in dichloromethane and added Pyridine (5 ml) under 0 °C. To this mixture, 1-ethyl-3-dimethyl amino propyl carbo di imide, (173 mg; 1.11 mmol) and 5mg of 4-dimethylaminopyridine were added. This mixture was allowed to react under constant stirring for 15 mins before 2-aminophenol (74.47 mg; 0.683 mmol) was added into the reaction mixture. This reaction was continued for 6 h at room temperature with constant stirring. After the reaction was over, pyridine was evaporated under vacuum and the mixture was dissolved in ethyl acetate and washed with water. The organic portion was then collected and excess solvent was evaporated. The crude compound was then purified using column chromatography (Solvent system – hexane and ethyl acetate (60: 40)) in silica 230 - 400 mesh to finally obtain the final compound in its pure form. (Yield: 30%). ^{1}H NMR (400 MHz, DMSO -d_6) δ : 11.83 (s, 1H), 9.96 (s, 1H), 9.24 (s, 1H), 8.31 (d, J = 3.2 Hz, 1H), 8.17 (d, J = 1.6 Hz, 1H), 7.75 (dd, J = 1.2, 1.2 Hz, 1H), 7.49 (dd, J = 1.2, 1.6 Hz, 1H), 7.20 (dd, J = 1.6, 2.0 Hz, 2H), 6.95 (dd, J = 1.2, 1.2 Hz, 3H).^{13}C NMR (101 MHz, DMSO-d_6) δ : 164.15, 148.74, 136.81, 129.97, 127.29, 126.24, 125.14, 123.19, 122.70, 121.12,120.84 – 120.68, 119.69, 116.83, 112.69, 110.50. HRMS (AP-ESI) *m/z* calcd for $C_{15}H_{12}N_2O_2$ $[M+H]^+$ 253.0932 $[M+H]^+$ found 253.0984 $[M+H]^+$.

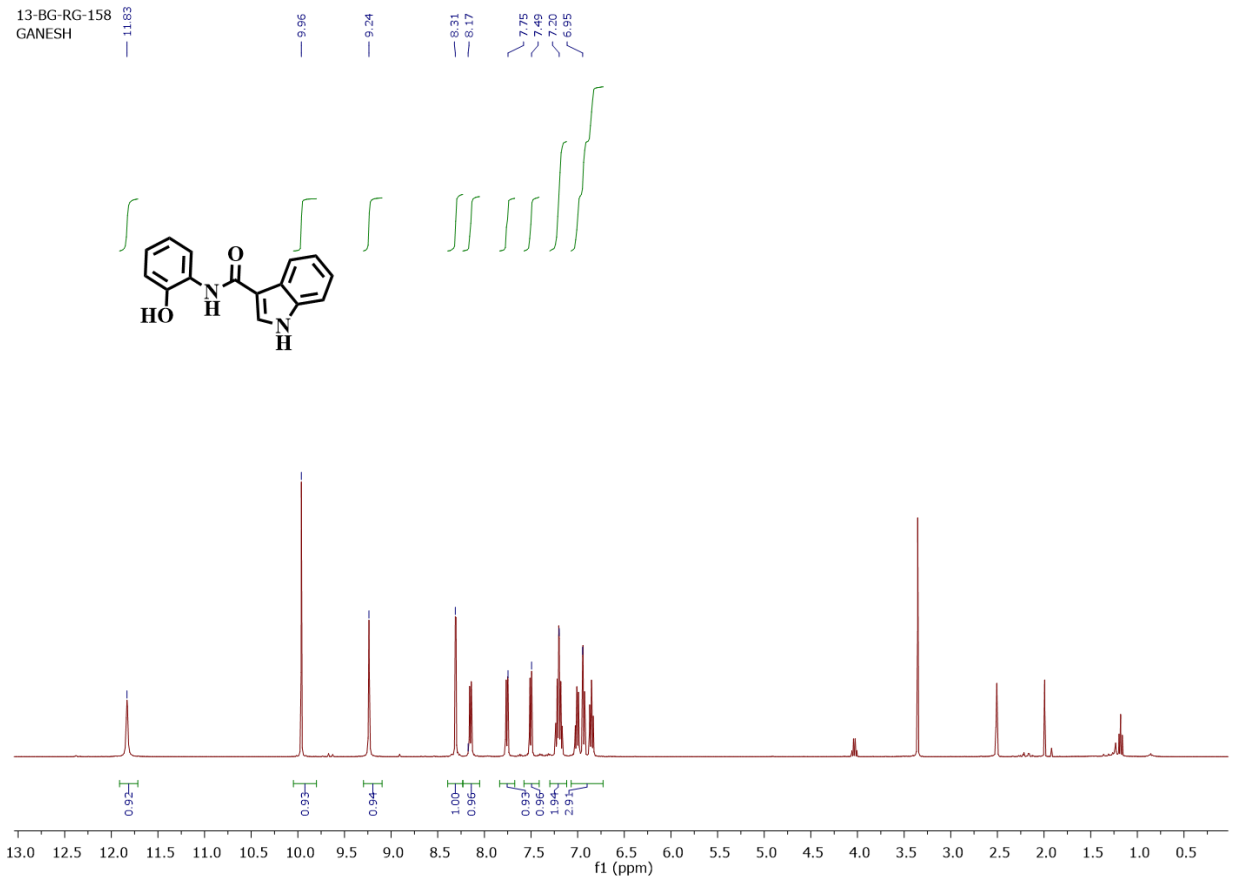
13-BG-RG-158
GANESH
11.83
9.96
9.24
8.31
8.17
7.75
7.49
7.20
6.95
HO
N
H
O
N
H
0.92
0.93
0.94
1.00
0.96
0.93
0.96
1.94
2.94
13.0 12.5 12.0 11.5 11.0 10.5 10.0 9.5 9.0 8.5 8.0 7.5 7.0 6.5 6.0 5.5 5.0 4.5 4.0 3.5 3.0 2.5 2.0 1.5 1.0 0.5
f1 (ppm)

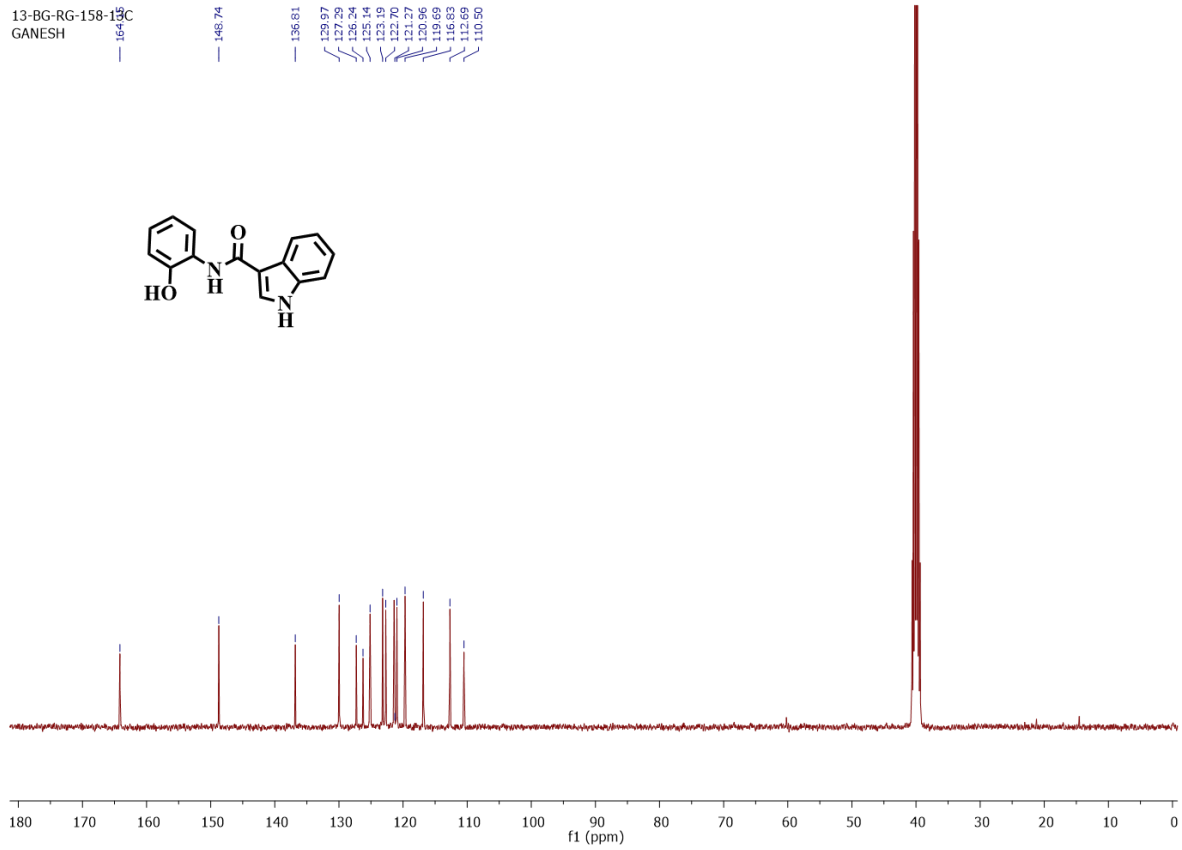
13-BG-RG-158-13C
GANESH
164.74
148.74
136.81
129.97
127.29
126.24
125.14
123.19
122.70
121.27
120.96
119.69
116.83
112.69
110.50
HO
N
H
O
N
H
180
170
160
150
140
130
120
110
100
90
80
70
60
50
40
30
20
10
0
f1 (ppm)

HPLC:

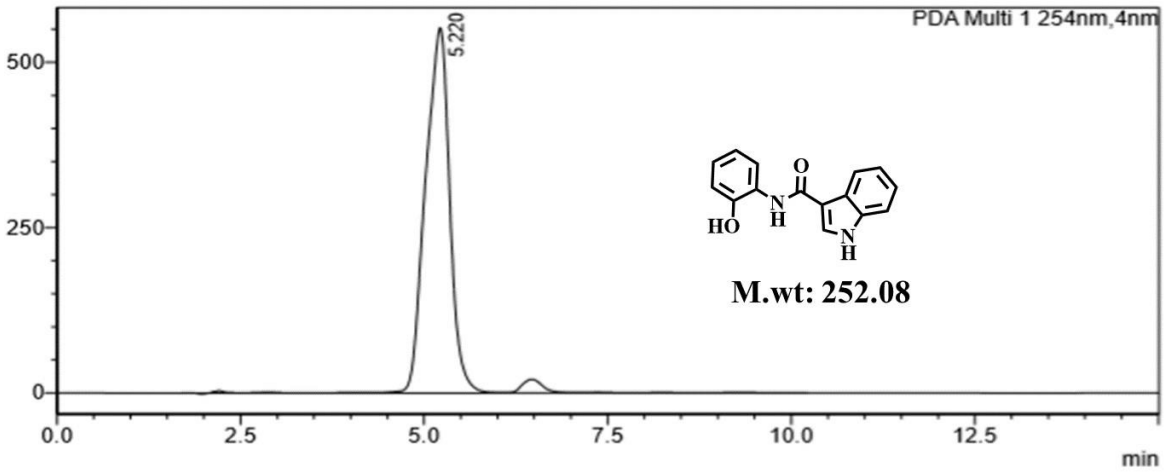
PDA Multi 1 254nm,4nm
5.220
500
250
0
0.0
2.5
5.0
7.5
10.0
12.5
min
HO
N
H
O
N
H
M.wt: 252.08

LCMS:

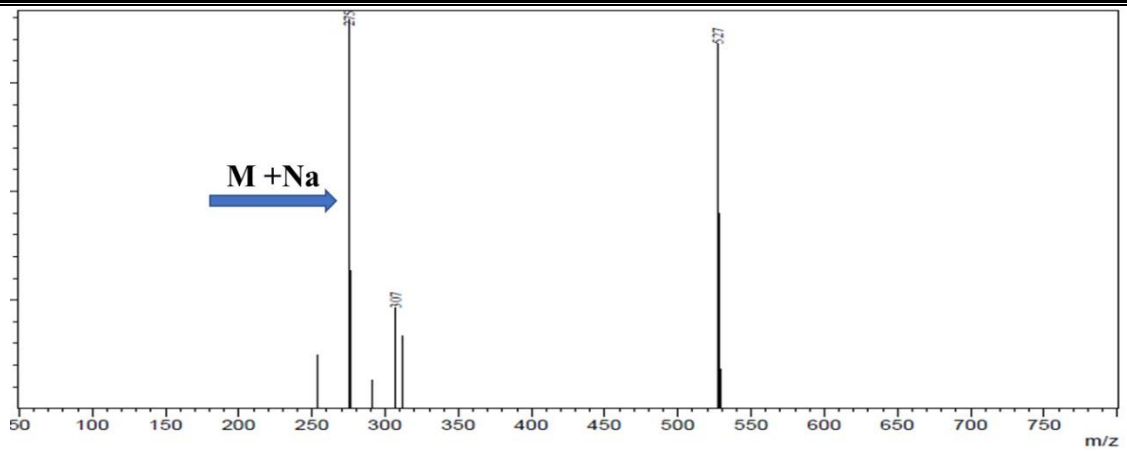
M +Na
275
307
527
50 100 150 200 250 300 350 400 450 500 550 600 650 700 750
m/z

HRMS:

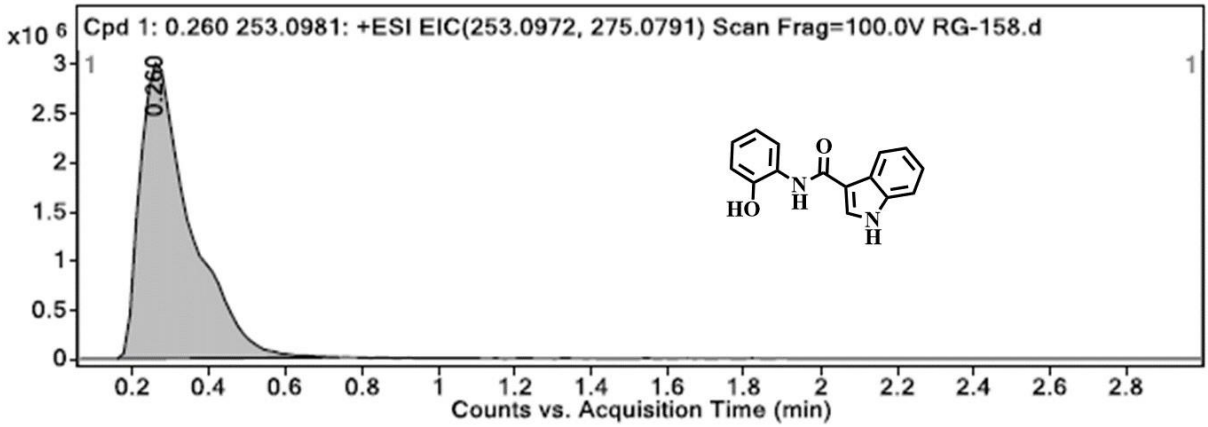
Cpd 1: 0.260 253.0981: +ESI EIC(253.0972, 275.0791) Scan Frag=100.0V RG-158.d
x10 6
0.260
HO
N
H
O
N
H
0.2 0.4 0.6 0.8 1 1.2 1.4 1.6 1.8 2 2.2 2.4 2.6 2.8
Counts vs. Acquisition Time (min)

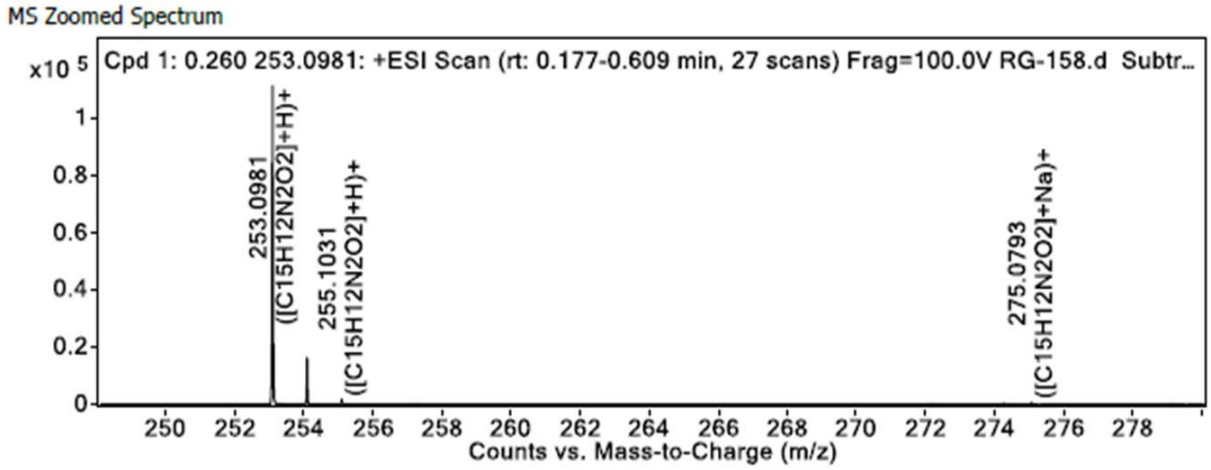
MS Zoomed Spectrum
Cpd 1: 0.260 253.0981: +ESI Scan (rt: 0.177-0.609 min, 27 scans) Frag=100.0V RG-158.d Subtr...
x10 5
253.0981
([C15H12N2O2]+H)+
255.1031
([C15H12N2O2]+H)+
275.0793
([C15H12N2O2]+Na)+
250 252 254 256 258 260 262 264 266 268 270 272 274 276 278
Counts vs. Mass-to-Charge (m/z)

3.4.1.8. Preparation of N-(2-amino-5-floro- phenyl)-1H-indole-3-carboxamide (13b)

Indole-3-carboxylic acid (8) (100 mg; 0.621 mmol) was dissolved in dichloromethane and added Pyridine (5 ml) under 0 °C. To this mixture, 1-ethyl-3-dimethyl amino propyl carbo di imide (173.25 mg; 1.11 mmol) and 5 mg of 4-dimethylaminopyridine were added. This mixture was subjected to react for 15 mins under continuous stirring before adding 2-amino-5-fluoro phenol (173.135 mg; 1.117 mmol) into the reaction mixture. The reaction was then continued at room temperature for overnight under continuous stirring. After removal of pyridine, the mixture was then dissolved in ethyl acetate and washed with water. The organic part was then collected and excess solvent was then evaporated under vacuum. The crude compound was then purified using column chromatography (Solvent system - hexane and ethyl acetate (75:25)) in silica 230 - 400 mesh to obtain the final compound in its pure form. (Yield: 48%). 1H NMR (400 MHz, DMSOd_6) δ : 11.81 (s, 1H), 10.42 (s, 1H), 9.21 (s, 1H), 8.30 (d, J = 2.8 Hz, 1H), 8.14 (d, J = 7.6 Hz, 1H), 7.66 (d, J = 2.4 Hz, 1H), 7.49 (d, J = 7.6 Hz, 1H), 7.17 (t, J = 8.4 Hz, 2H), 6.68 (dd, J = 2.8, 2.4 Hz, 2H).13C NMR (101 MHz, DMSO-*d6*): δ 164.40, 160.94, 158.55, 150.73, 136.76, 129.85, 126.37, 124.95, 123.67, 122.84, 121.34, 121.08, 112.62, 110.47, 105.91, 103.96. HRMS (AP-ESI) *m/z* calcd for $C_{15}H_{11}FN_2O_2$ $[M+H]^+$ 271.0838 $[M+H]^+$ found 271.0887 $[M+H]^+$.

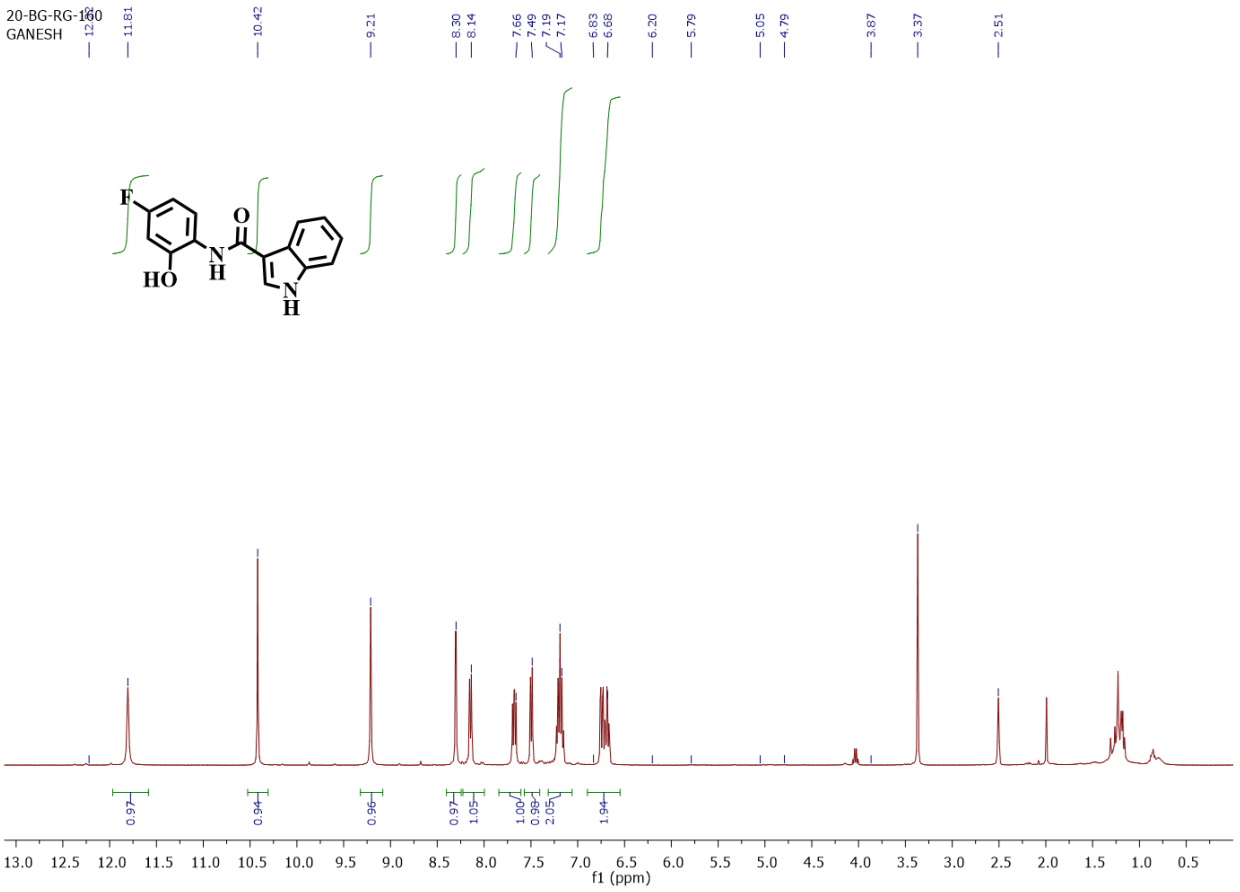
20-BG-RG-160
GANESH
12.02
11.81
10.42
9.21
8.30
8.14
7.66
7.49
7.19
7.17
6.83
6.68
6.20
5.79
5.05
4.79
3.87
3.37
2.51
F
HO
O
N
H
N
H
0.97
0.94
0.96
0.97
1.05
1.00
0.98
2.05
1.94
13.0 12.5 12.0 11.5 11.0 10.5 10.0 9.5 9.0 8.5 8.0 7.5 7.0 6.5 6.0 5.5 5.0 4.5 4.0 3.5 3.0 2.5 2.0 1.5 1.0 0.5
f1 (ppm)

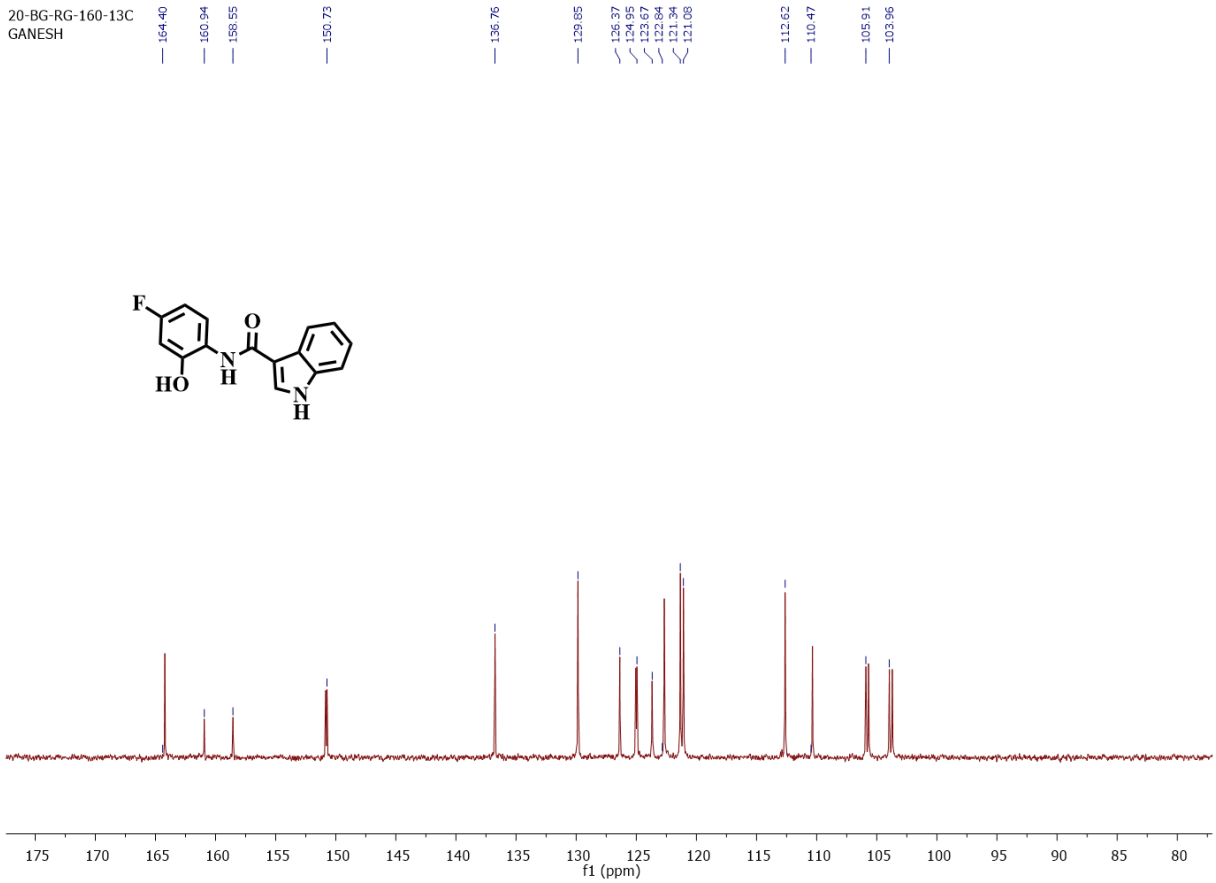
20-BG-RG-160-13C
GANESH
164.40
160.94
158.55
150.73
136.76
129.85
126.37
124.95
123.67
122.84
121.34
121.08
112.62
110.47
105.91
103.96
F
HO
O
N
H
N
H
175 170 165 160 155 150 145 140 135 130 125 120 115 110 105 100 95 90 85 80
f1 (ppm)

HPLC:

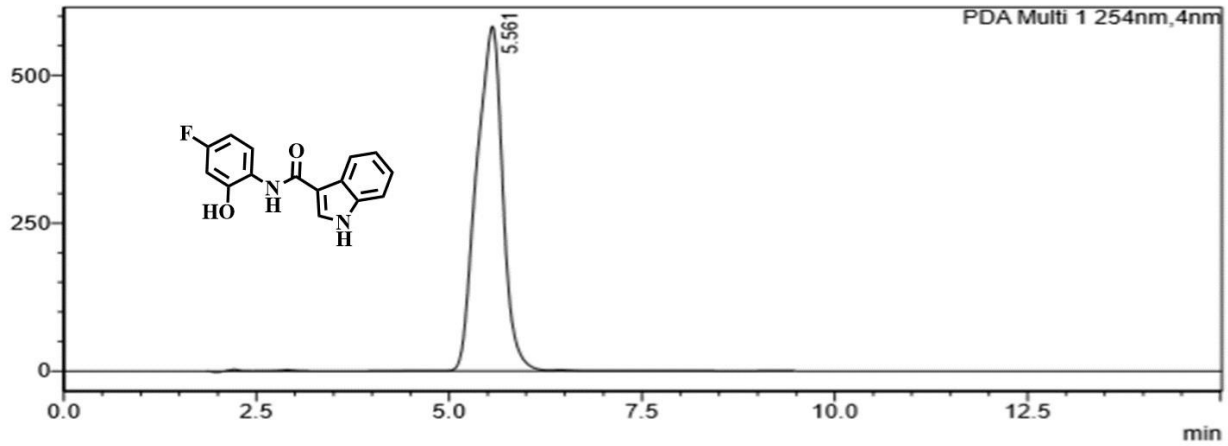
PDA Multi 1 254nm,4nm
5.561
500
250
0
F
HO
O
N
H
N
H
0.0
2.5
5.0
7.5
10.0
12.5
min

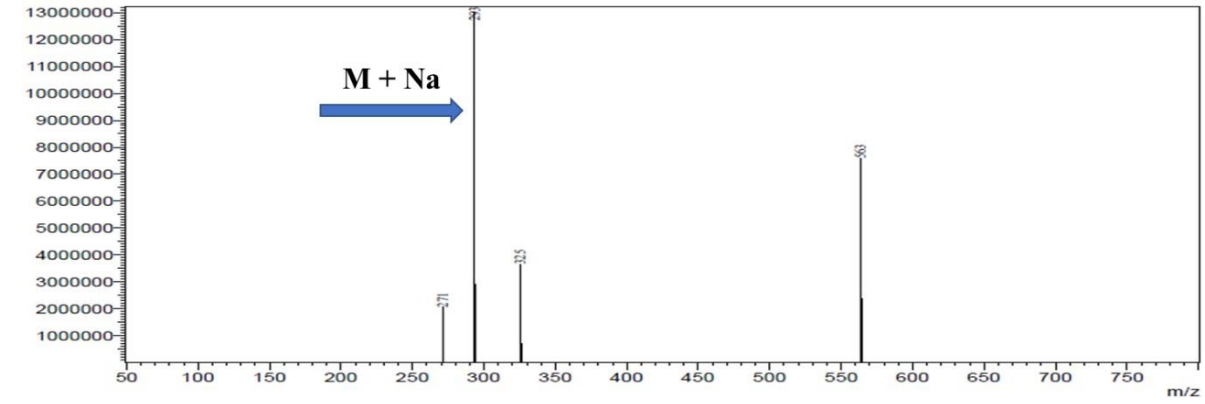

HRMS:

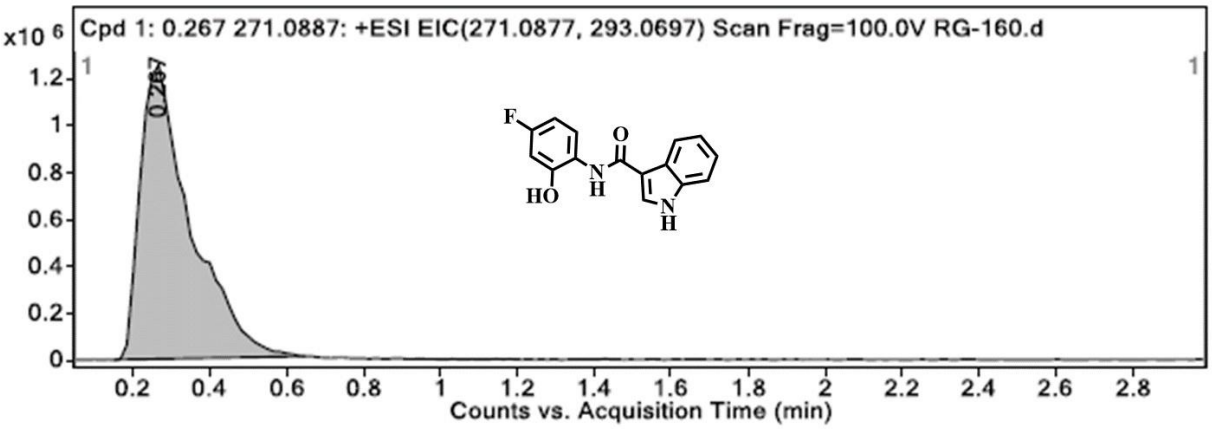

MS Zoomed Spectrum

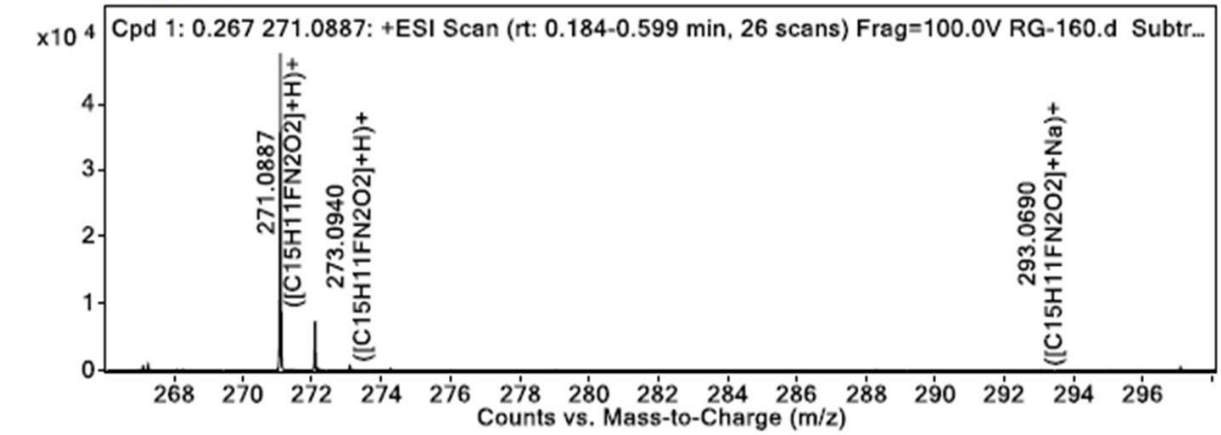

3.4.1.9. Preparation of N-(2-hydroxyphenyl) thiophene-3-carboxamide (14a)

Thiophene-3-carboxylic acid (9) (200 mg; 1.80 mmol) was dissolved in dichloromethane and added pyridine (5 ml) under 0 °C. To this mixture, 1-ethyl-3-dimethyl amino propyl carbo di imide (502 mg; 3.24 mmoles) and 5 mg of 4-dimethylaminopyridine were added. This mixture was subject to react with continuous stirring for 15 mins before 2-aminophenol (216 mg; 1.98 mmol) was added to the reaction mixture. This reaction was continued at room temperature for 6 h with continuous stirring. After removal of pyridine, the mixture was dissolved in ethyl acetate and washed with water. The organic part was isolated and excess solvent was evaporated under vacuum. The crude compound was purified using column chromatography (Solvent system – methanol and chloroform (5: 95)) in silica 230 - 400 mesh to finally obtain the final compound in its pure form. (Yield: 52%). ^{1}H NMR (400 MHz, DMSO-d_6) δ : 9.71 (s, 1H), 9.41 (s, 1H), 8.37 (s, 1H), 7.63 (dd, J = 1.2, 1.6 Hz, 3H), 7.04 (t, J = 7.6 Hz, 1H), 6.94 (dd, J = 1.2, 1.2 Hz, 1H), 6.83 (t, J = 7.2 Hz, 1H).^{13}C NMR (101 MHz, DMSO-*d6*) δ : 161.42, 149.93, 137.88, 130.24, 127.96, 127.53, 126.15, 126.22, 124.94, 119.49, 116.57. HRMS (AP-ESI) *m/z* calcd for $C_{11}H_9NO_2S$ $[M+H]^+$: 220.0388 $[M+H]^+$ found 220.0435.

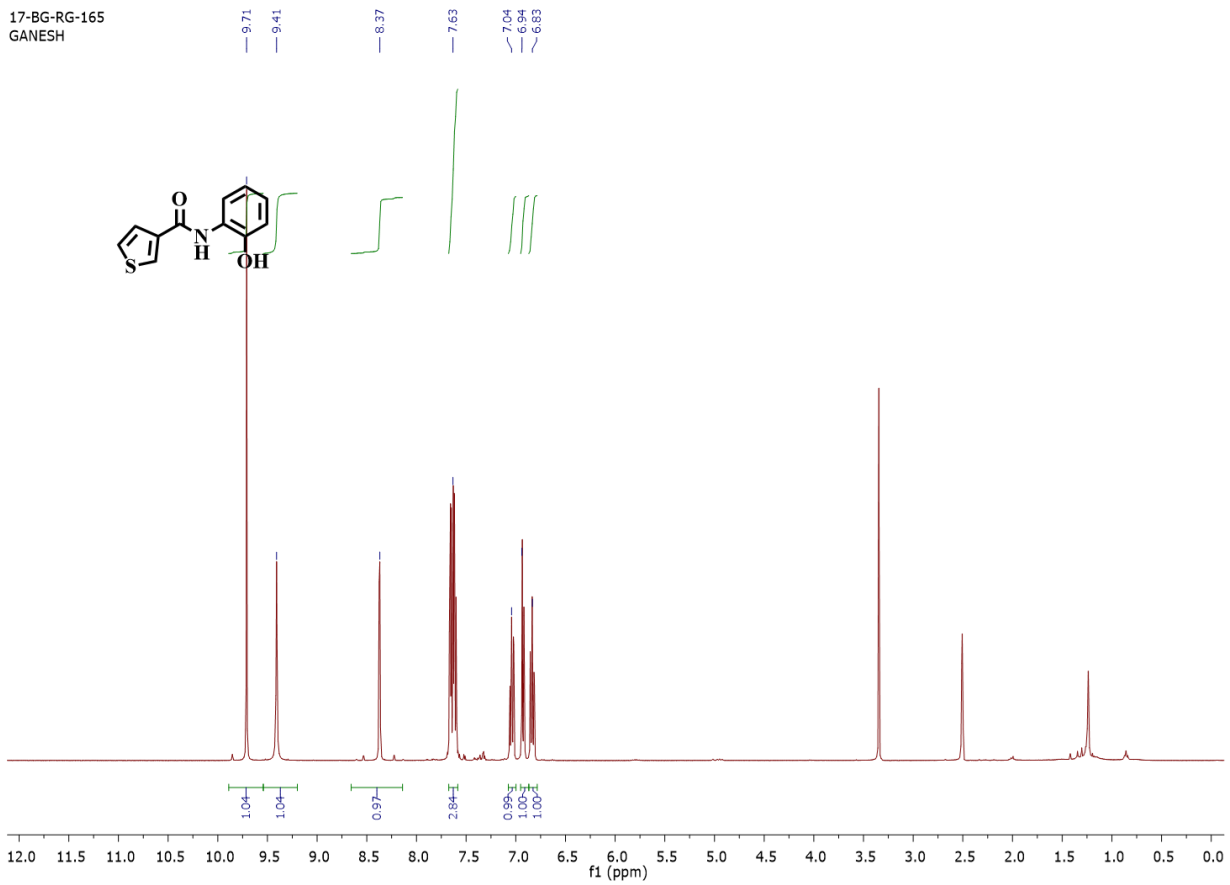
17-BG-RG-165
GANESH
9.71
9.41
8.37
7.63
7.04
6.94
6.83
O
N
H
S
OH
1.04
1.04
0.97
2.84
0.99
1.00
1.00
12.0 11.5 11.0 10.5 10.0 9.5 9.0 8.5 8.0 7.5 7.0 6.5 6.0 5.5 5.0 4.5 4.0 3.5 3.0 2.5 2.0 1.5 1.0 0.5 0.0
f1 (ppm)

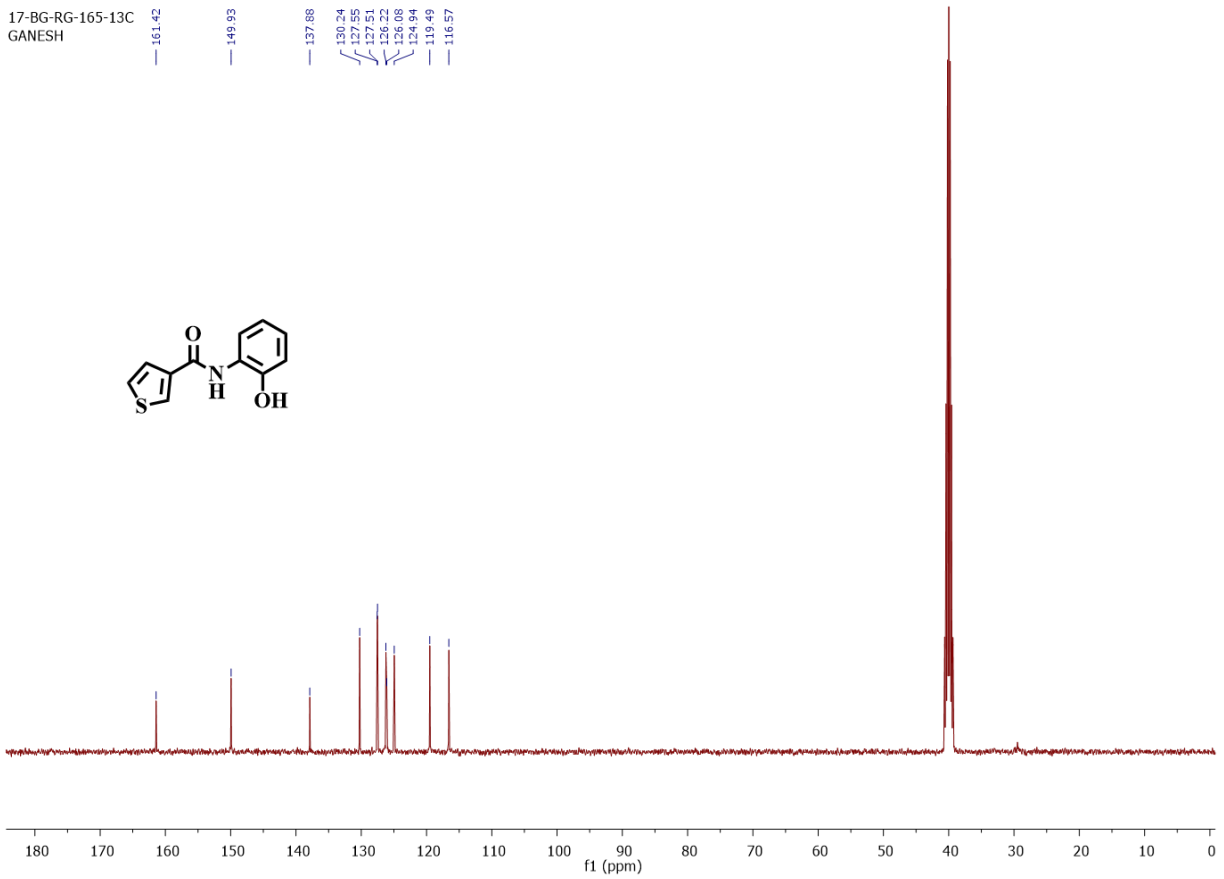
17-BG-RG-165-13C
GANESH
161.42
149.93
137.88
130.24
127.55
127.51
126.22
126.08
124.94
119.49
116.57
O
N
H
S
OH
180
170
160
150
140
130
120
110
100
90
80
70
60
50
40
30
20
10
0
f1 (ppm)

HPLC:

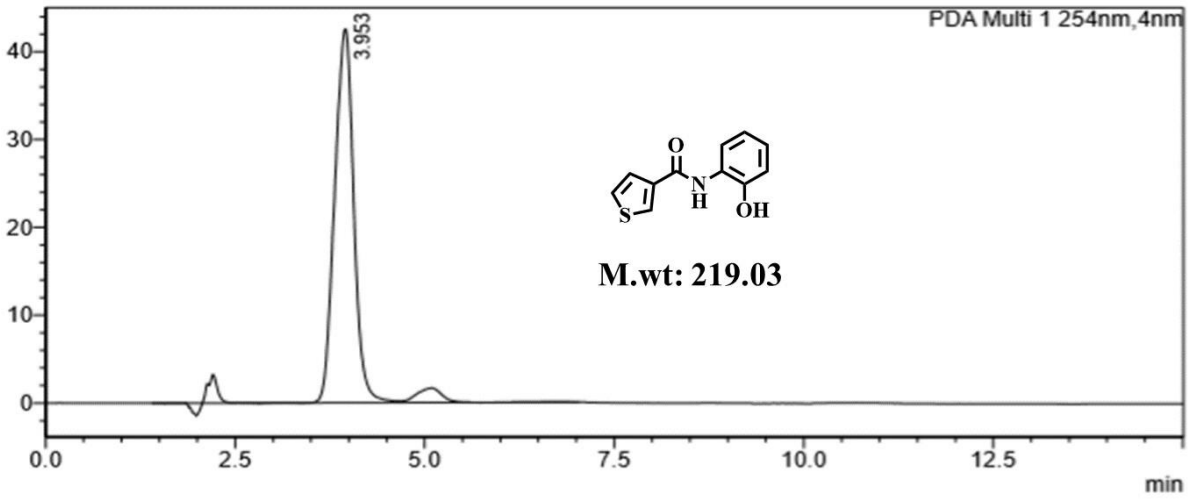
PDA Multi 1 254nm,4nm
3.953
40
30
20
10
0
0.0
2.5
5.0
7.5
10.0
12.5
min
O
N
H
S
OH
M.wt: 219.03

LCMS:

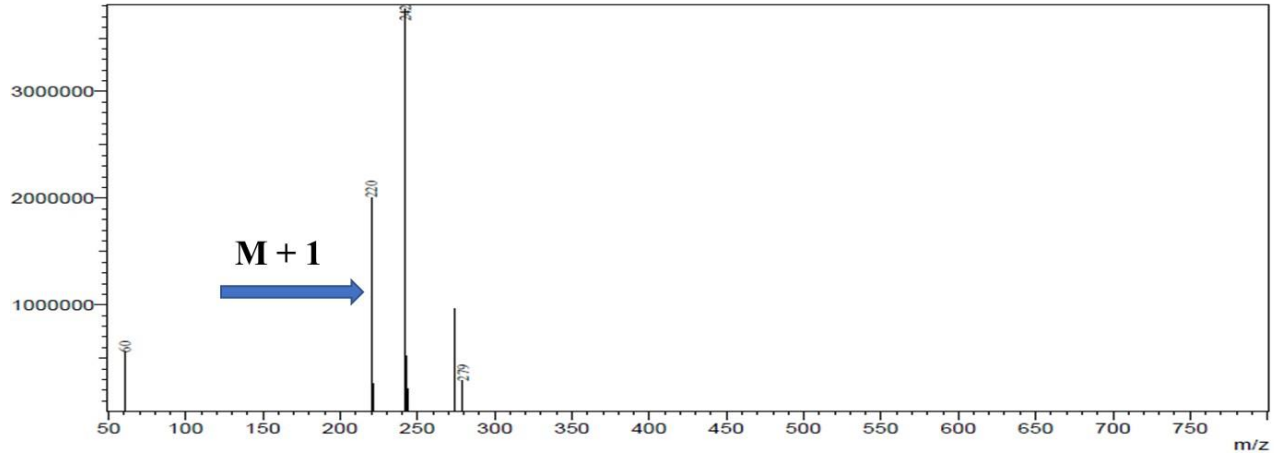
M + 1
3000000
2000000
1000000
50
100
150
200
250
300
350
400
450
500
550
600
650
700
750
m/z

HRMS:

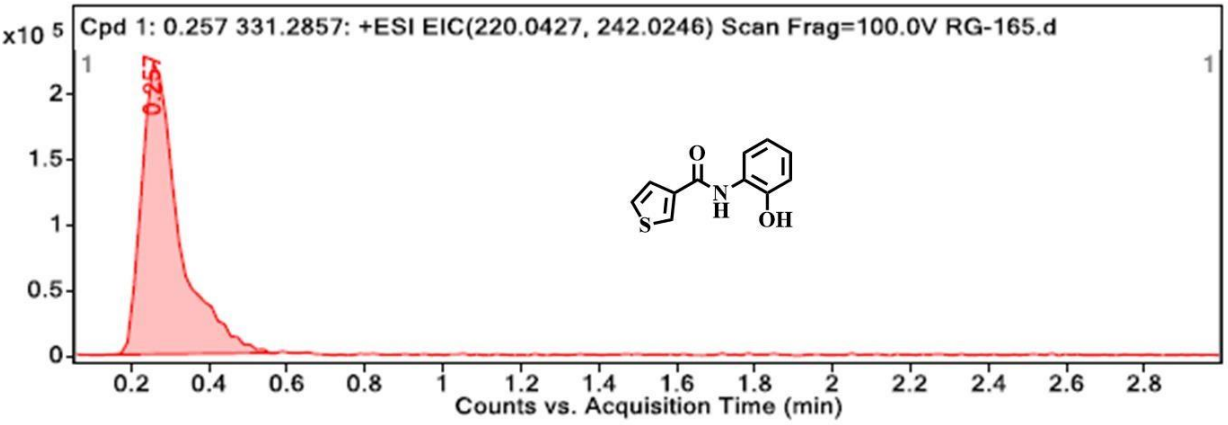
Cpd 1: 0.257 331.2857: +ESI EIC(220.0427, 242.0246) Scan Frag=100.0V RG-165.d
x10 5
0.257
O
N
H
S
OH
Counts vs. Acquisition Time (min)

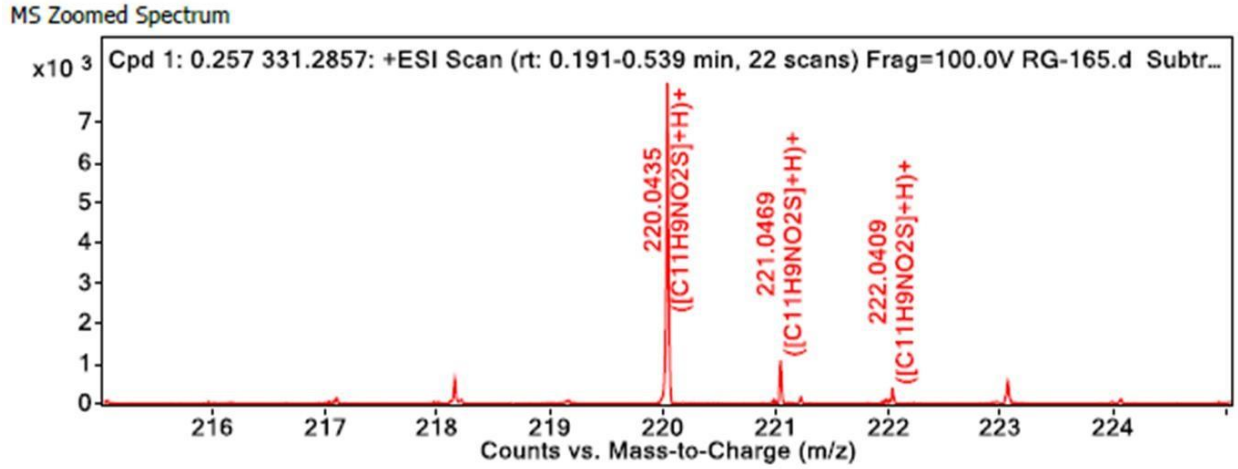
MS Zoomed Spectrum
Cpd 1: 0.257 331.2857: +ESI Scan (rt: 0.191-0.539 min, 22 scans) Frag=100.0V RG-165.d Subtr...
x10 3
220.0435
([C11H9NO2S]+H)+
221.0469
([C11H9NO2S]+H)+
222.0409
([C11H9NO2S]+H)+
Counts vs. Mass-to-Charge (m/z)

3.4.1.10. Preparation of N-(4-fluoro-2-hydroxyphenyl) thiophene-3-carboxamide (14b)

Thiophene-3-carboxylic acid (9) (200 mg; 1.80 mmol) was dissolved in dichloromethane and added Pyridine (5 ml) under 0 °C. To this mixture, 1-ethyl-3-dimethyl amino propyl carbo di imide (502 mg; 3.24 mmoles) and 5 mg of 4-dimethylaminopyridine were added. This mixture was settled to react under continuous stirring for 15 mins before 2-amino-5 fluoro phenol (251.7 mg; 1.98 mmol) was added to it. This reaction was carried out under constant stirring at room temperature for 6h. After removal of pyridine, the mixture was dissolved in ethyl acetate and washed with water. The organic portion was then collected and excess solvent was removed under vacuum. The crude compound was then purified using column chromatography (Solvent system methanol: chloroform (5: 95)) in silica 230 - 400 mesh to finally obtain the final compound in its pure form. (Yield: 45%). ^{1}H NMR (400 MHz, DMSO-d_6) δ : 10.18 (s, 1H), 9.41 (s, 1H), 8.34 (s, 1H), 7.62 (dt, J = 2.0, 5.2 Hz, 2H), 7.51 (dd, J = 6.4, 6.8 Hz, 1H), 6.71 (dd, J = 2.8, 2.8 Hz, 1H), 6.66 (td, J = 8.6, 2.9 Hz, 1H). ^{13}C NMR (101 MHz, DMSO-d_6) δ : 161.52, 152.17, 137.83, 130.21, 127.55, 126.95, 122.32, 105.70, 105.49, 103.67, 103.43. HRMS (AP-ESI) *m/z* calcd for $C_{11}H_8FNO_2S$ $[M+H]^+$: 238.0293 $[M+H]^+$, found 238.0335 $[M+H]^+$.

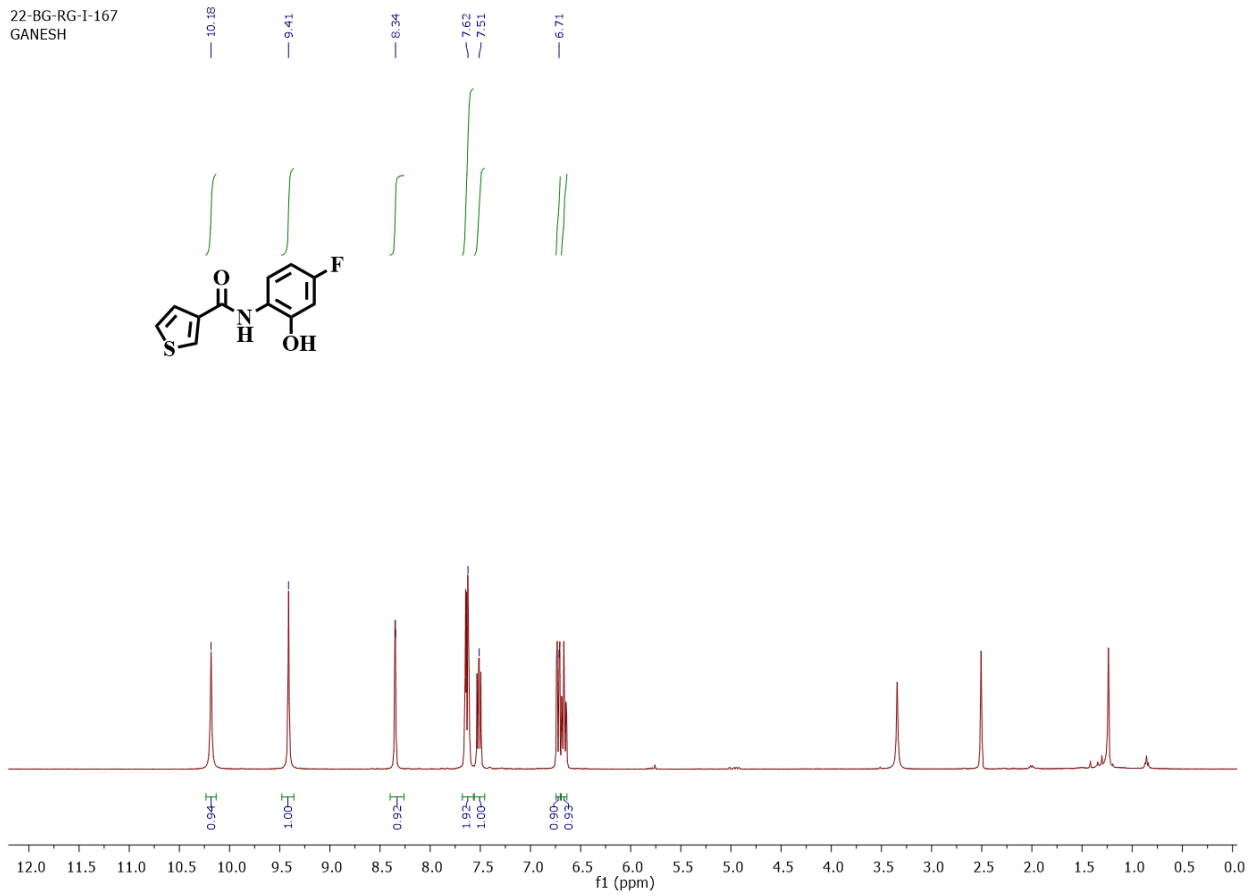
22-BG-RG-I-167
GANESH
10.18
9.41
8.34
7.62
7.51
6.71
O
N
H
S
F
OH
0.94
1.00
0.92
1.92
1.00
0.90
0.93
12.0 11.5 11.0 10.5 10.0 9.5 9.0 8.5 8.0 7.5 7.0 6.5 6.0 5.5 5.0 4.5 4.0 3.5 3.0 2.5 2.0 1.5 1.0 0.5 0.0
f1 (ppm)

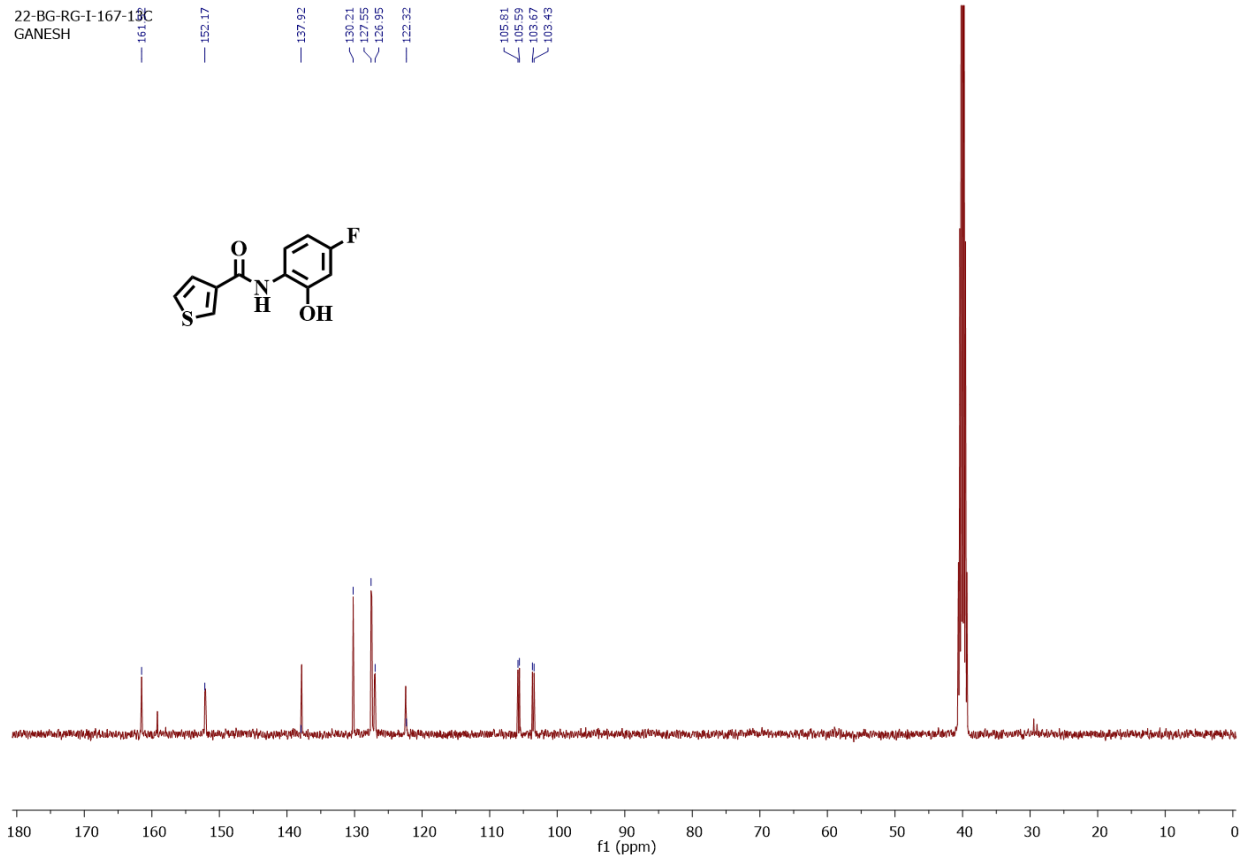
22-BG-RG-I-167-13C
GANESH
161.81
152.17
137.92
130.21
127.55
126.95
122.32
105.81
105.59
103.67
103.43
O
N
H
S
F
OH
180
170
160
150
140
130
120
110
100
90
80
70
60
50
40
30
20
10
0
f1 (ppm)

HPLC:

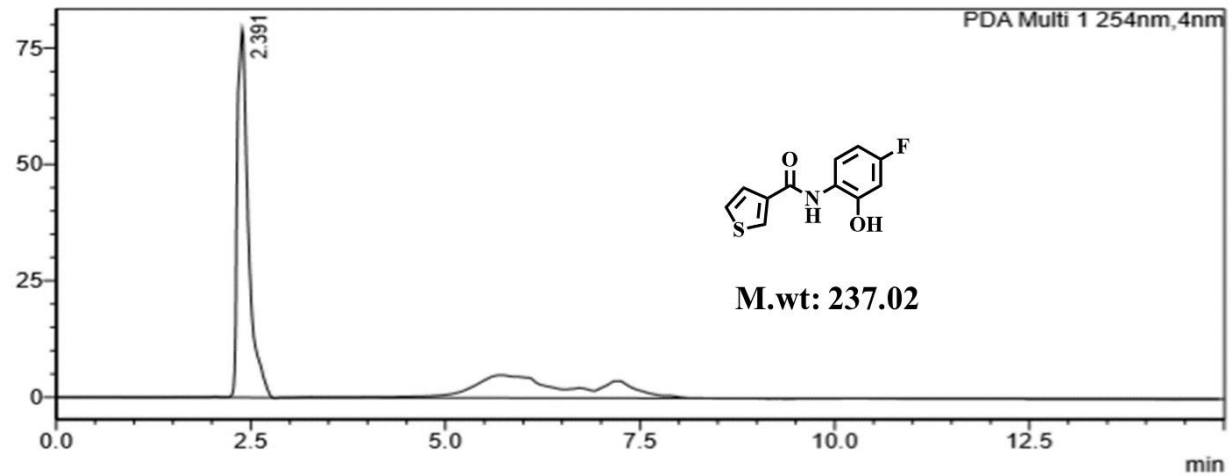
PDA Multi 1 254nm,4nm
2.391
75
50
25
0
0.0
2.5
5.0
7.5
10.0
12.5
min
O
N
H
S
F
OH
M.wt: 237.02

LCMS:

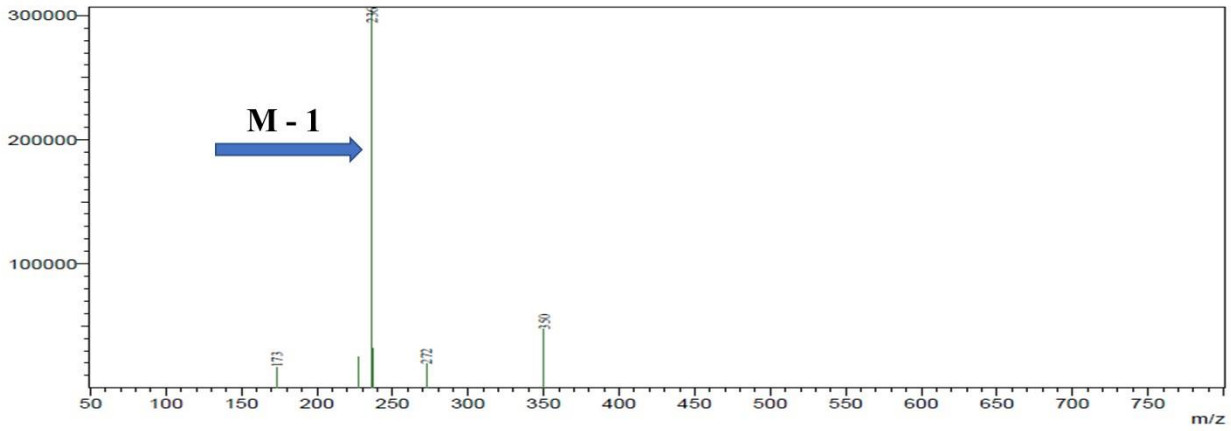
M - 1
m/z

HRMS:

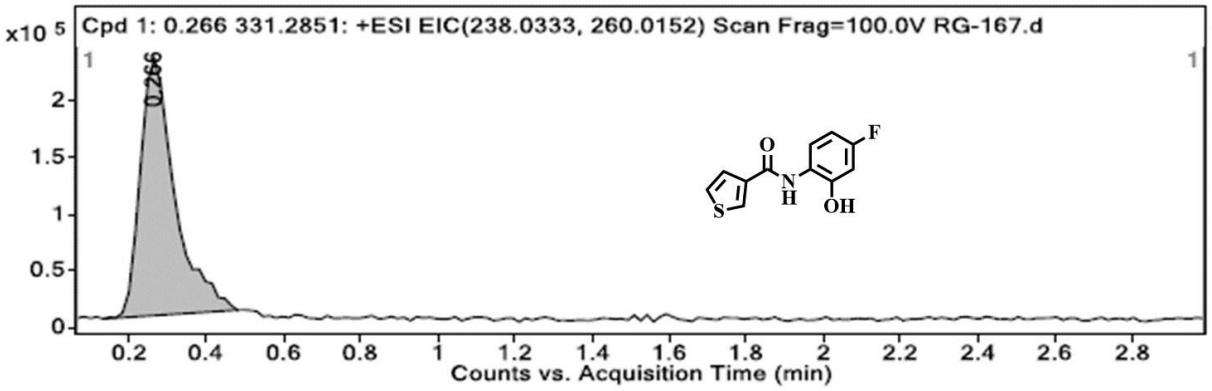
Cpd 1: 0.266 331.2851: +ESI EIC(238.0333, 260.0152) Scan Frag=100.0V RG-167.d
0.266
F
O
N
H
S
OH
Counts vs. Acquisition Time (min)

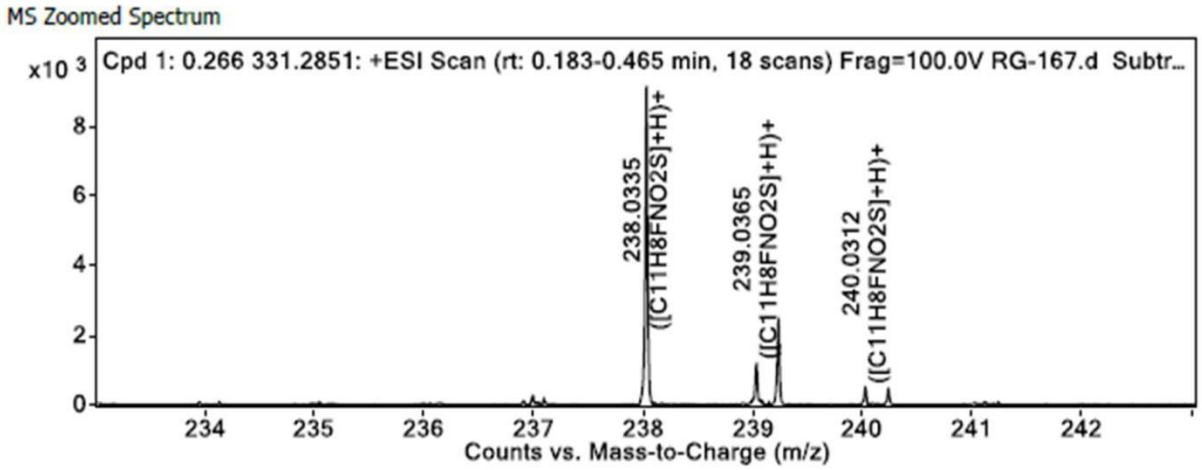
MS Zoomed Spectrum
Cpd 1: 0.266 331.2851: +ESI Scan (rt: 0.183-0.465 min, 18 scans) Frag=100.0V RG-167.d Subtr...
238.0335
([C11H8FNO2S]+H)+
239.0365
([C11H8FNO2S]+H)+
240.0312
([C11H8FNO2S]+H)+
Counts vs. Mass-to-Charge (m/z)

3.4.1.11. Preparation of tert-butyl 2-(benzamido)-5-fluoro phenyl carbamate (16a)

The solution of dichloromethane and pyridine (1:1) was added to benzoic acid (15a) (100 mg; 1.63 mmol). To this reaction mixture, 1-ethyl-3-dimethyl amino propyl carbo di imide (454.77 mg; 2.93 mmol) (EDC) and catalytic amount of DMAP were added. This mixture was stirred at room temperature for 15 mins. with stirring, *tert*-butyl 2-amino 5-fluoro phenyl carbamate (405.21 mg; 1.79 mmol) was added into the reaction mixture and reaction was continued for 12h and the reaction progress was tracked using TLC. After the reaction completion, pyridine was evaporated under rota evaporated. The mixture was diluted with ethyl acetate and washed with sodium bicarbonate solution. The organic layer was then separated and dried over Na2SO4. The dried solvent was evaporated under vacuum. The crude product was then purified using column chromatography (Solvent system – hexane and ethyl acetate (60:40)) in silica 230 – 400 mesh to obtain the final compound in its pure form. (Yield: 45%). ^{1}H NMR (400 MHz, CDCl3) δ : 8.74 (s, 1H), 7.95 (d, J = 7.1 Hz, 2H), 7.48 (d, J = 5.1 Hz, 4H), 7.20 (d, J = 9.6 Hz, 1H), 6.89 (s, 2H), 1.51 (s, 9H).

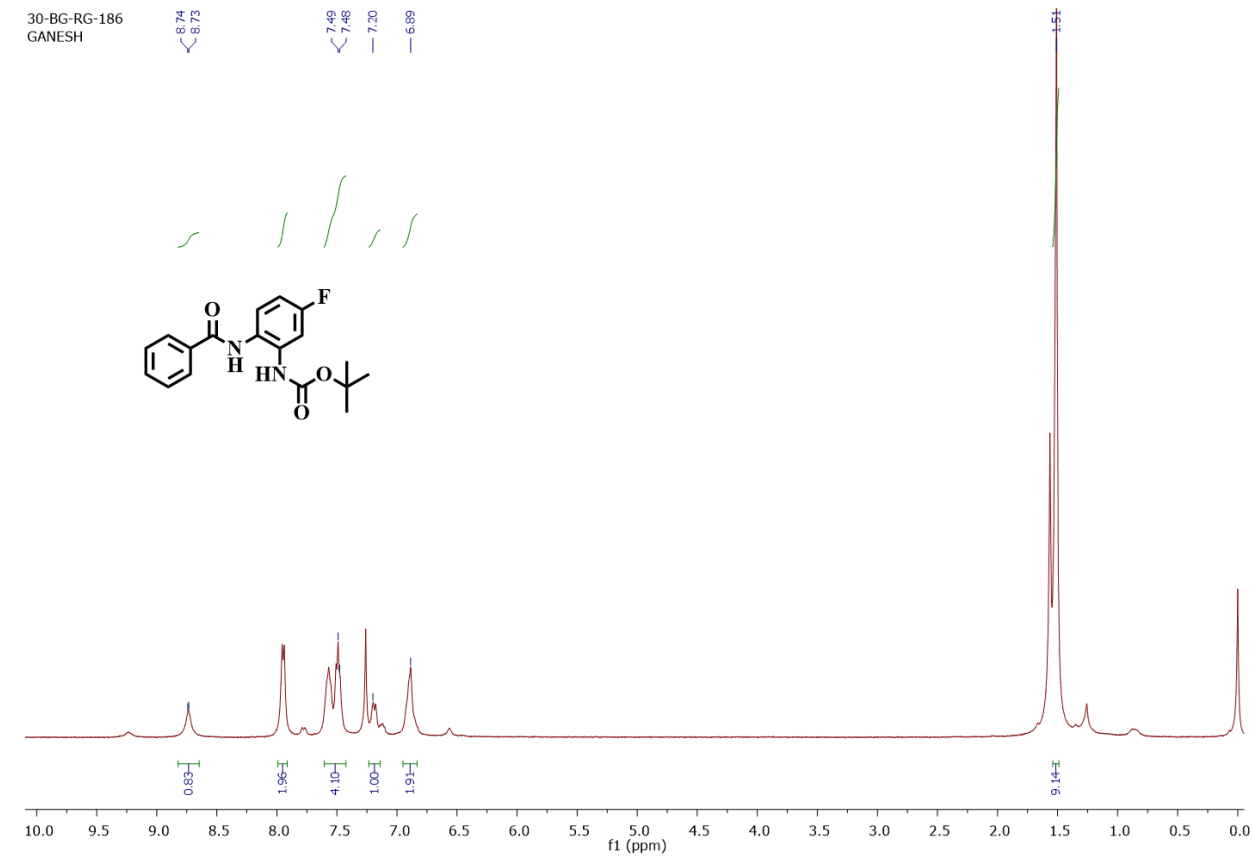

3.4.1.12. Preparation of N-(2-amino 5-fluoro phenyl) benzamide (17a)

The solution of compound *tert*-butyl-2-(benzamide) phenyl carbamate (16a) (70 mg; 0.212 mmol) in dichloromethane (5 ml) was stirred at 0 °C in 10min. After 10 mins to this reaction mixture the solution of 4M dioxane in HCl was added at 0°C. This mixture was then allowed to react under constant stirring at room temperature for 2h. The reaction was monitored with TLC. After completion, the dioxane was then evaporated under vacuum. To the resulting mixture, water was added and extracted with ethyl acetate. The organic layer was then separated, dried over Na2SO4 and solvent was evaporated under vacuum. The mixture was then washed with pentane to obtain Boc de-protected final compound. (Yield: 82%). 1H NMR (400 MHz, DMSO-*d6*) δ : 9.61 (s, 1H), 7.98 (d, *J* = 7.2 Hz, 2H), 7.51 (m, 3H), 7.13 (t, *J* = 6.4 Hz, 1H), 6.58 (dd, *J* = 2.8, 2.8 Hz, 1H), 6.37

(m, 1H), 5.24 (s, 2H). 13C NMR (101 MHz, DMSO-*d6*) δ : 166.07, 162.71, 160.33, 145.92, 134.98, 131.86, 129.10, 129.00, 128.71, 128.25, 119.73, 102.60, 101.79. HRMS (AP-ESI) *m/z* calcd for $C_{13}H_{11}FN_2O$ $[M+H]^+$ 231.0889 $[M+H]^+$ found 231.0940 $[M+H]^+$.

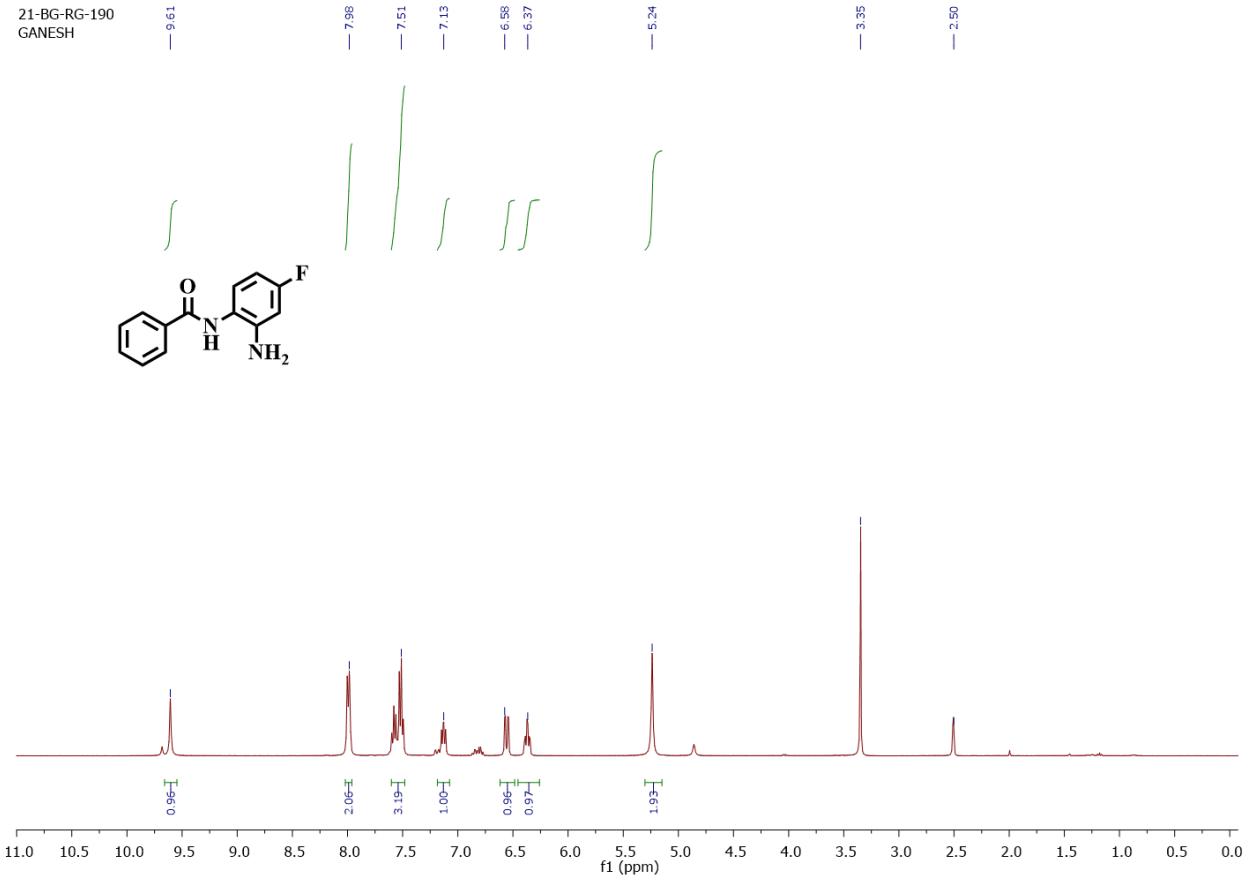

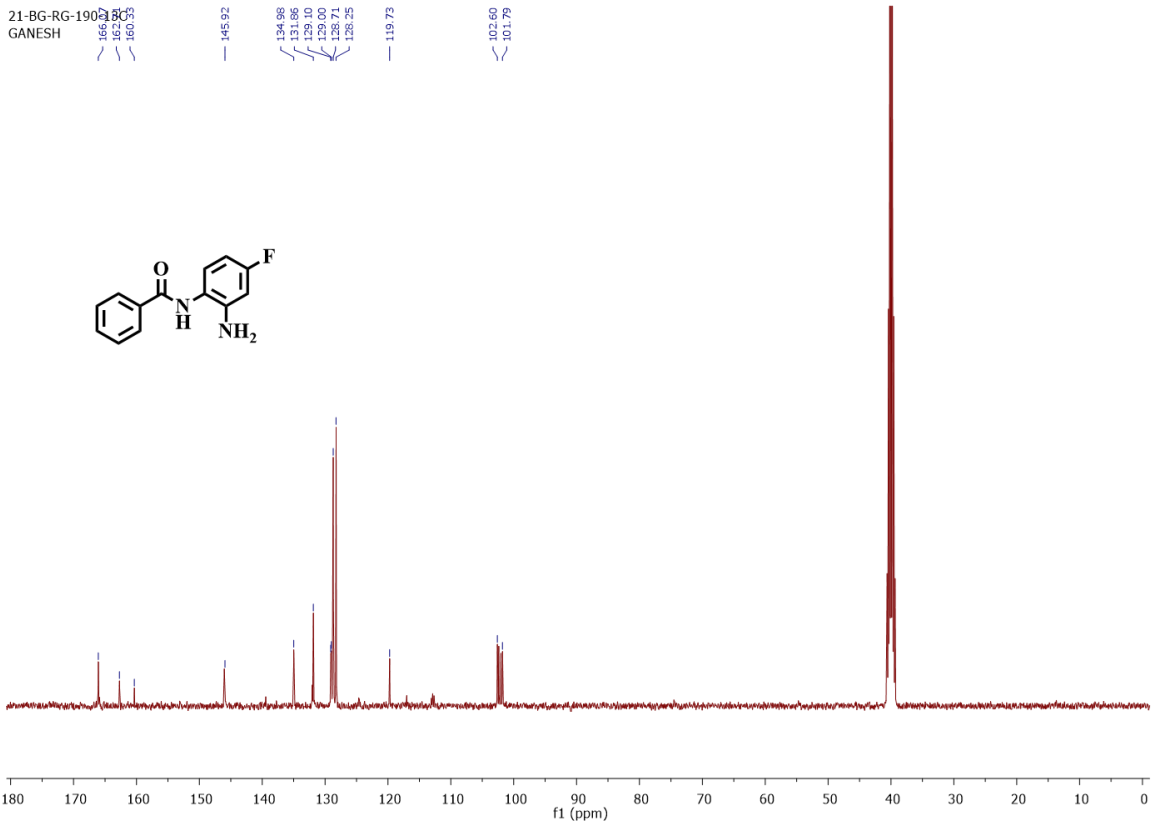
21-BG-RG-190-13C
GANESH
166.41
161.50
160.93
145.92
134.98
131.86
129.10
129.00
128.71
128.25
119.73
102.60
101.79
O
N
H
F
NH2
180 170 160 150 140 130 120 110 100 90 80 70 60 50 40 30 20 10 0
f1 (ppm)

HPLC:

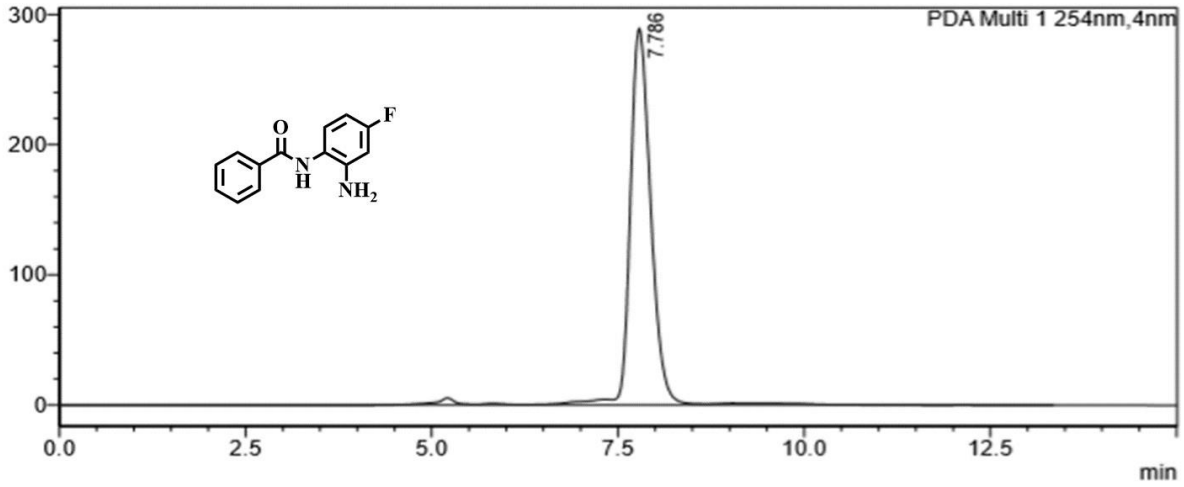
PDA Multi 1 254nm,4nm
7.786
300
200
100
0
O
N
H
F
NH2
0.0 2.5 5.0 7.5 10.0 12.5
min

LCMS:

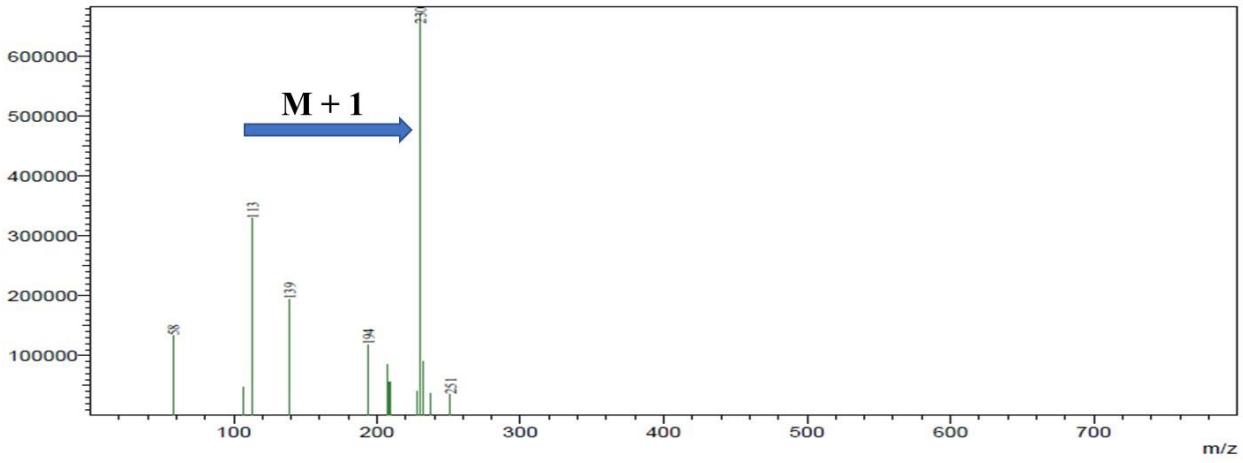
M + 1
600000
500000
400000
300000
200000
100000
100
200
300
400
500
600
700
m/z
58
113
139
194
230
251

HRMS:

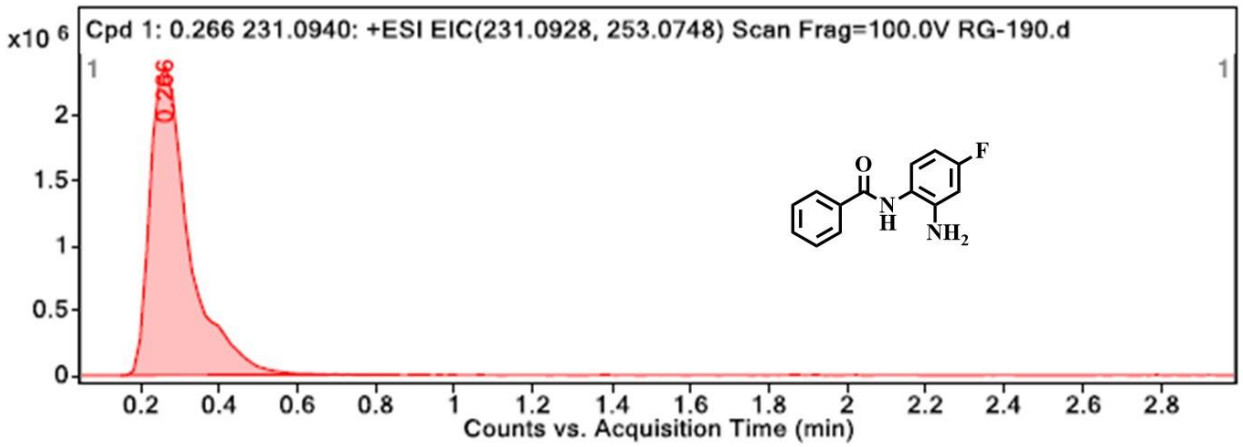
Cpd 1: 0.266 231.0940: +ESI EIC(231.0928, 253.0748) Scan Frag=100.0V RG-190.d
x10 6
2
1.5
1
0.5
0
0.2
0.4
0.6
0.8
1
1.2
1.4
1.6
1.8
2
2.2
2.4
2.6
2.8
Counts vs. Acquisition Time (min)
O
N
H
F
NH2

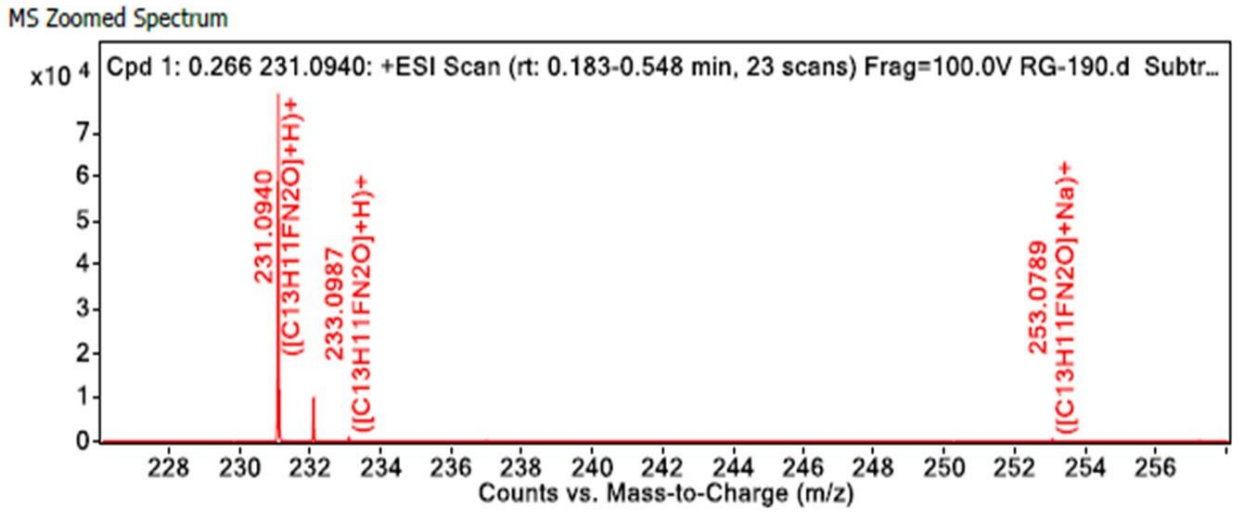

3.4.1.13. Preparation of tert-butyl 2-(1-naphthamido)-5-fluoro phenyl carbamate (16b)

The solution of dichloromethane and pyridine (1:1) was added to 1-naphthoic acid (15b) (100 mg; 0.581mmol). To this reaction mixture, 1-ethyl-3-dimethyl amino propyl carbo di imide (162.43 mg; 1.04 mmol) and catalytic amount of 4-di methyl amino pyridine were added. This mixture was stirred at room temperature for 15 mins. This reaction mixture was treated with *tert*-butyl 2-amino 5-fluoro phenyl carbamate (144.53 mg; 0.639 mmol) and reaction was continued to 12 h. After completion of the reaction, excess pyridine was evaporated under vacuum. To this reaction mixture, sodium bicarbonate solution was added and extracted with ethyl acetate. The organic layer was then separated and dried with Na_2SO_4. The dried solvent was removed under to get the crude, which was purified using column chromatography (Solvent system – hexane and ethyl acetate (60:40)) in silica 230 – 400 mesh to obtain the final compound in its pure form. (Yield:54%). 1H NMR (400 MHz, $CDCl_3$) δ : 8.42 (m, 2H), 7.88 (d, J = 8 Hz, 2H), 7.74 (s, 1H), 7.56 (m, 4H), 7.32 (d, J = 10 Hz, 1H), 7.11 (s, 1H), 6.88 (s, 1H), 1.45 (s, 9H).

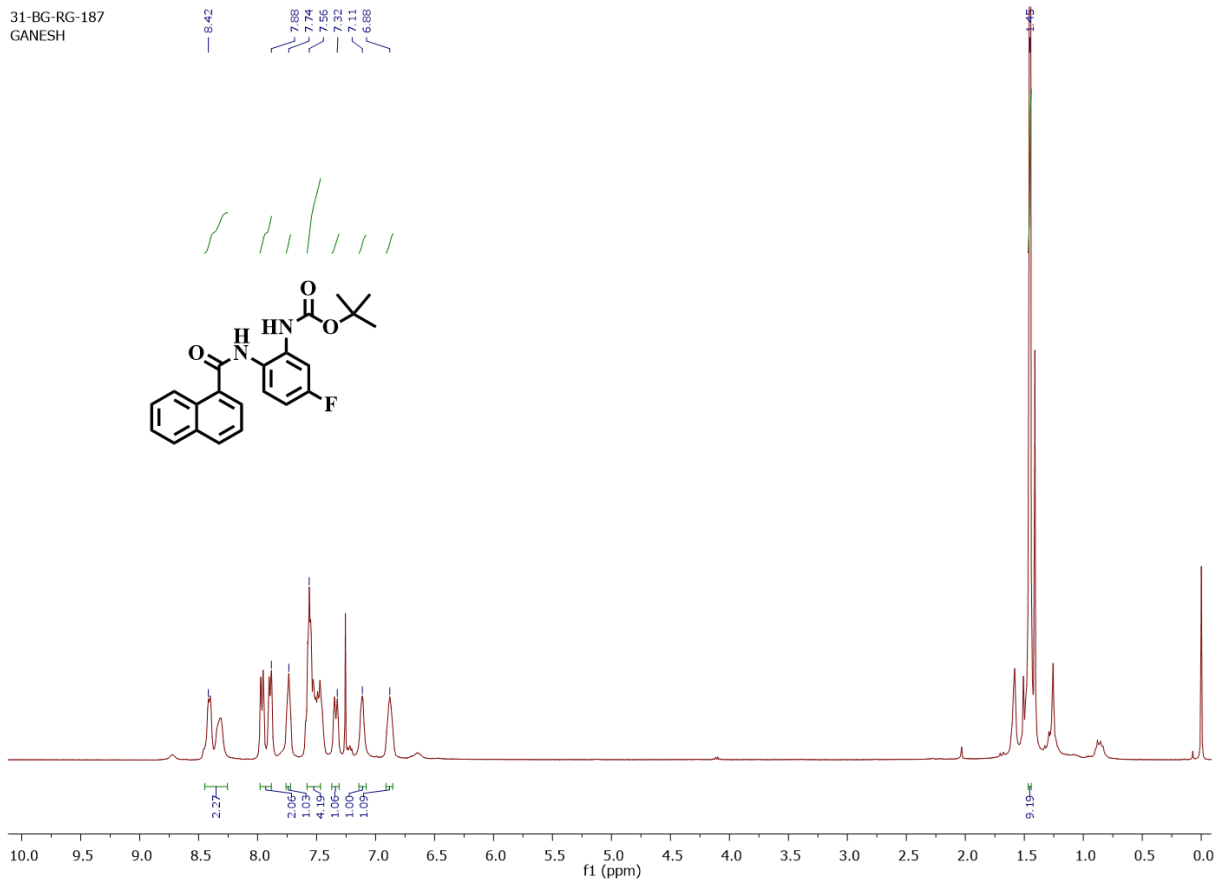

3.4.1.14. Preparation of N-(2-amino 5-fluoro phenyl) 1-naphthmide (17b)

To a solution containing a *tert*-butyl-2-(1-naphthamido)-5-fluoro phenyl carbamate (16b) (82 mg; 0.215 mmol) in dichloromethane (5mL) and 4M Dioxane in HCl was added to it at 0 °C. To the solution was stirred at room temperature for 2h. After dioxane was removed under reduced pressure, the residue was treated with sodium bicarbonate solution. The aqueous phase was extracted with ethyl acetate. The organic layer was then separated, dried with Na2SO4 and solvent was evaporated under vacuum. The mixture was then washed with pentane to obtain Boc deprotected final compound. (Yield: 66.66%). ^{1}H NMR (400 MHz, DMSO-*d6*) δ : 9.76 (s, 1H), 8.28 (d, *J* = 9.6 Hz, 1H), 8.06 (dd, *J* = 8.4 Hz, 9.6 Hz, 2H), 7.87 (d, *J* = 6.8 Hz, 1H), 7.62 (m, 3H), 7.37 (t, *J* = 8.4 Hz, 1H), 6.62 (dd, *J* = 2.8 Hz, 2.8 Hz, 1H), 6.43 (m, 1H), 5.30 (s, 2H). ^{13}C NMR

(101 MHz, DMSO-*d6*): δ 168.11, 162.53, 160.16, 145.19, 134.98, 133.64, 130.52, 128.74, 128.36, 127.33, 126.75,126.24, 125.84, 125.47, 119.84, 102.76, 102.18. HRMS (AP-ESI) *m/z* calcd for $C_{17}H_{13}FN_2O$ $[M+H]^+$ 281.1045 found 281.1090.

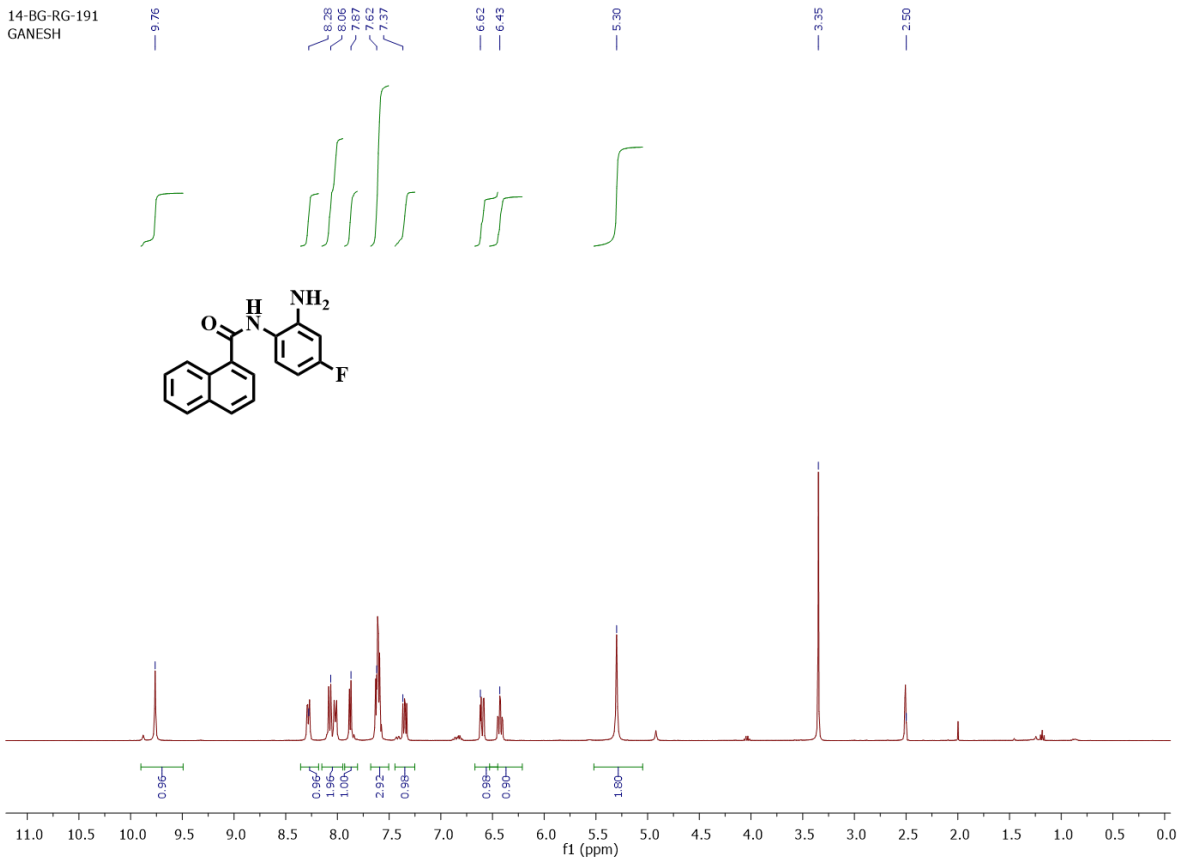

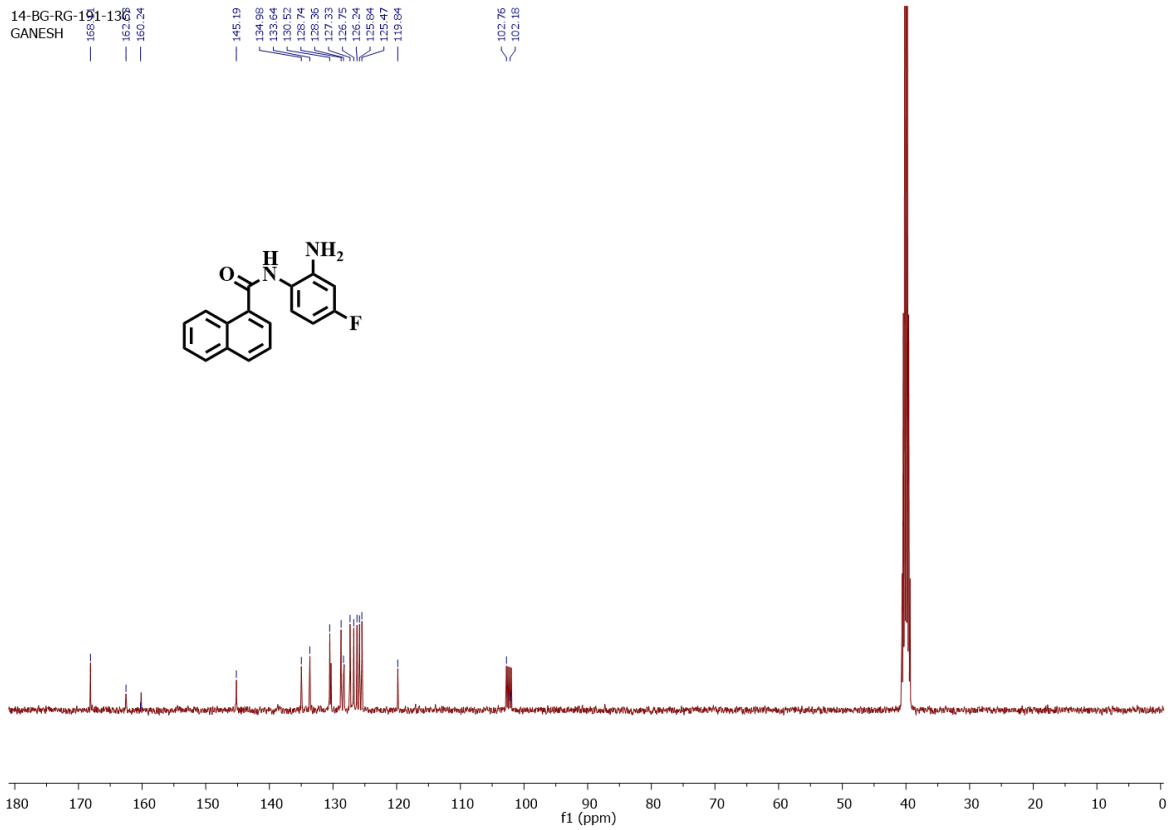
14-BG-RG-191-13C
GANESH
168.
162.25
160.24
145.19
134.98
133.64
130.52
128.74
128.36
127.33
126.75
126.24
125.84
125.47
119.84
102.76
102.18
NH2
H
N
O
F
180
170
160
150
140
130
120
110
100
90
80
70
60
50
40
30
20
10
0
f1 (ppm)

HPLC:

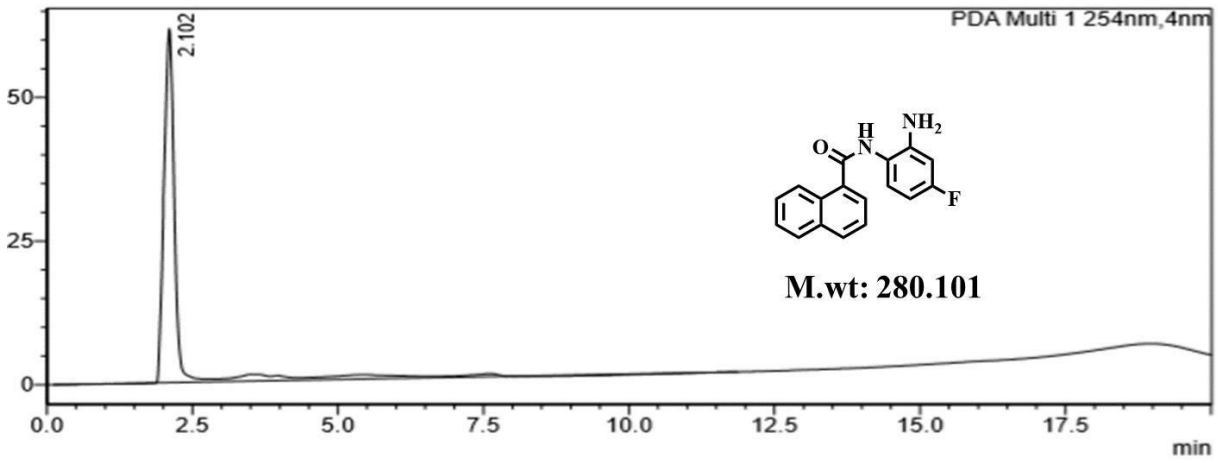
PDA Multi 1 254nm,4nm
2.102
50
25
0
0.0
2.5
5.0
7.5
10.0
12.5
15.0
17.5
min
NH2
H
N
O
F
M.wt: 280.101

LCMS:

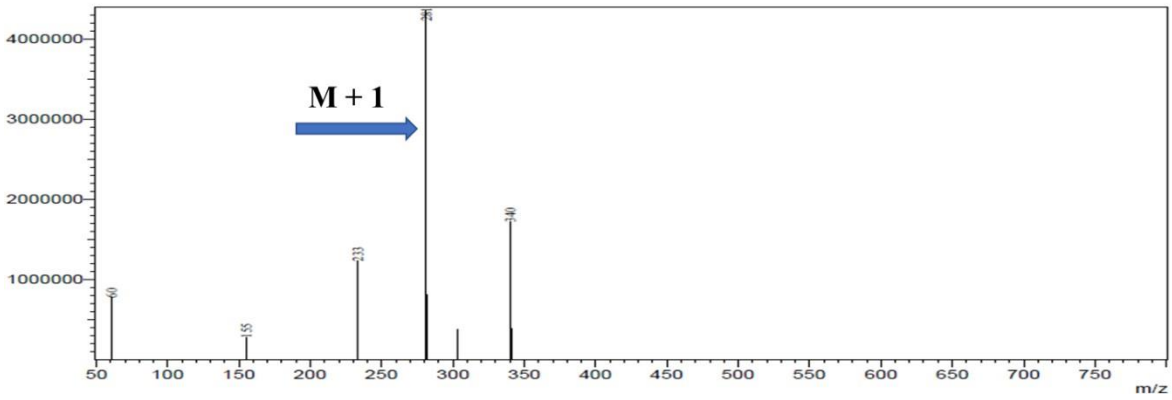

HRMS:

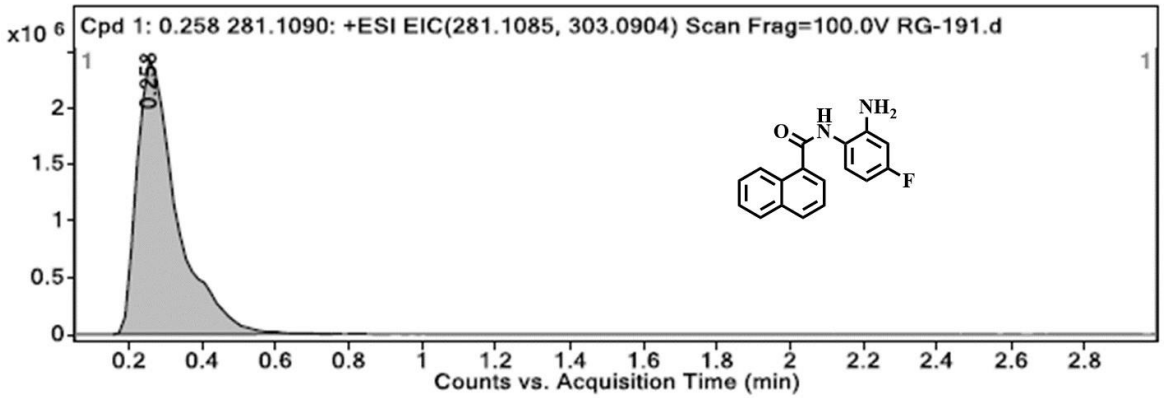

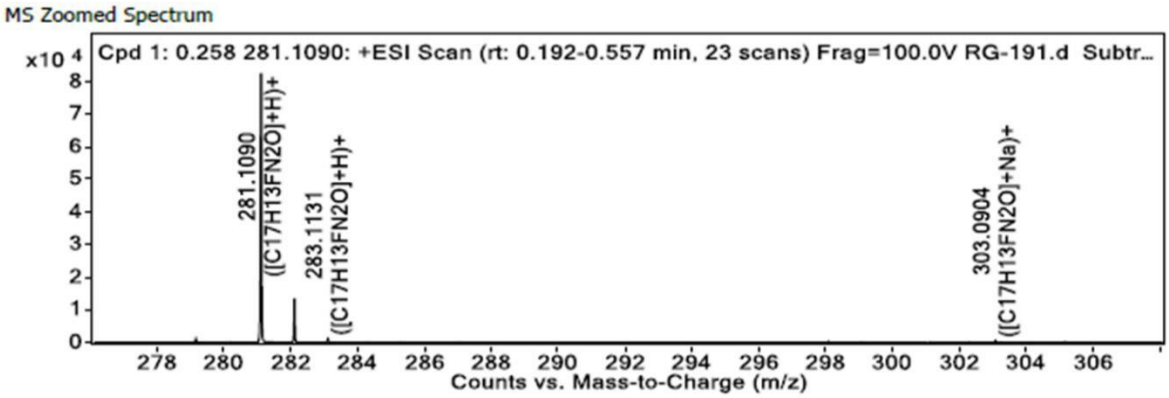

3.4.1.15. Preparation of tert-butyl 2-(2-naphthamido)-5-fluoro phenyl carbamate (16c)

The solution of dichloromethane and pyridine (1:1) was added to 2-naphthoic acid (15c) (100 mg;

0.900 mmol). To this reaction mixture, 1-ethyl-3-dimethyl amino propyl carbo di imide (251 mg; 1.62 mmol) and catalytic amount of 4-di methyl amino pyridine were added. This mixture was stirred at room temperature for 15 mins. After 15 mins, *tert*-butyl 2-amino 5-fluoro phenyl carbamate (206 mg; 0.990 mmol) was added into the reaction mixture and reaction was continued for 12h. After completion of the reaction, pyridine was evaporated under vacuum. The mixture was then dissolved in ethyl acetate and washed with sodium bicarbonate. The organic layer was then separated and dried with Na2SO4. The dried solvent was evaporated under vacuum. The crude product was then purified using column chromatography (Solvent system – hexane and ethyl acetate (50:50)) in silica 230 – 400 mesh to obtain the final compound in its pure form. (Yield:51%). ^{1}H NMR (400 MHz, $CDCl_3$) δ : 9.11 (s, 1H), 8.47 (s, 1H), 7.99 (d, J = 7.2 Hz, 1H), 7.92 (dd, J = 2.8, 9.2 Hz, 3H), 7.56 (m, 3H), 7.15 (d, J = 9.6 Hz, 1H), 7.11 (s, 1H), 6.825 (m, 1H), 1.51 (s, 9H).

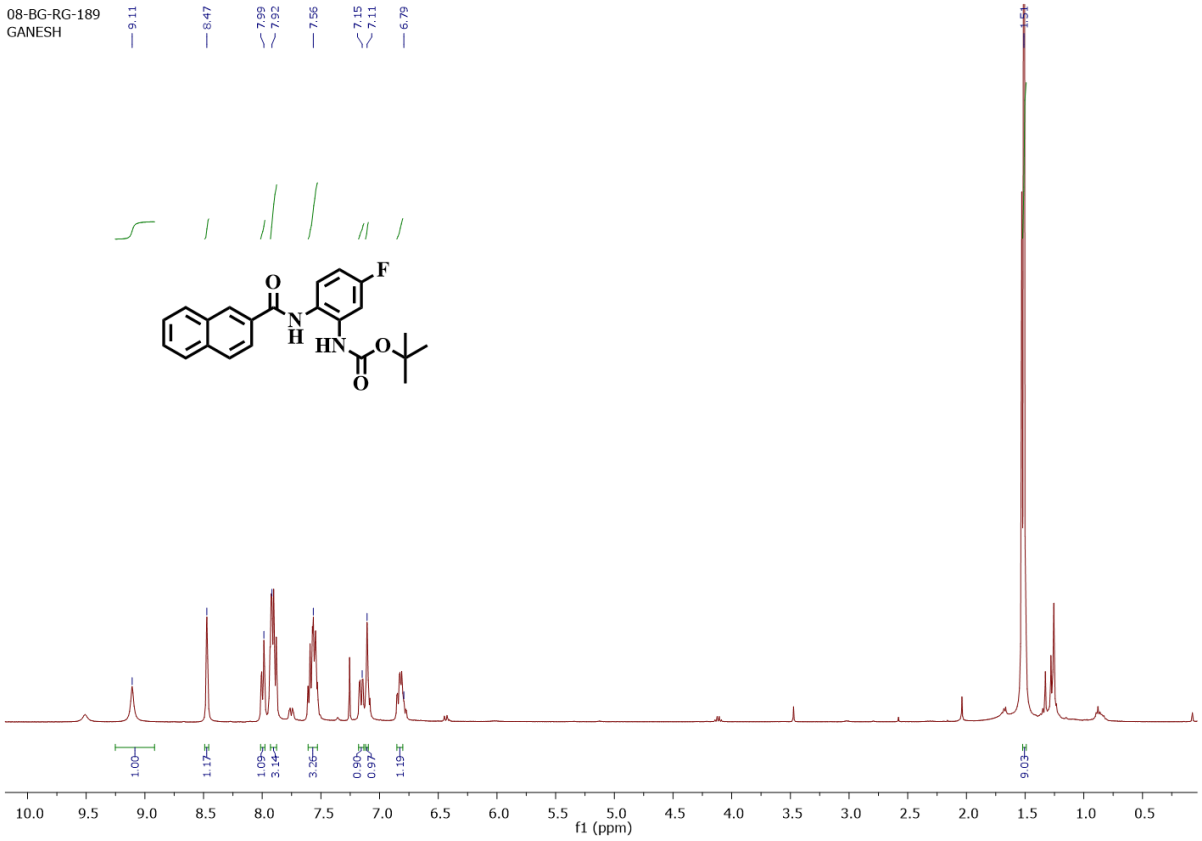

3.4.1.16. Preparation of N-(2-amino 5-fluoro phenyl)-2-naphthamide (17c)

The compound *tert*-butyl-2-(2-naphthamido)-5-fluoro phenyl carbamate (16c) (100 mg; 0.314 mmol) was dissolved in dichloromethane (5mL) and solution of 4M Dioxane in HCl was added to it at 0 °C. This mixture was then allowed to react under constant stirring at room temperature for 2h. The excess dioxane was evaporated under vacuum. The resulting compound was then dissolved in ethyl acetate and washed with water. The organic layer was separated, dried with Na2SO4 and solvent was evaporated under vacuum. The mixture was then washed with pentane to obtain Boc de-protected final compound. (Yield: 61.78%). ^{1}H NMR (400 MHz, DMSO-d_6) δ : 9.79 (s, 1H), 8.63 (s, 1H), 8.08 (m, 3H), 7.63 (s, 2H), 7.19 (dt, J = 10 Hz, 6.8 Hz, 1H), 6.84 (m, 1H), 6.58 (d, J = 10 Hz, 1H), 6.40 (t, J = 6.8 Hz, 1H), 5.30 (s, 2H). ^{13}C NMR (101 MHz, DMSO-

d_6) δ : 166.36 162.73, 160.36, 145.93, 139.43, 134.70, 132.59, 129.39, 128.86, 128.63, 128.12, 127.22, 119.80, 117.30, 113.15, 102.41, 101.83. HRMS (AP-ESI) *m/z* calcd for $C_{17}H_{13}FN_2O$ [M+H]+ 281.1045 found 281.1094.

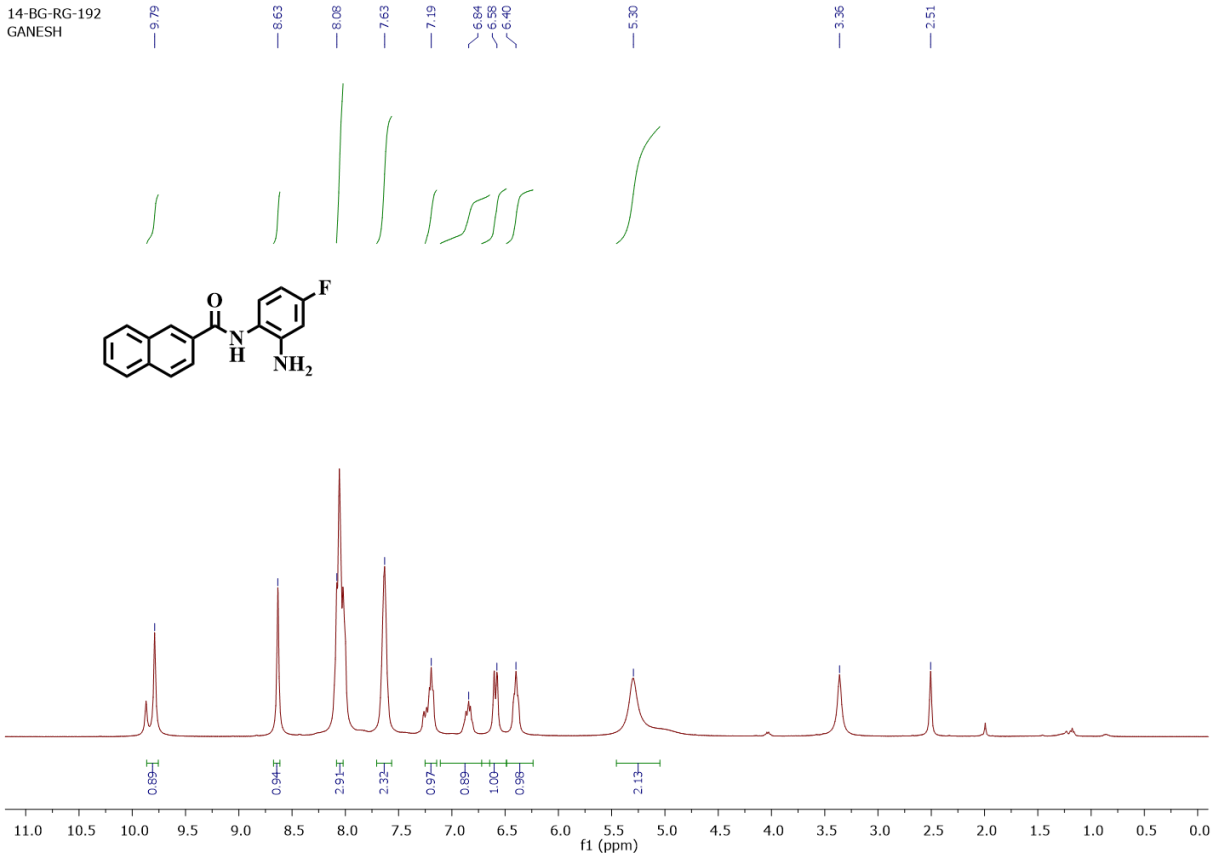

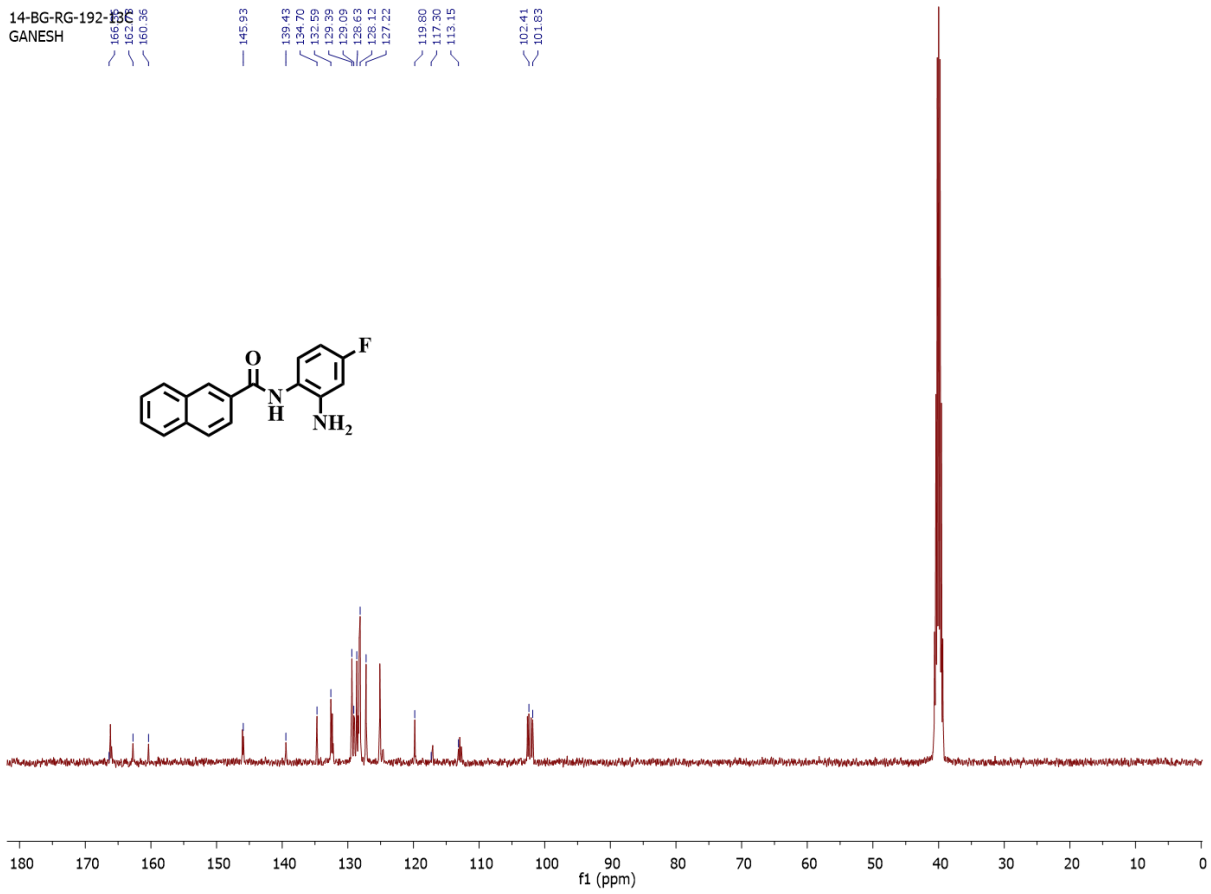
14-BG-RG-192-13C
GANESH
166.36
162.78
160.36
145.93
139.43
134.70
132.59
129.39
129.09
128.63
128.12
127.22
119.80
117.30
113.15
102.41
101.83
O
N
H
NH2
F
180 170 160 150 140 130 120 110 100 90 80 70 60 50 40 30 20 10 0
f1 (ppm)

HPLC:

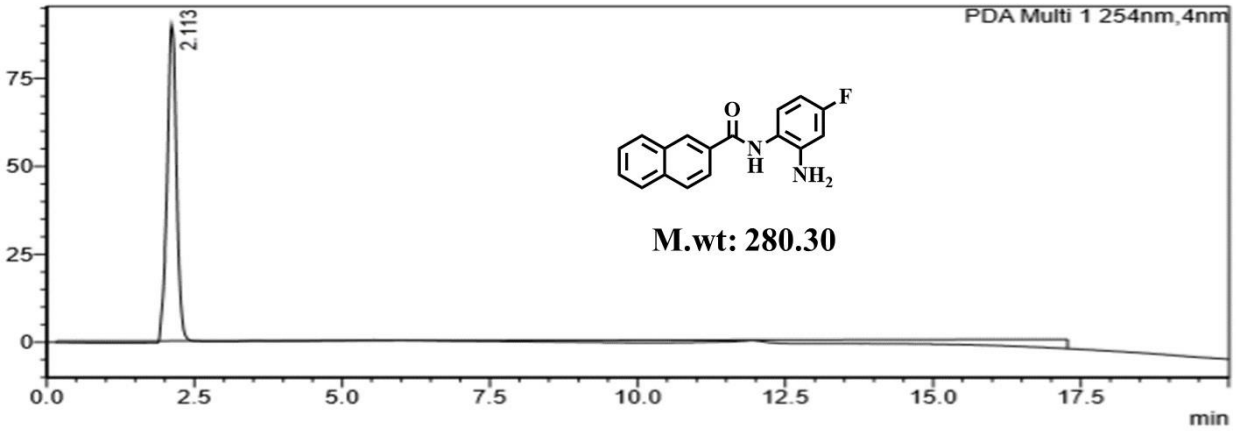
PDA Multi 1 254nm,4nm
2.113
75
50
25
0
0.0 2.5 5.0 7.5 10.0 12.5 15.0 17.5
min
O
N
H
NH2
F
M.wt: 280.30

LCMS:

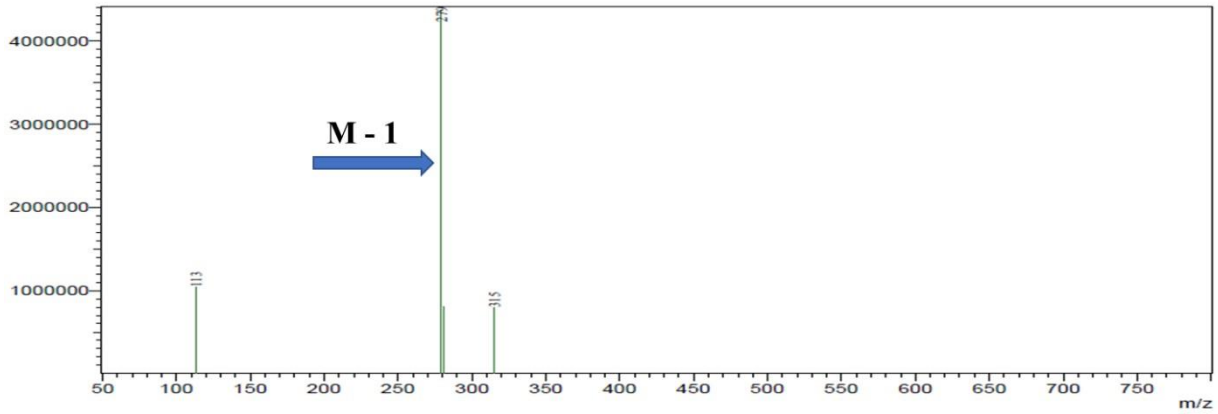
M - 1
4000000
3000000
2000000
1000000
113
279
315
50
100
150
200
250
300
350
400
450
500
550
600
650
700
750
m/z

HRMS:

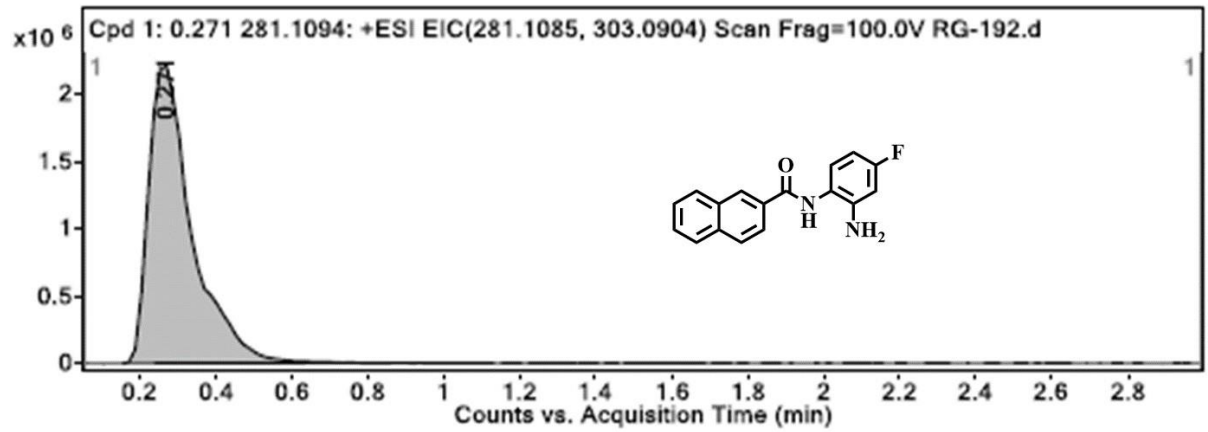
x10 6
Cpd 1: 0.271 281.1094: +ESI EIC(281.1085, 303.0904) Scan Frag=100.0V RG-192.d
0.271
O
N
H
F
NH2
2
1.5
1
0.5
0
0.2
0.4
0.6
0.8
1
1.2
1.4
1.6
1.8
2
2.2
2.4
2.6
2.8
Counts vs. Acquisition Time (min)

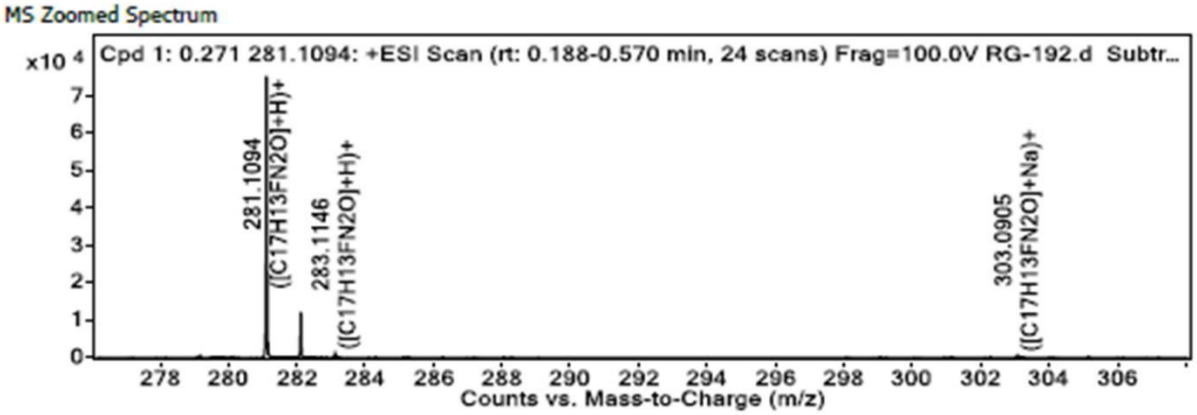

3.4.1.17. Preparation of tert-butyl 2-(amino-4-fluoro phenyl)-6- (phenyl amino) pyrazine-2carbamate (21).

The solution of dichloromethane and pyridine (1:1) was added to 6-(phenyl amino) pyrazine -2carboxylic acid (20**)** (80 mg; 0.232 mmol). To this reaction mixture, 1-ethyl-3-dimethyl amino propyl carbo di imide (64.728 mg; 0.417 mmol) and catalytic amount of 4-di methyl amino pyridine were added. This mixture was stirred at room temperature for 15 mins. After 15 mins, *tert*-butyl 2-amino 5-fluoro phenyl carbamate (57.81 mg; 0.255 mmol) was added into the reaction mixture and reaction was continued for 12h. After completion of the reaction pyridine was evaporated under vacuum. The mixture was then dissolved in ethyl acetate and washed with sodium bicarbonate. The organic layer was then separated and dried with Na2SO4. The dried solvent was evaporated under vacuum. The crude product was then purified using column chromatography (Solvent system – hexane and ethyl acetate (70:30)) in silica 230 – 400 mesh to obtain the final compound in its pure form. (Yield: 48.78). ^{1}H NMR (400 MHz, CDCl3) δ : 9.46 (s, 1H), 8.86 (s, 1H), 8.43 (s, 1H), 7.41 (m, 8H), 6.84 (s, 2H), 1.48 (s, 9H). $C_{22}H_{22}FN_5O_3$ [M]: 423.4484; MS (ESI) m/z; $[M + H]^+$: 424.6684 $[M + H]^+$.

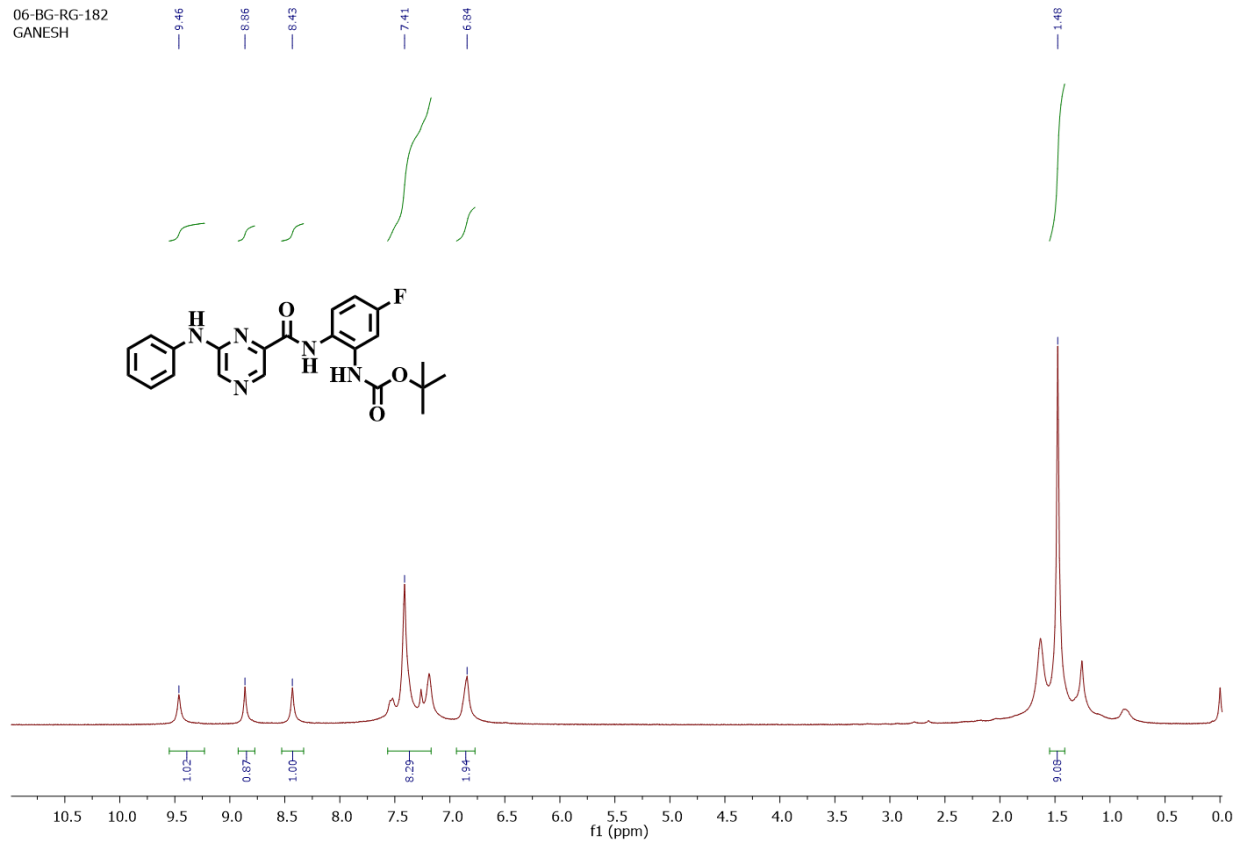

3.4.1.18. Preparation of N-(2-aminophenyl)-6-phenylamino pyrazine-2-carboxamide (22)

The compound *tert*-butyl 2-(amino-4-fluoro phenyl)-6- (phenyl amino) pyrazine-2-carbamate (21) (38 mg; 0.966 mmol) was dissolved in dichloromethane (5 ml) and the solution of 4M dioxane in HCl was added to it at 0 °C. This mixture was then allowed to react under constant stirring at room temperature for 2h. The excess dioxane was then evaporated under vacuum. The resulting compound was then dissolved in ethyl acetate and washed with water. The organic layer was then separated, dried over Na2SO4 and solvent was evaporated under vacuum. The mixture was then washed with pentane to obtain boc de-protected final compound. (Yield: 62.28%). 1H NMR (400 MHz, $CDCl_3$) δ : 9.20 (s, 1H), 8.81 (s, 1H), 8.37 (s, 1H), 7.39 (t, J = 9.6 Hz, 5H), 7.15 (d, J = 5.2 Hz, 1H), 6.86 (s, 1H), 6.52 (d, J = 6.0 Hz, 2H), 3.97 (s, 2H).13C NMR (101 MHz, $CDCl_3$) δ : 162.15, 150.54, 140.93, 138.13, 136.67, 134.36, 130.03, 126.29, 126.07, 124.59, 121.05, 106.54,

105.95, 104.52, 104.25. HRMS (AP-ESI) *m/z* calcd for $C_{17}H_{14}FN_5O$ $[M+H]^+$ 324.1216 $[M + H]^+$ found 324.1254 $[M + H]^+$.

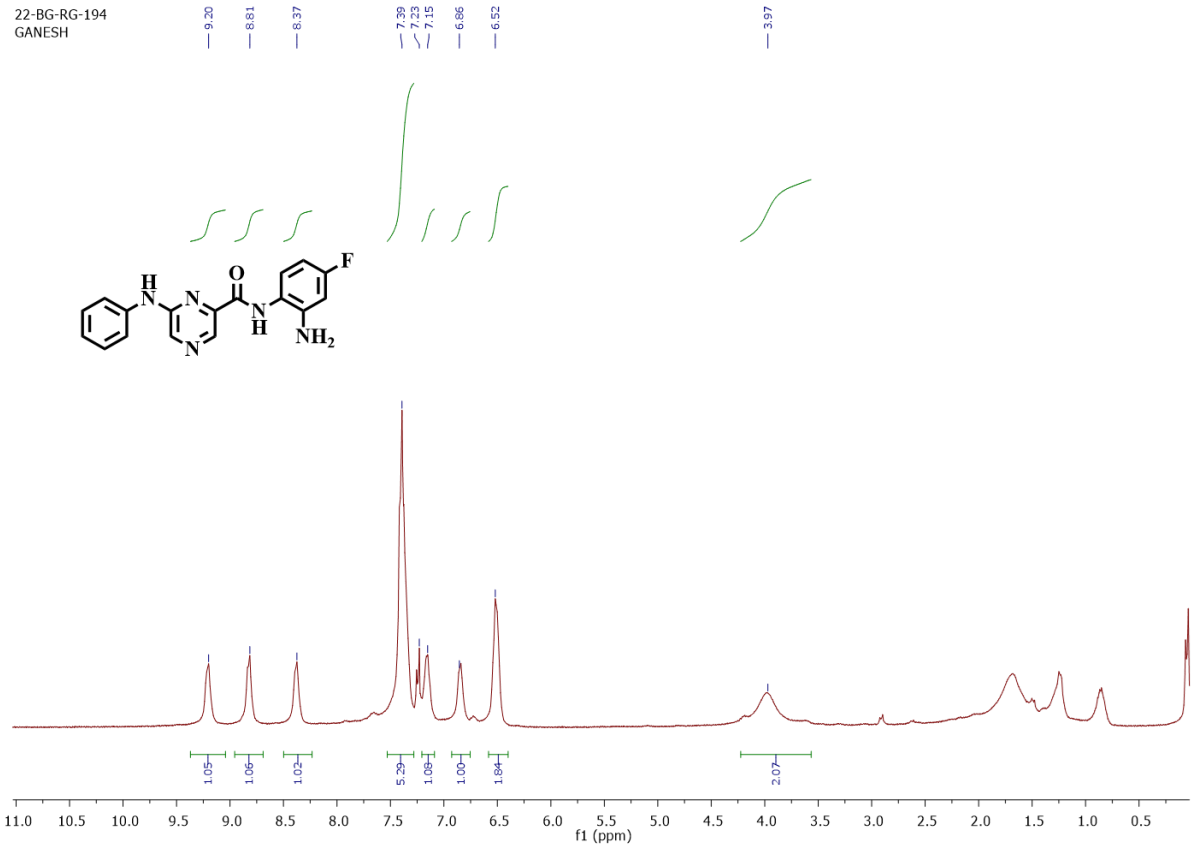

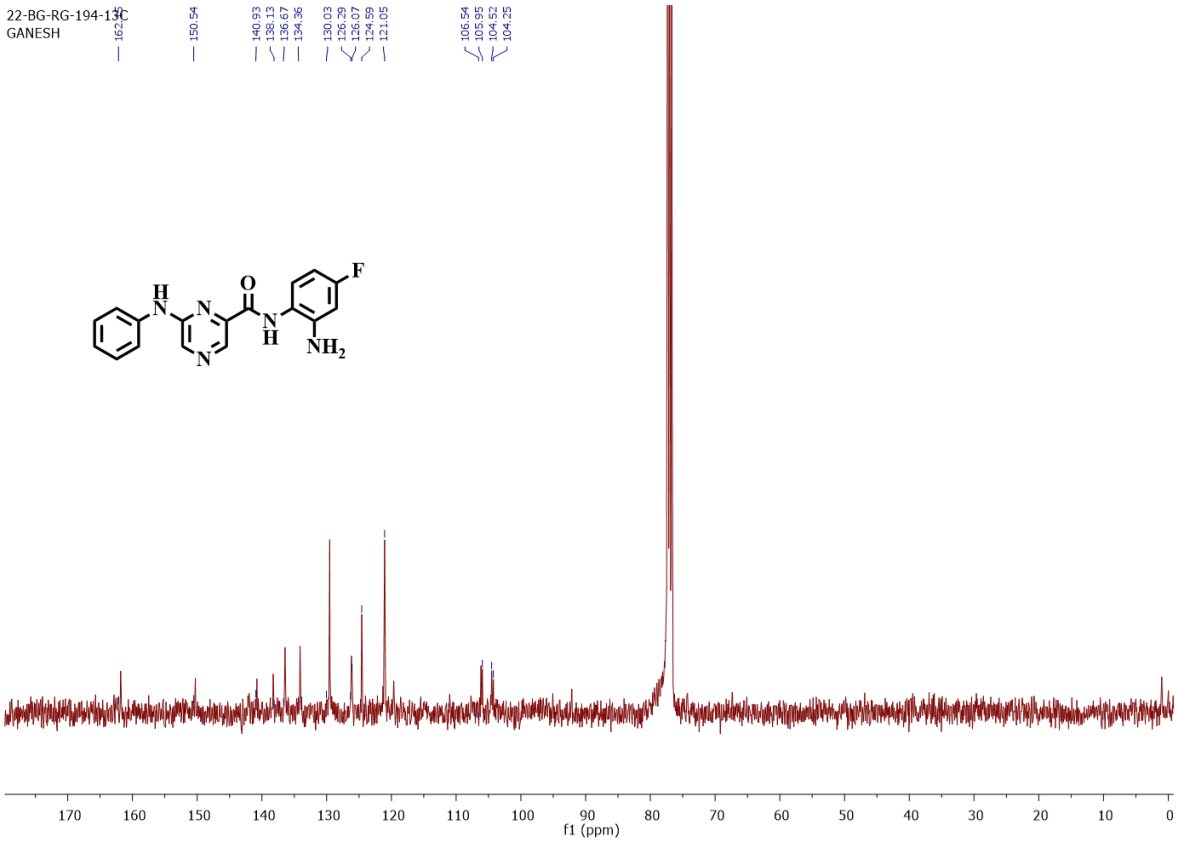
22-BG-RG-194-13C
GANESH
162.16
150.54
140.93
138.13
136.67
134.36
130.03
126.29
126.07
124.59
121.05
106.54
105.95
104.52
104.25
F
O
H
N
N
N
N
H
NH2
170
160
150
140
130
120
110
100
90
80
70
60
50
40
30
20
10
0
f1 (ppm)

HPLC:

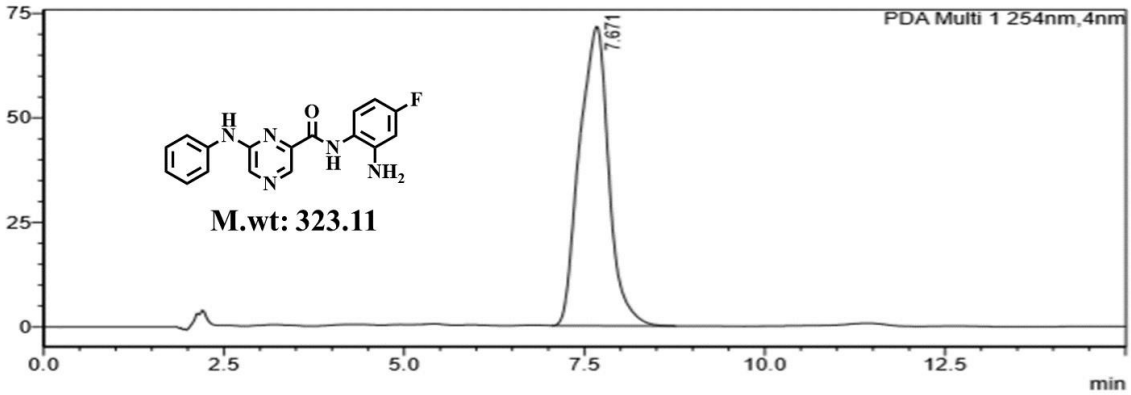
PDA Multi 1 254nm,4nm
7.671
75
50
25
0
0.0
2.5
5.0
7.5
10.0
12.5
min
F
O
H
N
N
N
N
H
NH2
M.wt: 323.11

LCMS:

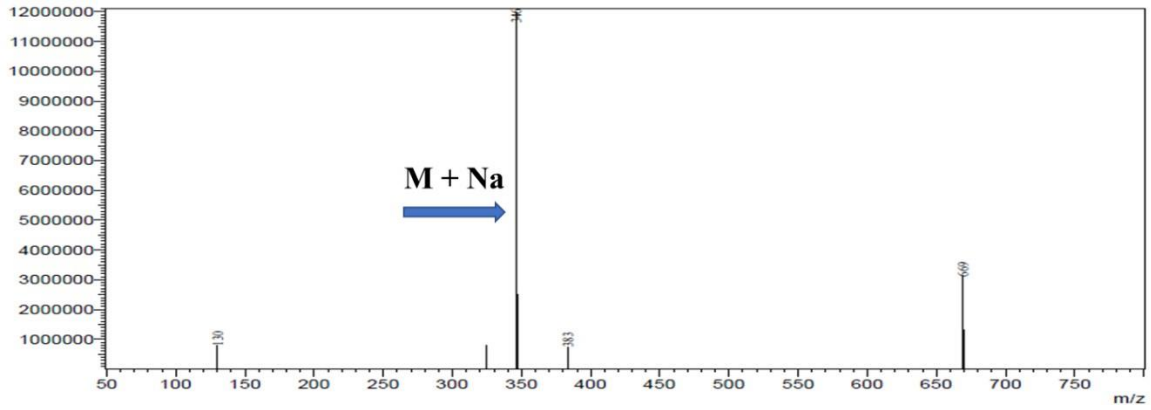

HRMS:

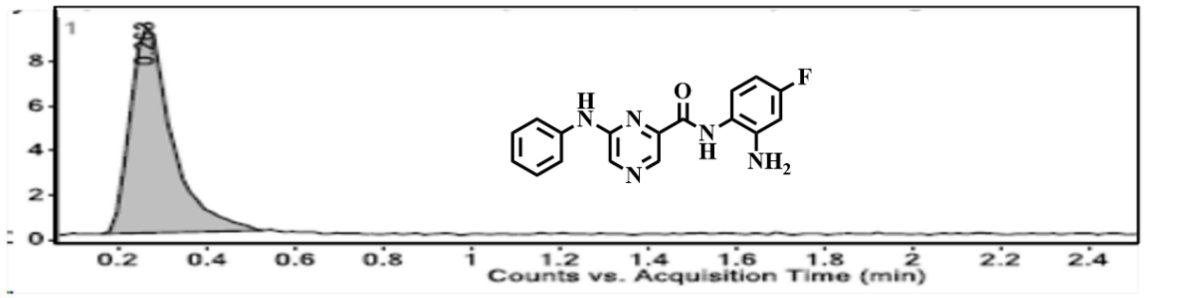

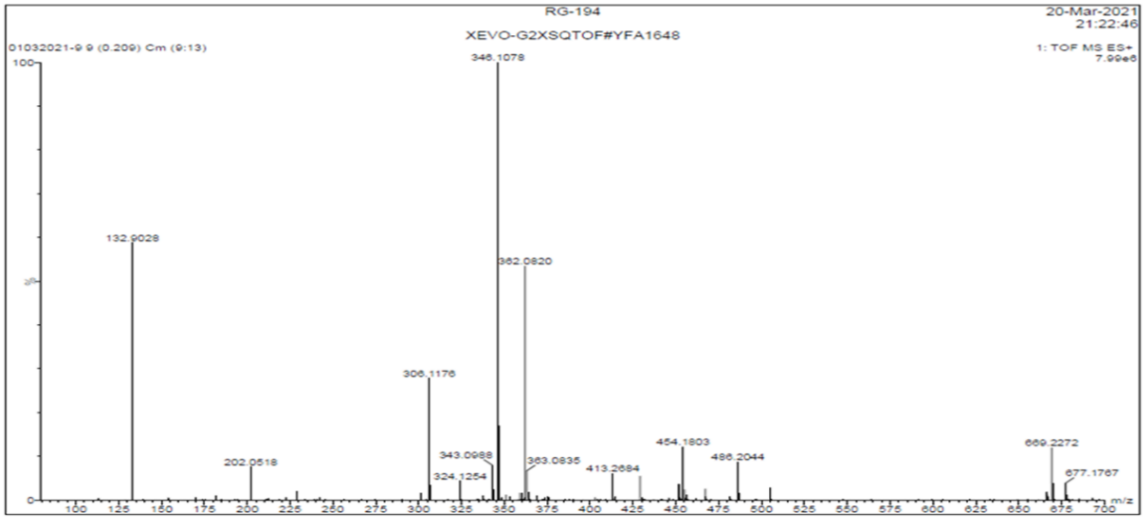

3.4.2. Biology

3.4.2.1. Cell culture

Three distinct cell lines, i.e., mouse breast cancer cell line (4T1), murine melanoma cancer cell line (B16F10) and human breast cancer cell line (MDA-MB-231) were taken into consideration for anticancer evaluation of these synthesized novel compounds by MTT [3-(4,5-dimethylthiazol2-yl)-2,5-diphenyltetrazolium bromide] assay. These cell lines were collected from National Centre for Cell Science (NCCS, Pune, India). B16F10 and MDA-MB-231 cell lines were cultured in Dulbecco's modified eagle medium (high glucose media: AL007S) and 4T1 cell line was cultured in Minimum essential medium (AT154,) along with 10% foetal bovine serum (FBS) and 1% antibiotic (Pen strep: A001) under incubation at 37°C and 5% CO_2 atmosphere. All the chemicals and reagents were bought from Hi media Laboratories Pvt. Ltd., Mumbai, India.

3.4.2.2. Chemicals and antibodies

The synthesized compounds were dissolved in DMSO stock solution and were stored in -20°C. Primary antibodies - rabbit mAb H3K9 acetylated histone H3 (catalogue #9649), rabbit mAb H4K12 acetylated histone H4 (catalogue #13944), mouse mAb beta-Actin primary antibodies (catalogue #58169), rabbit mAb Caspase-3 (catalogue #9662), rabbit mAb Caspase-7 (catalogue #12827) and secondary antibodies – anti-rabbit HRP linked antibody and anti-mouse IgG HRP-Linked antibody were bought from cell signalling technology. DAPI (4′, 6-diamidino-2-phenylindole) and AO (acridine orange), PI (propidium iodide) and RNase were bought from Sigma. TACs Annexin-V/FITC – PI assay kit was bought from Bio legend and was used according to the protocol provided by the vendor.

3.4.2.3. MTT Assay

MTT assay was carried out as per the standardized protocol described in our earlier reports (Trivedi *et al.,* 2018b; Hamoud *et al*., 2020b). Accordingly, a 96 well plate was seeded with 100 µL of cell

suspension at each well (cell density of 1×10^4/well) and was incubated for 24 hr. The medium was then aspirated, and the cells were treated with the molecules synthesized taking CI-994 as a positive control at a concentration of 100 µM and 10 µM in 150 µl into the respective media in duplicate and incubated further for 72 h. The culture medium was then aspirated and subsequently, 50 µl of 5 mg/ml concentrated solution of MTT in phenol red was added in each well and incubated further for 3 h for the production of formazan crystals. After that, 150 µl of DMSO was added to dissolve the formazan crystals and subsequently, the absorbance was recorded using multi-well plate reader Spectramax (Molecular Devices, USA) at two different wavelengths (570 nm and 650 nm). The % cell viability was determined as a fraction of absorbance generated from the treated cells from the absorbance of untreated control cells. The same methodology was followed for all these three cell lines used for the study.

For the IC_{50} measurement of all these compounds in the series along with CI-994, the same procedure was followed as mentioned above. The selected compounds were dissolved in DMSO and these were further diluted to 200 µM, 100 µM, 50 µM, 25 µM, 12.5 µM, 6.25 µM, 3.125 µM, 1.562 µM and 0.781 µM with the DMEM complete media and MEM media, respectively including a blank control containing DMSO in medium and CI-994 as positive control and were incubated for 72 h. Depending on the described protocol, the experiment was repeated in all these three cell lines and the cell viability was determined. Determination of IC_{50} by MTT assay was also carried out for these compounds to judge their cytotoxicity using Human embryonic kidney (HEK293) cell line sub-cultured in DMEM with 10% FBS and 1% antibiotic and were incubated at 37 °C in 5% CO_2 atmosphere. The DMSO solutions of the selected compounds were prepared and they were further diluted to 2mM, 1mM, 500 µM, 250 µM, 125 µM, 62.5 µM, 31.25 µM, 15.62 µM and

7.81 μM with the DMEM complete media for the estimation of IC_{50} values along with a blank control containing DMSO in medium and were incubated for 72 h (Hamoud *et al*., 2020b).

3.4.2.4. HDAC Inhibition Assays

HDAC enzyme inhibition assays were carried out as per the experimental protocol given in the enzyme kits of pan-HDAC (BML-AK501), HDAC1 (BML-AK511), HDAC2 (BML-AK512), HDAC3/NCoR1 (BML-AK531-0001), HDAC8 (BML-AK518) from Enzo life sciences ltd. andHDAC6 (K465-100) from Biovision ltd. that were purchased from Bionova suppliers, Hyderabad. The absorbance values for HDAC enzyme inhibition were estimated with the help of a microplate reader (Spectramax™, Molecular Devices) (Pulya, Mahale, *et al*., 2021b).

3.4.2.5. HDAC inhibition Assay

The enzyme inhibition assay was performed using HDAC colorimetric assay kit (BML-AK501, ENZO life sciences) Routholla *et al.,* 2021). Initially, 5 μL of HeLa nuclear extract (BML-KI137–0500), 10 μL of assay buffer (BMLKI143–0020), 10 μL of sample solution was added per well of a microtiter plate. The reaction was initiated with addition of 25 μL Color de Lys® substrate solution (BML-KI138–0050). After that, the reaction was incubated for 30 min at 37 °C, which was terminated by the addition of 50 μl mixture of developer (BML-KI139-0300) plus stop solution. The plate was incubated further at 37 °C for 15 min and the absorbance was measured at 405 nm. All these synthesized compounds were evaluated at 10μM concentration in duplicate.

3.4.2.5.1. HDAC1 inhibition assay

The HDAC1 enzyme inhibition assay was conducted as per our earlier reported methods (Trivedi *et al*., 2018b; Routholla *et al*., 2021) with the help of HDAC1 fluorimetric drug discovery assay kit (BML-AK511, ENZO life sciences). In the 96 well microtiter plate, 10μ L of the test sample solution and 15 μL diluted HDAC1 complex solution (BML-SE456-0050) were added/ well and

25 µL Fluor de Lys® substrate solution (BML-KI177-0005) was added. The plate was incubated at 37°C for 15 min for reaction. For terminating the reaction, 50µL of mixture of Fluor de Lys® developer II (BML-KI176-1250) and Trichostatin A ((BML-GR309-9090) was added/well and incubated at 37°C for 45 min as per the protocol. The fluorescence intensity was recorded at Excitation and Emission wavelengths of 360 nm and 460 nm, respectively using Spectra max M4 (Molecular Devices, USA). All the selected promising compounds **11a, 12b** along with reference molecule CI-994 were evaluated at 10µM concentration in duplicate. Again, all these selected compounds were tested in duplicate at the concentration range of 1.25µM – 80µM to determine the IC_{50} values following the same protocol (Trivedi *et al*., 2018b; Routholla *et al*., 2021). The IC_{50} values of these compounds were estimated using nonlinear regression analysis method by means of the Graph Pad Prism 5.

3.4.2.5.2. ***HDAC2 inhibition assay***

The HDAC2 enzyme inhibition assay was conducted using HDAC2 fluorimetric drug discovery assay kit (BML-AK512, ENZO life sciences). In the 96 well microtiter plate, 10µL of test sample solution and 15µL diluted HDAC2 complex solution (BML-KI575-0030) were added to each well and 25µL Fluor de Lys® substrate solution (BML-KI572-0050) was added. The plate was incubated at 37°C for 30 min for the reaction. For terminating the reaction, 50µL of mixture of Fluor de Lys® developer II (BML-KI105-0300) and Trichostatin A ((BML-GR309-9090) was added to each well and further incubated at 37 °C for 15 min as per the protocol (Trivedi *et al*., 2018b; Routholla *et al.,* 2021). The fluorescence intensity was recorded at Excitation and Emission wavelengths of 485 nm and 530 nm respectively with the help of Spectra max M4 (Molecular Devices, USA). All the selected compounds **11a, 12b** as well as CI-994 were tested at 10µM concentration in duplicate. Further, all these compounds were tested in duplicate at the

concentration range of 0.625μM – 80μM to determine the IC_{50} values following the same procedure (Trivedi *et al*., 2018b; Routholla *et al*., 2021). The IC_{50} values of these compounds were estimated by means of the nonlinear regression analysis method using Graph Pad Prism 5.

3.4.2.5.3. HDAC3/NCOR1 inhibition assay

The HDAC3 enzyme inhibition assay was performed using HDAC3/NCOR1 fluorimetric drug discovery assay kit (BML-AK531-0001, ENZO life sciences) following the earlier reported method (Trivedi *et al*., 2018b; Routholla *et al*., 2021). In the 96 well microtiter plate, 10μL of test sample solution and 15μL diluted HDAC3/NCOR1 complex solution (BMLKI574-0030) were added/well and 25μL Fluor de Lys® substrate solution (BML-KI177-0005) was added to each well. The plate was incubated at 37 °C for 15 min for the reaction. For terminating the reaction, 50μL of mixture of Fluor de Lys® developer II (BML-KI176-1250) along with Trichostatin A ((BML-GR309-9090) was added/well and incubated further at 37°C for 45 min according to the protocol (Trivedi *et al*., 2018b; Routholla *et al.*, 2021). The fluorescence intensity was recorded at Excitation and Emission wavelengths of 360 nm and 460 nm, respectively with the help of Spectramax M4 (Molecular Devices, USA). All the compounds including CI-994 were screened at 1μM concentration in duplicate. The promising test compounds **11a, 11b and 12b** as well as CI-994 were tested in duplicate at the concentration range of 0.25μM – 8μM to determine the IC_{50} values following the same procedure (Trivedi *et al*., 2018b; Routholla *et al*., 2021). The IC_{50} values of these compounds were determined by means of nonlinear regression analysis method in Graph Pad Prism 5.

3.4.2.5.4. HDAC6 inhibition assay

The HDAC6 enzyme inhibition assay was carried out using HDAC6 fluorimetric inhibitor screening kit (K465-100, Biovision). To the 96 well microtiter plate provided in the kit, 2 μL of

test sample solution and 50 µL diluted HDAC2 complex solution (K465-100-2) were added to each well and incubated at 37°C for 15 mins. Again, 48µL Fluor de Lys® substrate solution (K465100-3) was added to this. The plate was incubated at 37°C for 30 min the reaction. For terminating the reaction, 10µL of developer II (K465-100-4) was added/well and incubated further at 37°C for 10 min according to the protocol (Trivedi *et al*., 2018b; Routholla *et al.,* 2021). The fluorescence intensity was recorded at Excitation and Emission wavelengths of 380 nm and 490 nm, respectively with the help of Spectra max M4 (Molecular Devices, USA). All the selected compounds **11a, 12b** as well as CI-994 were evaluated in duplicate at 20 µM concentration. Moreover, all these compounds were evaluated in duplicate at the concentration range of 10µM – 320µM to determine the IC_{50} values following the same procedure (Trivedi *et al*., 2018b; Routholla *et al.,* 2021). The IC_{50} values of these compounds were estimated by means of the nonlinear egression analysis method in Graph Pad Prism 5.

3.4.2.5.5. HDAC8 inhibition assay

The HDAC8 enzyme inhibition assay was conducted using HDAC8 fluorimetric drug discovery assay kit (BML-AK518, ENZO life sciences). 10µL of test sample solution and 15µL diluted HDAC8 complex solution (BML-SE145-0100) were added/ well and 25µL Fluor de Lys® substrate solution (BML-KI178-0005) was added to each well of the 96 well microtiter plate. The plate was incubated at 37°C for 10 min for the reaction. For terminating the reaction, 50µL of mixture of Fluor de Lys® developer II (BML-KI176-1250) and Trichostatin A ((BML-GR3099090) was added/well and incubated further at 37°C for 45 min according to the protocol (Trivedi *et al*., 2018b; Routholla *et al.,* 2021). The fluorescence intensity was recorded at Excitation and Emission wavelengths of 360 nm and 460 nm, respectively with the help of Spectra max M4 (Molecular Devices, USA). Initially, all the selected compounds **11a, 12b** as well as CI-

994 were tested in duplicate at 5μM concentration. Again, all the compounds were evaluated in duplicate at the concentration range of 0.625μM – 40μM to determine the IC_{50} values following the same procedure (Trivedi *et al*., 2018b; Routholla *et al*., 2021). The IC_{50} values of these compounds were estimated by means of the nonlinear regression analysis method in Graph Pad Prism 5.

3.4.2.6.Western blot analysis of histone acetylation in B16F10 cells

The western blot analysis of histone acetylation in B16F10 cells was conducted as per the earlier reported method (Routholla *et al.,* 2021). For western blot analysis of the acetylated Histone H3 (H3K9) and acetylated Histone H4 (H4K12), B16F10 murine melanoma cells were plated in flat bottom 96 well plate and subjected to grow overnight. These cells were treated with compounds **11a**, **12b** and CI-994 at 5μM, 20μM final concentrations for 12h. After that, the cells were harvested by trypsinization and centrifuged for 5 min at 1250 rpm. The cells pallet was then washed by ice cold PBS, and the total protein was extracted by means of 100μL, 1X RIPA lysis buffer (Millipore, Billerica, MA, USA), supplemented with 0.5 mM phenyl methyl sulfonyl fluoride (PMSF) and protease inhibitor. Then the suspension was vertexed and centrifuged at 4°C for 15 min at 14000 rpm. The whole-cell lysates 20μL and 5μL of loading buffer (4X) was heated for 5 min at 95°C followed by sodium dodecyl sulfate-polyacrylamide gel electrophoresis on 15% Bis-Tris 10-well gels at 60V for approximately 180min in SDS Running Buffer. Gels were transferred to the polyvinylidene fluoride membranes (Bio-Rad, Laboratones, Inc.) and run at 60V for 80 min. Membranes were blocked in 5% non-fat skimmed milk (Bio-Rad, Laboratones, Inc.) in tris-buffered saline with 1% Tween 20 (TBST), and incubated with rabbit mAb H3K9 acetylated histone H3, rabbit mAb H4K12 acetylated histone H4 and mouse mAb beta-Actin primary antibodies overnight at 4°C, which were diluted up-to 1:7000 in 5% (w/v) milk. The membranes

were then incubated with Horseradish peroxidase (HRP)-conjugated anti-rabbit secondary antibody and anti-mouse secondary antibody and then visualized with a chemiluminescence kit (Bio-Rad, Laboratories, Inc.) and exposed using a Fusion plus 6 Imaging System (Vilber Lourmat, France). Beta-Actin was used as an internal control (Pulya, Mahale, *et al.*, 2021b).

3.4.2.7. Nuclear staining assay

The Nuclear staining was conducted as per the earlier reported protocol (Routholla *et al*., 2021) to know the status of nuclear disintegration of cancer cells after treating with compounds **11a**, **12b** and standard molecule CI-994 by means of staining with DAPI and AO. For this purpose, B16F10 murine melanoma cells were plated in a flat bottom 12 well plate and subjected to grow overnight. After that, the cells were treated with compounds **11a** (18.55 µM), **12b** (40.71 µM) and reference standard CI-994 (14.59 µM) and incubated for 48h. After that, control and compounds **11a, 12b** and **CI-994** treated group were fixed with 4% paraformaldehyde solution. Then both the control and compounds treated cells were stained with DAPI and AO. The nuclear staining of both control and treated cells was visualized under fluorescence microscope (Leica microsystems, Germany) on 20x Magnification.

3.4.2.8. Apoptosis assay

The apoptotic assay was performed as per the standardized protocol of the manufacturer (Bio Legend, US) reported earlier (Routholla *et al.*, 2021). B16F10 cells, having cell density of 0.5×10^6/well were seeded for overnight in 12 well tissue culture plates. After that, the cells were treated with compounds **11a** (18.55 µM), **12b** (40.71 µM) and **CI-994** (14.59 µM) for 72h and were incubated at 37°C in CO_2 incubator. The cells were washed with ice cold PBS, subsequently trypsinized and subjected to centrifuge to obtain cell pellet. The pellet was resuspended in 100µL reagent comprising AnnexinV buffer, FITC (1 µL) and PI (10 µL) and incubated for 30 min at

room temperature. AnnexinV binding buffer, 1X (400µl) was added to each sample and characterized by flow cytometer (BDAria^{TM} III). The cells with no treatment were considered as controls. FITC versus PI with quadrant gating was conducted as dot plot (Q1 – Necrotic cells, Q2 - late apoptosis, Q3 – Live cells, Q4 – early apoptotic cells). To estimate the apoptosis, early and late apoptotic events were considered.

3.4.2.9. Cell cycle analysis

The cell cycle analysis was conducted with the help of flow cytometry analysis as per the standardized protocol reported earlier (Routholla et al., 2021). Prior to incubation for overnight, the B16F10 cells were taken into consideration for seeding having density of 0.5×10^6 cells/well. After that, 15µM of compounds **11a**, **12b** and **CI-994** were added to cells and subsequently, incubated further for 48 h. After that, the cells were harvested with trypsin and subsequently, the cell pellet was washed with ice cold PBS. The cells were fixed by dropwise incorporation of 70% ethanol in the cell suspension with gentle vortexing. The clumping of cell was avoided and single cell fixation was visualized for cross-verification under microscope and kept overnight in -20°C. After that, the fixed samples were subjected to centrifuge at 1000 rpm for 7 min at 4°C to produce cell pellet. Finally, the cells were re-suspended in 500 µL of PI and RNAse staining solution. The staining solution was made by adding 20% w/v RNAse and 2% w/v PI in 0.1% v/v of Triton X100 in PBS. The samples were incubated for 30 min in dark condition at room temperature and subsequently, analyzed by flow cytometry (BDAria^{TM} III). The dot plot of PI width against PI area was recorded and histogram of PI area on X axis and counts on Y axis was plotted. The % of cells in each phase of the cell cycle was evaluated with the help of the FCS express software.

3.4.2.10. Animals

For *in vivo* studies, female BALB/c mice of 6–8 weeks age and having 18-22 g of weight were purchased from the National Centre for Laboratory Animal Sciences, National Institute of Nutrition (Hyderabad, India). The protocols were followed as per the CPCSEA guidelines under the strict compliance of Institutional Animal Ethics Committee, of Department of pharmacy, BITS Pilani, Hyderabad campus, Hyderabad (Pulya, Mahale, *et al*., 2021b). The room with conditions of 23±2◦C and 60±10% humidity and 12h light/dark cycle was prepared for animals. Food and water were provided ad libitum. Maximum six mice were placed in one cage at any time during the experiment. The total number of tumor-bearing mice used for the *in vivo* study was 12.

3.4.2.10. Xenograft mouse model

The subcutaneous tumor was developed by subcutaneously injecting 4T1 cells (1.5×10^6 cells suspended in 100µL of PBS) into the dorsal flank region of female BALB/c mice. The mice were supervised and the appearance of tumor was observed for 7-10 days. With the help of vernier caliper, the tumor volume [(length ×width2)/2] was measured. After tumor volume reached about 50 mm3, mice were divided into 3 groups (n=4). Mice were treated intraperitoneally with vehicle itself (5% DMSO, 30% Cremophor, 65% saline), 25 mg/kg and 50 mg/kg of compound **11a** (dissolved in vehicle). The mice were treated for 21 days, five days per week. During the experiment, body weight and tumor volume were measured once in every 3 days. The mice were sacrificed at the end of the study and tumor masses were isolated and weighed. All data represented the mean ± S.E.M. from at least four individual experiments. Animal experiments were performed in accordance with relevant guidelines and regulations and followed ethical standards (Baklaushev *et al.*, 2017; Chiu *et al.*,

2013). Further, towards the survival study, after the treatment period, the mice were shaved in the tumor area, anesthetized in an induction chamber with 2% isoflurane/O2 flow and the primary tumors were then surgically removed following the standard protocol (Pulaski & Ostrand-Rosenberg, 2000; Paschall & Liu, 2016; B. H. Kim *et al.*, 2019). under sterilised conditions. The surgical site was closed using auto-clip applier and the mice were left in separate cages and were taken care following institutional guidelines. The survival study was conducted post-tumor resection for 21 days and the data was presented using Kaplan-Meier plots and were analyzed using GraphPad Prism 5.0.

3.4.2.10. In vivo Bioluminescence imaging analysis

Further, *in vivo* tumor growth was monitored by *in vivo* imaging system IVIS® Lumina III, PerkinElmer, USA. The treated mice were taken to the imaging facility and were anesthetized in an induction chamber with 2% isoflurane/O_2 flow. About 100µl of Luciferin D (100 mg/kg in PBS) was injected intraperitoneally to the mice before imaging. The tumor growth was monitored in treated mice one from each group selected randomly on day 10 and day 21 post injection by acquiring images with IVIS®. After day 21, the mice were sacrificed and tumors along with various organs like heart, lungs, liver, spleen and kidney were isolated and were embedded in tissue freezing medium for immunohistochemistry analysis. To the endpoint, tumors were harvested and lysed in cold 1X RIPA lysis buffer (Millipore, Billerica, MA, USA), supplemented with 0.5 mM phenylmethylsulfonyl fluoride (PMSF) and protease inhibitor and used for western blotting analysis. Bioluminescence signals were measured (photons/sec/cm^2 /sr) by selecting the region of interest in the tumor area (Lim *et al.*, 2009).

3.4.2.11. Western blot analysis

The western blot analysis was performed based on the standardized protocol reported in our earlier report (Routholla *et al*., 2021). For this purpose, tumors were collected from treated mice and washed briefly with chilled 1X PBS. Homogenize the tumor tissue and the total cell lysate was extracted with the help of 100 µL, 1X RIPA lysis buffer (Millipore, Billerica, MA, USA), supplemented with 0.5 mM PMSF and protease inhibitor. After lysing was done, the suspension was subjected to vertex and subsequently centrifuged for 15 min at 14000 rpm at 4°C. After that, 15µL of the whole-cell lysates and 5µL of loading buffer (4X) was heated for 5 min at 95°C and was subjected further to sodium dodecyl sulphate (SDS)-polyacrylamide gel electrophoresis on 15% Bis-Tris 10-well gels at 60V for about 3h in SDS Running Buffer. Gels were transferred to the polyvinylidene fluoride membranes (Bio-Rad, Laboratones, Inc.) and was run at 60V for 80 min. After that, the membranes were blocked in 5% non-fat skimmed milk (Bio-Rad, Laboratones, Inc.) in tris-buffered saline with 1% Tween 20 (TBST), and incubated with rabbit mAb H3K9 acetylated histone H3, rabbit mAb H4K12 acetylated histone H4, rabbit mAb Caspase 3, rabbit mAb Caspase 7 and mouse mAb β-Actin primary antibodies overnight at 4°C, which were diluted up-to 1:7000 in 5% (w/v) milk. Then the membranes were incubated with Horseradish peroxidase (HRP)-conjugated anti-rabbit and anti-mouse secondary antibodies and then visualized by means of a chemiluminescence kit (Bio-Rad, Laboratories, Inc.) and exposed with the help of a Fusion plus 6 Imaging System (Vilber Lourmat, France). The blots were quantified using Image J software by normalising against beta-Actin as an internal control (Pulya, Mahale, *et al*., 2021b).

3.4.2.11. Immunohistochemistry

3.4.2.10.1. TUNEL assay in tumor cryosections

TUNEL assay (Terminal deoxynucleotidyl transferase mediated nickend labeling) was performed to determine extent of apoptosis in the tumor tissue. The tumors were harvested from mice and sectioned with the thickness of 5µm using a cryostat (Leica biosystems, Germany). Then tumor sections were fixed with 4% paraformaldehyde and treated with TUNEL reagent kit (Fragel DNA Fragmentation Detection Kit, Merck, Darmstadt, Germany). The level of apoptosis in tumor sections was determined as per the methodology provided by the manufacturer. The stained tumor sections were viewed under fluorescent microscope using blue and green filters. The images were processed and analyzed in Image J software.

3.4.2.10.2. ROS production in tumor tissues

The production of ROS was evaluated in tumors using a DCFH-DA fluorescence probe. The treated mice were taken to the imaging facility and were anesthetized in an induction chamber with 2% isoflurane/O2 flow. The treated mice (n=2) were then injected intra-tumorally on day 21 with the DCFH-DA probe (100µL, 25µM). The extent of ROS production was monitored post injection by acquiring images with IVIS®. ROS generation was quantified in terms of fluorescence intensity [(p/sec/cm^2/sr)/µW/cm^2] by selecting the region of interest. After 30 min, the mice were sacrificed and the tumors were isolated and sectioned into 5 µm thickness and observed under fluorescence microscope.

3.4.2.10.3. Immuno-histochemical analysis of Ki-67

Ki-67 immuno-histochemical analysis on tumor sections was performed to study cell proliferation. After the treatment protocol, the tumor bearing mice were sacrificed, and fixed with 4% paraformaldehyde for 24 h. With the help of cryotome, 5µm slices were cut from the embedded

tumor tissues for Ki-67 immuno-histochemical analysis. The tumor sections were incubated overnight with Ki-67 (catalogue#9129S) with dilution of 1:500, at 4°C. Then the sections were washed using 1X PBS and incubated further with Alexa Fluor® 488 conjugate secondary antibody for 2h. Then, tissue sections were washed with 1X PBS and covered with coverslip and observed under fluorescence microscope. Microscopic images of the tissues were captured with the utilization of microscope (Lieca).

3.4.2.10.4. H & E staining analysis of tumor and organ sections

H&E staining was performed on various organs isolated from tumor bearing mice. After the completion of treatment, the major organs like liver, heart, spleen, kidney and lung were removed, fixed in tissue freezing media and sectioned into 5μm thickness using a cryotome (Leica biosystems, Germany). The manufacturer's protocol was followed to stain the sections with Harris's hematoxylin-eosin (H and E) reagent. The sections were observed under light microscope for histological studies.

3.4.3. Molecular docking

Molecular docking studies on compounds **11a** and **12b** compounds were performed by the Glide module of Schrodinger Maestro v12.1 to the binding site of HDAC3 enzyme. The protein structure was obtained from the Protein Data Bank and processed by using ''protein preparation wizard'' protocol in the Maestro wizard v12.1. The generating states and refinement steps automatically added hydrogen atoms and some essential bonds in the missing sites of proteins. The refinement steps include the optimization of groups having hydrogen bonding, restrained minimization with the help of the default OPLS_3e force field. After the optimization was over, receptor grid generation was processed to locate the binding pocket. The docking results were found with different docked ligand conformations including their binding energy scores. These conformations

ranked depending on the scores and selected as per their interactions with the enzymes as well as docking scores **(*Docking and Scoring | Schrödinger*).**

Chapter-4

SUMMARY & CONCLUSION

SUMMARY AND CONCLUSION:

By reversibly modifying the acetylation status of histone and nonhistone proteins, studies over the past few decades have shown that HDACs play a crucial role in the development of cancer. HDACs have been found dysregulate and function incorrectly in cancer, providing a crucial attractive target against cancer. HDACs are a key modulator of proliferation and tumorigenic potential, but their precise role in these processes is still remains. HDACs are genetically down regulated or knocked out, which causes cell cycle arrest and apoptosis in a variety of cancer cells.

However, in some situations, HDACs are also seen to have a potential tumour suppressor function. The role of individual HDACs in different cancer types at various stages of tumorigenesis is not clearly understood yet. Currently, broad-spectrum nonselective HDACi are the most common HDAC inhibitors being tested in both preclinical and clinical settings. The current focus is on developing HDAC inhibitor that are more effective and less toxic. In addition, research is increasingly indicating that combination therapy may be another important way to develop the therapeutic efficacy of HDAC inhibitor.

In first objective we have synthesis, biological evaluation, and molecular docking analysis of novel linker-less benzamide based potent and selective HDAC3 inhibitors. All the compounds were studied for their *pan*-HDAC and HDAC3 inhibitory activity. Further, the selected lead compounds **5e** and **5f** were studied for their HDAC 1, 2, 3, 8 and 6 enzyme inhibitory profiles to judge the selectivity towards HDAC3. Two lead compounds **5e** and **5f** were found to be potent and highly selective HDAC3 inhibitors over other Class-I HDACs and HDAC6. Compound **5e** bearing a 6quinolinyl moiety as the cap group was found to be a highly potent HDAC3 inhibitor (IC_{50} = 560 nM) and displayed 46-fold selectivity for HDAC3 over HDAC2, and 33-fold selectivity for HDAC3 over HDAC1. Moreover, the HDAC3 selectivity of the lead molecules found to be much

better than the reference compound **CI994**. All these compounds exhibited effective antiproliferative activity against various cancer cell lines (4T1, B16F10 and MDA-MB-231) with less cytotoxicity against normal cells (HEK293) when compared with reference compound **CI994** and interestingly the most promising molecule (**5e**) showed least toxicity towards normal cells. Further, the acetylation levels of cellular histone (H3K9 and H4K12) were examined and both the lead compounds were able to enhance the acetylation level significantly in a dose-dependent manner in B16F10 cells. Moreover, compounds **5e** and **5f** were found to cause apoptotic cell death and were causing G2/M cell cycle phase arrest in B16F10 cells. The molecular docking study revealed similar binding interactions of the lead molecules and reference compound at the active site of HDAC3. The higher HDAC3 inhibitory potency along with selectivity for HDAC3 of compound **5e** over compound **5f** was also justified by the molecular docking analysis. Based on the findings, it can be inferred that most potent and HDAC3 selective lead molecule **5e** might serve as a potential therapeutic as anticancer agent.

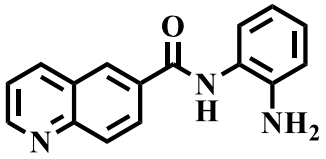

Compound 5e (ch.2)

Figure 4.1. Lead compound from the first series of 2-aminobenzamide derivatives additionally, all the biological studies indicated compound 5e (ch.2) can be further explored as a promising compound for anticancer therapy.

In the second objective, in this study, a series of novel substituted benzamides consisting of various aryl and heteroaryl cap groups with *o*-hydroxy and *p*-fluoro substituted benzamides as effective ZBG were designed and synthesized. These compounds were studied as potential and selective

HDAC3 inhibitors possessing effective anticancer activities. These novel compounds were screened against cancer cell lines 4T1, B16F10 and MCF-7 and are found to possess significant antiproliferative activity when compared to class-I selective HDAC inhibitor **CI-994** as a reference molecule. These molecules were also relatively nontoxic to the normal cell line HEK-293. Among compounds in the series, compounds **11a** and **12b** were the most potent and HDAC3-selective over other Class-I HDACs and HDAC6. Compound **11a** possessing a 6-quinolyl scaffold in the cap region and hydroxyl function substituted at the *ortho* position of the benzamide scaffold was found to be the most promising with over 20 and 16-fold HDAC3 selectivity over HDAC2 and HDAC1, respectively. Compounds **11a** and **12b** were found to induce significant upregulation of acetylated H3K9 and H4K12 in B16F10 cells in a dose-dependent fashion *in vitro*. Molecular docking analysis with compounds **11a** and **12b** at the HDAC3 active site were found to be a good fit with the docking scores correlating the *in vitro* HDAC3 inhibitory assay results. They were found to induce apoptosis and cause the cell cycle arrest in G2/M phase as evidenced in B16F10 cells. The *in vivo* antitumor efficacy studies in 4T1-Luc breast cancer xenograft model in female Balb/c mice indicated that the compound **11a** (25 mg/kg and 50 mg/kg) exhibited a significant reduction in tumor volume compared to control group mice which are treated with vehicle alone. No change in body weights during the treatment period suggested no general toxicity of the compound **11a** even at 50 mg/kg dose. TUNEL assay results indicated the extent of apoptosis increased with 50 mg/kg when compared to 25 mg/kg dose treatment with a greater number of TUNEL (+ve) staining in the tissue of 50 mg/kg. Compound **11a** also significantly induced ROS generation leading to apoptosis. Moreover, a decrease in cell proliferation has been indicated by the significant reduction in Ki-67 positive stained tumor tissue as in the case of treated tumor tissue sections when compared to control group tumor tissues. No significant toxicity was found in major organs, as evidenced by

H&E staining of various organs of compound **11a** treated mice. Western blot analysis of tumor tissues of compound **11a** treated mice also showed the upregulation of acetylated H3K9 and H4K12 levels along with the upregulation of apoptotic markers such as caspase-3 and caspase-7 levels further indicating the significant apoptotic activity through enhanced histone acetylation due to the inhibition of HDAC3 enzyme *in vivo*. Altogether, the results obtained from the *in vitro* and *in vivo* antitumor experiments pointed out that compound **11a** from the series of HDAC3 specific inhibitors might be promising anticancer therapeutics and can be taken further for the clinical translation as an emerging anticancer drug candidate.

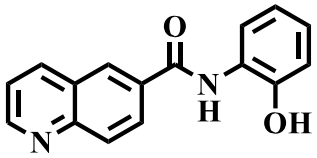

Compound 11a (ch.3)

Figure 4.2. Lead compound from the second series of 2-hydroxy benzamide derivative

Compound name / **Parameters**	**5e (chapter 2)**	**11a (chapter 3)**	**CI-994 (Standard reference cpd.)**
HDAC3 IC_{50} (µM)	0.563±0.11	1.586 ± 0.120	0.902
HDAC3 selectivity over HDAC1 and 2	33-fold over HDAC1 46-fold over HDAC2	16 -fold over HDAC1 20-fold over HDAC2	Equally potent across all three isoforms (HDAC1 and HDAC2 and HDAC3
IC_{50} (µM)	17.89±1.31 (B16F10)	10.29 ± 3.58 (4T1)	14.34 ± 1.68 (B16F10)
Normal cell line IC_{50} (µM)	1084±10.6 (HEK)	449.7 ± 6.98 (HEK)	216.2 ± 4.69 (HEK)
Cancer cell selectivity over normal cells	60.59	43.70	15.08

FUTURE PERSPECTIVES

Histone deacetylase inhibitors are a large group of diverse molecules intrinsically able to inhibit cell proliferation in various cancer cell lines. Their apoptotic effects have been linked to the modulation in the expression of several regulatory tumor suppressor genes caused by the modified status of histone acetylation, a key event in chromatin remodelling. As the initial histone deacetylase activity of HDAC has been extended to other proteins, the possible other biological mechanisms modified by HDAC inhibitor treatments are still to be clarified. The need for HDAC isoform selective inhibitors is an important issue to serve this goal.

In this study, we have developed molecules with preferential selectivity towards specific HDAC3 isoform. The lead compounds were found as potent and highly selective HDAC3 inhibitors over other class-1 HDACs. It can be helpful for further development of these molecules. These compounds possess efficient anti-cancer potential. They can be further studied for their pathway specific activity and can be modified to enhance their efficacy.

Currently many HDAC inhibitors are focusing on strategies for achieving higher efficacy by combination therapies, including phoshoinositide-3-kinase (PI3K) and EGFR inhibitors, and hormone- or immunotherapy. This also includes new bifunctional inhibitors as well as novel approaches for HDAC degradation via PROteolysis-Targeting Chimeras (PROTACs).

The lead compounds from the two series can be evaluated side by side in *in vivo* animal model to assess their difference of efficacy even when administered equal dose and same route of administration.

BIBLIOGRAPHY

Abdizadeh, T., Kalani, M. R., Abnous, K., Tayarani-Najaran, Z., Khashyarmanesh, B. Z., Abdizadeh, R., Ghodsi, R., & Hadizadeh, F. (2017). Design, synthesis and biological evaluation of novel coumarin-based benzamides as potent histone deacetylase inhibitors and anticancer agents. *European Journal of Medicinal Chemistry*, *132*, 42–62. https://doi.org/10.1016/J.EJMECH.2017.03.024

Adhikari, N., Amin, S. A., Trivedi, P., Jha, T., & Ghosh, B. (2018). HDAC3 is a potential validated target for cancer: An overview on the benzamide-based selective HDAC3 inhibitors through comparative SAR/QSAR/QAAR approaches. *European Journal of Medicinal Chemistry*, *157*, 1127–1142. https://doi.org/10.1016/J.EJMECH.2018.08.081

Adhikari, N., Jha, T., & Ghosh, B. (2021). Dissecting Histone Deacetylase 3 in Multiple Disease Conditions: Selective Inhibition as a Promising Therapeutic Strategy. *Journal of Medicinal Chemistry*, *64*(13), 8827–8869. https://doi.org/10.1021/ACS.JMEDCHEM.0C01676

Adimoolam, S., Sirisawad, M., Chen, J., Thiemann, P., Ford, J. M., & Buggy, J. J. (2007). HDAC inhibitor PCI-24781 decreases RAD51 expression and inhibits homologous recombination. *Proceedings of the National Academy of Sciences of the United States of America*, *104*(49), 19482–19487. https://doi.org/10.1073/PNAS.0707828104

Almouzni, G., & Cedar, H. (2016). Maintenance of Epigenetic Information. *Cold Spring Harbor Perspectives in Biology*, *8*(5). https://doi.org/10.1101/CSHPERSPECT.A019372

Amin, S. A., Adhikari, N., Jha, T., & Ghosh, B. (2019). Designing potential HDAC3 inhibitors to improve memory and learning. *Journal of Biomolecular Structure & Dynamics*, *37*(8), 2133–2142. https://doi.org/10.1080/07391102.2018.1477625

Amin, S. A., Adhikari, N., Kotagiri, S., Jha, T., & Ghosh, B. (2019a). Histone deacetylase 3 inhibitors in learning and memory processes with special emphasis on benzamides. *European Journal of Medicinal Chemistry*, *166*, 369–380.

Angiolilli, C., Kabala, P. A., Grabiec, A. M., van Baarsen, I. M., Ferguson, B. S., García, S., Fernandez, B. M., McKinsey, T. A., Tak, P. P., Fossati, G., Mascagni, P., Baeten, D. L., & Reedquist, K. A. (2017). Histone deacetylase 3 regulates the inflammatory gene expression programme of rheumatoid arthritis fibroblast-like synoviocytes. *Annals of the Rheumatic Diseases*, *76*(1), 277–285. https://doi.org/10.1136/ANNRHEUMDIS-2015-209064

Baidya, S. K., Amin, S. A., Banerjee, S., Adhikari, N., & Jha, T. (2019). Structural exploration of arylsulfonamide-based ADAM17 inhibitors through validated comparative multi-QSAR modelling studies. *Journal of Molecular Structure*, *1185*, 128–142. https://doi.org/10.1016/J.MOLSTRUC.2019.02.081

Baklaushev, V. P., Kilpeläinen, A., Petkov, S., Abakumov, M. A., Grinenko, N. F., Yusubalieva, G. M., Latanova, A. A., Gubskiy, I. L., Zabozlaev, F. G., Starodubova, E. S., Abakumova, T. O., Isaguliants, M. G., & Chekhonin, V. P. (2017). Luciferase expression allows bioluminescence imaging but imposes limitations on the orthotopic mouse (4T1) model of breast cancer. *Scientific Reports*, *7*(1). https://doi.org/10.1038/S41598-017-07851-Z

Bardai, F. H., & D'Mello, S. R. (2011). Selective toxicity by HDAC3 in neurons: regulation by Akt and GSK3beta. *The Journal of Neuroscience: The Official Journal of the Society for Neuroscience*, *31*(5), 1746–1751. https://doi.org/10.1523/JNEUROSCI.5704-10.2011

Beckers, T., Burkhardt, C., Wieland, H., Gimmnich, P., Ciossek, T., Maier, T., & Sanders, K. (2007). Distinct pharmacological properties of second generation HDAC inhibitors with the benzamide or hydroxamate head group. *International Journal of Cancer*, *121*(5), 1138–1148. https://doi.org/10.1002/IJC.22751

Bhaskara, S., Knutson, S. K., Jiang, G., Chandrasekharan, M. B., Wilson, A. J., Zheng, S., Yenamandra, A., Locke, K., Yuan, J. L., Bonine-Summers, A. R., Wells, C. E., Kaiser, J. F., Washington, M. K., Zhao, Z., Wagner, F. F., Sun, Z. W., Xia, F., Holson, E. B., Khabele, D., & Hiebert, S. W. (2010). Hdac3 is essential for the maintenance of chromatin structure and genome stability. *Cancer Cell*, *18*(5), 436. https://doi.org/10.1016/J.CCR.2010.10.022

Bishton, M. J., Harrison, S. J., Martin, B. P., McLaughlin, N., James, C., Josefsson, E. C., Henley, K. J., Kile, B. T., Prince, H. M., & Johnstone, R. W. (2011). Deciphering the molecular and biologic processes that mediate histone deacetylase inhibitor-induced thrombocytopenia. *Blood*, *117*(13), 3658–3668. https://doi.org/10.1182/BLOOD-2010-11-318055

Biswas, S., & Rao, C. M. (2017). Epigenetics in cancer: Fundamentals and Beyond. *Pharmacology & Therapeutics*, *173*, 118–134. https://doi.org/10.1016/J.PHARMTHERA.2017.02.011

Boissinot, M., Inman, M., Hempshall, A., James, S. R., Gill, J. H., Selby, P., Bowen, D. T., Grigg, R., & Cockerill, P. N. (2012). Induction of differentiation and apoptosis in leukaemic cell lines by the novel benzamide family histone deacetylase 2 and 3 inhibitor MI-192. *Leukemia Research*, *36*(10), 1304–1310. https://doi.org/10.1016/J.LEUKRES.2012.07.002

Bolden, J. E., Peart, M. J., & Johnstone, R. W. (2006). Anticancer activities of histone deacetylase inhibitors. *Nature Reviews. Drug Discovery*, *5*(9), 769–784.

Bolden, J. E., Shi, W., Jankowski, K., Kan, C. Y., Cluse, L., Martin, B. P., MacKenzie, K. L., Smyth, G. K., & Johnstone, R. W. (2013). HDAC inhibitors induce tumor-cell-selective pro-apoptotic transcriptional responses. *Cell Death & Disease*, *4*(2).

Bradbury, C. A., Khanim, F. L., Hayden, R., Bunce, C. M., White, D. A., Drayson, M. T., Craddock, C., & Turner, B. M. (2005). Histone deacetylases in acute myeloid leukaemia show a distinctive pattern of expression that changes selectively in response to deacetylase inhibitors. *Leukemia*, *19*(10), 1751–1759. https://doi.org/10.1038/SJ.LEU.2403910

Butler, L. M., Zhou, X., Xu, W. S., Scher, H. I., Rifkind, R. A., Marks, P. A., & Richon, V. M. (2002). The histone deacetylase inhibitor SAHA arrests cancer cell growth, up-regulates thioredoxinbinding protein-2, and down-regulates thioredoxin. *Proceedings of the National Academy of Sciences of the United States of America*, *99*(18), 11700–11705. https://doi.org/10.1073/PNAS.182372299

Chandler, V. L. (2007). Paramutation: from maize to mice. *Cell*, *128*(4), 641–645. https://doi.org/10.1016/J.CELL.2007.02.007

Chen, C. L., Sung, J., Cohen, M., Chowdhury, W. H., Sachs, M. D., Li, Y., Lakshmanan, Y., Yung, B. Y. M., Lupold, S. E., & Rodriguez, R. (2006). Valproic acid inhibits invasiveness in bladder cancer but not in prostate cancer cells. *The Journal of Pharmacology and Experimental Therapeutics*, *319*(2), 533–542. https://doi.org/10.1124/JPET.106.106658

Chen, C. S., Wang, Y. C., Yang, H. C., Huang, P. H., Kulp, S. K., Yang, C. C., Lu, Y. S., Matsuyama, S., Chen, C. Y., & Chen, C. S. (2007). Histone deacetylase inhibitors sensitize prostate cancer cells to agents that produce DNA double-strand breaks by targeting Ku70 acetylation. *Cancer Research*, *67*(11), 5318–5327. https://doi.org/10.1158/0008-5472.CAN-06-3996

Chen, Y., Feng, J., Hu, Y., Wang, X., Song, W., & Zhang, L. (2020). Discovery of N-(2-Amino-4Fluorophenyl)-4- [bis-(2-Chloroethyl)-Amino]-Benzamide as a Potent HDAC3 Inhibitor. *Frontiers in Oncology*, *10*. https://doi.org/10.3389/FONC.2020.592385

Chen, Y., He, R., Chen, Y., D'Annibale, M. A., Langley, B., & Kozikowski, A. P. (2009). Studies of benzamide- and thiol-based histone deacetylase inhibitors in models of oxidative-stress-induced neuronal death: identification of some HDAC3-selective inhibitors. *ChemMedChem*, *4*(5), 842–852. https://doi.org/10.1002/CMDC.200800461

Chiu, H. W., Yeh, Y. L., Wang, Y. C., Huang, W. J., Chen, Y. A., Chiou, Y. S., Ho, S. Y., Lin, P., & Wang, Y. J. (2013). Suberoylanilide hydroxamic acid, an inhibitor of histone deacetylase, enhances radiosensitivity and suppresses lung metastasis in breast cancer in vitro and in vivo. *PloS One*, *8*(10). https://doi.org/10.1371/JOURNAL.PONE.0076340

Cui, Z., Xie, M., Wu, Z., & Shi, Y. (2018). Relationship Between Histone Deacetylase 3 (HDAC3) and Breast Cancer. *Medical Science Monitor: International Medical Journal of Experimental and Clinical Research*, *24*, 2456–2464. https://doi.org/10.12659/MSM.906576

Dawson, M. A., & Kouzarides, T. (2012). Cancer epigenetics: From mechanism to therapy. *Cell*, *150*(1), 12–27. https://doi.org/10.1016/J.CELL.2012.06.013 de Ruijter, A. J. M., van Gennip, A. H., Caron, H. N., Kemp, S., & van Kuilenburg, A. B. P. (2003). Histone deacetylases (HDACs): characterization of the classical HDAC family. *The Biochemical Journal*, *370*(Pt 3), 737–749. https://doi.org/10.1042/BJ20021321

Dirice, E., Ng, R. W. S., Martinez, R., Hu, J., Wagner, F. F., Holson, E. B., Wagner, B. K., & Kulkarni, R. N. (2017). Isoform-selective inhibitor of histone deacetylase 3 (HDAC3) limits pancreatic islet infiltration and protects female nonobese diabetic mice from diabetes. *The Journal of Biological Chemistry*, *292*(43), 17598–17608.

Docking and Scoring | Schrödinger. (n.d.). Retrieved December 14, 2022, from https://www.schrodinger.com/science-articles/docking-and-scoring

Dokmanovic, M., Clarke, C., & Marks, P. A. (2007b). Histone deacetylase inhibitors: overview and perspectives. *Molecular Cancer Research : MCR*, *5*(10), 981–989.

Falkenberg, K. J., & Johnstone, R. W. (2014b). Histone deacetylases and their inhibitors in cancer, neurological diseases and immune disorders. *Nature Reviews Drug Discovery 2014 13:9*, *13*(9), 673–691. https://doi.org/10.1038/nrd4360

Finnin, M. S., Donigian, J. R., Cohen, A., Richon, V. M., Rifkind, R. A., Marks, P. A., Breslow, R., & Pavletich, N. P. (1999a). Structures of a histone deacetylase homologue bound to the TSA and SAHA inhibitors. *Nature*, *401*(6749), 188–193. https://doi.org/10.1038/43710

Fournel, M., Bonfils, C., Hou, Y., Yan, P. T., Trachy-Bourget, M. C., Kalita, A., Liu, J., Lu, A. H., Zhou, N. Z., Robert, M. F., Gillespie, J., Wang, J. J., Ste-Croix, H., Rahil, J., Lefebvre, S., Moradei, O., Delorme, D., MacLeod, A. R., Besterman, J. M., & Li, Z. (2008). MGCD0103, a novel isotypeselective histone deacetylase inhibitor, has broad spectrum antitumor activity in vitro and in vivo.

Molecular Cancer Therapeutics, *7*(4), 759–768. https://doi.org/10.1158/1535-7163.MCT-072026

Frew, A. J., Johnstone, R. W., & Bolden, J. E. (2009). Enhancing the apoptotic and therapeutic effects of HDAC inhibitors. *Cancer Letters*, *280*(2), 125–133.

Galli, M., Salmoiraghi, S., Golay, J., Gozzini, A., Crippa, C., Pescosta, N., & Rambaldi, A. (2010). A phase II multiple dose clinical trial of histone deacetylase inhibitor ITF2357 in patients with relapsed or progressive multiple myeloma. *Annals of Hematology*, *89*(2), 185–190. https://doi.org/10.1007/S00277-009-0793-8

Gong, P., Wang, Y., & Jing, Y. (2019). Apoptosis Induction by Histone Deacetylase Inhibitors in Cancer Cells: Role of Ku70. *International Journal of Molecular Sciences*, *20*(7). https://doi.org/10.3390/IJMS20071601

Guenther, M. G., Barak, O., & Lazar, M. A. (2001). The SMRT and N-CoR Corepressors Are Activating Cofactors for Histone Deacetylase 3. *Molecular and Cellular Biology*, *21*(18), 6091– 6101. https://doi.org/10.1128/MCB.21.18.6091-6101.2001/ASSET/C0193855-7D01-47F4BD88-DC859A78BB1A/ASSETS/GRAPHIC/MB1810338009.JPEG

Gupta, M., Han, J. J., Stenson, M., Wellik, L., & Witzig, T. E. (2012). Regulation of STAT3 by histone deacetylase-3 in diffuse large B-cell lymphoma: implications for therapy. *Leukemia*, *26*(6), 1356–1364. https://doi.org/10.1038/LEU.2011.340

Hamoud, M. M. S., Pulya, S., Osman, N. A., Bobde, Y., Hassan, A. E. A., Hassan, A. E. A., Abdel Fattah, H. A., Ghosh, B., & Ghanim, A. M. (2020b). Design, synthesis, and biological evaluation of novel nicotinamide derivatives as potential histone deacetylase-3 inhibitors. *New Journal of Chemistry*, *44*(23), 9671–9683. https://doi.org/10.1039/D0NJ01274B

Harada, T., Ohguchi, H., Grondin, Y., Kikuchi, S., Sagawa, M., Tai, Y. T., Mazitschek, R., Hideshima, T., & Anderson, K. C. (2017). HDAC3 regulates DNMT1 expression in multiple myeloma: therapeutic implications. *Leukemia*, *31*(12), 2670–2677.

He, P., Li, K., Li, S. B., Hu, T. T., Guan, M., Sun, F. Y., & Liu, W. W. (2018). Upregulation of AKAP12 with HDAC3 depletion suppresses the progression and migration of colorectal cancer. *International Journal of Oncology*, *52*(4), 1305–1316.

He, R., Chen, Y., Chen, Y., Ougolkov, A. v., Zhang, J. S., Savoy, D. N., Billadeau, D. D., & Kozikowski, A. P. (2010). Synthesis and biological evaluation of triazol-4-ylphenyl-bearing histone deacetylase inhibitors as anticancer agents. *Journal of Medicinal Chemistry*, *53*(3), 1347–1356. https://doi.org/10.1021/JM901667K/ASSET/IMAGES/LARGE/JM-200901667K_0007.JPEG

Hess-Stumpp, H., Bracker, T. U., Henderson, D., & Politz, O. (2007). MS-275, a potent orally available inhibitor of histone deacetylases--the development of an anticancer agent. *The International Journal of Biochemistry & Cell Biology*, *39*(7–8), 1388–1405.

Hirata, Y., Sasaki, T., Kanki, H., Choong, C. J., Nishiyama, K., Kubo, G., Hotei, A., Taniguchi, M., Mochizuki, H., & Uesato, S. (2018). New 5-Aryl-Substituted 2-Aminobenzamide-Type HDAC Inhibitors with a Diketopiperazine Group and Their Ameliorating Effects on Ischemia-Induced Neuronal Cell Death. *Scientific Reports 2018 8:1*, *8*(1), 1–10. https://doi.org/10.1038/s41598-01819664-9

H. Ozdag, A.E. Teschendorff, A.A. Ahmed, S.J. Hyland, C. Blenkiron, L. Bobrow, A. Veerakumarasivam, G. Burtt, T. Subkhankulova, M.J. Arends, V.P. Collins, D. Bowtell, et al, Differential expression of selected histone modifier genes in human solid cancers, BMC Genomics 7 (2006) 90. - Google Search. (n.d.). Retrieved November 21, 2022, from https://www.google.com/search

Hsieh, H. Y., Chuang, H. C., Shen, F. H., Detroja, K., Hsin, L. W., & Chen, C. S. (2017b). Targeting breast cancer stem cells by novel HDAC3-selective inhibitors. *European Journal of Medicinal Chemistry*, *140*, 42–51. https://doi.org/10.1016/J.EJMECH.2017.08.069

Huang, B. H., Laban, M., Leung, C. H. W., Lee, L., Lee, C. K., Salto-Tellez, M., Raju, G. C., & Hooi, S. C. (2005). Inhibition of histone deacetylase 2 increases apoptosis and p21Cip1/WAF1 expression, independent of histone deacetylase 1. *Cell Death and Differentiation*, *12*(4), 395–404. https://doi.org/10.1038/SJ.CDD.4401567

Huang, H., Sabari, B. R., Garcia, B. A., David Allis, C., & Zhao, Y. (2014). SnapShot: histone modifications. *Cell*, *159*(2). https://doi.org/10.1016/J.CELL.2014.09.037

Hubeek, I., Comijn, E. M., van der Wilt, C. L., Merriman, R. L., Padron, J. M., Kaspers, G. J. L., & Peters, G. J. (2008). CI-994 (N-acetyl-dinaline) in combination with conventional anti-cancer agents is effective against acute myeloid leukemia in vitro and in vivo. *Oncology Reports*, *19*(6), 1517–1523. https://doi.org/10.3892/OR.19.6.1517

Hu, G., He, N., Cai, C., Cai, F., Fan, P., Zheng, Z., & Jin, X. (2019). HDAC3 modulates cancer immunity via increasing PD-L1 expression in pancreatic cancer. *Pancreatology : Official Journal of the International Association of Pancreatology (IAP) ... [et Al.]*, *19*(2), 383–389. https://doi.org/10.1016/J.PAN.2019.01.011

Imai, S., Johnson, F. B., Marciniak, R. A., McVey, M., Park, P. U., & Guarante, L. (2000). Sir2: An NAD-dependent Histone Deacetylase That Connects Chromatin Silencing, Metabolism, and Aging. *Cold Spring Harbor Symposia on Quantitative Biology*, *65*, 297–302. https://doi.org/10.1101/SQB.2000.65.297

Inoue, A., & Fujimoto, D. (1969). Enzymatic deacetylation of histone. *Biochemical and Biophysical Research Communications*, *36*(1), 146–150. https://doi.org/10.1016/0006-291X(69)90661-5

Jeong, M. H., Ko, H., Jeon, H., Sung, G. J., Park, S. Y., Jun, W. J., Lee, Y. H., Lee, J., Lee, S. wook, Yoon, H. G., & Choi, K. C. (2016). Delphinidin induces apoptosis via cleaved HDAC3-mediated p53 acetylation and oligomerization in prostate cancer cells. *Oncotarget*, *7*(35), 56767. https://doi.org/10.18632/ONCOTARGET.10790

Johnstone, R. W. (2002). Histone-deacetylase inhibitors: novel drugs for the treatment of cancer. *Nature Reviews. Drug Discovery*, *1*(4), 287–299. https://doi.org/10.1038/NRD772

Johnstone, R. W., Ruefli, A. A., & Lowe, S. W. (2002). Apoptosis: A link between cancer genetics and chemotherapy. *Cell*, *108*(2), 153–164. https://doi.org/10.1016/S0092-8674(02)00625-6

Karagianni, P., & Wong, J. (2007). HDAC3: taking the SMRT-N-CoRrect road to repression. *Oncogene*, *26*(37), 5439–5449. https://doi.org/10.1038/SJ.ONC.1210612

Khan, N., Jeffers, M., Kumar, S., Hackett, C., Boldog, F., Khramtsov, N., Qian, X., Mills, E., Berghs, S. C., Carey, N., Finn, P. W., Collins, L. S., Tumber, A., Ritchie, J. W., Jensen, P. B., Lichenstein, H. S., & Sehested, M. (2008). Determination of the class and isoform selectivity of small-molecule histone deacetylase inhibitors. *The Biochemical Journal*, *409*(2), 581–589. https://doi.org/10.1042/BJ20070779

Kim, B. H., Lee, H., Song, Y., Park, J. S., Gadhe, C. G., Choi, J., Lee, C. G., Pae, A. N., Kim, S., & Ye, S. K. (2019). Development of Oxadiazole-Based ODZ10117 as a Small-Molecule Inhibitor of STAT3 for Targeted Cancer Therapy. *Journal of Clinical Medicine*, *8*(11). https://doi.org/10.3390/JCM8111847

Kim, H. C., Choi, K. C., Choi, H. K., Kang, H. B., Kim, M. J., Lee, Y. H., Lee, O. H., Lee, J., Kim, Y. J., Jun, W., Jeong, J. W., & Yoon, H. G. (2010). HDAC3 selectively represses CREB3-mediated transcription and migration of metastatic breast cancer cells. *Cellular and Molecular Life Sciences*, *67*(20), 3499–3510. https://doi.org/10.1007/S00018-010-0388-5/FIGURES/5

Kim, M. S., Kwon, H. J., Lee, Y. M., Baek, J. H., Jang, J. E., Lee, S. W., Moon, E. J., Kim, H. S., Lee, S. K., Chung, H. Y., Kim, C. W., & Kim, K. W. (2001). Histone deacetylases induce angiogenesis by negative regulation of tumor suppressor genes. *Nature Medicine*, *7*(4), 437–443. https://doi.org/10.1038/86507

Knipstein, J., & Gore, L. (2011a). Entinostat for treatment of solid tumors and hematologic malignancies. *Expert Opinion on Investigational Drugs*, *20*(10), 1455–1467. https://doi.org/10.1517/13543784.2011.613822

Kretsovali, A., Hadjimichael, C., & Charmpilas, N. (2012). Histone deacetylase inhibitors in cell pluripotency, differentiation, and reprogramming. *Stem Cells International*, *2012*. https://doi.org/10.1155/2012/184154

Kriaucionis, S., & Tahiliani, M. (2014). Expanding the epigenetic landscape: novel modifications of cytosine in genomic DNA. *Cold Spring Harbor Perspectives in Biology*, *6*(10). https://doi.org/10.1101/CSHPERSPECT.A018630

Laubach, J. P., Moreau, P., San-Miguel, J. F., & Richardson, P. G. (2015). Panobinostat for the Treatment of Multiple Myeloma. *Clinical Cancer Research : An Official Journal of the American Association for Cancer Research*, *21*(21), 4767–4773.

Lauffer, B. E. L., Mintzer, R., Fong, R., Mukund, S., Tam, C., Zilberleyb, I., Flicke, B., Ritscher, A., Fedorowicz, G., Vallero, R., Ortwine, D. F., Gunzner, J., Modrusan, Z., Neumann, L., Koth, C. M., Kaminker, J. S., Heise, C. E., & Steiner, P. (2013). Histone Deacetylase (HDAC) Inhibitor Kinetic Rate Constants Correlate with Cellular Histone Acetylation but Not Transcription and Cell Viability. *The Journal of Biological Chemistry*, *288*(37), 26926. https://doi.org/10.1074/JBC.M113.490706

Lee, J. H., Choy, M. L., Ngo, L., Foster, S. S., & Marks, P. A. (2010a). Histone deacetylase inhibitor induces DNA damage, which normal but not transformed cells can repair. *Proceedings of the National Academy of Sciences of the United States of America*, *107*(33), 14639–14644. https://doi.org/10.1073/PNAS.1008522107

Lee, J. H., Choy, M. L., Ngo, L., Foster, S. S., & Marks, P. A. (2010b). Histone deacetylase inhibitor induces DNA damage, which normal but not transformed cells can repair. *Proceedings of the National Academy of Sciences of the United States of America*, *107*(33), 14639–14644. https://doi.org/10.1073/PNAS.1008522107/-/DCSUPPLEMENTAL

Legube, G., & Trouche, D. (2003). Regulating histone acetyltransferases and deacetylases. *EMBO Reports*, *4*(10), 944–947. https://doi.org/10.1038/SJ.EMBOR.EMBOR941

Li, E., & Zhang, Y. (2014). DNA methylation in mammals. *Cold Spring Harbor Perspectives in Biology*, *6*(5). https://doi.org/10.1101/CSHPERSPECT.A019133

Life at Schrödinger | Schrödinger. (n.d.). Retrieved December 13, 2022, from https://www.schrodinger.com/working-here/life-schrodinger

Lim, E., Modi, K. D., & Kim, J. B. (2009). In vivo bioluminescent imaging of mammary tumors using IVIS spectrum. *Journal of Visualized Experiments : JoVE*, *26*.

Liu, X., Wang, J. H., Li, S., Li, L. L., Huang, M., Zhang, Y. H., Liu, Y., Yang, Y. T., Ding, R., & Ke, Y. Q. (2015). Histone deacetylase 3 expression correlates with vasculogenic mimicry through the phosphoinositide3-kinase / ERK-MMP-laminin5γ2 signaling pathway. *Cancer Science*, *106*(7), 857–866. https://doi.org/10.1111/CAS.12684

Li, X., Zhang, Y., Jiang, Y., Wu, J., Inks, E. S., Chou, C. J., Gao, S., Hou, J., Ding, Q., Li, J., Wang, X., Huang, Y., & Xu, W. (2017). Selective HDAC inhibitors with potent oral activity against leukemia and colorectal cancer: Design, structure-activity relationship and anti-tumor activity study. *European Journal of Medicinal Chemistry*, *134*, 185–206. https://doi.org/10.1016/J.EJMECH.2017.03.069

Li, Y., & Seto, E. (2016a). HDACs and HDAC Inhibitors in Cancer Development and Therapy. *Cold Spring Harbor Perspectives in Medicine*, *6*(10).

Li, Y., Wang, Y., Xie, N., Xu, M., Qian, P., Zhao, Y., & Li, S. (2015). Design, synthesis and antiproliferative activities of novel benzamides derivatives as HDAC inhibitors. *European Journal of Medicinal Chemistry*, *100*, 270–276.

Li, Z. yang, Li, Q. zhong, Chen, L., Chen, B. dong, Wang, B., Zhang, X. jun, & Li, W. ping. (2016). Histone Deacetylase Inhibitor RGFP109 Overcomes Temozolomide Resistance by Blocking NFκB-Dependent Transcription in Glioblastoma Cell Lines. *Neurochemical Research*, *41*(12), 3192– 3205. https://doi.org/10.1007/S11064-016-2043-5

Lombardi, P. M., Cole, K. E., Dowling, D. P., & Christianson, D. W. (2011). Structure, mechanism, and inhibition of histone deacetylases and related metalloenzymes. *Current Opinion in Structural Biology*, *21*(6), 735–743. https://doi.org/10.1016/J.SBI.2011.08.004

Long, J., Fang, W. Y., Chang, L., Gao, W. H., Shen, Y., Jia, M. Y., Zhang, Y. X., Wang, Y., Dou, H. B., Zhang, W. J., Zhu, J., Liang, A. B., Li, J. M., & Hu, J. (2017). Targeting HDAC3, a new partner protein of AKT in the reversal of chemoresistance in acute myeloid leukemia via DNA damage response. *Leukemia*, *31*(12), 2761–2770.

Loprevite, M., Tiseo, M., Grossi, F., Scolaro, T., Semino, C., Pandolfi, A., Favoni, R., & Ardizzoni, A. (2005). In vitro study of CI-994, a histone deacetylase inhibitor, in non-small cell lung cancer cell lines. *Oncology Research*, *15*(1), 39–48.

LoRusso, P. M., Demchik, L., Foster, B., Knight, J., Bissery, M. C., Polin, L. M., Leopold, W. R., & Corbett, T. H. (1996). Preclinical antitumor activity of CI-994. *Investigational New Drugs 1996 14:4*, *14*(4), 349–356. https://doi.org/10.1007/BF00180810

Lundh, M., Galbo, T., Poulsen, S. S., & Mandrup-Poulsen, T. (2015). Histone deacetylase 3 inhibition improves glycaemia and insulin secretion in obese diabetic rats. *Diabetes, Obesity & Metabolism*, *17*(7), 703–707. https://doi.org/10.1111/DOM.12470

Luo, Y., Liu, H. M., Su, M. B., Sheng, L., Zhou, Y. B., Li, J., & Lu, W. (2011). Synthesis and biological evaluation of piperamide analogues as HDAC inhibitors. *Bioorganic & Medicinal Chemistry Letters*, *21*(16), 4844–4846. https://doi.org/10.1016/J.BMCL.2011.06.046

Lu, X., Ning, Z., Li, Z., Cao, H., & Wang, X. (2016). Development of chidamide for peripheral T-cell lymphoma, the first orphan drug approved in China. *Intractable & Rare Diseases Research*, *5*(3), 185–191. https://doi.org/10.5582/IRDR.2016.01024

Madsen, A. S., Kristensen, H. M. E., Lanz, G., & Olsen, C. A. (2014). The effect of various zinc binding groups on inhibition of histone deacetylases 1-11. *ChemMedChem*, *9*(3), 614–626. https://doi.org/10.1002/CMDC.201300433

Malvaez, M., McQuown, S. C., Rogge, G. A., Astarabadi, M., Jacques, V., Carreiro, S., Rusche, J. R., & Wood, M. A. (2013). HDAC3-selective inhibitor enhances extinction of cocaine-seeking behavior in a persistent manner. *Proceedings of the National Academy of Sciences of the United States of America*, *110*(7), 2647–2652. https://doi.org/10.1073/PNAS.1213364110

Mann, B. S., Johnson, J. R., Cohen, M. H., Justice, R., & Pazdur, R. (2007). FDA Approval Summary: Vorinostat for Treatment of Advanced Primary Cutaneous T-Cell Lymphoma. *The Oncologist*, *12*(10), 1247–1252. https://doi.org/10.1634/THEONCOLOGIST.12-10-1247

Marks, P. A. (2006). THIOREDOXIN IN CANCER-ROLE OF HISTONE DEACEYLASE INHIBITORS. *Seminars in Cancer Biology*, *16*(6), 436.

Marks, P. A., Richon, V. M., & Rifkind, R. A. (2000). Histone deacetylase inhibitors: inducers of differentiation or apoptosis of transformed cells. *Journal of the National Cancer Institute*, *92*(15), 1210–1216. https://doi.org/10.1093/JNCI/92.15.1210

Marson, C. M., Matthews, C. J., Atkinson, S. J., Lamadema, N., & Thomas, N. S. B. (2015). Potent and Selective Inhibitors of Histone Deacetylase-3 Containing Chiral Oxazoline Capping Groups and a N-(2-Aminophenyl)-benzamide Binding Unit. *Journal of Medicinal Chemistry*, *58*(17), 6803–6818. https://doi.org/10.1021/ACS.JMEDCHEM.5B00545

Marson, C. M., Matthews, C. J., Yiannaki, E., Atkinson, S. J., Soden, P. E., Shukla, L., Lamadema, N., & Thomas, N. S. B. (2013). Discovery of potent, isoform-selective inhibitors of histone deacetylase containing chiral heterocyclic capping groups and a N-(2-aminophenyl)benzamide binding unit. *Journal of Medicinal Chemistry*, *56*(15), 6156–6174. https://doi.org/10.1021/JM400634N

Ma, Y., Baltezor, M., Rajewski, L., Crow, J., Samuel, G., Staggs, V. S., Chastain, K. M., Toretsky, J. A., Weir, S. J., & Godwin, A. K. (2019). Targeted inhibition of histone deacetylase leads to suppression of Ewing sarcoma tumor growth through an unappreciated EWS-FLI1/HDAC3/HSP90 signaling axis. *Journal of Molecular Medicine (Berlin, Germany)*, *97*(7), 957–972. https://doi.org/10.1007/S00109-019-01782-0

Ma, Y., Yue, Y., Pan, M., Sun, J., Chu, J., Lin, X., Xu, W., Feng, L., Chen, Y., Chen, D., Shin, V. Y., Wang, X., & Jin, H. (2015). Histone deacetylase 3 inhibits new tumor suppressor gene DTWD1 in gastric cancer. *American Journal of Cancer Research*, *5*(2), 663. /pmc/articles/PMC4396045/

McClure, J. J., Inks, E. S., Zhang, C., Peterson, Y. K., Li, J., Chundru, K., Lee, B., Buchanan, A., Miao, S., & Chou, C. J. (2017). Comparison of the Deacylase and Deacetylase Activity of Zinc-Dependent HDACs. *ACS Chemical Biology*, *12*(6), 1644–1655. https://doi.org/10.1021/ACSCHEMBIO.7B00321

McClure, J. J., Zhang, C., Inks, E. S., Peterson, Y. K., Li, J., & James Chou, C. (2016). Development of Allosteric Hydrazide-Containing Class I Histone Deacetylase Inhibitors for Use in Acute Myeloid Leukemia. *Journal of Medicinal Chemistry*, *59*(21), 9942–9959. https://doi.org/10.1021/ACS.JMEDCHEM.6B01385

McLeod, A. B., Stice, J. P., Wardell, S. E., Alley, H. M., Chang, C. Y., & McDonnell, D. P. (2018). Validation of histone deacetylase 3 as a therapeutic target in castration-resistant prostate cancer. *The Prostate*, *78*(4), 266–277. https://doi.org/10.1002/PROS.23467

McQuown, S. C., Barrett, R. M., Matheos, D. P., Post, R. J., Rogge, G. A., Alenghat, T., Mullican, S. E., Jones, S., Rusche, J. R., Lazar, M. A., & Wood, M. A. (2011). HDAC3 is a critical negative regulator of long-term memory formation. *The Journal of Neuroscience: The Official Journal of the Society for Neuroscience*, *31*(2), 764–774.

Mehdipour, P., Santoro, F., Botrugno, O. A., Romanenghi, M., Pagliuca, C., Matthews, G. M., Johnstone, R. W., & Minucci, S. (2017). HDAC3 activity is required for initiation of leukemogenesis in acute promyelocytic leukemia. *Leukemia*, *31*(4), 995–997.

Miller, T. A., Witter, D. J., & Belvedere, S. (2003a). Histone deacetylase inhibitors. *Journal of Medicinal Chemistry*, *46*(24), 5097–5116. https://doi.org/10.1021/JM0303094

Minami, J., Suzuki, R., Mazitschek, R., Gorgun, G., Ghosh, B., Cirstea, D., Hu, Y., Mimura, N., Ohguchi, H., Cottini, F., Jakubikova, J., Munshi, N. C., Haggarty, S. J., Richardson, P. G., Hideshima, T., & Anderson, K. C. (2014a). Histone deacetylase 3 as a novel therapeutic target in multiple myeloma. *Leukemia*, *28*(3), 680–689. https://doi.org/10.1038/LEU.2013.231

Miyake, K., Yoshizumi, T., Imura, S., Sugimoto, K., Batmunkh, E., Kanemura, H., Morine, Y., & Shimada, M. (2008). Expression of hypoxia-inducible factor-1alpha, histone deacetylase 1, and metastasis-associated protein 1 in pancreatic carcinoma: correlation with poor prognosis with possible regulation. *Pancreas*, *36*(3).

Mottamal, M., Zheng, S., Huang, T. L., & Wang, G. (2015). Histone deacetylase inhibitors in clinical studies as templates for new anticancer agents. *Molecules (Basel, Switzerland)*, *20*(3), 3898–3941. https://doi.org/10.3390/MOLECULES20033898

Munshi, A., Kurland, J. F., Nishikawa, T., Tanaka, T., Hobbs, M. L., Tucker, S. L., Ismail, S., Stevens, C., & Meyn, R. E. (2005). Histone deacetylase inhibitors radiosensitize human melanoma cells by suppressing DNA repair activity. *Clinical Cancer Research : An Official Journal of the American Association for Cancer Research*, *11*(13), 4912–4922. https://doi.org/10.1158/1078-0432.CCR04-2088

Narita, N., Fujieda, S., Tokuriki, M., Takahashi, N., Tsuzuki, H., Ohtsubo, T., & Matsumoto, H. (2005). Inhibition of histone deacetylase 3 stimulates apoptosis induced by heat shock under acidic conditions in human maxillary cancer. *Oncogene*, *24*(49), 7346–7354. https://doi.org/10.1038/SJ.ONC.1208879

Nepali, K., Chang, T. Y., Lai, M. J., Hsu, K. C., Yen, Y., Lin, T. E., Lee, S. B., & Liou, J. P. (2020). Purine/purine isoster based scaffolds as new derivatives of benzamide class of HDAC inhibitors. *European Journal of Medicinal Chemistry*, *196*, 112291–112291. https://doi.org/10.1016/J.EJMECH.2020.112291

Nielsen, T. K., Hildmann, C., Dickmanns, A., Schwienhorst, A., & Ficner, R. (2005). Crystal structure of a bacterial class 2 histone deacetylase homologue. *Journal of Molecular Biology*, *354*(1), 107–120. https://doi.org/10.1016/J.JMB.2005.09.065

Ning, Z. Q., Li, Z. bin, Newman, M. J., Shan, S., Wang, X. H., Pan, D. S., Zhang, J., Dong, M., Du, X., & Lu, X. P. (2012). Chidamide (CS055/HBI-8000): a new histone deacetylase inhibitor of the benzamide class with antitumor activity and the ability to enhance immune cell-mediated tumor cell cytotoxicity. *Cancer Chemotherapy and Pharmacology*, *69*(4), 901–909. https://doi.org/10.1007/S00280-011-1766-X

Oehme, I., Deubzer, H. E., Wegener, D., Pickert, D., Linke, J. P., Hero, B., Kopp-Schneider, A., Westermann, F., Ulrich, S. M., von Deimling, A., Fischer, M., & Witt, O. (2009). Histone deacetylase 8 in neuroblastoma tumorigenesis. *Clinical Cancer Research : An Official Journal of the American Association for Cancer Research*, *15*(1), 91–99. https://doi.org/10.1158/10780432.CCR-08-0684

Paschall, A. v., & Liu, K. (2016). An Orthotopic Mouse Model of Spontaneous Breast Cancer Metastasis. *Journal of Visualized Experiments : JoVE*, *2016* (114).

Phiel, C. J., Zhang, F., Huang, E. Y., Guenther, M. G., Lazar, M. A., & Klein, P. S. (2001). Histone deacetylase is a direct target of valproic acid, a potent anticonvulsant, mood stabilizer, and teratogen. *The Journal of Biological Chemistry*, *276*(39), 36734–36741.

Pili, R., Salumbides, B., Zhao, M., Altiok, S., Qian, D., Zwiebel, J., Carducci, M. A., & Rudek, M. A. (2012). Phase I study of the histone deacetylase inhibitor entinostat in combination with 13-cis retinoic acid in patients with solid tumours. *British Journal of Cancer*, *106*(1), 77–84. https://doi.org/10.1038/BJC.2011.527

Poole, R. M. (2014). Belinostat: first global approval. *Drugs*, *74*(13), 1543–1554. https://doi.org/10.1007/S40265-014-0275-8

Prakash, S., Foster, B. J., Meyer, M., Wozniak, A., Heilbrun, L. K., Flaherty, L., Zalupski, M., Radulovic, L., Valdivieso, M., & Lorusso, P. M. (2001). Chronic oral administration of CI-994: a phase 1 study. *Investigational New Drugs*, *19*(1), 1–11.

Pulaski, B. A., & Ostrand-Rosenberg, S. (2000). Mouse 4T1 Breast Tumor Model. *Current Protocols in Immunology*, *39*(1), 20.2.1-20.2.16.

Pulya, S., Amin, S. A., Adhikari, N., Biswas, S., Jha, T., & Ghosh, B. (2021). HDAC6 as privileged target in drug discovery: A perspective. *Pharmacological Research*, *163*. https://doi.org/10.1016/J.PHRS.2020.105274

Pulya, S., Mahale, A., Bobde, Y., Routholla, G., Patel, T., Swati, Biswas, S., Sharma, V., Kulkarni, O. P., & Ghosh, B. (2021). PT3: A Novel Benzamide Class Histone Deacetylase 3 Inhibitor Improves Learning and Memory in Novel Object Recognition Mouse Model. *ACS Chemical Neuroscience*, *12*(5), 883–892. https://doi.org/10.1021/ACSCHEMNEURO.0C00721

Qian, D. Z., Kachhap, S. K., Collis, S. J., Verheul, H. M. W., Carducci, M. A., Atadja, P., & Pili, R. (2006). Class II histone deacetylases are associated with VHL-independent regulation of hypoxiainducible factor 1 alpha. *Cancer Research*, *66*(17), 8814–8821.

Rajak, H., Singh, A., Raghuwanshi, K., Kumar, R., Dewangan, P. K., Veerasamy, R., Sharma, P. C., Dixit, A., & Mishra, P. (2014). A structural insight into hydroxamic acid based histone deacetylase inhibitors for the presence of anticancer activity. *Current Medicinal Chemistry*, *21*(23), 2642–2664. https://doi.org/10.2174/0929867313209990191

Ropero, S., Fraga, M. F., Ballestar, E., Hamelin, R., Yamamoto, H., Boix-Chornet, M., Caballero, R., Alaminos, M., Setien, F., Paz, M. F., Herranz, M., Palacios, J., Arango, D., Orntoft, T. F., Aaltonen, L. A., Schwartz, S., & Esteller, M. (2006). A truncating mutation of HDAC2 in human cancers confers resistance to histone deacetylase inhibition. *Nature Genetics*, *38*(5), 566–569. https://doi.org/10.1038/NG1773

Routholla, G., Pulya, S., Patel, T., Abdul Amin, S., Adhikari, N., Biswas, S., Jha, T., & Ghosh, B. (2021). Synthesis, biological evaluation, and molecular docking analysis of novel linker-less benzamide based potent and selective HDAC3 inhibitors. *Bioorganic Chemistry*, *114*. https://doi.org/10.1016/J.BIOORG.2021.105050

Sadikovic, B., Al-Romaih, K., Squire, J., & Zielenska, M. (2008a). Cause and consequences of genetic and epigenetic alterations in human cancer. *Current Genomics*, *9*(6), 394–408. https://doi.org/10.2174/138920208785699580

Sadikovic, B., Al-Romaih, K., Squire, J., & Zielenska, M. (2008b). Cause and Consequences of Genetic and Epigenetic Alterations in Human Cancer. *Current Genomics*, *9*(6), 394. https://doi.org/10.2174/138920208785699580

Saito, A., Yamashita, T., Mariko, Y., Nosaka, Y., Tsuchiya, K., Ando, T., Suzuki, T., Tsuruo, T., & Nakanishi, O. (1999b). A synthetic inhibitor of histone deacetylase, MS-27-275, with marked in vivo antitumor activity against human tumors. *Proceedings of the National Academy of Sciences of the United States of America*, *96*(8), 4592–4597. https://doi.org/10.1073/PNAS.96.8.4592

Santo, L., Hideshima, T., Kung, A. L., Tseng, J. C., Tamang, D., Yang, M., Jarpe, M., van Duzer, J. H., Mazitschek, R., Ogier, W. C., Cirstea, D., Rodig, S., Eda, H., Scullen, T., Canavese, M., Bradner, J., Anderson, K. C., Jones, S. S., & Raje, N. (2012). Preclinical activity, pharmacodynamic, and pharmacokinetic properties of a selective HDAC6 inhibitor, ACY-1215, in combination with bortezomib in multiple myeloma. *Blood*, *119*(11), 2579–2589. https://doi.org/10.1182/BLOOD2011-10-387365

Sarkar, R., Banerjee, S., Amin, S. A., Adhikari, N., & Jha, T. (2020a). Histone deacetylase 3 (HDAC3) inhibitors as anticancer agents: A review. *European Journal of Medicinal Chemistry*, *192*. https://doi.org/10.1016/J.EJMECH.2020.112171

Sathishkumar, C., Prabu, P., Balakumar, M., Lenin, R., Prabhu, D., Anjana, R. M., Mohan, V., & Balasubramanyam, M. (2016). Augmentation of histone deacetylase 3 (HDAC3) epigenetic signature at the interface of proinflammation and insulin resistance in patients with type 2 diabetes. *Clinical Epigenetics*, *8*(1). https://doi.org/10.1186/S13148-016-0293-3

Schrump, D. S., Fischette, M. R., Nguyen, D. M., Zhao, M., Li, X., Kunst, T. F., Hancox, A., Hong, J. A., Chen, G. A., Kruchin, E., Wright, J. J., Rosing, D. R., Sparreboom, A., Figg, W. D., & Steinberg, S. M. (2008). Clinical and molecular responses in lung cancer patients receiving Romidepsin. *Clinical Cancer Research : An Official Journal of the American Association for Cancer Research*, *14*(1), 188–198. https://doi.org/10.1158/1078-0432.CCR-07-0135

Seto, E., & Yoshida, M. (2014). Erasers of histone acetylation: the histone deacetylase enzymes. *Cold Spring Harbor Perspectives in Biology*, *6*(4).

Shan, X., Fu, Y. S., Aziz, F., Wang, X. Q., Yan, Q., & Liu, J. W. (2014). Ginsenoside Rg3 Inhibits Melanoma Cell Proliferation through Down-Regulation of Histone Deacetylase 3 (HDAC3) and Increase of p53 Acetylation. *PLoS ONE*, *9*(12).

Shao, Y., Gao, Z., Marks, P. A., & Jiang, X. (2004). Apoptotic and autophagic cell death induced by histone deacetylase inhibitors. *Proceedings of the National Academy of Sciences of the United States of America*, *101*(52), 18030–18035.

Sharma, S., Kelly, T. K., & Jones, P. A. (2010). Epigenetics in cancer. *Carcinogenesis*, *31*(1), 27–36. https://doi.org/10.1093/CARCIN/BGP220

Silva, G., Cardoso, B. A., Belo, H., & Almeida, A. M. (2013). Vorinostat induces apoptosis and differentiation in myeloid malignancies: genetic and molecular mechanisms. *PloS One*, *8*(1). https://doi.org/10.1371/JOURNAL.PONE.0053766

Singh, T. R., Shankar, S., & Srivastava, R. K. (2005). HDAC inhibitors enhance the apoptosis-inducing potential of TRAIL in breast carcinoma. *Oncogene*, *24*(29), 4609–4623. https://doi.org/10.1038/SJ.ONC.1208585

Siu, L. L., Pili, R., Duran, I., Messersmith, W. A., Chen, E. X., Sullivan, R., MacLean, M., King, S., Brown, S., Reid, G. K., Li, Z., Kalita, A. M., Laille, E. J., Besterman, J. M., Martell, R. E., & Carducci, M. A. (2008). Phase I study of MGCD0103 given as a three-times-per-week oral dose in patients with advanced solid tumors. *Journal of Clinical Oncology : Official Journal of the American Society of Clinical Oncology*, *26*(12), 1940–1947. https://doi.org/10.1200/JCO.2007.14.5730

Somoza, J. R., Skene, R. J., Katz, B. A., Mol, C., Ho, J. D., Jennings, A. J., Luong, C., Arvai, A., Buggy, J. J., Chi, E., Tang, J., Sang, B. C., Verner, E., Wynands, R., Leahy, E. M., Dougan, D. R., Snell, G., Navre, M., Knuth, M. W., … Tari, L. W. (2004a). Structural snapshots of human HDAC8 provide insights into the class I histone deacetylases. *Structure*, *12*(7), 1325–1334. https://doi.org/10.1016/j.str.2004.04.012

Spurling, C. C., Godman, C. A., Noonan, E. J., Rasmussen, T. P., Rosenberg, D. W., & Giardina, C. (2008a). HDAC3 overexpression and colon cancer cell proliferation and differentiation. *Molecular Carcinogenesis*, *47*(2), 137–147. https://doi.org/10.1002/MC.20373

Stockhausen, M. T., Sjölund, J., Manetopoulos, C., & Axelson, H. (2005). Effects of the histone deacetylase inhibitor valproic acid on Notch signalling in human neuroblastoma cells. *British Journal of Cancer*, *92*(4), 751–759. https://doi.org/10.1038/SJ.BJC.6602309

Suzuki, T., Kasuya, Y., Itoh, Y., Ota, Y., Zhan, P., Asamitsu, K., Nakagawa, H., Okamoto, T., & Miyata, N. (2013). Identification of highly selective and potent histone deacetylase 3 inhibitors using click chemistry-based combinatorial fragment assembly. *PloS One*, *8*(7). https://doi.org/10.1371/JOURNAL.PONE.0068669

Taddei, M., Cini, E., Giannotti, L., Giannini, G., Battistuzzi, G., Vignola, D., Vesci, L., & Cabri, W. (2014). Lactam based 7-amino suberoylamide hydroxamic acids as potent HDAC inhibitors. *Bioorganic & Medicinal Chemistry Letters*, *24*(1), 61–64. https://doi.org/10.1016/J.BMCL.2013.11.072

Tashima, T., Murata, H., & Kodama, H. (2014). Design and synthesis of novel and highly-active panhistone deacetylase (pan-HDAC) inhibitors. *Bioorganic & Medicinal Chemistry*, *22*(14), 3720– 3731. https://doi.org/10.1016/J.BMC.2014.05.001

The histone deacetylase inhibitor MS-275 promotes differentiation or apoptosis in human leukemia cells through a process regulated by generation of reactive oxygen species and induction of p21CIP1/WAF1 1 - PubMed. (n.d.). Retrieved December 8, 2022, from https://pubmed.ncbi.nlm.nih.gov/12839953/

Timmermann, S., Lehrmann, H., Polesskaya, A., & Harel-Bellan, A. (2001). Histone acetylation and disease. *Cellular and Molecular Life Sciences : CMLS*, *58*(5–6), 728–736. https://doi.org/10.1007/PL00000896

Trivedi, P., Adhikari, N., Amin, S. A., Bobde, Y., Ganesh, R., Jha, T., & Ghosh, B. (2019). Design, synthesis, biological evaluation and molecular docking study of arylcarboxamido piperidine and piperazine-based hydroxamates as potential HDAC8 inhibitors with promising anticancer activity. *European Journal of Pharmaceutical Sciences : Official Journal of the European Federation for Pharmaceutical Sciences*, *138*. https://doi.org/10.1016/J.EJPS.2019.105046

Trivedi, P., Adhikari, N., Amin, S. A., Jha, T., & Ghosh, B. (2018a). Design, synthesis and biological screening of 2-aminobenzamides as selective HDAC3 inhibitors with promising anticancer effects. *European Journal of Pharmaceutical Sciences : Official Journal of the European Federation for Pharmaceutical Sciences*, *124*, 165–181.

Vandermolen, K. M., McCulloch, W., Pearce, C. J., & Oberlies, N. H. (2011). Romidepsin (Istodax, NSC 630176, FR901228, FK228, depsipeptide): a natural product recently approved for cutaneous T-cell lymphoma. *The Journal of Antibiotics*, *64*(8), 525–531. https://doi.org/10.1038/JA.2011.35

Vannini, A., Volpari, C., Filocamo, G., Casavola, E. C., Brunetti, M., Renzoni, D., Chakravarty, P., Paolini, C., de Francesco, R., Gallinari, P., Steinkühler, C., & di Marco, S. (2004). Crystal structure of a eukaryotic zinc-dependent histone deacetylase, human HDAC8, complexed with a hydroxamic acid inhibitor. *Proceedings of the National Academy of Sciences of the United States of America*, *101*(42), 15064. https://doi.org/10.1073/PNAS.0404603101

Wagner, F. F., Lundh, M., Kaya, T., McCarren, P., Zhang, Y. L., Chattopadhyay, S., Gale, J. P., Galbo, T., Fisher, S. L., Meier, B. C., Vetere, A., Richardson, S., Morgan, N. G., Christensen, D. P., Gilbert, T. J., Hooker, J. M., Leroy, M., Walpita, D., Mandrup-Poulsen, T., … Holson, E. B. (2016). An Isochemogenic Set of Inhibitors To Define the Therapeutic Potential of Histone Deacetylases in β-Cell Protection. *ACS Chemical Biology*, *11*(2), 363–374. https://doi.org/10.1021/ACSCHEMBIO.5B00640

Watson, P. J., Fairall, L., Santos, G. M., & Schwabe, J. W. R. (2012). Structure of HDAC3 bound to co-repressor and inositol tetraphosphate. *Nature*, *481*(7381), 335–340.

Weichert, W., Röske, A., Gekeler, V., Beckers, T., Ebert, M. P., Pross, M., Dietel, M., Denkert, C., & Röcken, C. (2008a). Association of patterns of class I histone deacetylase expression with patient prognosis in gastric cancer: a retrospective analysis. *The Lancet. Oncology*, *9*(2), 139–148. https://doi.org/10.1016/S1470-2045(08)70004-4

Weichert, W., Röske, A., Gekeler, V., Beckers, T., Stephan, C., Jung, K., Fritzsche, F. R., Niesporek, S., Denkert, C., Dietel, M., & Kristiansen, G. (2008). Histone deacetylases 1, 2 and 3 are highly expressed in prostate cancer and HDAC2 expression is associated with shorter PSA relapse time after radical prostatectomy. *British Journal of Cancer*, *98*(3), 604–610. https://doi.org/10.1038/SJ.BJC.6604199

Wells, C. E., Bhaskara, S., Stengel, K. R., Zhao, Y., Sirbu, B., Chagot, B., Cortez, D., Khabele, D., Chazin, W. J., Cooper, A., Jacques, V., Rusche, J., Eischen, C. M., McGirt, L. Y., & Hiebert, S. W. (2013). Inhibition of histone deacetylase 3 causes replication stress in cutaneous T cell lymphoma. *PloS One*, *8*(7).

Wilson, A. J., Byun, D. S., Popova, N., Murray, L. B., L'Italien, K., Sowa, Y., Arango, D., Velcich, A., Augenlicht, L. H., & Mariadason, J. M. (2006). Histone Deacetylase 3 (HDAC3) and Other Class I HDACs Regulate Colon Cell Maturation and p21 Expression and Are Deregulated in Human Colon Cancer. *Journal of Biological Chemistry*, *281*(19), 13548–13558. https://doi.org/10.1074/JBC.M510023200

Witt, O., Deubzer, H. E., Milde, T., & Oehme, I. (2009a). HDAC family: What is the cancer relevant targets? *Cancer Letters*, *277*(1), 8–21.

World Health Organization (WHO). (n.d.). Retrieved December 13, 2022.

Wu, C. T., & Morris, J. R. (2001). Genes, genetics, and epigenetics: A correspondence. *Science*, *293*(5532), 1103–1105. https://doi.org/10.1126/SCIENCE.293.5532.1103

Xu, Z., Tong, Q., Zhang, Z., Wang, S., Zheng, Y., Liu, Q., Qian, L. B., Chen, S. Y., Sun, J., & Cai, L. (2017). Inhibition of HDAC3 prevents diabetic cardiomyopathy in OVE26 mice via epigenetic regulation of DUSP5-ERK1/2 pathway. *Clinical Science (London, England : 1979)*, *131*(15), 1841–1857. https://doi.org/10.1042/CS20170064

Yang, X. J., & Seto, E. (2007). HATs and HDACs: from structure, function and regulation to novel strategies for therapy and prevention. *Oncogene*, *26*(37), 5310–5318. https://doi.org/10.1038/SJ.ONC.1210599

Yin, Y., Zhang, M., Dorfman, R. G., Li, Y., Zhao, Z., Pan, Y., Zhou, Q., Huang, S., Zhao, S., Yao, Y., & Zou, X. (2017). Histone deacetylase 3 overexpression in human cholangiocarcinoma and promotion of cell growth via apoptosis inhibition. *Cell Death & Disease*, *8*(6). https://doi.org/10.1038/CDDIS.2016.457

Younes, A., Oki, Y., Bociek, R. G., Kuruvilla, J., Fanale, M., Neelapu, S., Copeland, A., Buglio, D., Galal, A., Besterman, J., Li, Z., Drouin, M., Patterson, T., Ward, M. R., Paulus, J. K., Ji, Y., Medeiros, L. J., & Martell, R. E. (2011). Mocetinostat for relapsed classical Hodgkin's lymphoma: an open-label, single-arm, phase 2 trial. *The Lancet. Oncology*, *12*(13), 1222–1228. https://doi.org/10.1016/S1470-2045(11)70265-0

Yue, L., Sharma, V., Horvat, N. P., Akuffo, A. A., Beatty, M. S., Murdun, C., Colin, C., Billington, J. M. R., Goodheart, W. E., Sahakian, E., Zhang, L., Powers, J. J., Amin, N. E., Lambert-Showers, Q. T., Darville, L. N., Pinilla-Ibarz, J., Reuther, G. W., Wright, K. L., Conti, C., … EplingBurnette, P. K. (2020). HDAC11 deficiency disrupts oncogene-induced hematopoiesis in myeloproliferative neoplasms. *Blood*, *135*(3), 191–207. https://doi.org/10.1182/BLOOD.2019895326

Yun, F., Cheng, C., Ullah, S., He, J., Zahi, M. R., & Yuan, Q. (2019). Thioether-based 2aminobenzamide derivatives: Novel HDAC inhibitors with potent in vitro and in vivo antitumor activity. *European Journal of Medicinal Chemistry*, *176*, 195–207. https://doi.org/10.1016/J.EJMECH.2019.05.007

Yu, X., Yang, F., Jiang, H., & Fan, L. (2020). RGFP966 Suppresses Tumor Growth and Migration Through Inhibition of EGFR Expression in Hepatocellular Carcinoma Cells in vitro. *Drug Design, Development and Therapy*, *14*, 121–128. https://doi.org/10.2147/DDDT.S234871

Zang, J., Liang, X., Huang, Y., Jia, Y., Li, X., Xu, W., Chou, C. J., & Zhang, Y. (2018). Discovery of Novel Pazopanib-Based HDAC and VEGFR Dual Inhibitors Targeting Cancer Epigenetics and Angiogenesis Simultaneously. *Journal of Medicinal Chemistry*, *61*(12), 5304–5322. https://doi.org/10.1021/ACS.JMEDCHEM.8B00384

Zhang, J., & Zhong, Q. (2014). Histone deacetylase inhibitors and cell death. *Cellular and Molecular Life Sciences : CMLS*, *71*(20), 3885–3901. https://doi.org/10.1007/S00018-014-1656-6

Zhang, X. D., Gillespie, S. K., Borrow, J. M., & Hersey, P. (2003). The histone deacetylase inhibitor suberic bishydroxamate: A potential sensitizer of melanoma to TNF-related apoptosis-inducing ligand (TRAIL) induced apoptosis. *Biochemical Pharmacology*, *66*(8), 1537–1545. https://doi.org/10.1016/S0006-2952(03)00509-4

Zhang, Z., Hao, C., Wang, L., Liu, P., Zhao, L., Zhu, C., & Tian, X. (2013). Inhibition of leukemic cells by valproic acid, an HDAC inhibitor, in xenograft tumors. *OncoTargets and Therapy*, *6*, 733–740. https://doi.org/10.2147/OTT.S46135

Zhang, Z., Yamashita, H., Toyama, T., Sugiura, H., Omoto, Y., Ando, Y., Mita, K., Hamaguchi, M., Hayashi, S. I., & Iwase, H. (2004). HDAC6 expression is correlated with better survival in breast cancer. *Clinical Cancer Research : An Official Journal of the American Association for Cancer Research*, *10*(20), 6962–6968. https://doi.org/10.1158/1078-0432.CCR-04-0455

Zhou, N., Moradei, O., Raeppel, S., Leit, S., Frechette, S., Gaudette, F., Paquin, I., Bernstein, N., Bouchain, G., Vaisburg, A., Jin, Z., Gillespie, J., Wang, J., Fournel, M., Yan, P. T., Trachy-Bourget, M. C., Kalita, A., Lu, A., Rahil, J., … Delorme, D. (2008). Discovery of N-(2Aminophenyl)-4-[(4-pyridin-3-ylpyrimidin-2-ylamino) methyl]benzamide(MGCD0103), an orally active histone deacetylase inhibitor. *Journal of Medicinal Chemistry*, *51*(14), 4072–4075. https://doi.org/10.1021/JM800251W

LIST OF PUBLICATIONS

From thesis work:

1. **Routholla G**, Pulya S, Patel T, Adhikari N, Abdul Amin S, Paul M, Bhagavatula S, Biswas S, Jha T, Ghosh B. Design, synthesis and binding mode of interaction of novel small molecule o-hydroxy benzamides as HDAC3-selective inhibitors with promising antitumor effects in 4T1-Luc breast cancer xenograft model. ***Bioorg Chem***. 2021 Dec;117:105446. Doi : 10.1016/j.bioorg.2021.105446. Epub 2021 Oct 22. PMID: 34717237.
2. **Routholla G**, Pulya S, Patel T, Abdul Amin S, Adhikari N, Biswas S, Jha T, Ghosh B. Synthesis, biological evaluation, and molecular docking analysis of novel linker-less benzamide based potent and selective HDAC3 inhibitors. ***Bioorg Chem***. 2021 Sep; 114:105050. Doi : 10.1016/j.bioorg.2021.105050. Epub 2021 Jun 4. PMID: 34120025

Other Publications:

1. Pulya S, Patel T, Paul M, Adhikari N, Banerjee S, **Routholla G**, Biswas S, Jha T, Ghosh B. Selective inhibition of histone deacetylase 3 by novel hydrazide based small molecules as therapeutic intervention for the treatment of cancer. ***Eur J Med Chem.*** 2022 Aug 5; 238:114470. Doi : 10.1016/j.ejmech.2022.114470. Epub 2022 May 18. PMID: 35635949.
2. Pulya S, Mahale A, Bobde Y, **Routholla G,** Patel T, Swati, Biswas S, Sharma V, Kulkarni OP, Ghosh B. PT3: A Novel Benzamide Class Histone Deacetylase 3 Inhibitor Improves Learning and Memory in Novel Object Recognition Mouse Model. ***ACS Chem Neurosci***. 2021 Mar 3;12(5):883-892. Doi : 10.1021/acschemneuro.0c00721. Epub 2021 Feb 12. PMID: 33577290.
3. Sk. Abdul Amin, Prakruti Trivedi, Nilanjan Adhikari, **Ganesh Routholla**, Dhanya Vijayasarathi, Sanjib Das, Balaram Ghosh and Tarun Jha. Quantitative activity–activity relationship (QAAR) driven design to develop hydroxamate derivatives of pentanoic acids as selective HDAC8 inhibitors: synthesis, biological evaluation and binding mode of

interaction studies. ***New Journal of Chemistry*** 2021, **45**, 17149-17162. Doi : 10.1039/D1NJ02636D.

4. Trivedi P, Adhikari N, Amin SA, Bobde Y, **Ganesh R**, Jha T, Ghosh B. Design, synthesis, biological evaluation and molecular docking study of arylcarboxamido piperidine and piperazine-based hydroxamates as potential HDAC8 inhibitors with promising anticancer activity. ***Eur J Pharm Sci.*** 2019 Oct 1;138:105046. Doi : 10.1016/j.ejps.2019.105046. Epub 2019 Aug 14. PMID: 31421254.
5. Karnam K, Sedmaki K, Sharma P, **Routholla G**, Goli S, Ghosh B, Venuganti VVK, Kulkarni OP. HDAC6 inhibitor accelerates wound healing by inhibiting tubulin mediated IL-1β secretion in diabetic mice. ***Biochim Biophys Acta Mol Basis Dis***. 2020 Nov 1;1866(11):165903. Doi : 10.1016/j.bbadis.2020.165903. Epub 2020 Jul 23. PMID: 32712153.
6. Kavitha Sedmaki; Kalyani Karnam; Pravesh Sharma; Ashutosh Mahale; ***Ganesh Routholla***, **Balaram Ghosh;** Onkar Kulkarni. HDAC6 inhibition attenuates renal injury by reducing IL-1β secretion and RIP kinase mediated necroptosis in acute oxalate nephropathy. ***International Immunopharmacology***. 2022. Jun 17; 110:108919. Doi :10.1016 /j.intimp. 2022.108919.
7. Gautam AK, Kumar P, Maity B, **Routholla G,** Ghosh B, Chidambaram K, Begum MY, Al Fatease A, Rajinikanth PS, Singh S, Saha S, M R V. Synthesis and appraisal of dalberginloaded PLGA nanoparticles modified with galactose against hepatocellular carcinoma: *Invitro*, pharmacokinetic, and *in-silico* studies. ***Front Pharmacol***. 2022 Oct 28; 13:1021867. Doi: 10.3389/fphar.2022.1021867. PMID: 36386226; PMCID: PMC9650263
8. Tarun patel; Ruchi Gaikwad; Kavita Jain; **Routholla Ganesh**; Yamini Bobde; **Balaram Ghosh;** Kalpataru Das; Shovanlal Gayen. First report on 3-(3-oxoaryl) indole derivatives as anticancer agents: Microwave assisted synthesis, in vitro screening and molecular docking studies. ***Chemistry Select*** 2019, 4, 4478–4482 Doi: 10.1002/slct.201900088.
9. Ruchi Gaikwad, Yamini Bobde, **Routholla Ganesh**, Tarun Patel, **Balaram Ghosh**, Kalpataru Das, Shovanlal Gayen. 2-phenylindole derivatives as anticancer agents: synthesis and screening against murine melanoma, human lung and breast cancer cell lines. ***Synthetic Communications*** 2019**,** Doi.org/10.1080/00397911.2019.1620282.

Patents:

1.Benzamide Based HDAC3 Selective Inhibitors: ***Balaram Ghosh,*** *Swati Biswas,* ***Ganesh Routholla,*** *Sravani Pulya*; Patent Authority BITS-Pilani**: Indian Patent Application Number 202011056177.** Filed on 23/12/**2020.**

2. Hydrazide based HDAC3 selective inhibitors ***Balaram Ghosh****, Swati Biswas, Sravani Pulya,* ***Ganesh Routholla****, Tarun Kumar Patel.* Patent Authority BITS-Pilani: Indian Patent Application Number 202111022553**,** Filed on May 20, **2021.**

Conference Presentations:

1. Development of Histone Deacetylase (HDAC) Inhibitors with Preferential Isoform Selectivity for HDAC3: *Ganesh Routholla, Sravani Pulya, Tarun Patel, Swati Biswas,* ***Balaram Ghosh***: 8th Annual Conference on Navigating Translational Discoveries under the auspices of *International Chemical Biology Society (ICBS)* at the CSIR-Indian Institute of Chemical Technology, Hyderabad (IICT-Hyd) between 02^{th}-04^{th} Nov, 2019.

2. Development of novel *o*-hydroxy benzamide based HDAC3-selective inhibitors as anticancer agents with promising *in vivo* potential: *Ganesh Routholla, Sravani Pulya, Tarun Patel, Milan Paul, Swati Biswas,* ***Balaram Ghosh******: the 10^{th} annual conference of the International Chemical Biology Society, ICBS 2021: November 11^{th}-13^{th}, 2021.

3. I took part as volunteer in the International Conference on Drug Discovery – 2020, Organized by Schrodinger in Bits-Pilani Hyderabad campus, collaboration with USA. February 29^{th} – March 2^{nd}, 2020.

4. Participated in Two-day National Symposium on Convergence of Chemistry and Materials (CCM-2023) in BITS-Pilani Hyderabad Campus, Hyderabad. January 6^{th}-7^{th}, 2023

5. Participated in ACS chemistry for life workshop organised by ACS publication in collaboration with BITS- Pilani, Hyderabad campus. October 4^{th} 2021.

BIOGRAPHY OF R GANESH

Mr. Ganesh Routholla completed his M.Sc. degree in organic chemistry from Osmania University, Hyderabad. He has two years of research experience in an organic chemistry laboratory under the supervision of Dr. D. Srinivas Reddy at NCL Pune. He has also qualified CSIR-NET(LS) examination. He has joined Epigenetic Research Laboratory as a project fellow under our SERBDST sponsored project in September 2017 and he got the admission in PhD programme in the following semester in January 2018. He has been converted to Institute Ph.D. fellow from August 2020 after the SERB sponsored project got over. He has published 13 international journals and he is the inventors of two Indian patent filed. He has presented four posters in various national and international scientific conferences.

BIOGRAPHY OF Prof. BALARAM GHOSH

Prof. Balaram Ghosh is presently working as an Associate Professor, in the Department of Pharmacy, Birla Institute of Technology and Science, Pilani, Hyderabad Campus. He received his B. Pharm degree (1998) and M. Pharm (2000) from Jadavpur University, India. He was awarded his Ph.D. in Pharmaceutical Sciences in the year 2009 from Wayne State University, Michigan, USA. After completion of doctoral studies, he pursued his postdoctoral studies at the Centre for Human Genetic Research (CHGR), Harvard Medical School, Harvard University, USA (2013). He has been involved in research for the last 22 years. He has published more than 125 research publications, four US patents, two WIPO patents, one European patent and thirteen Indian Patents. He has authored 12 book chapters. One of the research molecules (BG45) developed by him at Harvard Medical School has been commercialized with Sigma-Aldrich. He has successfully completed many projects sponsored by Pharmaceutical Industries such as SUN PHARMA, DR. Reddy's Lab, Dacwoong Pharmaceuticals and also Sponsored by Indian Govt funding agencies such as DST, DBT, ICMR, SERB, and CSIR. Currently he is handling projects sponsored by CSIR-EMR, DBTBUILDER and DHR-ICMR. Two students have successfully completed Ph.D. under his supervision. Currently eight students are pursuing their Ph.D. under his principal supervision and three students under his co-supervision and one RA-II student are working under his guidance.